

# Late Quaternary geochemical history of lithogenic sedimentation in the Andaman Sea

A thesis submitted to the Goa University for the award of  
Doctor of Philosophy

In the Department of Marine Sciences



By

**Pavan Miriyala**

Under the guidance of



**Dr. B. Nagender Nath**  
Chief Scientist (Retired)  
Geological Oceanographic Division  
CSIR-National Institute of Oceanography, Goa  
October 2017



*Dedicated to  
my Parents and Chelli!*

# Contents

	Page
<b>Statement</b>	v
<b>Certificate</b>	vi
<b>Acknowledgements</b>	viii
<b>Preface</b>	ix
<b>List of Tables</b>	xvi
<b>List of Figures</b>	xvii

<b>Chapter 1</b>	<b><i>Introduction</i></b>	
1.1	General Introduction	2
1.2	Geological and Oceanographic settings of Andaman Sea	7
1.3	Previous studies	9
	1.3.1. Tectonic history of Andaman back arc basin	9
	1.3.2. Sediment sources to the Andaman basin	10
1.4	Scientific rationale	16
1.5	Objectives	18
<b>Chapter 2</b>	<b><i>Materials and Methods</i></b>	
2.1	Surface sediments	20
2.2	Sediment cores	22
2.3	Age model and Chronostratigraphy	24
2.4	Sedimentation rates in the Andaman Sea	27
2.5	Elemental analyses	29
	2.5.1 Leaching protocols	29
	2.5.2 Measuring with XRF instrument	30
	2.5.2.1. Procedure for making Glass Beads for XRF analyses	30
	2.5.3. Analyses with ICP-MS	31
2.6	Radiogenic isotopic analyses	32
	2.6.1. Leaching protocols	32
	2.6.1.1. Extraction of lithogenic fraction for isotopic studies	32
	2.6.1.2. Leaching of calcium carbonate	33
	2.6.1.3. Reductive leaching of Fe-Mn oxides in sediments	34
	2.6.1.4. Acid digestion of the detrital fraction for isotope analysis	35
	2.6.1.5. Dissolution (Parr vessels in oven)	35
	2.6.1.6. Chemical Separation	36
	2.6.2. Analyses with MC-ICPMS	37
	2.6.2.1. Mass Spectrometry	37

<b>Chapter 3</b>	<b><i>Lithogenic sources to the Andaman Sea, northeastern Indian Ocean</i></b>	
3.1	Introduction	40
3.2	Results	43
3.3	Discussion	56
	3.3.1 Indo-Burman Ranges	57
	3.3.2 Sino-Burman Ranges	59
	3.3.3. Andaman-Nicobar Islands	62
	3.3.4. Western Andaman fault	65
	3.3.5. Nd-Hf based provenance inferences	66
	3.3.6. Sr-Nd mixing diagram	69
	3.3.7. Sm-Nd based $T_{DM}$ calculations	70
3.4	Conclusions	71
	Data tables of the present study	74
<b>Chapter 4</b>	<b><i>Climatic control on lithogenic sedimentation in the Andaman Sea during late Quaternary period</i></b>	
4.1	Introduction	96
4.2	Results & Preliminary observations	99
	4.2.1. Chemical weathering proxies	99
	4.2.2. Radiogenic Isotopes in lithogenic fraction	104
4.3	Discussion	105
	4.3.1. Past climatic reconstructions using chemical weathering proxies	105
	4.3.2. Climatic forcing on lithogenic sedimentation	107
	4.3.3. Global linkage of Indian Ocean dynamics	113
	4.3.3.1. Wind proxies during Holocene	118
4.4	Conclusions	124
<b>Chapter 5</b>	<b><i>Summary and Conclusions</i></b>	128
	<b><i>Bibliography</i></b>	135
	<b><i>Annexure (Publications)</i></b>	148

# Statement

As required under the university ordinance OB-9.9 (vi), I hereby state that the present thesis entitled “Late Quaternary geochemical history of lithogenic sedimentation in the Andaman Sea”, is my original contribution and the same has not been submitted on any previous occasion. To the best of my knowledge, the present study is the first comprehensive work of its kind from the area mentioned.

The literature related to the problem investigated has been cited. Due acknowledgements have been made wherever facilities and suggestions have been availed of.

Pavan Miriyala  
National Institute of Oceanography  
Council of Scientific and Industrial Research  
Dona Paula, Goa-403004  
October 2017

# Certificate

As required under the university ordinance OB-9.9 (vi), I certify that the thesis entitled “Late Quaternary geochemical history of lithogenic sedimentation in the Andaman Sea”, submitted by Mr. Pavan Miriyala, for the award of the degree of Doctor of Philosophy in Marine Sciences, is based on original studies carried out by him under my supervision. The thesis or any part thereof has not been previously submitted for any other degree or diploma in any university or institution.

Dr. B. Nagender Nath  
Chief Scientist (Retired)  
Geological Oceanography Division  
National Institute of Oceanography  
Council of Scientific and Industrial Research  
Dona Paula, Goa-403004  
October 2017

# ACKNOWLEDGMENTS

Over the last eight years, I had the privilege of meeting several influential people, who have helped and tuned me in many ways.

First and far most is to my supervisor, ***Dr. B.Nagender Nath*** – thank you for giving me various options and allowed me to choose this topic of research. Your continuous support – personal and professional – has made it a true pleasure to work both onboard and onshore laboratories. I am constantly inspired by your concern about students and dedication that inspired me to seek the depth of subject and increase my enthusiasm for science. You are the best example that I can show the world, how a mentor and a researcher should be. I will never forget your care that showed me the essence of life and research. They are always interested in hearing about his research and has been highly supportive. He has always been available for discussing my research and helping me through problems (technical and career) and I have learned a great deal about doing science from him in the field and in discussing about Himalayan, Indo-Burman geology and northern Indian Ocean.

To my project leaders, Drs. Shyam Prasad, M., Bhaskar Rao, YJ and Babu EVSSK for their continuous support during my stay at NIO and at NGRI. To Dr. Sukumaran, who played a crucial role to rise& fall of my views in exiting directions, through your tolerance about my silly thoughts and invoking me to move in a proper way, many thanks! To Dr. Abhay Mudholkar, for inviting me for various deep-sea expeditions and listening my views patiently, moreover for your advice to work on basement rocks in order to fulfil my scientific thirst, HOPE I can contribute to improve the existing knowledge on the tectonic evolution of the Andaman basin. I am thankful To Dr. Sridhar Iyer for his advise as VC's nominee, and other scientists at NIO and NGRI Kamesh Raju, Borole, Pattan, Banerjee, Ramaswamy, Srinivas.K, Durbar Ray, Prakash Babu, Sreenivas.B, Vijaykumar.Tand Yatheesh for their encouragement. I also want to thank Shri Ceaser Moraes, Dr. Parthiban for their kind support during major and trace elemental analyses.

***“Oceanography is a costly science”***, it costs not only visible bucks but invisible emotions. I owe my gratitude to my friends Milind, Anthony, Sheldon, Kalathian, Ramesh, Kuldeep and Miliketan, without whom I wouldn't have spent those isolated ship days happily. To Shri. Ramalingeswara Rao and Drs. Muralidhar Kocherla, they taught me geological sample procuring-preserving-utilizing onboard. To Shri. Arvapalli, Drs.

Subbaiah, Aditya, Suryaprakash, Sunil, Sriram and Damodararao for accompanying me numerous tours, gave a chance to see other world and eventually to bring innovative views '*out of the box*'.

To friends from back to my masters in Marine Geology at Waltair located in east coast of India, namely Jakkula, Gummadi, Saripalli, Chirukuri, Noolu and Dindi who gave me enough confidence to my thought of joining in NIO located in west coast of India for further research in the field of my favorite 'marine geology'. To friends, Reshma, Manasa, Armoury and Jaleena who have always wanted me to discover new things, ever since I joined in Ph.D in this pioneer institute "National Institute of Oceanography".

A special "thanks" goes to Drs.Vineesh, Brenda, Sijin and Manju who taught me what to do and what not to do in research career. Thanks to Ramamurty and Kinnu of NGRI; Cliffa, Poonam, Teena, Sampada, Niyati-Mahesh, Linshy, Sujatha, Domnica, Dalaiah, Arindam, Kiran, Pooja, Simonthini, Shami, Linsy-Tyson, Savitri, Pushkraj, Purnina, Saranya, Aswini, Darwin, Agnelo, Ajeesh, Suresh.K, Robin, Kiranmai, Ankita, Surabhi, Sarun, Manual, Tanvi, Amol, Sushil, Gobardhan, Rajaneesh, Bhagyasri and Shabnam of NIO and GU and many others who assisted me in the laboratories onboard and onshore. I will miss the commiserating and camaraderie that we have shared over many wada-pav and mirchi-pavmeets at Dona Paula and Habsiguda the past 8 years. Jaggu, Rajkumar, Kartheek, Krushna, Tulasi,Darsipudi, Yenne, Nagendra, Deeksha, Sunny, Babji, Sundar, Dinesh, Sandeep, Ashok, Rana, Balu, Lohith, Sujai for their support in various stages of my life. Special regards to kids Yaswanth, Sanju, Geethika, Joel, Nehal, Sreshta and Dhruv Narayan.

I thank Dean, Life Sciences, Heads of the Department and faculty of Department of Marine Sciences, Goa University for their guidance and support throughout the tenure. My five years stay at CSIR-NIO was supported through funds from MoES Project PMN Surveys. Cruises and analytical work at NIO and NGRI were funded by various CSIR projects such as COR-0006, GENIAS, GEOSINKS, INDEX without which this work would not have been completed. My sincere thanks to Directors (present and past) of CSIR-NIO and CSIR-NGRI for the permissions given and facilities provided.

*...Pavan Miriyala*

# Preface

The Andaman Sea (AS) is a marginal sea in the northeastern part of the Indian Ocean situated between the east of Andaman Nicobar Ridge (ANR) and west of Malayan Peninsula, with a maximum water depth of 4400 m. Andaman Sea receives terrigenous sediments mainly from major south Asian Rivers of Irrawaddy and Salween [Rodolfo, 1969; Roonwal, 1996]. The Irrawaddy delta-shelf is accumulating 90% of the sediment [Rodolfo, 1968], the riverine and shelf sediments reach the deeper areas through canyons and Gulf of Martaban [Ramaswamy *et al.*, 2004] and the traces of influence of Irrawaddy sedimentation are also noticed in the equatorial Indian Ocean [Ahmad *et al.*, 2005]. Seismic studies have also shown evidences of accumulation of detrital sediment in the eastern part of the Andaman Back arc Basin presumably derived from Irrawaddy shelf [Kamesh Raju *et al.*, 2012]. The rivers contributing these sediments flow through Indo-Burman ranges, which mainly consist of Tertiary & Cretaceous sedimentary formations [Colin *et al.*, 2006] and the sediments in the Andaman Sea would record the changes in removal processes at source terrains. Deep-water sediment exchange between Andaman Sea and the Bay of Bengal is not possible as sills separating these two seas only allow the exchange of intermediate waters. The Himalayas has the world's highest physical and chemical erosion rates [Milliman and Meade, 1983; Milliman and Syvitski, 1992]. Similar processes are expected to occur in Indo-Burman mountain ranges, eastern syntaxis of Himalayas (Sino-Burman ranges) and thus an interesting region to establish a relationship between erosion and climate [Colin *et al.*, 1999]. The sediments of Andaman Sea fed by Myanmar rivers, thus provide an excellent record of variability of the intensity of erosion in Burman ranges, and also the paleoclimatic & paleoenvironmental changes affecting the erosion, weathering and removal processes prevailed in SW Asia. Degree and nature of

weathering would depend on the prevailing climate at the time of break-down and removal. Key climatic feature in the region is the monsoon and the monsoonal variation during the glacial-interglacial periods will definitely influence the type of weathering. Understanding the variability in silicate weathering is important as it involves in the consumption of atmospheric CO<sub>2</sub>, and it is the major sink for atmospheric CO<sub>2</sub> than carbonate weathering [Broecker, 1994; MacFarlane *et al.*, 1994; Nath *et al.*, 2000]. On geological time scales, silicate weathering plays a key role in driving the global climate. The Andaman Sea has a moderate to high sedimentation rate of ~8.32 to 23 cm/ka and a depocenter for sediments discharged by the Myanmar rivers Irrawaddy, Salween and Sittang. As Kurian, Nath *et al.*, [Kurian *et al.*, 2008] have found that the Andaman Back-arc basin also receives sediments of volcanogenic, hydrothermal origin. As eroded sediments are depositing in Andaman Sea, the lithogenic fraction in the sediments from this area allows reconstructing the history of sediment deposition. The paleoclimatic interpretation of detrital geochemical records requires knowledge of the source areas. Elemental abundances in sediments were effectively used in inferring the sources, erosional events, dispersal patterns, paleoweathering trends of siliciclastic deposits [Nath and Mudholkar, 1989; Fedo *et al.*, 1995; Nath *et al.*, 2000, 2005; Nath, 2001]. In addition, radiogenic isotopes of Nd, Sr are reliable tracers of source for sediments which are preserved in the ocean basin [Ahmad *et al.*, 2005; Colin *et al.*, 2006].

***The thesis has been organized to 5 chapters and a brief outline is presented below:***

### **Chapter 1: Introduction**

This chapter provides a general introduction about the importance of lithogenic fraction in marine sediments, climatic influence on elemental removal during erosion and weathering, transportation and depositional environment of sediment. This chapter also includes the detailed description of the various proxies in understanding the past chemical weathering conditions, terrigenous material pathways. The chapter also describes the previous studies on sediment dispersal patterns in the Andaman Sea, gaps in our understanding of the sedimentary processes, provenance and deposition with time and changing climate leading to the description of scope of this work and the scientific objectives of the investigations carried out. This chapter also describes the geology, tectonics, depositional setting and oceanography of the study area.

### **Chapter 2: Materials and Methods**

This chapter describes the materials used and methods followed to fulfill the projected research objectives. Also described are the age model and stratigraphy of the sediment cores used in this study. The study comprises of analyses of 1) surface sediments from different depositional settings to decipher the distal and proximal sources and to tie the isotopic and geochemical signatures to riverine and local volcanogenic and island sources and to understand the present day geographical control over neighbor geological reservoirs to the basin. (2) 3 sediment cores in a near north-south transect. northern core from Alcock seamount complex, second one from central Andaman Trough, the southern core is from Nicobar earthquake swarm area. All the three cores were dated by (AMS)  $^{14}\text{C}$  either at NOSAMS facility at WHOI, USA or AMS facility of Division of Ion Physics, Uppsala University, Sweden and the sedimentation rates are published. The mean sedimentation rates for these cores are 8, 11 and 23 cm/ka respectively and dates back to a maximum time period of 54ka. The geochemical analyses were carried on carbonate and salt-free basis and thus represent the lithogenic fraction. All the major and trace, rare earth elemental studies were carried out at National Institute of Oceanography (CSIR-NIO), Goa using XRF (X-Ray Fluorescence) and ICP-MS (Inductively Coupled Plasma Mass Spectrometry) respectively. Sediment leaching, separation of lithogenic fraction, power

bomb digestions, column separation, purification and analyses of strontium, neodymium, hafnium and lead isotopes were carried out at MC-ICP-MS national facility at Geochronology and Isotope studies division of National Geophysical Research Institute (CSIR-NGRI), Hyderabad.

### **Chapter 3: Lithogenic sources to the Andaman Sea, northeastern Indian Ocean**

This chapter defines the distribution of terrigenous sediments in the Andaman Sea to decipher the geographical distribution of various terrigenous sources which contribute them. A total of 44 surface sediments were used for this study which were either collected by grab or represent core tops. The sample set also includes four sediments from Myanmar continental shelf to help in defining the different terrigenous end-members. The data generated during the present study was combined with the published core top data to define the sources. The geochemical data of lithogenic fraction was used to generate discriminative plots A-CN-K, A-CNK-FM, La-Th-Sc and total alkalies vs silica (TAS) to decipher the provenance changes within the basin. In addition, robust source indicators of Sr-Nd-Hf isotopes in lithogenic fraction were also measured to strengthen the understand the sediment sources to the basin. The geochemical and isotopic data suggest that the central part of the basin (the Central Andaman Basin -CAB) receives terrigenous material mainly from Myanmar rivers Salween and Sittang with relatively lesser supply from Irrawaddy, while the western Andaman Basin (WAB) receives sediments from Andaman and Nicobar archipelago and Irrawaddy river. The presence of mafic-ultramafic suites in these islands might have been played a key role in differentiating the WAB from the CAB. The more radiogenic  $\epsilon_{Nd}$  in Irrawaddy mouth is very similar to the Arakan shelf, and agrees well with reported Irrawaddy sediment value of  $\epsilon_{Nd} -8.3$  and implies that the eastern and western part of Indo-Burman ranges (IBR) are contributing near similar Nd signal to the open ocean, either through Arakan, Rakhine rivers in western IBR or through Irrawaddy river on eastern IBR. The similar isotopic signatures in material derived from Andaman Islands and that comes through IBR makes a second dominated source of sediment to the basin. Whereas WAF chain of seamounts in southern basin which are connected to Indonesia volcanic chain in southeastern part and Barren-Narcondam islands in the north defines a third but minor source. The similarity in  $\epsilon_{Nd}$  of a seamount top sediment in the southern basin to the Barren rocks/derived ash layers in northern basin suggests a minor but a visible terrigenous source.

#### **Chapter 4: Climatic control on lithogenic sedimentation in the Andaman Sea during late Quaternary period**

This chapter describes the temporal variations of geochemical ratios and its deposition with response to the last glacial-interglacial climatic oscillations reflected mainly on the Myanmar river plains. The present study provides the first report on hafnium isotopes in the Northern Indian Ocean. The Hf isotopes have been used here to decipher the weathering intensity and its linkage to the fluctuations in monsoonal strength. From the high resolution study on strontium and hafnium isotopes along with Al/K, Rb/Sr of northern deep sea core SK168, it appears that these geochemical and isotopic tracers seem to trace the climate related erosional and weathering changes in the source regions. The glacial-interglacial variation is clearly seen in all chemical weathering proxies and provenance indicators and suggests the Andaman Sea is the best place to understand the past climatic studies from the weathering residues due to its confined nature and enormous sediment and fresh water delivery of Myanmar rivers. While Sr and Hf isotopes were used as an index of weathering changes, Nd isotope seem to trace even the small changes in provenance. A small change in radiogenic nature in Nd during deglaciation suggests a control of climate change in shifting of source material of Myanmar river watersheds. This work has been published in journal *Scientific Reports* (<http://www.nature.com/articles/srep44310>). The absence of high radiogenic Nd in this central Andaman core (SK168) during glacials contradicts the earlier observations; 1) that attributing increased radiogenic Nd in Bay of Bengal (Stoll et al, 2007) to the Arakan/Rakhine coast and 2) radiogenic pulses to ninetyeast ridge core during Heinrich events (Ahmad et al, 2005). Though the dramatic change in North Atlantic events (Heinrich events) are reported in the Andaman Sea (Sijinkumar et al, 2016a), this present study purely based on lithogenic sedimentation suggests there was no effect of these far climatic events on the weathering intensity or provenance changes in the Myanmar river watersheds.

This chapter also discusses the observed rainfall contrast during Holocene period with in the Northern and equatorial Indian Ocean. Sr-isotope and geochemical data based interpretations have shown that the 3 alternating periods (8.5 to 6.5ka, 6.5 to 5ka and 5-3.8ka) of humidity and aridity in the eastern and the western Indian Ocean regions during the Holocene period. The observed rainfall contrast in E-W Indian Ocean is supported by published monsoonal records suggests the occurrence of Indian Ocean dipole like phenomenon. If this contrast is similar to present day short term rainfall anomalies (like

Indian Ocean Dipole), this study reflects the prevalence of longer period IOD events in the longer time scale. Though of low resolution, this forms the first report of Holocene IOD changes. This study also suggests that there are monsoonal (precipitation) contrasts within the Northern Indian Ocean or South Asia and the entire Northern Indian Ocean cannot be considered as a single entity as far as the prevalence of monsoon is concerned.

## **Chapter 5: Conclusions**

This chapter summarizes the results and major conclusions obtained from the present research work.

## List of Tables

<b>Tables</b>	<b>Descriptions</b>	<b>Page No.</b>
Table 2.1	<i>Location and water depth details of surface sediments used in the present work.</i>	21
Table 2.2	<i>Details of sediment cores used in the present work.</i>	24
Table 2.3	<i>AMS <sup>14</sup>C dates of foraminifera and calibrated ages of sediment samples for SK168, AAS11 and RVS02 [Sijinkumar et al., 2015].</i>	26
Table 2.4	<i>Thickness of sediments deposited during each MIS stages of three cores.</i>	28
Table 3.1.	<i>Location and water depths of all sediment samples studied here. Also shown are details of published literature on sediment samples in and around Andaman Sea used in the interpretations. Serial Numbers are same as those shown in Fig. 2.1</i>	74
Table 3.2.	<i>Major element content and calculated weathering indices Al/K, CIA*, CIW and PIA of surface sediments of Andaman Sea</i>	76
Table 3.3.	<i>Trace elemental content (in ppm), ratios of Rb/Sr, La<sub>n</sub>/Yb<sub>n</sub> and Total REE concentrations of surface sediments of Andaman Sea</i>	78
Table 3.4.	<i>Nd, Sr and Hf isotopic composition of surface sediments of Andaman Sea</i>	79
Table 3.5.	<i>Major element content and calculated Al/K, CIA*, CIW and PIA in sediments from the core SK168/GC01 shown against subsurface depth and age.</i>	80
Table 3.6.	<i>Major element content and calculated Al/K, CIA*, CIW and PIA in sediments from the core AAS11/GC01 shown against subsurface depth and age.</i>	82
Table 3.7.	<i>Major element content and calculated Al/K, CIA*, CIW and PIA in sediments from the core RVS02/GC03 shown against subsurface depth and age.</i>	84
Table 3.8.	<i>Trace elemental content (ppm), ratios of Ni/Co, Rb/Sr, Th/Yb, La<sub>n</sub>/Yb<sub>n</sub> and Total REE concentrations of the core SK168/GC01 shown against sediment depth and age</i>	86
Table 3.9.	<i>Trace elemental content (ppm), ratios of Ni/Co, Rb/Sr, Th/Yb, La<sub>n</sub>/Yb<sub>n</sub> and Total REE concentrations of the core AAS11/GC01 shown against sediment depth and age</i>	88
Table 3.10.	<i>Trace elemental content (ppm), ratios of Ni/Co, Rb/Sr, Th/Yb, La<sub>n</sub>/Yb<sub>n</sub> and Total REE concentrations of the core RVS02/GC03 shown against sediment depth and age</i>	91

Table 3.11.	<i>Nd, Sr and Hf isotopic composition of core SK168/GC01.</i>	93
Table 3.12.	<i>Nd and Sr isotopic compositions of core RVS02/GC03.</i>	94

## List of Figures

<b>Figure</b>	<b>Description</b>	<b>Page No.</b>
Fig. 1.1:	<i>Geographical and bathymetry map of northern Indian Ocean and Indian sub-continent. This map is generated by using ArcGIS programme, E.S.R.I. "10.1."Redlands, California: ESRI [2012].</i>	4
Fig. 1.2:	<i>Geological map of south Asia, including all major river channels. Modified from Colin et al., [2006].</i>	8
Fig. 1.3:	<i>Morphological and geological structure of Andaman Sea and Myanmar, modified from Raju et al., 2004</i>	11
Fig. 2.1:	<i>Location map of surface and core sediments studied here. Also plotted locations from the published literature in the area. The numbers are identification of each station, the details of these stations are found in Table 3.1.</i>	23
Fig. 2.2a:	<i>Age-depth model with sedimentation rates of a) northern core SK168; b) central core AAS11 and c) southern core RVS02, modified from Sijinkumar et al, [2015].</i>	25
Fig. 2.2b:	<i>Sedimentation rates (cm/ka) of the Andaman Sea. RODO1 to 14 are from Rodolfo [1969] and details of other samples can be found in Table 3.1.</i>	27
Fig. 2.3:	<i>Schematic representation steps involved during glass bead making procedure for sediment samples.</i>	29
Fig. 2.4:	<i>Inductively Coupled Plasma Mass Spectrometer (ICP-MS) facility at CSIR-National Institute of Oceanography, Goa.</i>	32
Fig. 2.5:	<i>Multi collector Inductively Coupled Plasma Mass Spectrometer (MC-ICPMS) facility at CSIR-National Geophysical Research Institute, Hyderabad.</i>	37
Fig. 3.1a:	<i>Total alkalies versus silica plot (TAS diagram) [Le Bas et al., 1986] of all surface sediments along with seamount rocks of southern basin [Kamesh Raju et al., 2012], rocks and ash of Barren and Narcondam islands of northern basin [Luhr and Haldar, 2006; Chandrasekharam et al., 2009; Streck et al., 2011].</i>	42
Fig. 3.1b:	<i>Total alkalies versus silica plot (TAS diagram) [Le Bas et al., 1986] of glacial and-interglacial sediments of all three sediment cores of this study. The sediments from southern location (RVS) plot distinctly away from northern cores on silica axis.</i>	44
Fig. 3.1c:	<i>Total alkalies versus silica plot (TAS diagram) [Le Bas et al., 1986] of sediments collected in and around Barren and Narcondam islands and seamounts of southern Andaman basin – Western Andaman Fault (this study) along with rocks and ash of Barren and Narcondam [Luhr and Haldar, 2006; Chandrasekharam et al., 2009; J.Streck et al., 2011], various Indonesian volcanoes [Chesner and Rose, 1991; Turner et al., 2003; Gardner et al., 2013], plume derived nintyeast ridge [Weis and Frey, 1996]and Afanasiy Nikitan seamounts</i>	45

	<i>[Mahoney et al., 1996]. The decrease in alkalis and silica content is observed (red arrow) from Indonesian volcanoes to Barren and Narcondam island material. The similar trend is observed in southern Andaman rocks [Kamesh Raju et al, 2012] and sediments of the present study with decrease in alkalis (green arrow) content and constant silica content.</i>	
Fig. 3.2:	<i>The downcore variation of major elemental composition with age for the 3 sediment cores studied here. Compositionally, the southern core (RVS) is different from the northern cores.</i>	46
Fig. 3.3a:	<i>A-CN-K diagram of all surface sediments studied for this work along with seamount rocks of southern Andaman basin. Most of the sediment samples fall in between weathering trends of granite-illite and gabbro-smectite suggesting their mixed nature. Some points fall close to average andesite values.</i>	47
Fig. 3.3b:	<i>A-CN-K diagram of all subsections of three sediment cores. Glacial and interglacial sediments are plotted with a different symbol. Subtle differences are seen these two sets of sediments. The differences are relatively more visible in two northern stations.</i>	48
Fig. 3.4a:	<i>A-CNK-FM diagram of surface sediments of this study along with southern basin rocks. Clear geographic differences are seen within the Andaman Sea.</i>	49
Fig. 3.4b:	<i>A-CNK-FM diagram of subsurface sediments of 3 sediment cores. Glacial and interglacial sediments are plotted with a different symbol. Temporal and spatial changes in composition are seen.</i>	51
Fig. 3.5a:	<i>La-Th-Sc ternary diagram of all surface sediments studied here. Discriminatory spaces of continental margins and island arcs are shown.</i>	54
Fig. 3.5b:	<i>La-Th-Sc diagram of all subsurface sediments from three sediment cores. Glacial and interglacial sediments are plotted with a different symbol.</i>	55
Fig. 3.6:	<i>Downcore variation of <math>\Sigma REE</math>, <math>(La/Yb)_n</math>, Ni/Co and Th/Yb ratios of SK168, AAS11 and RVS02 cores. The southern core shows different La/Yb and Th/Yb ratios, similar to major elemental variation.</i>	57
Fig. 3.7a:	<i>A plot of <math>^{87}Sr/^{86}Sr</math> vs <math>\epsilon_{Nd}</math> of all sediments used for this study and other available sediments from the northeastern Indian Ocean. The discriminative spaces are re-drawn from Colin et al, [1999]. Most of the samples fall in a broad field defining Higher Himalayan crystalline series where the 3 Myanmar river end-members also fall.</i>	58
Fig. 3.7b:	<i>A plot of <math>^{87}Sr/^{86}Sr</math> vs <math>\epsilon_{Nd}</math> of all available downcore data of Andaman Sea. Distinct geographic zonation is seen in the</i>	60

	<i>elemental data too.</i>	
Fig. 3.7c:	<i>A mixing diagram of <math>^{87}\text{Sr}/^{86}\text{Sr}</math> vs <math>\epsilon_{\text{Nd}}</math> showing all available surface sediment and downcore data plotted along with data generated for this present study. Four possible end-members viz., the IBR, Irrawaddy, Salween-Sittang and Mergui Plateau are plotted. While the CAB and SAB sediments fall within the end-members, WAS sediments seems to have additional source</i>	62
Fig. 3.7d:	<i>Sr-Nd isotopic data of all available sediment cores of the Andaman Sea along with northern and southern cores (SK168 and RVS02) of this study. WAS sediments plot away from CAB cores.</i>	63
Fig. 3.8:	<i><math>\epsilon_{\text{Nd}}</math> vs. <math>\epsilon_{\text{Hf}}</math> of all available surface sediments and 44 subsections of core SK168 of Andaman Sea along with Ganges sediment in India and Bangladesh as well MORB-Mid-Oceanic Ridge Basalt and OIB-Oceanic Island Basalt composition. The seawater array is re-drawn from Vervoort et al, [2007] and zircon-free and zircon-bearing arrays are re-drawn from Bayon et al, [2009].</i>	67
Fig. 4.1:	<i>Different indices of alteration of all three gravity cores obtained from major element analysis plotted against age. CIA=Chemical index of alteration [Nesbitt and Young, 1982]; CIW=Chemical index of weathering [Harnois, 1988]; PIA=Plagioclase index of alteration [Fedo et al., 1995] and elemental ratio of alumina and potassium.</i>	100
Fig. 4.2:	<i>Downcore variation of <math>\Sigma\text{REE}</math>, <math>(\text{La}/\text{Yb})_n</math>, <math>\text{Ni}/\text{Co}</math> and <math>\text{Th}/\text{Yb}</math> ratios of all three cores plotted against age. <math>n</math>=normalized to Post Australian Archean Shale [Taylor and McLennan, 1985].</i>	101
Fig. 4.3:	<i>CIA vs <math>\text{Al}/\text{Na}</math> binary plot of glacial and interglacial sediments of all three cores along with shelf sediments off Myanmar river mouths and seamount rocks [Kamesh Raju et al, 2012]. Majority of the samples fall in the intermediate/moderate weathering domain</i>	102
Fig. 4.4:	<i><math>\epsilon_{\text{Nd}}</math> versus <math>^{87}\text{Sr}/^{86}\text{Sr}</math> of glacial and interglacial sediments of published data [Colin et al, 2006; Awasthi et al, 2015; Ali et al, 2015; Cao et al, 2015] and two cores of the present study [SK168 and RVS02].</i>	103
Fig. 4.5:	<i>Downcore plots of SK168 (northern core); (a) <math>\text{La}_n/\text{Yb}_n</math> ratio and 3-point moving average; (b) Chemical Index of Alteration* and 3-point moving average (CIA*-excluding CaO [Colin et al, 2006]) calculated from molar proportions of major elements; (c) elemental ratio of rubidium to strontium and it's 3-point moving average; (d) elemental ratio of aluminium to potassium; (e) <math>^{87}\text{Sr}/^{86}\text{Sr}</math>; (f) <math>\epsilon_{\text{Nd}}</math>; (g) mean effective moisture of Asia [Herzschuh, 2006]; (h) summer insolation at <math>30^\circ\text{N}</math> [Berger, 1978]. <math>\text{La}_n/\text{Yb}_n</math>, <math>\text{Rb}/\text{Sr}</math> and <math>\text{Sr}/\text{Sr}</math> are in reverse order</i>	105

	<i>to get best fit with other plots.</i>	
Fig. 4.6:	<i>Present day and reconstructed river catchments during interglacial and glacial periods respectively. Increased catchments during interglacials due to increased vegetated and soil zone areas. Additional catchments (orange) during interglacials would facilitate produce more weathered material. During glacials, due to less catchment area, low infiltration and high runoff are expected. Exposed shelf during glacials (reconstructed-shaded area, below 120MSL of present day).</i>	107
Fig. 4.7:	<i>Downcore plots of (a) <math>^{87}\text{Sr}/^{86}\text{Sr}</math> of SK168; (b) <math>\epsilon\text{Nd}</math> of SK168; (c) <math>\delta^{18}\text{O}_{\text{sw}}</math> of Andaman Sea of RC12-344 [Rashid et al., 2007]; (d) Planktonic foraminifer (<i>Globigerina Bulloides</i>) % in SK168 [Sijinkumar et al., 2010]; (e) Salinity record in 126KL core of Bay of Bengal [Kudrass et al., 2001]; (f) <math>p\text{CO}_2</math> [Petit et al., 1999]; (g) <math>\delta^{18}\text{O}_{\text{sw}}</math> of middle-west Bay of Bengal from SK218 [Govil and Naidu, 2011]; (h) <math>\delta^{18}\text{O}</math> of stalagmites of Chinese caves [Wang, 2001; Yuan et al., 2004]; (i) summer insolation at <math>30^\circ\text{N}</math> [Berger, 1978]; (j) <math>\delta^{18}\text{O}</math> of ice core from Greenland ice-sheet program GISP2 [Blunier and Brook, 2001]. For clarity we have restricted the time series records to 32ka. The blue color shaded region represents the period with coeval increase in chemical weathering and the deglacial monsoon.</i>	109
Fig. 4.8:	<i>a) downcore plots of <math>\epsilon\text{Nd}</math> of SK168 (north central basin), MD169 (south central basin), RVS02 (southern basin); b) downcore plots of <math>^{87}\text{Sr}/^{86}\text{Sr}</math> of SK168 (north central basin), MD169 (south central basin), RVS02 (southern basin); c) <math>\text{Rb}/\text{Sr}</math> of SK168 (north central basin), AAS11 (south central basin), RVS02 (southern basin); d) <math>\text{Al}/\text{K}</math> of SK168 (north central basin), AAS11 (south central basin), RVS02 (southern basin); e) <math>\text{CIA}^*</math> of SK168 (north central basin), AAS11 (south central basin), RVS02 (southern basin); f) Mean effective Moisture of [Herzschuh, 2006] and Summer Insolation at <math>30^\circ\text{N}</math> [Berger, 1978].</i>	112
Fig. 4.9:	<i>Holocene monsoonal precipitation changes in the Andaman Sea compared with those from the western and eastern Arabian Sea and from the Bay of Bengal and Africa which are inferred from proxy data: a) <math>\delta^{13}\text{C}_{\text{wax}}</math> of Tanganyika lake [Tierney and DeMenocal, 2013]; b) <math>^{87}\text{Sr}/^{86}\text{Sr}</math> data of dust fraction of 905 core off Somalia [Jung et al, 2014]; c) <i>G.Bullodies</i> (%) of ODP723A core [Naidu and Melmgren, 1995]; d) <math>\delta^{15}\text{N}</math> of RC27-23 and RC27-14 cores off Oman [Altabet et al, 2002]; e) Perij lake level fluctuations [Raj et al, 2015]; f) <i>G.bullodies</i> (%) of Malabar core [Saraswat et al, 2016]; h) <i>G.Bullodies</i> (%) of ODP716A core [Gupta et al, 2010]; i) <math>\delta^{18}\text{O}_{\text{sw}}</math> record of SK218core of western BoB [Govil and Naidu, 2011]; j) Salinity record of Ganges mouth core [Kudrass et al, 2001]; k)</i>	114

	<i>G.bulloides</i> (%) of SK168 core [Sijinkumar et al, 2010] and l) Coral reef record of Mentawai island [Abram et al, 2003].	
Fig. 4.10:	<i>Erosional and weathering proxy data of SK168 core during Holocene period. a) Aluminium to potassium ratio; b) Chemical Index of Alteration* (CIA-Nesbitt and Young, 1982) calculated from molar proportions of major elements and CIA*-excluding CaO [Colin et al, 2006]; c) <math>^{87}\text{Sr}/^{86}\text{Sr}</math> isotopic ratio variation; d) Potassium to rubidium ratio; e) Mass accumulation ratio of terrigenous matter, based on titanium concentration [Yarincik et al, 2000] and f) <math>e_{\text{Nd}}</math> used as a provenance indicator.</i>	117
Fig. 4.11:	<i>Climatic and precipitational proxy data of northern Indian Ocean. References can be found in figure 4.9 except BIT index of Challa lake of Kenya [Wolff et al, 2011], total fertile species of SK168 core [Sijinkumar et al, unpublished data], Asian mean moisture content [Herzschuh, 2006] and summer insolation curve [Berger, 1979].</i>	119
Fig. 4.12:	<i>Historical rainfall (for the last 112 years) contrast between east Indian and west Indian Ocean land masses. In the top panel, Bangladesh and Oman data have been used and in the bottom panel, Indonesia data is compared with Kenya. The data is taken from CRU [Haris et al, 2014].</i>	120
Fig. 4.13:	<i>Regional variability of precipitation and East-West monsoonal contrast during three periods of Holocene epoch in the Northern Indian Ocean reconstructed from paleo-data.</i>	122
Fig. 4.14:	<i>Sr isotope records of western (published) and eastern Indian Ocean (this study) are compared with wind proxies (upwelling indicators in oceans), monsoonal records from land in Africa, NE India. <math>^{87}\text{Sr}/^{86}\text{Sr}</math> isotope record off Somalia [Jung et al., 2004]; <math>\delta^{13}\text{C}</math> record from lake Tanganyika [Tierney and DeMenocal, 2013]; Variation of <i>G.bulloides</i> population from west to east Indian Ocean records [Naidu and Melmgren, 1995, Gupta et al., 2010, Sijinkumar et al., 2010]; SST record off Indonesia [Mohtadi et al., 2014]; <math>^{87}\text{Sr}/^{86}\text{Sr}</math> isotope record of Andaman Sea core (this study); <math>\delta^{18}\text{O}</math> record of Mawmulah cave [Dutt et al., 2015]; the boxes and ellipsoids on the right end indicate lake level fluctuations (red – low level; black – increased lake levels) in India. Boxes on the extreme left indicate Holocene IOD events reported in an Indonesian island [Abram et al., 2003].</i>	123

# CHAPTER 1

## Introduction

## 1.1. General Introduction:

1.1.1. Climate refers to the average weather condition and variations over a large area for a period, generally more than 30 years. **Paleoclimatology** is the study of reconstructing ancient climates. Since direct observations are not available paleoclimates are inferred from proxy records in marine sediments, sediments in lake beds, ice-cores, tree-rings and corals. Concentrations of various gases, especially greenhouse gases in the atmosphere play a key role to establish the climatic and environmental conditions on earth. **Carbon-dioxide** (CO<sub>2</sub>), among other greenhouse gases plays a vital role in regulating the Earth's temperatures. While the ocean-atmosphere exchange, plant and animal respiration, soil respiration and decomposition and the volcanic eruptions are the major natural suppliers of CO<sub>2</sub> to the atmosphere (<https://whatsyourimpact.org/greenhouse-gases/carbon-dioxide-emissions>), plant respiration, terrestrial and oceanic photosynthesis and silicate weathering are the major natural sinks which in turn regulate the global temperatures. In addition to being a CO<sub>2</sub> sink, the process of weathering is critical in controlling the chemistry of natural waters, global biogeochemical cycles, and soil formation [e.g., *Baumeister*, 2012]. The silicate weathering process assumes importance as the Earth's crust is composed roughly 92 weight percent silicate minerals. The Palaeocene-Eocene boundary was recognized as the maximum thermal conditions (PETM) and after this event [*Crowley and North*, 1991] of Cenozoic, climate observed greater climate cooling since ~50Ma. The impact of 'icehouse effect' promoted the growth of ice sheets. Since the end of Eocene, the possible ice-free conditions were reduced and the Earth has witnessed numerous glacial cycles. Milankovitch proposed cyclicality in earth's rotation makes perihelion and aphelion impacts which tends to move away and close to the heat source the 'SUN', in a rough periodicity of 110ka ultimately makes warm and cold climate over earth's surface. These gradual warming and cooling of earth's atmosphere tends to freeze and melt oceanic water

content and leads to greenhouse (interglacials) and icehouse (glacials) conditions. On these glacial-interglacial scales, silicate weathering played a crucial role in consuming excess CO<sub>2</sub> content to stabilize the warm atmospheric conditions. The effect of carbonated rain water acts as an acid due to increased acidity by H<sub>2</sub>O (rain water) +CO<sub>2</sub> (carbon-dioxide) =2HCO<sub>3</sub> (Carbonic acid). The increased acidic rain water (lower pH) will attack various mineral groups (like olivine, feldspars, pyroxene, amphiboles, etc) and chemically leaches more solute to weathered products during humid periods. There is two school of hypotheses described the role of chemical weathering in regulating global temperatures. Several workers like *Walker* (1981), *Berner* (1983), *Volk* (1987) and *Lasaga* (1994) proposed the increased global temperatures rise the rate of chemical weathering by consuming atmospheric CO<sub>2</sub> and further neutralized the global temperatures by negative feedbacks. Whereas the other hypothesis by *Raymo and Ruddiman* (1992) suggested, the 'weathering rates increases are correlated with falling global temperatures.' They have proposed that over past 40Ma, the Tibetan plateau uplift has resulted in intense monsoonal circulation, increased rainfall on the Himalaya, increased rates of chemical weathering ultimately leading to lowered atmospheric CO<sub>2</sub> concentrations. They have called for more studies to understand the tectonics-climate linkages. In this direction, few studies have been carried out in this part of the world at different time-scales.

Present day silicate weathering has been interpreted from solute chemistry of major Himalayan and peninsular rivers in India [*Krishnaswami et al.*, 1992; *Sarin et al.*, 1992; *Gaillardet et al.*, 1999; *Galy and France-Lanord*, 1999; *Das et al.*, 2006; *Gupta et al.*, 2011 and others]. Based on Rb, Sr concentrations and <sup>87</sup>Sr/<sup>86</sup>Sr isotopic ratios on dissolved load of the Ganges and Brahmaputra river systems, both silicate and carbonate weathering were found play a dominant role in controlling the solute chemistry [*Krishnaswami et al.*, 1992; *Jacobson et al.*, 2003]. New estimates of global silicate weathering fluxes and

associated CO<sub>2</sub> consumption fluxes were presented by *Gaillardet et al.*, (1999) from major ion chemistry of major rivers of the world. On kiloyear time scales very few, but important studies on past weathering from the Northern Indian Ocean were published. In the northern Arabian Sea, *Limmer et al.*, (2012a and b) studied two Indus shelf cores spanning the last 14ka and observed enhanced summer monsoon during 11 to 8ka of early Holocene

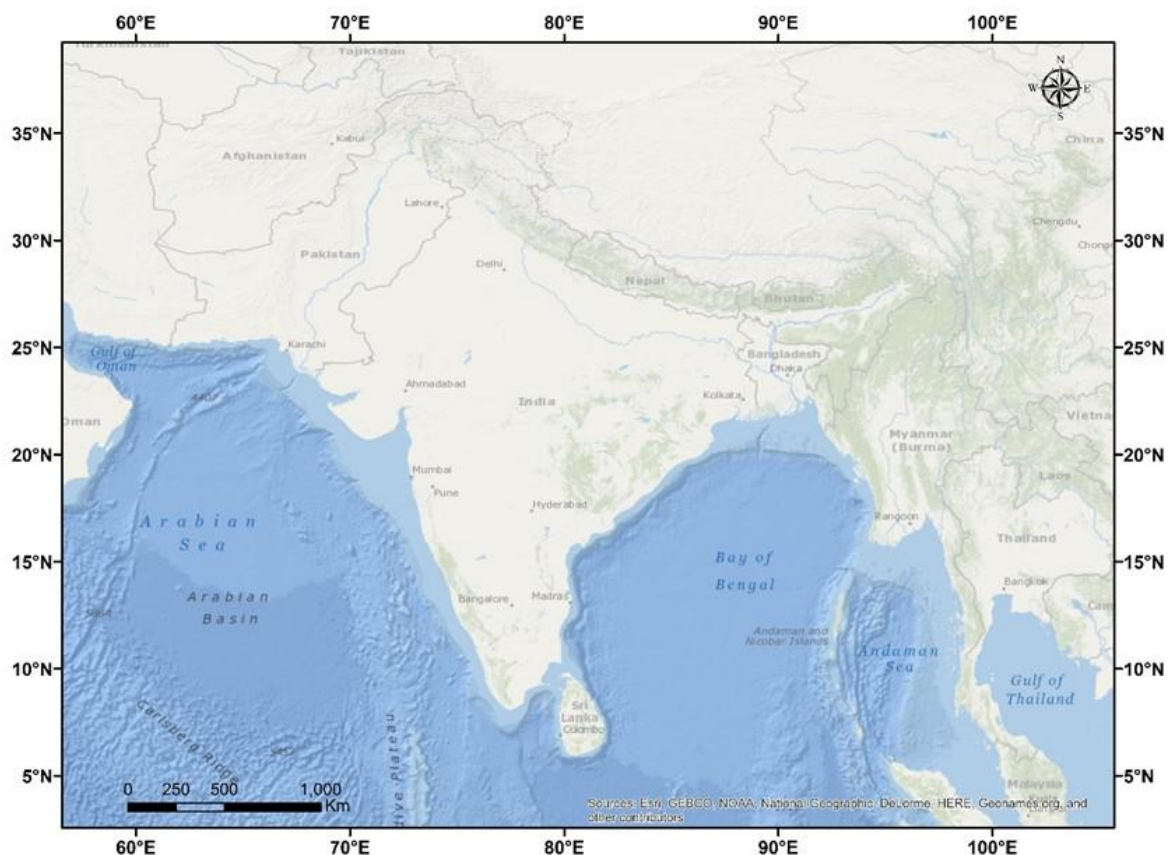


**Fig. 1.1:** Geographical and bathymetry map of northern Indian Ocean and Indian sub-continent. This map is generated by using ArcGIS programme, E.S.R.I. "10.1."Redlands, California: ESRI [2012].

and their K/Al data has shown that silicate weathering in the Indus plains peaked ca. 4–6ka. However, they suspect the impact of reworked shelf sediments (during deglacial transgression of sea level) on major chemical weathering indices like CIA, <sup>87</sup>Sr/<sup>86</sup>Sr except on K/Al ratio. *Thamban et al.*, (2002) studied two sediment cores from the southwestern continental margin of India. The grain size and clay mineralogy data has shown intensified summer monsoon during ~28ka, 22ka, 15.7 to 14.8ka and 8.8 to 6.4ka. The first two events occurred during last glaciations, while other two time periods (15.7 to 14.8ka and 8.8 to

6.4ka) corresponds to deglacial intensification of summer monsoon and Holocene climatic optimum (HCO) respectively. The occurrence of gibbsite along with increased kaolinite content during 15.7 to 14.8ka [*Thamban et al.*, 2002] also suggests the enhanced warm and humid conditions on hinterland [*Chamley*, 1989]. reconstructed climatic control on the erosion of Himalayas. A 100ka record of climatic control on Himalayan erosion [*Rahaman et al.*, 2009] has shown reduced monsoonal precipitation during 20 and 70ka ago due to increased glacial cover in the Higher Himalaya sources. Impact of climate on erosion in the Himalaya was also reported from western Bay of Bengal [*Tripathy et al.*, 2011], identifying reduced erosion rate over the Himalaya during LGM driven by reduced southwest monsoon intensity and glacier cover over the Higher Himalaya. From the abundance of chlorite (the clays produced in arid cold climate), magnetic grains and silt content, a reduced chemical weathering during glacials, physical weathering during Pre-Holocene and an intensified chemical weathering from 9.2 ka onwards was reported from the northern Bay of Bengal [*Chauhan et al.*, 2004].

On tectonic timescales, a 17-million year record of Neogene weathering history of Himalaya was presented by *Derry and France Lanord* (1996), who have shown late Miocene-Pliocene decrease in Himalayan erosion rates, followed by a return to physically dominated and rapid erosion in the Pleistocene in response to orogeny and climatic changes. *Filippelli* (1997) also suggests the excess drawdown of CO<sub>2</sub> by chemical weathering is the major reason for Pliocene climate destabilization. A detailed chemical weathering study of *Clift et al.* (2008) on three deep drilled cores (ODP1148-South China Sea; ODP718-distal Bay of Bengal and Indus Marine A1-off Indus river in north Arabian Sea) has shown imprints of increased chemical weathering in response to Asian monsoon during 16.0 to 10.0Ma and reduced monsoon between 10.0 and 3.0Ma. The consistent results in all three cores around the Himalayas, suggests the role of exhumation of the

Himalayas, especially Tibetan plateau to establish monsoonal conditions over Asia, and thus the global climate. However, by now, it is clear that chemical weathering neutralizes the global temperatures with negative feedback that gradually reduces atmospheric CO<sub>2</sub> or with positive feedback that consumes more CO<sub>2</sub> and establishes global cooling.

As shown above, most of the studies to understand the present-day and past weathering patterns heavily tilted towards the main Himalayan region (including the Karakoram in the west) and peninsular Indian regions leaving major portion of Indo-Burman ranges, Arakan mountains, Sino-Burman ranges, Tenasserim Hills, mainland Myanmar, Thailand through which some of the major rivers like Irrawaddy, Salween, Sittang and rivers such as Tanintharyi River flow through. In this context, it is pertinent to mention a recent study of *Hein et al.*, (2017) wherein the variations in the degree of chemical weathering of sediment exported by the G-B rivers were not found to follow climate variations in a straightforward manner, based on which it was argued for a possible late Holocene decoupling of climate forcing and silicate weathering in the Himalayas [*Hein et al.*, 2017]. However, the decoupling could be due to other reasons such as changes in the source of sediment which is fully not known (the low resolution of the provenance indicators such as Sr-Nd isotopes). The G-B river systems were recognised to have carried different sediment sources during glacial and interglacial climatic periods [*Stoll et al.*, 2007; *Rahaman et al.*, 2009]. Further, the Bay of Bengal is host of multiple sediment sources like peninsular rivers Mahanadi, Godavari, Krishna, Pennar and Cauveri apart from heterogeneity among Ganges-Brahmaputra river systems. The Andaman Sea, part of northeastern Indian Ocean on the hand which is recognized to have similar water column signatures [*Milliman and Syvitski*, 1992; *Naqvi et al.*, 1994; *Colin et al.*, 1999], but a restricted depocenter, and a semi locked basin (Andaman-Nicobar archipelago on the west, limited connection with Bay of Bengal, no deep-water exchange with Bay of Bengal) can

record host of the sediment and fresh water discharge of major river systems like Irrawaddy and Salween of the eastern Himalayas. In view of this and to decipher the sediment sources, the present-day and late Quaternary lithogenic sedimentation patterns in the Andaman Sea are elucidated in this work. While the chemical weathering records in general have been used as a manifestation of orogeny and tectonics-climate link as it was considered that the climatic impact will be seen on geological time-scales. Here, an attempt is made to employ the chemical weathering changes as a proxy to study the past climate in water-sheds of Myanmar where hardly few studies are available on erosion, weathering, climate, monsoonal changes, river-run off changes.

## 1.2. Geological and Oceanographic settings of Andaman Sea

The Andaman Sea is a semi enclosed marginal sea, in the eastern part of the northeastern Indian Ocean situated between the east of Andaman Nicobar Ridge (ANR) and west of Malayan Peninsula, with a maximum water depth of 4400m. The Andaman Sea is 1200km long, 650km wide and has an area of 8,00,000km<sup>2</sup> and its physiographic features are aligned to north south and parallel to the rift valleys. The Andaman Sea exchanges water with the Bay of Bengal in the northern Indian Ocean and marginal seas of western Pacific mainly via shallow channels. It is interconnected with the Bay of Bengal by the Deep Preparaes Channel, Ten Degree Channel and the Great Channel. The oceanographic processes in these seas (Andaman Sea and Bay of Bengal) are however comparable only up to a depth of about 1000m, as the deep water exchange between these two regions is hampered by several sills which has significant influence on intermediate to deep water circulation in the Andaman Sea. The Sunda Shelf provides a shallow route to

the eastern seas and to the Pacific Ocean, which is the southeast extension of the continental shelf of Southeast Asia. The Strait of Malacca maintains the connection of the Pacific Ocean water flowing through the South China Sea to the Bay of Bengal.

The present day oceanography of the Andaman Sea has been well described [Sijinkumar *et al.*, 2016b] (and references therein). As in the case of the northern Bay of

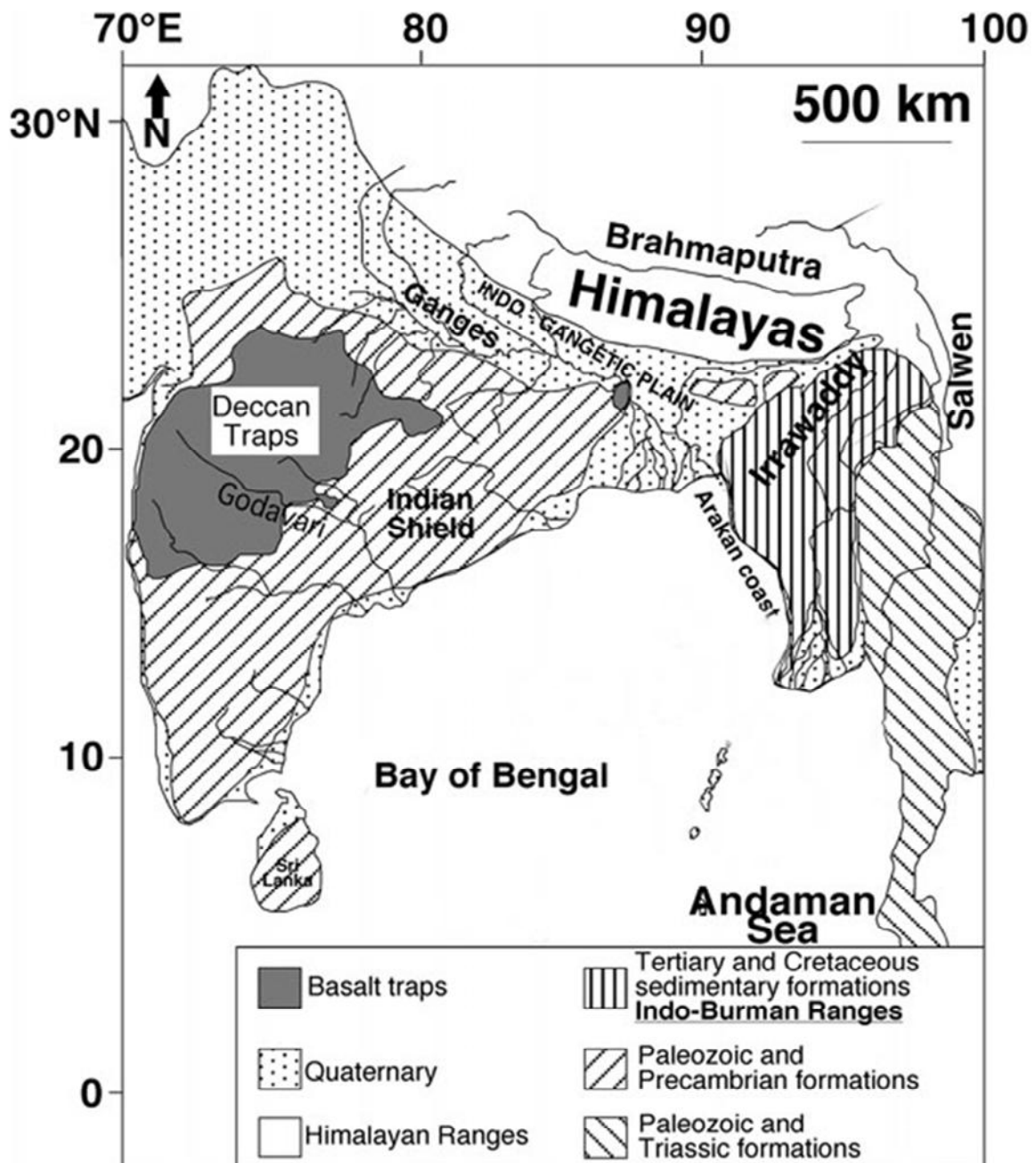


**Fig. 1.2:** Geological map of south Asia, including all major river channels. Modified from Colin *et al.*, [2006].

Bengal, the Andaman Sea receives annually large amount of fresh water from the

Irrawaddy catchment with most of the outflow occurring during the summer to late fall [Rashid *et al.*, 2007]. As a result of a fresh water influx, salinity reduces to a minimum value during summer monsoon (July to August [Varkey *et al.*, 1996]). The annual average salinity at north central Andaman Sea is nearly 31.5‰ [Sijinkumar *et al.*, 2016b and references therein]. As a result, a larger salinity gradient exists between the peak and inter monsoon periods. The annual surface water temperature ranges from 28 to 30°C and is well mixed to a depth of 50 m leading to stratification which hinders vertical mixing [Sarma and Narvekar, 2001]. The Andaman Sea experiences, a seasonal reversal in surface circulation similar to that of the Arabian Sea. The maximum water depth in the Andaman Sea is 4,400 m and it is inter-connected with the BoB via several openings viz., the Deep Prepares Channel, Ten Degree Channel, and the Great Channel. Similar to Arabian Sea, upwelling induced productivity changes is also reported from the Andaman Sea with a lower intensity mainly driven by cyclonic eddies. Biological productivity in the offshore Andaman region is ~0.8-1.0 mgC/m<sup>2</sup>/d compared to lesser values (<0.6 mg C/m<sup>2</sup>/d) observed in the coastal areas [Janekarn and Hylleberg, 1989].

### 1.3. Previous studies

#### 1.3.1 Tectonic history of the Andaman back arc basin:

The Andaman Sea extends from Myanmar in the north to Sumatra in the south and from the Malay Peninsula in the east to the Andaman and Nicobar Islands, which form a part of the Andaman Nicobar ridge, in the west. The basin is marked by prominent morphological features such as the Nicobar deep, Barren-Narcondam volcanic islands, Invisible bank, and Alcock and Sewell seamount complexes. Detailed study of multi-beam swath bathymetry, magnetic and single channel seismic data of Kamesh Raju *et al.*, (2004) over an area of about 30,000km<sup>2</sup> provided the basic understanding of tectonic evolution of

Andaman basin (Fig. 1.3). Swath bathymetry data revealed several morpho-tectonic features that divide the basin into a complex western part comprising arc-parallel seamount chains, N-S trending fault systems and a relatively smooth eastern part. A SW-NE trending spreading ridge bisects the central basin into Alcock (northern) and Sewell (southern) parts. A thick layer of sediment on Alcock than Sewell shows huge deposition of Myanmar sediments on northern basin due to its close proximity to river mouths. The new magnetic data shows that the true seafloor spreading started about 4Ma, rather than 10Ma postulated by *Curray* (1994). The initial spreading was very slow about 1.6cm/yr with an increase in the spreading rate to 3.8cm/yr later. The spreading center is connected to the Sagaing fault system in the eastern Burma highlands in the north and to the Semengko fault system in the south that longitudinally bisects Sumatra. The integrated analysis of swath bathymetry, magnetic and seismological data suggests that the basin has evolved as a consequence of extrusive tectonics that prompted extension and rifting along the plane joining the Sagaing on northeastern side and Semengko fault system on southeastern side of the basin. A major north-south trending fault system viz., the west Andaman fault (WAF) is located between Andaman-Nicobar ridge and Andaman basin [*Curray et al.*, 1979] is a major tectonic feature among other complex fault systems which, has been identified as active based on the seismic data [*Curray et al.*, 1979]. A line of this fault (WAF) is identified in the proximity of Barren and Narcondam islands by them. WAF has been said to form a lithospheric scale boundary and together with other tectonic elements modulate the occurrence of large earthquakes and their rupture pattern [*Kamesh Raju et al.*, 2007].

### 1.3.2. Sediment sources to the Andaman basin:

A first comprehensive study of sediments in the Andaman Sea was published by *Rodolfo* (1969), based on the samples collected during International Indian Ocean

Expedition (IIOE), and has identified the terrigenous material supply from rivers

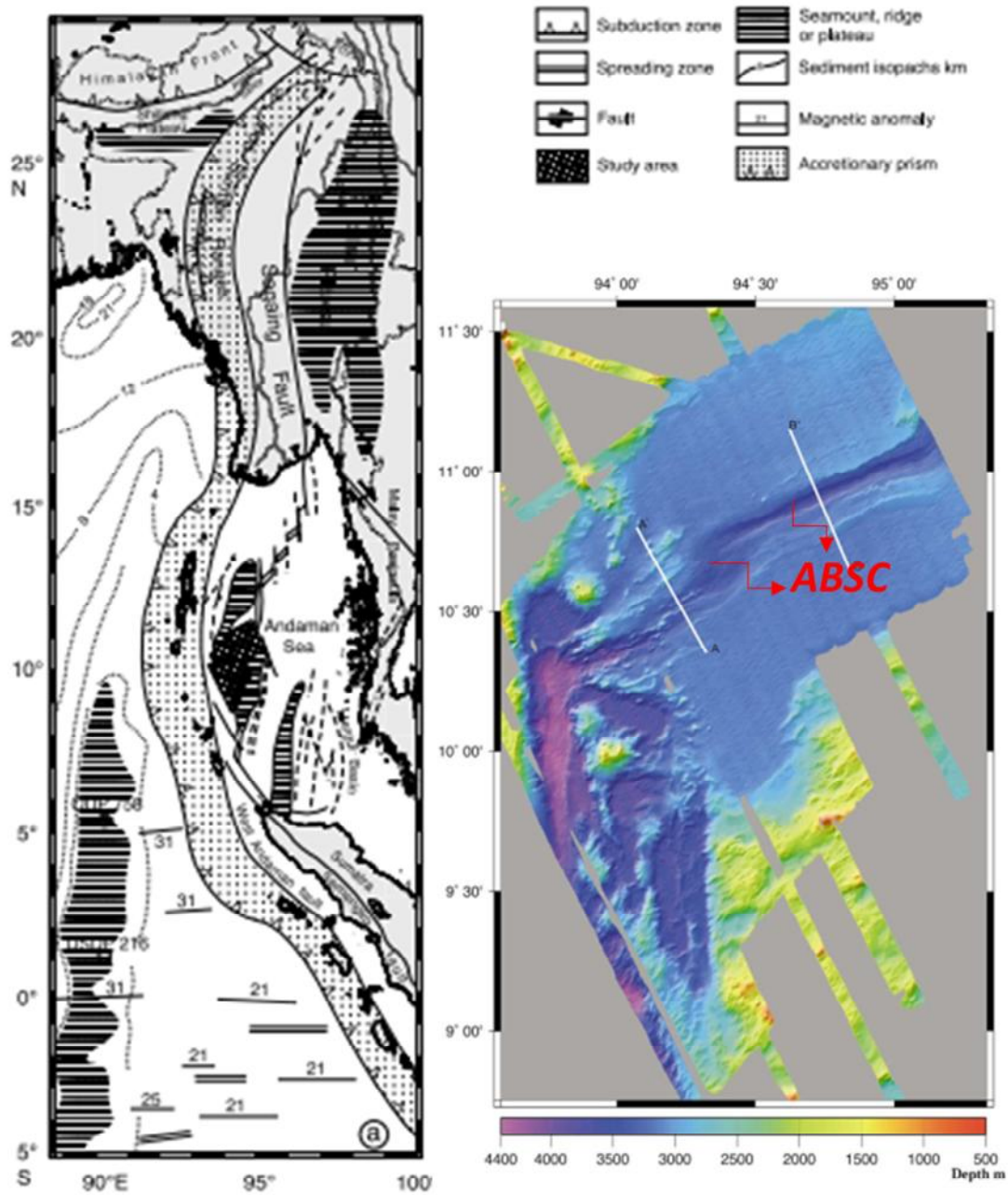


**Figure 1.3:** Morphological and geological structure of Andaman Sea and Myanmar, modified from Kamesh Raju et al, [2004]. ABSC-Andaman back-arc spreading center.

Irraw

addy. The Irrawaddy delta-shelf was found to accumulate about 90% of the sediment with the recent studies suggesting that these sediments were carried to deeper areas through canyons and gulf of Marthaban [Ramaswamy et al., 2004]. Colin et al, (2006) have studied a core retrieved from Sewell ridge complex of central basin for clay mineralogy, elemental

and Sr-Nd isotopes on carbonate free sediments for last 280ka. The small changes in isotopic data in their low resolution study made them to conclude that the source remained same throughout the record. The Nd isotopic data of this central basin core ( $\sim -10\epsilon_{Nd}$ ) closely resemble that of Irrawaddy sediment  $\epsilon_{Nd}$  value (-10.7) and have suggested that the river Irrawaddy remained as a major source for entire record. But, further studies on provenance of Irrawaddy sediment suggested heterogeneity in the Irrawaddy river watershed. *Allen et al*, (2008) for example have found an  $\epsilon_{Nd}$  isotopic value of -8 for Irrawaddy sediment. *Licht et al*, (2016) studied middle Irrawaddy sediments where river Chindwin joins Irrawaddy and found a large variation ( $\epsilon_{Nd}$  between -13.75 to +0.25) suggesting that the Irrawaddy has multiple source terrains and large local variability. *Licht* in another study [*Licht et al.*, 2013] shows how the central Myanmar basin (CMB) has evolved since early Cenozoic and suggested that the Irrawaddy watersheds flow through recent volcanic dykes, ophiolites, mud-volcanoes and flysch with basic, ultrabasic compositions like diorites, andesites, etc that provides high radiogenic (Nd) material. Whereas the Sino-Burman ranges (SBR) predominantly with older crustal material of Archean gneisses and granitic complexes may be responsible for low radiogenic (Nd) signal. The river Salween is originating in eastern Tibet and flows through the SBR (Fig. 1.2), whereas rivers Sittang and Tanintaryi originate from Shan plateau of SBR and western Thailand granitic complex respectively. The western Thailand granites are characterized by very low radiogenic Nd material with -25  $\epsilon_{Nd}$  [*Nakapadungrat et al.*, 1984] and the sediments carried by river Tanintaryi through this terrain to Mergui plateau has an  $\epsilon_{Nd}$  of -17 representing the lowest radiogenic Nd material supply to the Andaman basin [*Damodararao et al.*, 2016].

Despite the huge heterogeneity within Myanmar watersheds, a near similar  $\epsilon_{Nd}$  value of -10 for the entire 280ka [Colin *et al.*, 2006] of central Andaman sediment core is interesting and in the context of whether Irrawaddy remained a major sediment supplier even during glacials is to be assessed. Moreover, the neighbouring eastern Bay of Bengal (eBoB) was reported to have received high radiogenic Nd material during glacials than late Holocene [Stoll *et al.*, 2007; Tripathy *et al.*, 2011]. A reduction in SW monsoon and the sediment flux from mighty Ganges-Brahmaputra river systems during glacials was seen by Stoll *et al.*, (2007) as an effect of southward shifting of intertropical convergence zone (ITCZ). The increased presence of more radiogenic  $\epsilon_{Nd}$  in LGM sediments has been attributed to sediment supply from rivers in western Indo-Burman ranges, with high radiogenic values, flowing through Arakan coast to the eastern Bay of Bengal during glacials. A similar scenario of glacial to interglacial changes in isotopic signature can exist in the Andaman Sea. The domination of sand size among grain sizes (silt and clay) and presence of coral reefs of sediments in Andaman islands [Nobi *et al.*, 2010] limits the lithogenic supply to adjoining areas in the Andaman Sea. Two recent studies [Awasthi *et al.*, 2014; Ali *et al.*, 2015] from western Andaman Sea suggested a major sediment supply from Andaman archipelago with high radiogenic material. But the sediment supply from islands is unlikely as they are said to be bordered by coral reef systems since end of LGM [Awasthi *et al.*, 2014].

The pulses of Irrawaddy derived sediment were observed in a Sr-Nd isotopic study from distally located Bay of Bengal core SK157-14 [Ahmad *et al.*, 2005]. Though this core is located far away from the Irrawaddy river mouth, this ninety-east ridge sediment core clearly demonstrate the dominant role of Irrawaddy river in north-eastern Indian Ocean.

The fluctuations in  $\delta^{18}\text{O}$  of Globigerinoides sacculifer and clay mineral content were studied in a 250cm sediment core retrieved close to landfall island of north Andaman, about 200km away from Irrawaddy river mouth [Nagasundaram *et al.*, 2014] to reconstruct the intensity of SWM for the last 6.5 ka. High smectite content was interpreted to reflect the weathering product of mafic rocks from the islands in vicinity, whereas illite predominantly coming from Irrawaddy river. They identified coarser detritus during 6.5 to 5.4ka, strengthening of SWM and an overall weakening of SWM from ~6 to 2ka BP. The increased coarser detritus in this river mouth core during 6.5 to 5.4ka is attributed to increased SWM in Irrawaddy flood plains. This can alternately be due to other mechanism such as slumping or prevalence of high energy conditions. *Sijinkumar and Nath* have worked extensively [Sijinkumar *et al.*, 2010, 2011, 2015, 2016a, 2016b] on past monsoonal strength and interplay between SW monsoon and NE monsoon, past productivity signatures recorded in Andaman sedimentary records and relation with other records of Indian Ocean in a regional and global perspective. In another study of *Ahmad et al.*, (2000) on stable carbon and oxygen isotopes of the planktonic foraminifera (*G. ruber*) of a sediment core (GC-1) from Sewell ridge complex of central Andaman Sea, an increased pulse of  $\delta^{18}\text{O}$  during Younger Dryas cooling event and drastic reduction in fresh water influx were observed. The high  $\delta^{13}\text{C}$  values observed during isotopic stages 2 and 4 of glacial times were suggested to reflect enhanced productivity in the Andaman Sea.

*Kurian, Nath et al.*, (2008) have carried out a detailed geochemical study on sediments from the Andaman back-arc basin and highlighted the contrasting results compared to the previous studies viz.,

- 1) *Rodolfo (1969)* reported high smectite content for the deep Andaman Sea sediments, though the main fluvial source of sediments to the region has low smectite content (*Konta, 1985*).
- 2) Paleoclimatic reconstructions in the ABB were based on the assumption that the main source of sediments to the Andaman Sea is the Irrawaddy River (e.g. *Colin et al., 1999*). However, other sources are likely to play a role in the basinal sedimentation in view of its tectonic setting.
- 3) Backarc basins are known for hydrothermal mineralization. The ABB has a well-defined spreading axis (*Kamesh Raju et al., 2004*) and the possibility of hydrothermal signatures in the basin is reported by *Rao et al., (1996)*.

The close proximity of these cores to spreading centre enabled the possible sediment sources to the Andaman basin other than Myanmar river sediments. A detailed study on bulk, three selective leaches and residue gave a chance to explore the possible detrital, diagenetic and hydrothermal sources for Holocene sediments. Higher smectite in clay fraction, elemental ratios of trace elemental data and presence of volcanogenic glass in sand sized sediment fraction implies the supplies from local volcanic sources. Eu anomaly, Y/Ho ratio and the association of Mo with Pb, Zn and Cu in the HCl-insoluble residue suggests the presence of sulfidic material probably of hydrothermal origin. It is pertinent to mention that *Venkatesan et al., (2003)* have found biomarker lipids and suggested the role of thermal alteration of immature organic matter into hydrothermal petroleum.

The drilling carried out in the Andaman Sea for the National Gas Hydrates Programme has recovered cores of length of about 700 m and dates back to late Miocene [*Phillips et al., 2014*]. The site core had smectite likely derived from weathering of

volcanic rocks of the Andaman Islands and illite and chlorite likely derived from Irrawaddy River discharge with possible input from the Andaman Flysch. The site exhibits an overall decline in calcite from about 8Ma to 2.5Ma reflecting a local decrease in productivity since the Early Miocene. An increase in smectite compared to kaolinite at 8.5 Ma was attributed to the enhanced weathering of volcanic rock sources.

#### 1.4. Scientific rationale

The mighty Himalayas with an average altitude of ~5.5 km to the north of Indian Ocean provides a largest and unique monsoonal system. World's biggest river fan systems like Ganges and Indus were studied thoroughly to understand present and past sedimentary pathways and climatic control over it. Whereas the other major river systems like Irrawaddy and Salween were not studied fully. These Myanmar rivers that flow through eastern syntaxes of Himalayas and further Indo-Burman ranges (IBR) and Sino-Burman ranges (SBR) have a length of 2000 and 2800kms. These mountains consisting Tertiary and Cretaceous sedimentary formations [*Bender, 1983; Colin et al., 2006*] and Archean granitic terranes [*Mitchell et al., 2007; Licht et al., 2016*]. These Myanmar river systems Irrawaddy, Salween and small rivers like Sittang, Tanintaryi, Tavoy carry the terrigenous material and preserve in semi-locked and silled Andaman basin. The rivers Irrawaddy-Salween carries a sediment load equivalent to 57% of that carried by Ganges-Brahmaputra rivers [*Robinson et al, 2007*]. Despite this, the depocenters of these rivers are not as well as studied as the G-B derived fan systems. Further motivation is the lack of information on past climatic changes in the Myanmar watersheds. "Indian summer monsoon circulation can be characterized by mean tropospheric temperature (TT) gradient between ocean and land. Two major heat sources, one near the Myanmar Coast and the other near the Western

Ghats play seminal role in defining this TT gradient" [Kumar *et al.*, 2014]. While the climate change studies in Western Ghats influenced areas are relatively well known, the same is not the case in Myanmar area. Whether there was such a link between two major monsoon hot spots in the past is not known. The Andaman basin is the best place for studying such changes in climatically impacted geochemical/lithogenic sources. Few records are available for this area which are either close to Andaman islands [Awasthi *et al.*, 2014; Ali *et al.*, 2015] or at a single river mouth [Colin *et al.*, 2006], with one long record (280ka) available in central basin, which has missed the climatic impacts during the most important late Quaternary period because of the low age resolution of the study. Achyuthan *et al.*, (2014) studied a sedimentary core off landfall island of Andaman fore-arc basin of age spanning last ~6.5ka and overall warming and drying conditions were observed since 6.5ka with 4 to 3 ka being a period of increased chemical weathering. A recent sub-millennial 700 year record [Ota *et al.*, 2017] off Myanmar in the northern Andaman Sea has shown higher sedimentation rates after about AD 1600 which are attributed to higher ISM intensity. High resolution records of lithogenic sedimentation covering the last glacial, deglacial and present interglacial periods are nevertheless not available which can be useful in interpreting the climatic -erosion-weathering linkages in the Indo-Burman, Sino-Burman and Arakan areas. Relatively, high sedimentation rates in northeast Indian Ocean provides unique opportunity to study its archives, particularly during Holocene and the last deglaciation. Thus, a systematic study of lithogenic sedimentation using well dated sediment cores from the Andaman Sea is undertaken with the following specific objectives:

## 1.5. Objectives of the present study

1. To define the geochemical characteristics of lithogenic fraction of late Quaternary sediments of the Andaman Sea.
2. To study the provenance of Andaman Sea sediments and to understand the paleoweathering trends of the adjacent land mass.
3. To study the temporal variations of geochemical proxies in sediments with respect to last Glacial to Holocene climatic changes.
4. To understand the link between the depositional environment characters and the paleoclimatic and paleoceanographic changes.
5. To compare the paleoweathering and paleoerosion trends recorded in the Andaman Sea with the published records in other northern Indian Ocean records.

In order to accomplish the above objectives, 44 surface sediments from different topographic domains and three sediment cores (206 and 55 subsurface sediments for elemental and isotope geochemistry respectively) collected from different water depths (2064 – 2909m) in a north (11° 42'N) south (07° 42'N) transect were studied for lithogenic sedimentation using inorganic and isotope geochemical tracers to assess the spatial and temporal variability in sediment sources, lithogenic sedimentation and chemical weathering history of source areas during the late Quaternary period.

## CHAPTER 2

# Materials and Methods

The sediment samples used for the present investigation were collected from different types of tectonic settings and locations of the Andaman Sea. Elemental and radiogenic isotopic analyses were carried out on lithogenic fraction to identify the sources and to reconstruct past climatic and environmental conditions on the source areas of the sediments. All major, trace and rare earth elemental analyses were carried out at National Institute of Oceanography (CSIR-NIO), Goa and Sr-Nd-Hf isotopic analyses were carried at National Geophysical Research Institute (CSIR-NGRI), Hyderabad.

### **2.1. Surface sediments:**

Total 44 surface sediments collected from various tectonic settings varies from river mouths to volcanic arc were used for this study. The locations and water depths are furnished in Table 2.1 and displayed in Fig. 2.1. Surface sediments ( $n=7$ ) were collected off river mouths (Irrawaddy, Salween, Sittang of Myanmar and Rangat of middle Andaman island) to understand the nature of river sediment being transported to the adjoining shelf and the deep sea. Beach sediments collected at Corbyn's cove of southern Andaman island and Indira point of Nicobar archipelago of Andaman-Nicobar archipelago ( $n=2$ ) were also studied. This combined with the data on published beach sediments can help in ascertaining the control of islands on sedimentation in the western Andaman basin. Seven sediment samples were collected from western Andaman fault (WAF) which can represent arc derived material and 25 deep sea sediments were also studied. All surface samples were collected either by using van-veen grab or using the top 0-2cm of spade cores. The samples were collected during several expeditions of CSIR-NIO viz., the 33<sup>rd</sup>, 50<sup>th</sup> and 98<sup>th</sup> expeditions of *CRV Sindhu Sankalp* and 18<sup>th</sup> expedition of *ORV Sindhu Sadhana*. Except beach sediments, all sediments were in olive grey colour and texture ranges from sandy to clayey, while deep sea sediments are mostly of silty clay or clayey texture.

**Table 2.1:** Location and water depth details of surface sediments used in the present work.

Sr.No	Sample Name	Lat° N	Long° E	Water Depth (m)
1	SK175/Gr03	17.49	94.46	49
2	SK175/Gr38	15.4	95.23	18
3	SK175/Gr48	15.26	96.5	22
4	SK175/Gr52	15.01	97.25	28
5	SK168/SPC01	11.17	94.73	3047
6	SK168/SPC05	10.31	94.49	3132
7	RVS02/GC04	10.92	94.75	3618
8	SSK50/GC01	12.11	92.89	44
9	SSK50/GC02	11.52	92.82	608
10	SSK50/GC03A	10.76	93.11	1347
11	SSK50/SPC01	11.46	92.99	868
12	SSK50/SPC02	11.52	92.82	623
13	SSK50/SPC03	11.53	92.77	253
14	SSK50/SPC04R	12.05	92.87	54.2
15	SSK50/SPC04A	12.1	92.88	43.3
16	SSK33/Grab02	7.37	94.39	2557
17	SSD18/GC01	13.4	94.34	2137
18	SSD18/GC03	11.78	93.85	2181
19	SSD18/SPC02	12.4	94.27	1335
20	SSD18/SPC03	10.63	94.3	2880
21	SSD18/DR03	13.13	94.1	1664
22	SSD18/DR08	10.67	94.05	2618
23	SSD18/DR09	9.03	94.63	2000
24	SSD18/DR10	10	94.1	1321
25	SSK98/1/Gr-01	6.755	93.87	35.2
26	SSK98/1/GC-01	6.588	94.49	32
27	SSK98/1/Dr-06	6.911	94.59	1824
28	SSK98/1/Gr-07	12.78	94.19	63
29	Corbyn's cove beach	11.64	94.75	0.2
30	SSK98/2/SPC-01	12.29	93.84	724
31	SSK98/2/SPC-02	13.76	94.9	1122
32	SSK98/2/SPC-03	13.71	93.99	1397
33	SSK98/2/SPC-04	13.49	93.19	96
34	SSK98/2/SPC-06	12.49	93.08	85
35	SSK98/2/SPC-07	12.51	93.03	48
36	SSK98/2/SPC-08	12.45	92.97	30
37	SSK98/2/SPC-12	12.11	92.47	101
38	SSK98/2/SPC-13	12.1	92.36	158

**Table 2.1. continued...**

39	<b>SSK98/2/Gr-01</b>	12.12	92.26	515
40	<b>SSK98/2/Gr-04</b>	12.1	91.98	1604
41	<b>SSK98/2/Gr-05</b>	12.09	91.92	2030

## 2.2. Sediment cores:

Three sediment cores SK168/GC01 (hereafter SK168), AAS11/GC01 (hereafter AAS11) and RVS02/GC03 (hereafter RVS02) were collected by using a gravity corer having a coring capacity of 6m. The locations, lengths of the cores and water depths are furnished in Table 2.2 and displayed in Fig. 2.1. Although all three cores are from the deep sea, the core location of SK168 (~11°43' N) occupies northern part of the central basin, AAS11 (9° N) is from the central part of central basin and RVS02 (~7°43' N) covers southern basin and overall makes north to south transect geographically. As earlier studies suggested the major terrigenous material supply is from Myanmar river watersheds, these cores provide an ideal opportunity to study the variability in fluvial out flow spatially and temporally. Core SK168 was retrieved during 168<sup>th</sup> expedition of *ORV Sagar Kanya* (ship owned by Ministry of Earth Sciences, Government of India) from the Alcock ridge complex of central basin and recovered a length of 426cm. The core was sub sampled at a 2cm interval up to 52cm, 2-3cm interval from 52 to 200cm and at 5cm interval for rest of the core [Sijinkumar *et al.*, 2015]. The core comprises of three distinct sediment layers, dark yellowish brown coloured clays in the top 10 cm and olive grey sediments between 30cm to 420cm (bottom of the core), while the 20cm section of light olive grey sediments is sandwiched between these two layers. The sediments are extremely sticky and dominantly clayey in texture, containing tests of foraminifera. The downcore brown to grey colour transition is typical of hemipelagic sediments with an oxidized top.

The core AAS11 was collected from Sewell ridge complex of central basin during the 11<sup>th</sup> cruise of *RV AA Sidorenko* (Russian vessel chartered by CSIR-NIO), this core

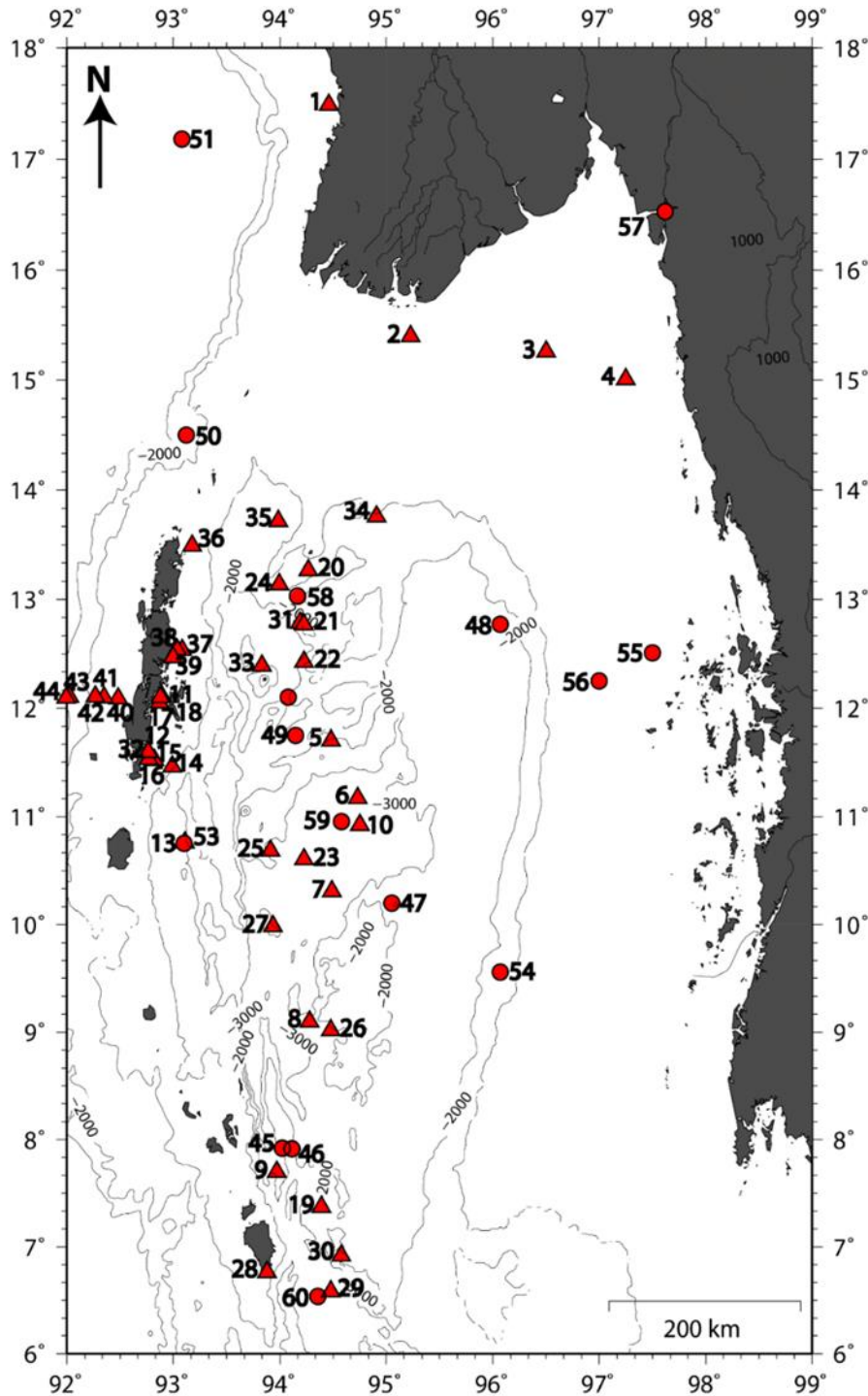


**Figure 2.1:** Location map of surface and core sediments studied here. Also plotted locations from the published literature in the area. The numbers are identification of each station, the details of these stations are found in Table 3.1.

was sub-sampled at 1cm interval in the top 20cm and 1-2cm alternatively from 20cm to 428cm. The core RVS02 was collected from southern Andaman basin during the Indian Ridge expedition on-board *RV Sonne* (German vessel chartered by CSIR-NIO), subsampled at 1cm interval in the top 100cm and 2cm interval for the rest of the core. A total 206 sub-sections (62 for SK168, 87 for AAS11 and 57 for RVS02) were selected for the elemental study, while 55 sub-sections (44 for SK168 and 11 for RVS02) for radiogenic isotopic analyses.

**Table 2.2:** Details of sediment cores used in the present work.

Sr. No	Core	Latitude (°N)	Longitude(°E)	Water depth(m)	Length in cm
1	SK168/GC01	11°42.463'	94°29.606'	2064	420
2	AAS11/GC01	9°00.00'	94°17.00'	2909	428
3	RVS02/GC03	07°42.501'	93°58.001'	2301	562

### 2.3. Age model and Chronostratigraphy of the Andaman Sea:

The law of superposition describes about the deposition of younger sediment on older sediments, thus gives chronological order of deposition and associated geological events if any occurred during its time of sediment deposition. Accurate dating of sedimentary sections obtained assumes importance to understand the sedimentation rates. In this present investigation both AMS radiocarbon dating of planktic foraminifera (Table 2.3) as well as oxygen isotope stratigraphy methods were employed. Combining and correlation of oxygen isotope stratigraphy gives more control on understanding the climatic events and also helps to know the lead and lag of events recorded in different sequences and regions. The three deep sea cores used for this study were well studied by Sijinkumar. A.V, and published in various articles [Sijinkumar *et al.*, 2010, 2011, 2015,

2016a,

2016b].

The

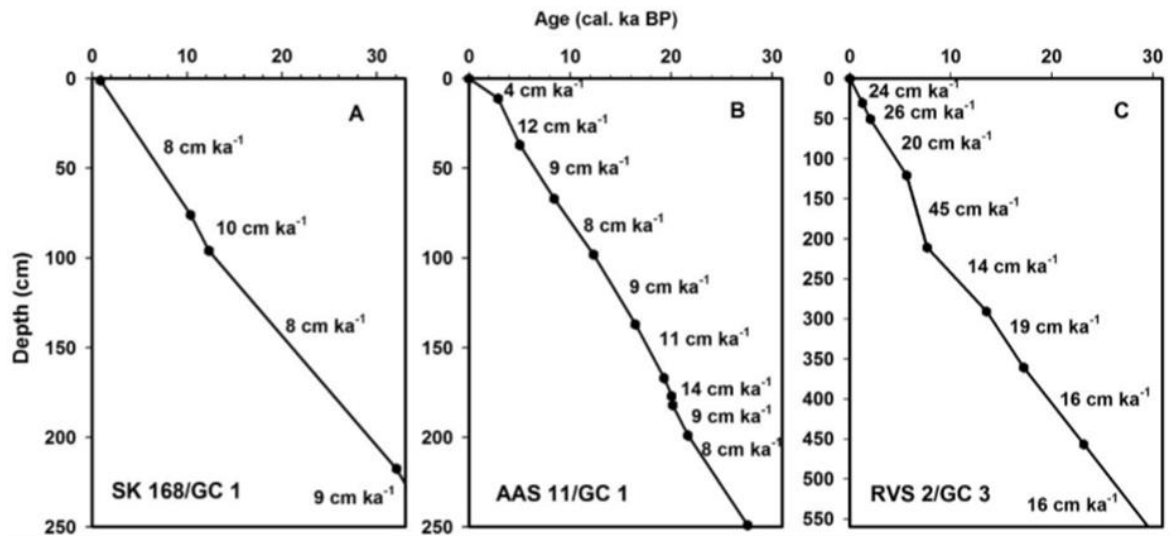


**Fig. 2.2a:** Age-depth model with sedimentation rates of a) northern core SK168; b) central core AAS11 and c) southern core RVS02, modified from Sijinkumar et al, [2015].

Accelerate Mass Spectrometer (AMS) <sup>14</sup>C dates of planktonic foraminiferal tests (mixed *G. ruber* and *G. sacculifer*) and calendar ages are presented in Table 2.3. In the present study, calendar age calibration was based on the CalPal 2007 programme [Weninger et al., 2007] for SK168 and AAS11 whereas, CALIB 5.0.2 program was used for RVS02 [Stuiver and Reimer, 1993].

**Table 2.3:** AMS  $^{14}\text{C}$  dates of foraminifera and calibrated ages of sediment samples for SK168, AAS11 and RVS02 [Sijinkumar et al., 2015].

Depth in core (cm)	Material	Radiocarbon age ( $^{14}\text{C}$ age in years)	Calendar age (Cal year BP)
<b>SK 168/GC01</b>			
0-2	Mixed Planktic foram	1440±30	883 ± 47
75-77	Mixed Planktic foram	9650±30	10361 ± 76
95-97	Mixed Planktic foram	10850±50	12321 ± 178
215-220	Mixed Planktic foram	27900±220	32055 ± 215
<b>AAS 11/GC01</b>			
10-12	Mixed Planktic foram	3085± 50	2807 ± 39
36-38	Mixed Planktic foram	4755± 35	4923 ± 45
66-68	Mixed Planktic foram	7995± 50	8406 ± 30
97-99	Mixed Planktic foram	10850± 70	12374 ± 185
136-138	Mixed Planktic foram	14245± 100	17070 ± 207
166-168	Mixed Planktic foram	16645± 120	19421 ± 334
176-178	Mixed Planktic foram	17310± 150	20154 ± 314
181-183	Mixed Planktic foram	17450± 130	20385 ± 387
198-200	Mixed Planktic foram	18700± 155	21969 ± 341
248-250	Mixed Planktic foram	23465± 260	27612 ± 480
<b>RVS 2/GC03</b>			
30-31	Mixed Planktic foram	1730± 30	1306 ± 14
50-51	Mixed Planktic foram	2430± 30	2059 ± 44
120-122	Mixed Planktic foram	5280± 30	5660 ± 38
210-212	Mixed Planktic foram	7190± 45	7676 ± 42
290-292	Mixed Planktic foram	12100± 50	13634 ± 127
360-362	Mixed Planktic foram	14800± 70	17588 ± 251
456-458	Mixed Planktic foram	19900± 90	23341 ± 340

Mixed Planktic foram (*Globigerinoides ruber* + *Globigerinoides sacculifer*)

## 2.4. Sedimentation rates in the Andaman Sea:

The accumulation of terrigenous materials in the ocean basins is generally controlled by climate and resultant strength of fluvial system or dominated geological agent. The rate of sedimentation varies with water depth and distance of land to the basin.

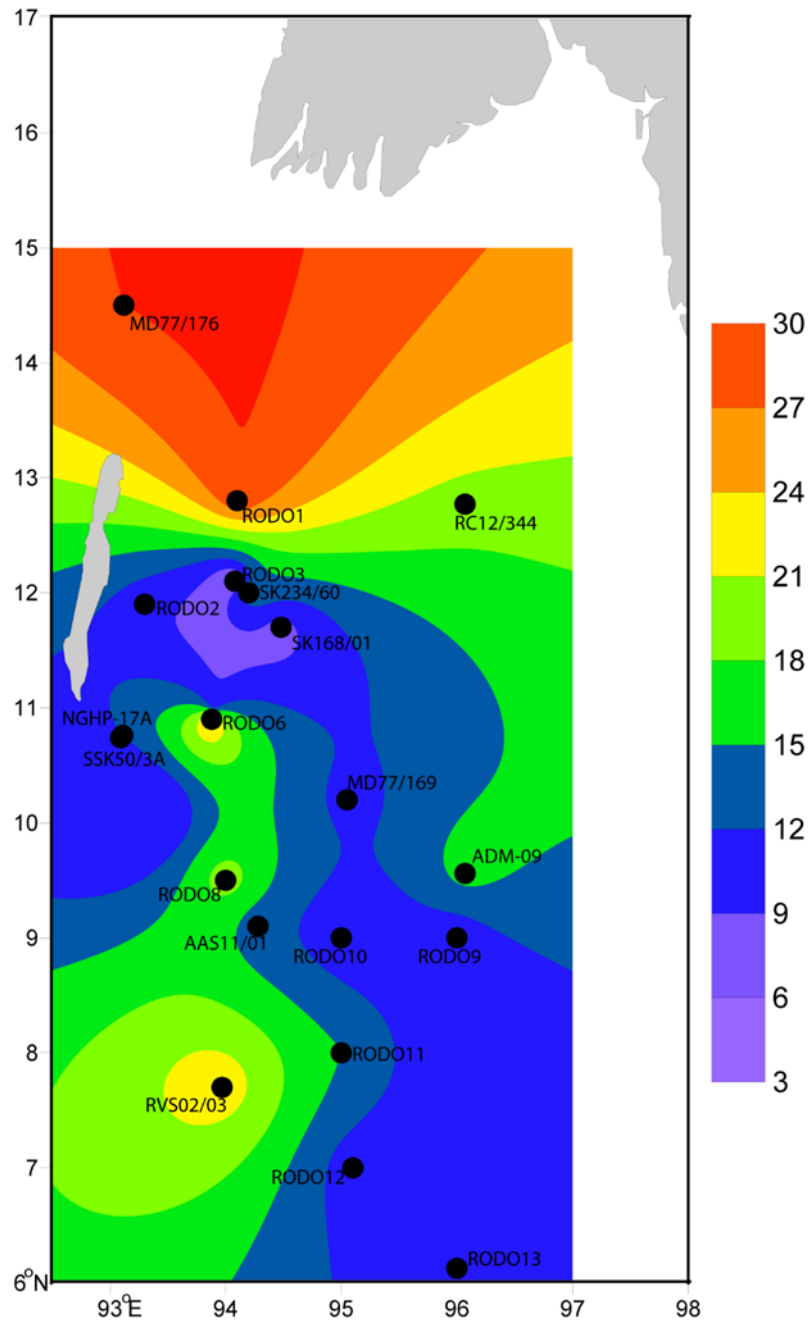


**Fig. 2.2b:** Sedimentation rates (cm/ka) of the Andaman Sea. RODO1 to 14 are from Rodolfo [1969] and details of other samples can be found in Table 3.1.

The accumulation of sediments on the seafloor is not evenly distributed and depends

basically on the bottom topography and hydrographical conditions. Andaman Sea topography is very irregular with seamounts and valleys [Rodolfo, 1969]. The changes in marine sedimentation rates provide preliminary clues about the past variation in fluvial erosion input, aeolian dust and the marine productivity [Prins *et al.*, 2000]. Linear sedimentation rate is also useful in estimating mass accumulation rates of the components at the seafloor. In core SK168, the average sedimentation rate was about 7.79cm/ka. The sedimentation rate was high during the Pleistocene to Holocene transition and low during the MIS 2/MIS 3 transition (Fig. 2.2a). In core AAS11, the linear extrapolation yielded an age of ~849yr BP at 2.5cm and age of 48.56ka at 427cm (Fig. 2.2b) and the average sedimentation rate was about 9.37cm/ ka. Core RVS02 has highest sedimentation rate with an average sedimentation rate of about 23.23cm/ka (Fig. 2.2c). The calculated sedimentation rates using the radiocarbon dates and depths at which various isotope stage boundaries are defined, isotope stage boundary timings, and the total thickness of the sediment represented by each isotope stage for SK168 are presented in Table 2.3 and Table 2.4.

Sedimentation rates in the Andaman basin of this study along with published literature are plotted in Fig 2.2b. The highest sedimentation rates (~30cm/ka) are found in the north, closer to the major terrigenous sediment sources of Myanmar rivers. Next in the order are the south-western and eastern Andaman basin areas with moderately high rates of deposition (~10-23 cm/ka). Entire central Andaman basin has intermediate sedimentation rates (~10cm/ka).

**Table 2.4:** *Thickness of sediments deposited during each MIS stages of three cores.*

Core Name	MIS 1	MIS 2	MIS 3
SK168/GC01	0-78cm	78-196cm	196-428cm
AAS11/GC01	0-82cm	82-239cm	239-426cm
RVS02/GC03	0-251cm	251-501cm	501-561cm

## 2.5. Elemental analyses:

Concentrations of major, trace and REE in the lithogenic fraction of the sediments were evaluated on 1N Hydrochloric (HCl) acid treated residue after removing the authigenic, biogenic and weakly bound exchangeable components. About 2g salt free, oven dried powdered samples were treated initially with 20ml 1N HCl for 4hrs, then with additional 15ml and agitated occasionally for every 30 minutes. Once the reactions ceased, the residues were washed thoroughly with MilliQ water four times, centrifuged and dried in an oven at 60°C.

**2.5.1. Leaching protocols:** Decarbonating the bulk sample: As the intention is to estimate the major alkalies which would have been contributed by lithogenous sources, calcium bound to carbonate was removed for extraction of lithogenic fraction by acid treatment.

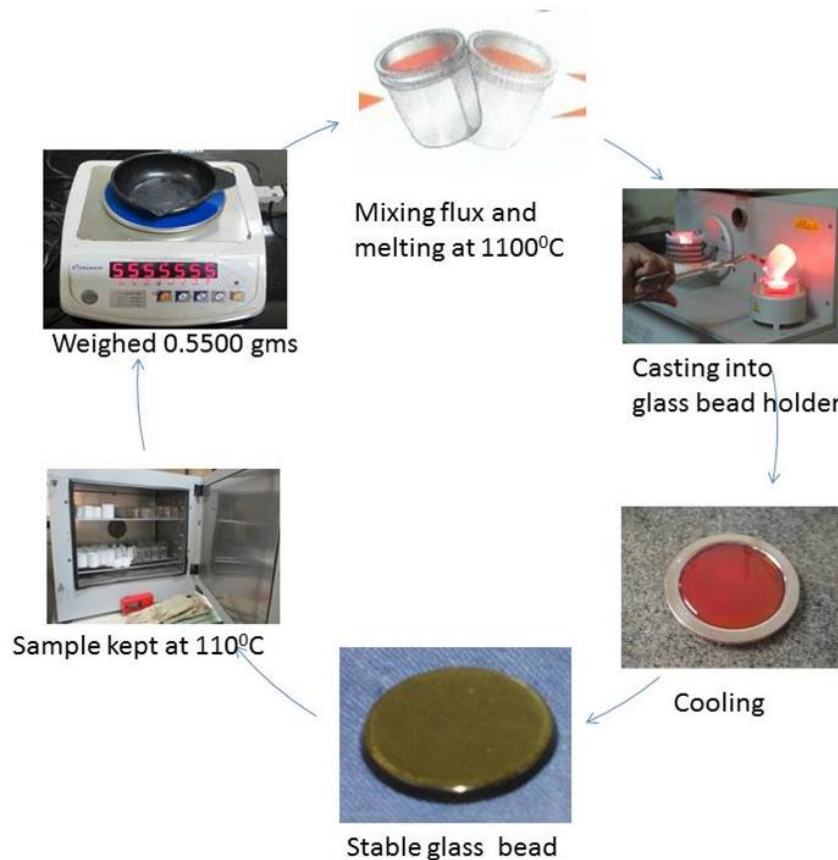


**Fig. 2.3:** Schematic representation steps involved during glass bead making procedure for sediment samples.

Here the sediments were decarbonated using ~25ml of 1 N HCl which was added to 8gms of wet/bulk samples. Samples were allowed to react with HCl. When the bubbling stopped, they were centrifuged and the residue was preserved by discarding the supernatant solution. Acid addition was repeated until the reaction has ceased. Samples were repeatedly washed with distilled water in order to remove the chlorides contributed by HCl and also sea salts. Thus, this step also allowed us to prepare the sediments free of seasalts allowing us to study Na bound to lithogenic fraction only. Later the HCl treated samples were dried at 60°C and grinded.

## **2.5.2. Measuring with XRF instrument:**

### **2.5.2.1. Procedure for making Glass Beads for XRF analyses:**

1. Taken ~ 1.2g of acid-treated sediment powder and kept in oven overnight at 110° C. [To remove moisture].
2. Weighed exactly 0.5500 gm. of sample powder.
3. Weighed 5.5000gm of flux Spectromelt A1000 of MERCK® (di-Lithium tetra-borate with Lithium bromide 0.07%) representing a sample to flux ratio of 1:10.
4. Sample and A1000 flux is mixed in the platinum crucible and placed in the bead making Minifuse-2 machine. After this, the pre-programmed method is run and the sample is fused/ melted with flux in the crucible using the furnace. Later on composite red hot melt is poured in casting dish and cooled into a glass bead which is ready for XRF analyses. This allowed complete homogenization.
5. Samples were analyzed for major rock forming oxides SiO<sub>2</sub>, Al<sub>2</sub>O<sub>3</sub>, TiO<sub>2</sub>, Fe<sub>2</sub>O<sub>3</sub>, MnO, CaO, Na<sub>2</sub>O, K<sub>2</sub>O, MgO and P<sub>2</sub>O<sub>5</sub>.

Major elements were measured on Wavelength-Dispersive X-ray Fluorescence (XRF-WD; Axios, PANanalytical, The Netherlands) at the National Institute of Oceanography (NIO), Goa. Geological Survey of Japan reference material, rhyolite powder-1 (JR-1) was analyzed simultaneously to monitor data quality. Accuracy and precision of the data are better than  $\pm 4\%$ . As the samples used were salt- and carbonate-free, Na and Ca values presented here represent those present in lithogenic fraction only and thus suitable for calculating the weathering index CIA.

**2.5.3. Analyses with ICP-MS:** For trace and REE analyses, 50mg of powdered samples was weighed into Teflon beakers and dissolved using a suprapure acid mixture of HF, HNO<sub>3</sub> and HClO<sub>4</sub> in a ratio of 7:3:1 on a hot plate. Following which, the digest was dissolved in 4 ml of 1:1 HNO<sub>3</sub> acid and made to 100ml final volume with Milli-Q water. Elemental concentrations were analyzed by Inductively Coupled Plasma Mass Spectrometer (Fig. 2.4) (ICP-MS, X-series2 of Thermo Fisher) at NIO, Goa, with Rh as internal standard. Along with the samples, geochemical reference standards of MAG-1, SCo-1, and AGV-1 were analyzed and the accuracy of trace and REE with reference to these standards was better than  $\pm 3\%$ .

## **2.6. Radiogenic isotopic analyses:**

### **2.6.1. Leaching protocols:**

**2.6.1.1. Extraction of lithogenic fraction for isotopic studies:** The inorganic lithogenic/aluminosilicate fraction was extracted from bulk sediment samples following a mild sequential leaching technique similar to that described by [Rutberg *et al.*, 2005]

and [Bayon *et al.*, 2002]. This chemical leaching ensures complete removal of biogenic calcium carbonate and authigenic Fe-Mn oxides in bulk sediments without altering clays.



**Fig. 2.4:** *Inductively Coupled Plasma Mass Spectrometer (ICP-MS) facility at CSIR-National Institute of Oceanography, Goa.*

All chemical procedures (leaching, digestions, chromatographic separations and purifications) were performed in over pressurized HEPA filtered laminar flow hoods/ clean benches at CSIR-National Geophysical Research Institute, Hyderabad. The reagents used for leaching purpose, glacial acetic acid (Optima, from Fisher scientific) and salts of hydroxylamine hydrochloride, sodium acetate (from Aldrich) were of high purity purchased commercially. Ultrapure acids of HF (~28M), HNO<sub>3</sub> (~14M) and HCl (~9M) used for chemical treatment of samples were prepared in house by sub-boiling distillation of reagent grade acids in quartz /Teflon stills. These ultrapure acids have very low blanks consistently less than a few pg/ml. Water with a resistivity of >18.2 MOhms from a Milli-Q system was used throughout for reagent preparation and cleaning of lab wares. Dilute

mineral acids necessary for the chromatography separation chemistry was prepared freshly for each batch of samples.

**2.6.1.2. Leaching of calcium carbonate:** Calcium carbonate was removed by leaching each sample for 2-3-hour periods with a 0.45 molar acetic acid leach solution. This leach solution was buffered to pH=5 with sodium acetate to dissolve the  $\text{CaCO}_3$  without attacking the clays. Following are the successive steps used for the removal of carbonate.

1. Weighed ~250-300mg oven dried bulk powdered sediment samples in an acid cleaned 50ml centrifuge Teflon tubes.
2. Added 10ml of buffered acetic acid very slowly to centrifuge tubes (2/3 capacity).
3. Used vortex mixer to disaggregate samples, placed in an ultrasonic bath for 2-3 hrs set at room temperature.
4. Agitated manually every 30 minutes.
5. Centrifuged at 1500 rpm for 10mts and poured the acetic acid with dissolved carbonate to waste.
6. Refilled the centrifuge tube with buffered acetic acid, disaggregated using vortex mixer, and placed in a sonic bath for 2-3 hrs.
7. Centrifuged again at 1500 rpm for 10mts and poured the acetic acid with dissolved carbonate to waste.
8. Repeated the leaching until all carbonate is removed, signs of which include:
  - a) Color of samples was uniform and dark-medium brown.
  - b) There was no  $\text{CO}_2$  gas pressure build-up during leaching.
  - c) No bubbles were found to form when tube was opened (except from shaking).

9) Rinsed the residue with Milli-Q about 3 to 4 times, used vortex mixer to agitate and centrifuge at high speed (2000 RPM) for 10 minutes to remove all acetate and discard the supernatant.

10) Dry the residues in an oven set at 80° to 100°C for a day or two and weigh the residue.

**2.6.1.3. Reductive leaching of Fe-Mn oxides in sediments:** To remove completely the Fe-Mn oxides in sediments, a strong leaching employing 1M HH/25% CH<sub>3</sub>COOH was followed.

1. Weighed ~200mg of carbonate free dried bulk sample and transferred to precleaned 15 ml PP Centrifuge Tubes (CT).
2. Added 10ml of the 1M HH solution, resulting in a reagent-to-solid sample ratio of 50ml: 1g.
3. Mixed the sample and the reagent with a vortex mixer
4. Placed the CT on a hotplate which was set at 90°C for 3hrs
5. Agitated manually every 30minutes
6. Removed from the hotplate and centrifuge at 3000RPM for 15minutes
7. Discarded the supernatant.
8. Added 4ml of MQ and agitated the CT with vortex mixer. Centrifuged and discarded the wash
9. Repeated step 7 three times with fresh aliquot of MQ, centrifuged and discarded the wash.
10. Dried the residue in an oven at 80° to 100°C for a day and it was reweighed. The difference in weight between the Centrifuge empty weight and the residue represents actual weight of the residue. This residue represents the carbonate-free and Fe-Mn oxide free terrigenous silicate fraction of the sediment and is referred as the pure detrital fraction of the sediment.

**2.6.1.4. Acid digestion of the detrital fraction for isotope analysis:**

1. Weighed and transferred ~100-140mg of sample detrital residue into an acid cleaned 15ml PFA savillex vials.
2. Added 3ml 48% sub-boiled HF and 1ml sub-boiled ~14N HNO<sub>3</sub>. This was swirled to take up all sample into a slurry. It was sonicated for one hour at room temperature.
3. The sample was dried on hot plate at ~150° C. This step is a rapid de-silicification step which generally proceeds with a vigorous evolution of SiF<sub>4</sub> as a volatile gas (open beaker HF attack) prior to sealing of samples in Parr vessels

**2.6.1.5. Dissolution (Parr vessels in oven):** Once dry, added 1ml conc HNO<sub>3</sub> to each vial and transferred the contents into the appropriate Parr vessel. Added 3ml conc. HF to each vial, swirled and again transferred into the Parr vessel.

4. Sealed the power bomb and placed in an oven at 180°C for 4 days.
5. Removed Parr vessels from oven and allowed them to cool overnight.
6. Next day, the Parr vessels were unsealed and transferred the contents to respective PFA vials.
7. Placed the vials on a hot plate at 120°C and dried the solution to a sample cake.
8. Added 1 ml of concentrated HNO<sub>3</sub> to sample, and again dried down to a dry sample cake.
9. Added 1ml concentration HCl to sample, capped, and swirled and dried. Added 6N HCl, capped and fluxed overnight on hot plate (100°C). At this stage, samples should be completely in solution. If the sample is not dissolved, then the solutions

are transferred to the appropriate Parr vessel, seal, and place in a 180°C oven overnight.

10. Following digestion and subsequent conversion to chlorides, all samples were taken up in 2.5N HCl for the chemical separation of Sr, Nd and Hf isotopes by ion exchange chromatography.

**2.6.1.6. Chemical Separation:** Primary separations of Hf, Sr and REE were performed in a Savillex teflon columns containing cation exchange resin (Bio-Rad® AG50W-X8, 200-400 µm mesh-size). Sample solutions were centrifuged prior to loading and the supernatant was loaded on the column. Hf with matrix was collected subsequent to three rinses with 2.5M HCl/0.1NHF. After washing out the cation matrix with 2.5M HCl including Rb, Sr was eluted in 2.5M HCl in a pre-cleaned 15ml PFA vial. REEs were then eluted using 6N HCl. The REE fraction was dried and the residue left overnight in 0.25N HCl. Nd was separated from REE and in particular from Sm on columns containing Teflon powder coated with HDEHP (di (2-ethylhexyl) ortho phosphoric acid. The primary Hf-cut was further processed to separate Hf, Zr and Ti from HFSEs in anion exchange columns (Bio-Rad® AG1-X8, 100-200µm mesh). Separation of Hf and Zr from Ti was accomplished on cation exchange columns in 2.5HCl/0.1NHF. Prior to mass spectrometry, the respective cuts of Nd, Hf and Sr sample concentrates were evaporated to dryness and re-dissolved in appropriate volume of 2% (v/v) HNO<sub>3</sub>; for Hf, a 2% HNO<sub>3</sub> with a trace of HF (0.1%) was preferred.

## 2.6.2. Analyses with MC-ICPMS:

**2.6.2.1. Mass Spectrometry:** Sr, Nd and Hf isotopic compositions were measured on a Nu Plasma HR multiple collector-inductively coupled plasma-mass spectrometer (MC-ICP-MS, Nu Instruments, Wrexham, UK) in static mode at National Geophysical Research Institute, Hyderabad (Fig. 2.5). This instrument is a double focusing mass spectrometer



**Fig. 2.5:** *Multi collector Inductively Coupled Plasma Mass Spectrometer (MC-ICPMS) facility at CSIR-National Geophysical Research Institute, Hyderabad.*

equipped with 12 faradays cups and three ion counters in a novel fixed collector configuration. Steering of the ion beams in to the collector array is achieved by means of a zoom lens which alters the dispersion of the mass spectrometer. At the beginning of each analytical session, Faraday cup amplifier gains were calibrated. Tuning of the instrument, gas flows, torch position and ion optics, was done to obtain maximum beam intensity. Peak shapes and coincidence were optimized with the automated Nu Instruments Quad lens routine. Hf, and Nd were measured in dry plasma mode using a Nu DSN-100 desolvating system and Sr analysis by direct nebulization, ‘wet plasma’.

Nd and Hf isotope measurements in samples were typically made at concentrations ranging from 50 to 100ng, whereas Sr was analyzed with an optimum concentration of

300-400ng. Analyses were bracketed with the similar concentrations of respective isotopic standards of SRM987 (Sr), JNdi (Nd) and JMC 475 (Hf). Mass bias corrections were made using  $^{88}\text{Sr}/^{86}\text{Sr} = 8.375209$ , and  $^{146}\text{Nd}/^{144}\text{Nd} = 0.7219$ . Typical sensitivities for all isotopes measured are ~100-250 V/ppm analyte for the DSN and 30 V/ppm analyte for the wet plasma. Typical on-peak backgrounds (instrument) are less than 1mV and are much less than 0.001% of the total signals intensities for the elements.

## CHAPTER 3

# Lithogenic sources to the Andaman Sea, northeastern Indian Ocean

### 3.1. Introduction:

Andaman Sea is a part of northeastern Indian Ocean and main depo-center of major Asian rivers drained through eastern syntaxes of Himalayan and Indo-Burman ranges (IBR), like Irrawaddy, Salween, Sittang and Tanintaryi that supplies more than 528mt/y of sediment load to the Indian Ocean. This is about 35% of sediment supply from Ganges-Brahmaputra river systems (excluding the sediments carried along the bottom). The work of terrigenous sources to the Andaman Sea by *Rodolfo* (1968) remains the first who has suggested that the northern Andaman Sea receives ~90% of its terrigenous material from Irrawaddy river alone [*Rodolfo*, 1968]. Based on Sr-Nd isotopes on surface sediments in Bay of Bengal and the Andaman Sea, *Colin et al.*, (1999) suggested Irrawaddy river is the major source to the entire Andaman basin since last 280ka. *Ramaswamy et al.*, (2004) suggested that the clock wise movement of summer (SW) monsoon currents distributes the Myanmar river sediments to entire basin through Marthaban shelf. Two recent studies [*Awasthi et al.*, 2014; *Ali et al.*, 2015] on western Andaman basin region has Andaman-Nicobar archipelago derived sediments and local volcanism derived sediments. But the lithogenic contribution of the arc (for example the Western Andaman Fault -WAF), as the same arc is in southern basin having numerous submarine volcanoes with varied petrological composition [*Kamesh Raju et al.*, 2012]. Geographically near north-south stretched Andaman and Nicobar archipelago separates the Andaman Sea from the Bay of Bengal in the northern Indian Ocean. *Kurian, Nath et al.*, (2008) have employed mineralogical and sediment geochemical (major, trace and REEs) studies of bulk as well as acid-treated residue and have identified multiple sediment sources to the Andaman back arc basin and for the first time reported a hydrothermal Mn component in sediments. While, pure Mn-rich hydrothermal oxides are reported from the volcanic arc system [*Kamesh Raju et al.*, 2012], venting systems such as those found on SW Pacific back-arc

basins are not reported yet. Two recent studies [*Cao et al.*, 2015; *Damodararao et al.*, 2016] shows the influence of Tanintaryi river material and Mergui shelf in the eastern side of the basin is another lithogenic sediment supplier in addition to Irrawaddy-Salween-Sittang derived lithogenic material in the north. Whereas the sediment transportation from Java Sea, south China Sea, gulf of Thailand through Malacca strait to southern Andaman basin is not fully known. Density flows are recognized as a major sediment transporting agents in this area [*Rodolfo*, 1968]. A study in and around Malacca Strait by *Keller and Richards*, (1967) show stiff clay overlies coarse sediment (sand), possibly due to the removal of fine fractions by intensified clock wise monsoonal currents in this southeast corner of the Andaman Sea. *Rodolfo*(1968) in his extensive sampling in this region also show the domination of coarse grained than fine grained sediments in Mergui Terrace and Malacca Strait, recognized as zone of non deposition further suggests the role of SW monsoon in sediment transport.

The Trans-Himalayan Batholith (THB) represents region of high radiogenic (Nd) material [*Galy and France-Lanord*, 2001] than Tethyan Sedimentary Series (TSS) and the Higher Himalayan Crystalline (HHC) region, probably due to the presence of hydrothermal deposits. The terranes of Myanmar watersheds are much more radiogenic than the central Himalaya probably due to complex tectonic evolution and the orogenic events mainly resulted by Sibumasu-IndoChina collision and Indian plate subduction under Sibumasu microplate. The off-scraping of underlain sediment of Indian plate gave rise to form Indo-Burman ranges (IBR) and Sibumasu-IndoChina collision gave rise to Sino-Burman ranges (SBR). Although Myanmar main land(central Myanmar basin CMB) consists of Archean-Proterozoic lithology, CMB is effectively controlled by debris of SBR from the east and IBR from the west. The presence of numerous volcanoes shows how the terranes were influenced by tectonic forces. This is represented by having very high radiogenic (Nd) than

neighboring Himalayas. The ranges of  $\epsilon_{Nd}$  of Myanmar watershed derived sediment varies between -8 and -12 [Colin *et al.*, 1999, 2006], though the southern Myanmar region has low radiogenic) material with  $\epsilon_{Nd}$  value of -26 may suggest the dominant influence of northern Myanmar watersheds compared to the sediment flux to open sea through Mergui

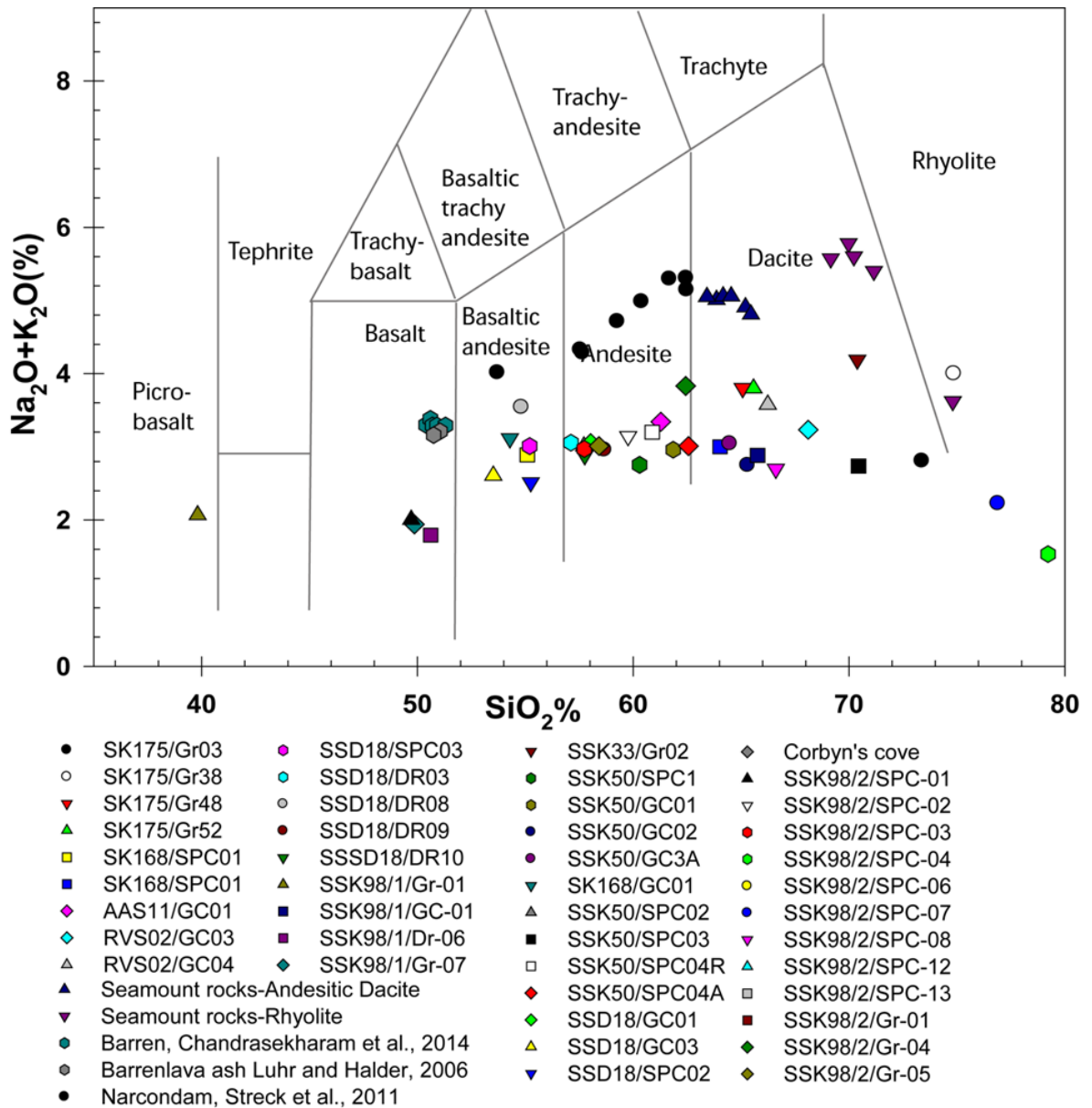


**Fig. 3.1a:** Total alkalies versus silica plot (TAS diagram) [Le Bas *et al.*, 1986] of all surface sediments along with seamount rocks of southern basin [Kamesh Raju *et al.*, 2012], rocks and ash of Barren and Narcondam islands of northern basin [Luhr and Halder, 2006; Chandrasekharam *et al.*, 2009; Streck *et al.*, 2011].

archipelago. In order to understand the relative contribution of these sources, an attempt is made to use another tracer viz., the hafnium isotopes in lithogenic fraction. The present

day lithogenic sources to the basin were deciphered using elemental and isotopic geochemical data of surface sediments from different geographic and geological domains.

### 3.2. Results:

Total 44 surface sediments and 206 subsections of three gravity cores along with 16 published records were used for this study (Fig. 2.1 and Table 3.1). The broad coverage of surface sediments provided detailed information about the imprints of geological reservoirs in and around the basin. On the other hand, the high resolution geochemical studies on three well dated cores provided a temporal control over sedimentary pathways since last 54ka of late Quaternary period. All 250 samples were extracted for lithogenic fraction and analyzed for major elements ( $\text{Al}_2\text{O}_3$ ,  $\text{SiO}_2$ ,  $\text{TiO}_2$ ,  $\text{Fe}_2\text{O}_3$ ,  $\text{MgO}$ ,  $\text{K}_2\text{O}$ ,  $\text{Na}_2\text{O}$ ,  $\text{CaO}$ ,  $\text{MnO}$ ,  $\text{P}_2\text{O}_5$ ) (Tables 3.2, 3.5, 3.6 and 3.7), 225 samples were analyzed for trace and rare earth elements (Li, Be, Sc, Ti, V, Cr, Mn, Co, Ni, Cu, Zn, Ga, Rb, Sr, Y, Zr, Nb, Mo, Cs, Ba, Hf, Ta, Pb, Bi, Th, U), rare earth elemental (La, Ce, Pr, Nd, Sm, Eu, Gd, Tb, Dy, Ho, Er, Tm, Yb, Lu) (Tables 3.3, 3.8, 3.9 and 3.10), 68 samples were analyzed for Sr-Nd isotopic studies ( $^{87}\text{Sr}/^{86}\text{Sr}$ ,  $^{143}\text{Nd}/^{144}\text{Nd}$ ) and 58 samples analyzed for Hf isotopic studies ( $^{176}\text{Hf}/^{177}\text{Hf}$ ) (Table 3.4, 3.11, 3.12). The lithogenic fraction was acquired after treating with 1N HCl for elemental analyses and sequential leaching procedure (buffered Acetic acid and hydroxylamine hydrochloride acid treatments) for isotopic analysis. The details of analytical protocols followed are described in Materials and Methods chapter (Chapter 2).

$\text{SiO}_2$  of surface sediments ranged between 39.8 and 78%,  $\text{CaO}$  ranged between 0.3 and 10.4%,  $\text{Al}_2\text{O}_3$  (3.6 and 20.9%),  $\text{Fe}_2\text{O}_3$  (1.1 and 21%),  $\text{MgO}$  (0.4 and 3.9%),  $\text{TiO}_2$  (0.4 and 1.1%),  $\text{K}_2\text{O}$  (0.3 and 2.9%),  $\text{Na}_2\text{O}$  (0.5 and 3%) and  $\text{P}_2\text{O}_5$  (0.1 and 0.9) with extreme values observed in beach sediments like 92%  $\text{SiO}_2$  in Corbyn's cove beach sediment, ~21%

$\text{Fe}_2\text{O}_3$  in Indira point sediment, ~10% CaO is observed in sediments from the proximity of Barren island and from the seamount chain in the south (Table 3.2). Similar high CaO is reported in Barren lavas, ash and scoria and Narcondam rocks (Table 3.2; *Luhr and Haldar, 2006; Chandrasekharam et al., 2009; Streck et al., 2011*). The down core major element

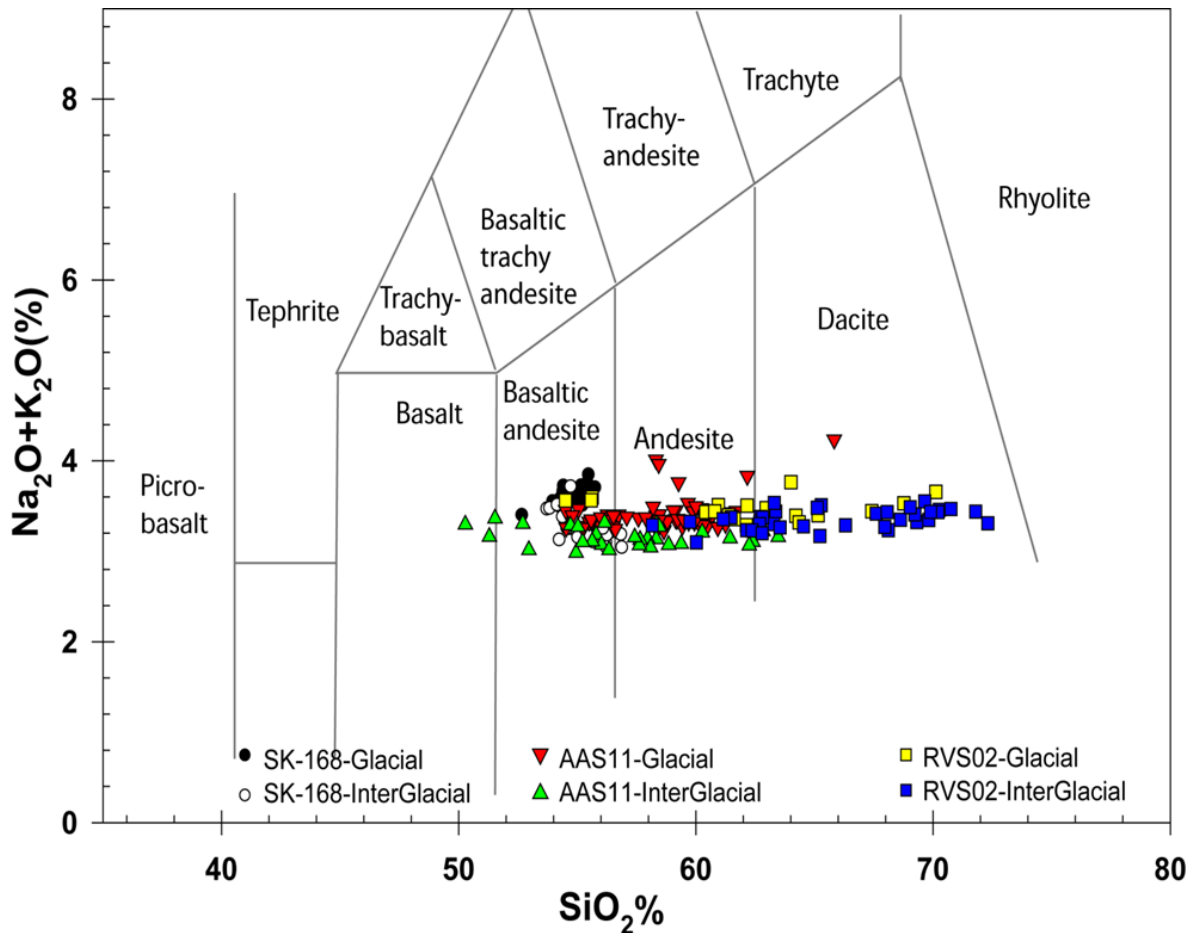


**Fig. 3.1b:** Total alkalis versus silica plot (TAS diagram) [Le Bas et al., 1986] of glacial and-interglacial sediments of all three sediment cores of this study. The sediments from southern location (RVS) plot distinctly away from northern cores on silica axis.

values like  $\text{SiO}_2$  ranged between 50.3 and 72.3%, and CaO ranged between 0.5 and 4.1% showing an increasing trend towards south (Fig. 3.2). In contrast,  $\text{Al}_2\text{O}_3$  (11.3 and 18.8%),  $\text{Fe}_2\text{O}_3$  (1.85 and 7.6%), MgO (0.71 and 2.8%) decrease towards south. N-S contrast is not well defined for other oxides  $\text{TiO}_2$ ,  $\text{K}_2\text{O}$ ,  $\text{Na}_2\text{O}$ ,  $\text{P}_2\text{O}_5$ . All the data in lithogenic fraction of sediments are plotted in geological discrimination plots in order to get an idea about source of these sediments. Primarily Total Alkalies-silica diagram [Le Bas et al., 1986] (Fig. 3.1a

and Fig. 3.1b) was used to identify the type of source rocks (alkalies can alter during the weathering), which broadly suggests that the Andaman basin received sediments from multiple sources that varies from basalt to dacite except few samples that are showing microbasalt with low silica or of rhyolite composition with high silica content (Fig. 3.1a).

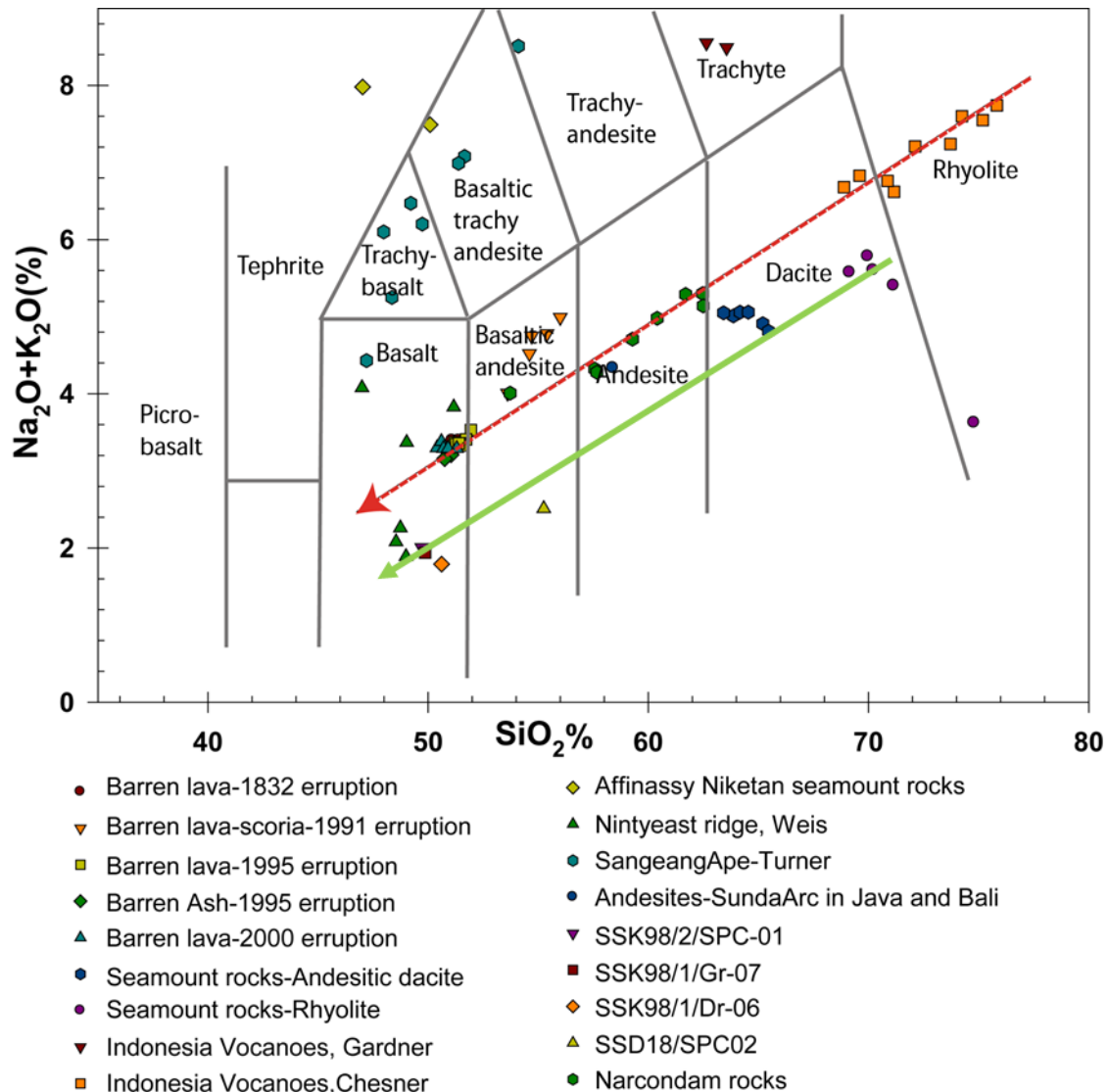


**Fig. 3.1c:** Total alkalis versus silica plot (TAS diagram) [Le Bas et al., 1986] of sediments collected in and around Barren and Narcondam islands and seamounts of southern Andaman basin – Western Andaman Fault (this study) along with rocks and ash of Barren and Narcondam [Lühr and Haldar, 2006; Chandrasekharam et al., 2009; J.Streck et al., 2011], various Indonesian volcanoes [Chesner and Rose, 1991; Turner et al., 2003; Gardner et al., 2013], plume derived nintyeast ridge [Weis and Frey, 1996] and Afanasiy Niketan seamounts [Mahoney et al., 1996]. The decrease in alkalies and silica content is observed (red arrow) from Indonesian volcanoes to Barren and Narcondam island material. The similar trend is observed in southern Andaman rocks [Kamesh Raju et al, 2012] and sediments of the present study with decrease in alkalies (green arrow) content and constant silica content.

The

chemistry data of rocks from the seamount [Kamesh Raju *et al.*, 2012] are also used in this study and plotted along with sediments of the present study (Fig. 3.1a). While both these sample sets have near similar silica values, sediments have lower alkalis compared to the seamount rocks. The downcore geochemical data of gravity cores are plotted separately (Fig. 3.1b) which show a composition varying from basalt to dacite composition. Among

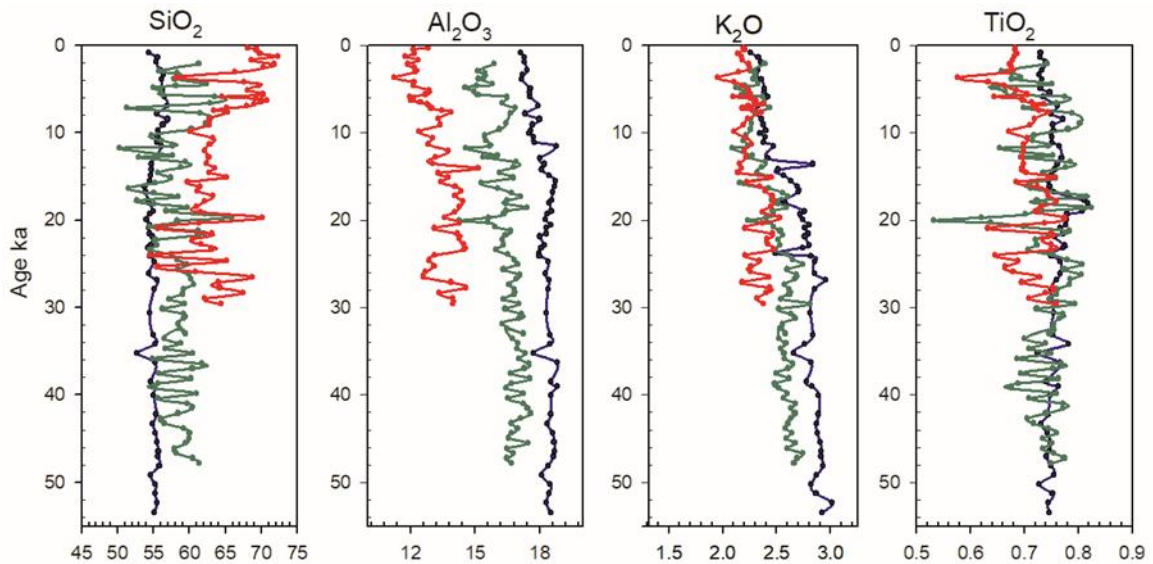


**Fig. 3.2:** The downcore variation of major elemental composition with age for the 3 sediment cores studied here. Compositionally, the southern core (RVS) is different from the northern cores.

the three cores, the northern area (represented by #SK168) received sediments from near similar source ‘basaltic andesite’ during both climatic periods. In contrast, the central and the southern cores have shown a large variability in silica content with time. The silica spread/variability (Fig. 3.1b) is large in the southern core (RVS-02) than that in central core AAS11. In the central core andesitic type of material deposited in general but the site has witnessed the deposition of basaltic type of material during interglacials. The  $\text{SiO}_2\%$  of Andaman sediments shows increased content both in surface sediments (Fig. 3.1a) and the cores (Fig. 3.1b) when moving to southward suggests reduced mafic material contribution towards south. Downcore plots of the cores (Fig. 3.2a) show reduced silica content and increased alumina content (Fig. 3.2b) with Ti and K remaining same (Fig. 3.2c and 3.2d) in the N-S transect suggests geographical variation in lithology of sediments that is supplied

to the Andaman basin. The central core AAS11 exhibits a relatively larger variation (Fig. 3.1b) than northern core SK168, with high silica during glacials and low silica during interglacials, the higher glacial values more closer to those in the southern core (RVS02).

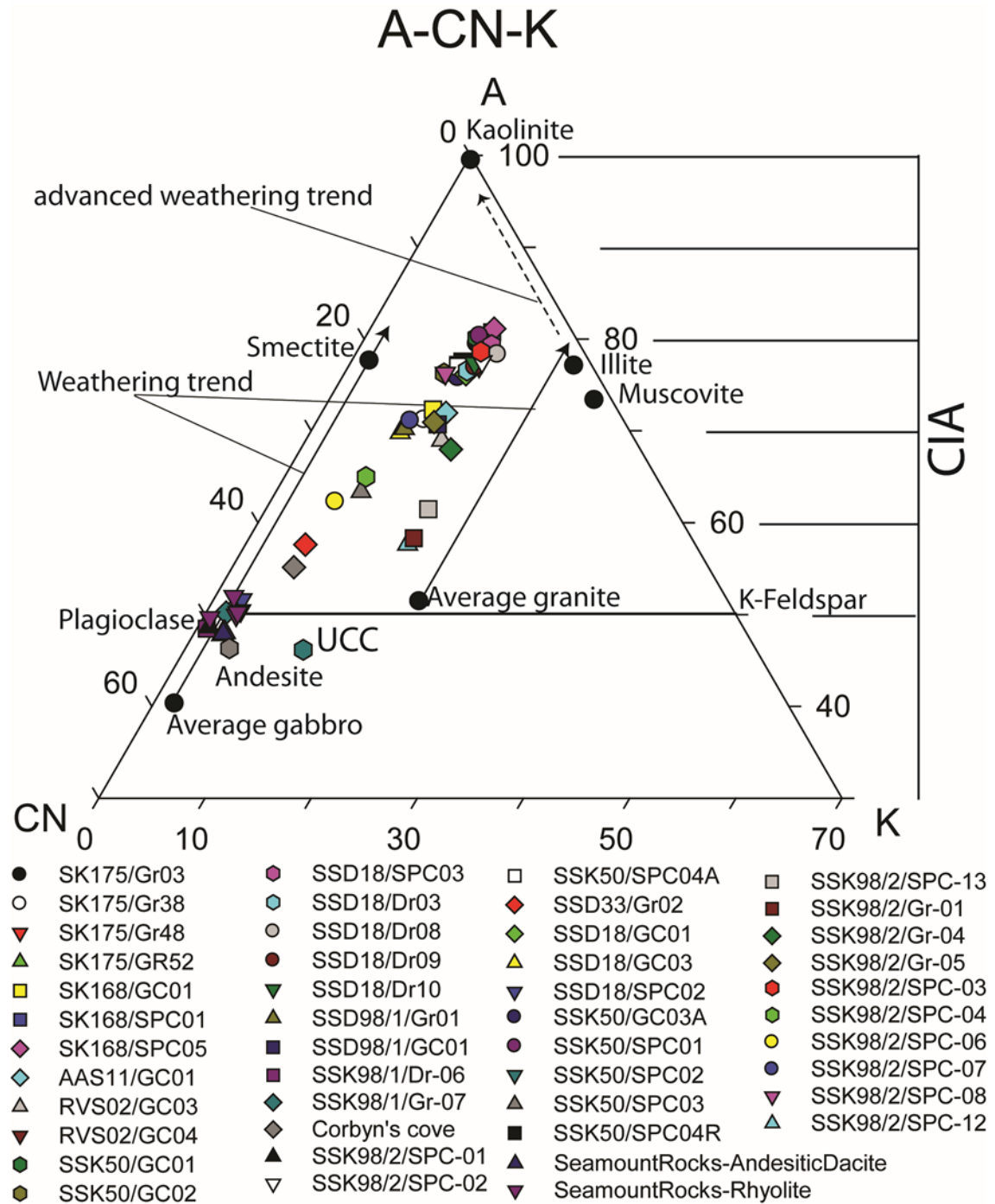


**Figure 3.3a:** A-CN-K diagram of all surface sediments studied for this work along with seamount rocks of southern Andaman basin. Most of the sediment samples fall in between weathering trends of granite-illite and gabbro-smectite suggesting their mixed nature. Some points fall close to average andesite values.

But the northern core (SK168) shows near similar composition in both glacial-interglacial

periods, implies the northern Andaman Sea had predominant supply from intermediate (felsic to mafic) sources. Whereas southern core (RVS02) shows a gradual rise in silica and a fall in alumina, titanium and potassium content (Fig. 3.2a) at ~9ka when the sedimentation in the core has rapidly increased from 14 to 45 cm/ka. Increase in the sedimentation rates possibly suggests an increased run-off during early Holocene. A gradual fall in the titanium content in southern and central cores during the early Holocene may probably indicating an increased terrigenous material from acidic type of sources. The

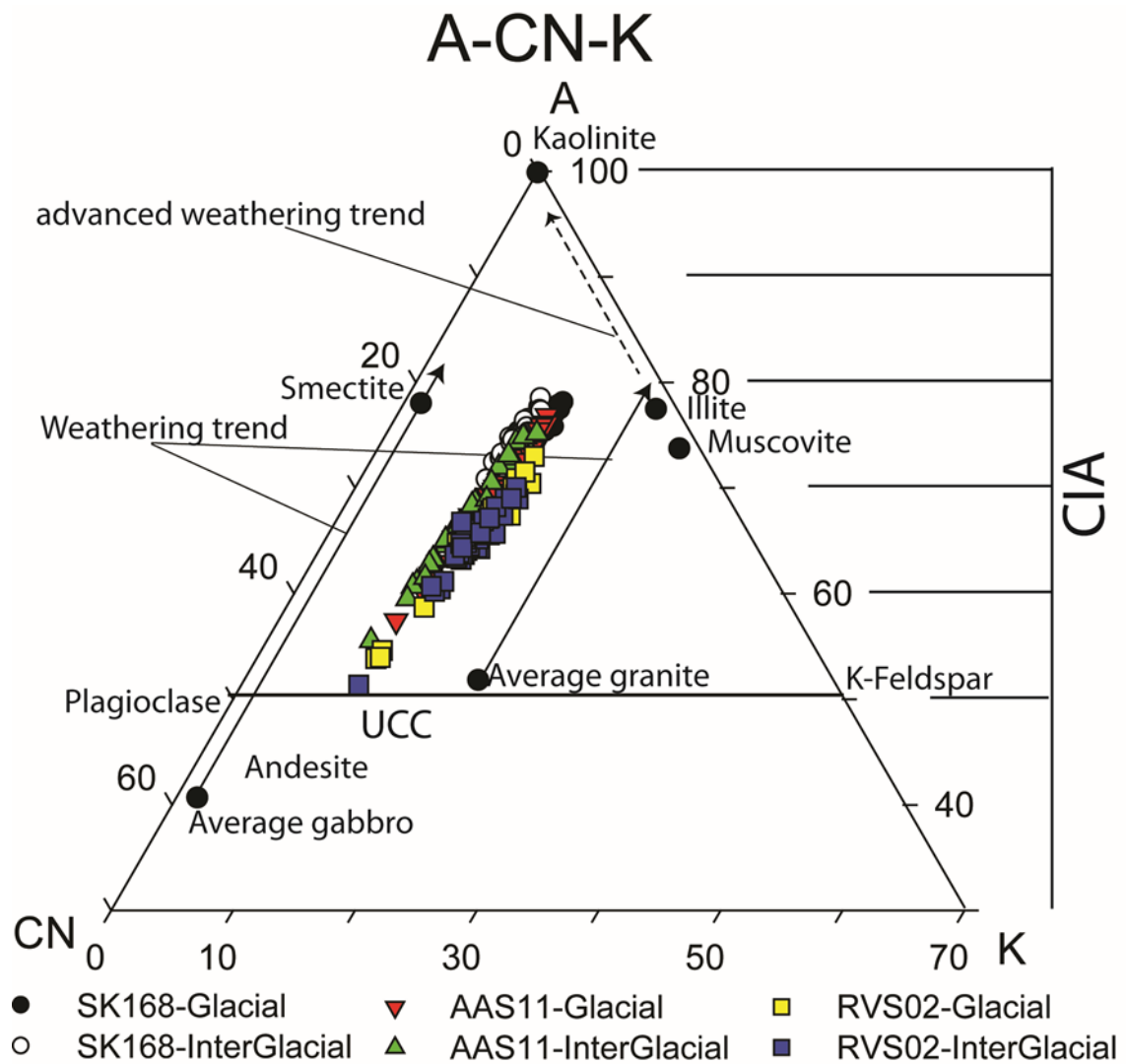


**Figure 3.3b:** A-CN-K diagram of all subsections of three sediment cores. Glacial and interglacial sediments are plotted with a different symbol. Subtle differences are seen these two sets of sediments. The differences are relatively more visible in two northern stations.

major lithogenic source has been earlier suggested as Irrawaddy River initially by

[Rodolfo, 1969] and followed by several researchers [Colin et al., 1999, 2006; Awasthi et al., 2014; Ali et al., 2015; Cao et al., 2015] but new data shows, increasing silica and decreasing aluminum content while moving away from Irrawaddy mouth suggesting possible additional sources to the Andaman Sea, likely through Great channel or Malacca strait.

Triangular plots A-CN-K (Fig. 3.3a and 3.3b), A-CNK-FM (Fig. 3.4a and 3.4b) [Nesbitt et al., 1980] and La-Th-Sc (Fig. 3.5a and 3.5b) [Bhatia and Crook, 1986] were also employed to assess the source of the sediments. The molar proportions were used to make

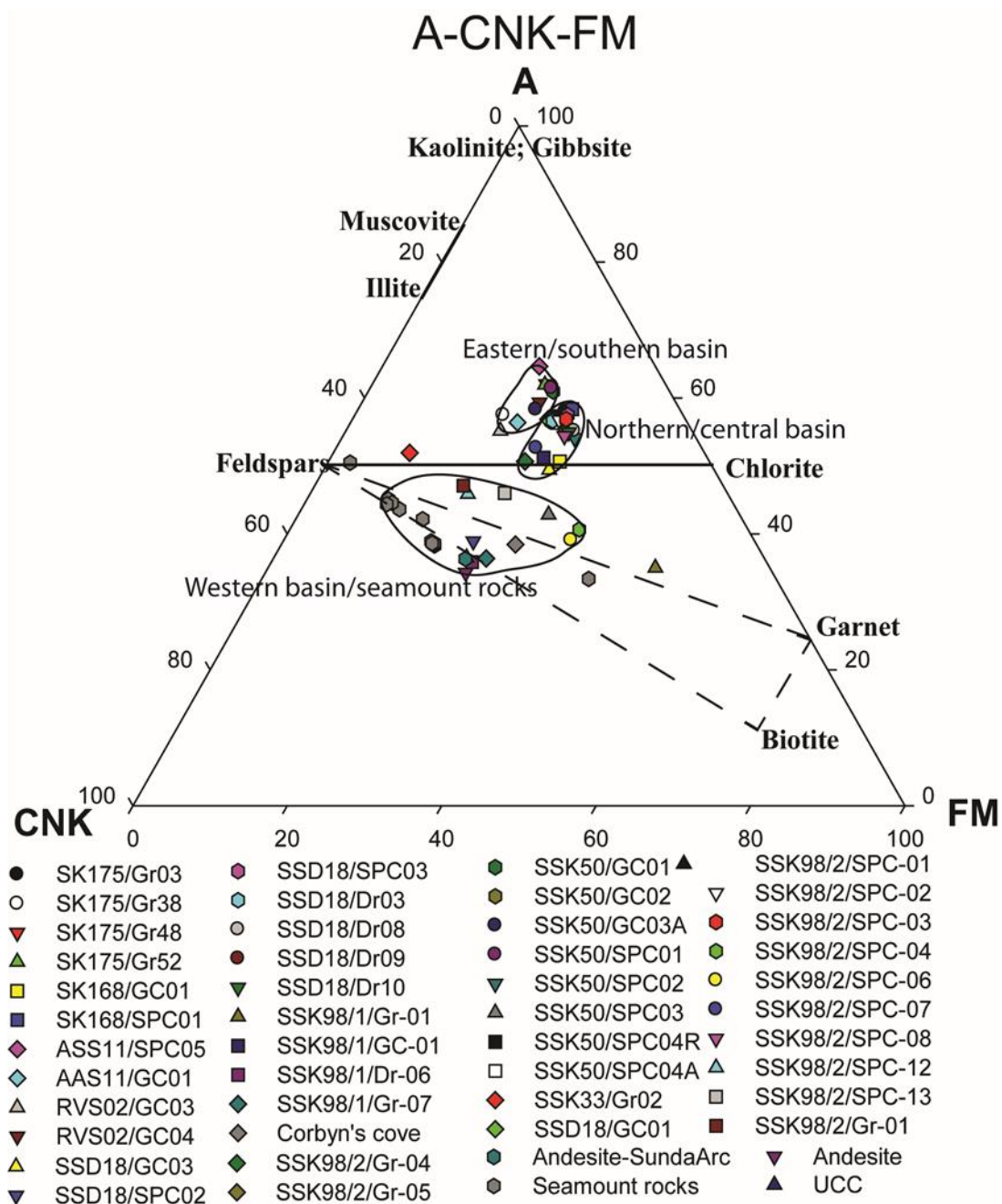


**Figure 3.4a:** A-CNK-FM diagram of surface sediments of this study along with southern basin rocks. Clear geographic differences are seen within the Andaman Sea.

these triangular plots; all three plots show the Andaman basin received sediments from various sources. A clear cut demarcation is seen in A-CN-K discriminative plot for surface sediments (Fig. 3.3a), with major population from the central basin falling in between weathering trends of granite and gabbro/andesite, while few samples from the western basin fall in a trend towards gabbro, suggesting the source of Andaman-Nicobar archipelago having mafic/basic composition to the western part of basin. Few other samples from eastern and southern basin trend towards the composition of average granite implying the dominant supply from felsic sources. The downcore values in A-CN-K plot (Fig. 3.3b) fall in near linear array between weathering trends of granite and gabbro with glacial sediments falling closer to granite trend and those deposited during interglacials plot closer to gabbro. The observations on TAS (Fig. 3.1b) is further supported in this A-CN-K plot. Another ternary plot A-CNK-FM (to represent mafics) of surface sediments (Fig. 3.4a) and downcore records (Fig. 3.4b) shows that the northern basin sediments fall closer to chlorite composition where as those from southern basin are closer to illite and muscovite compositional space. This indicates the type of source rocks from which these sediments are derived, chlorite being the weathering product of gabbro of mafic material, while illite and muscovite being the weathering products of felsic minerals. Those samples that have shown basaltic or picobasaltic nature in TAS diagram (Fig. 3.1a) fall in biotite-feldspar trend in A-CNK-FM diagram and close to the location of seamount rocks (Fig. 3.4a), indicates that this set of samples are derived from arc type of material, probably from the WAF.

The trace and REE data of surface and downcore sediments is presented in Tables 3.3, 3.8, 3.9 and 3.10. The similar downcore trends of specific trace elements and the major elements with respect to climatic changes clearly shows the role of climate on trace element data too. All the sediments were plotted in La-Th-Sc ternary plot to see which type

of arc they belong to, as the sediments are from back arc basin (Fig. 3.5a and 3.5b). A set of samples including central Andaman basin sediments and those derived from eastern Myanmar (through Salween, Sittang and Tanintaryi rivers) plot in continental island arc space, while other sediments collected close to Andaman-Nicobar archipelago and

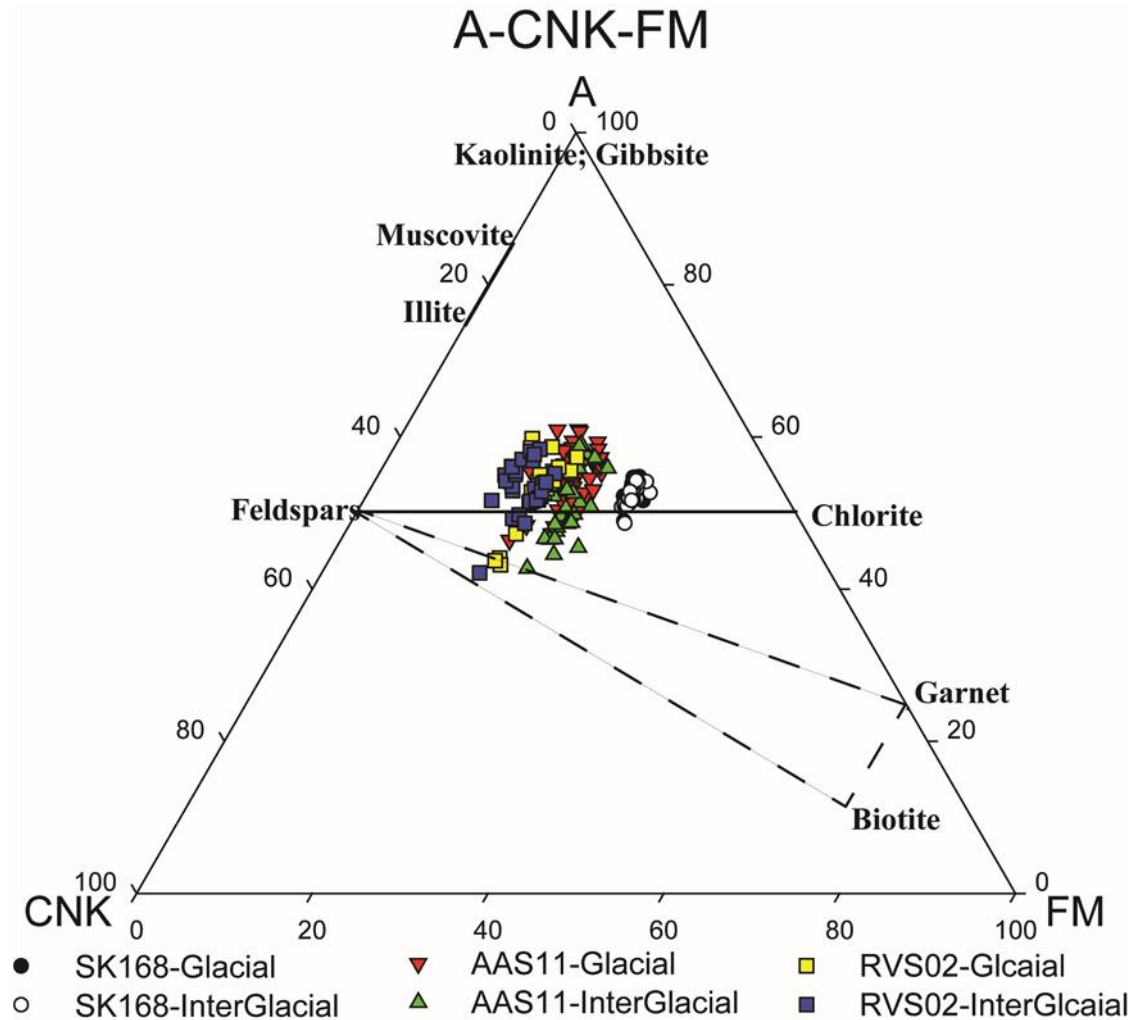


**Figure 3.4b:** A-CNK-FM diagram of subsurface sediments of 3 sediment cores. Glacial and interglacial sediments are plotted with a different symbol. Temporal and spatial changes in composition are seen.

Irrawaddy-Arakan shelves does not fall in any of the discriminative spaces, but plot in an area sandwiched between continental island arc and the active/passive continental margin fields. The downcore data of all the 3 cores fall within continental island arc space with the data of northern sediment core plotting towards oceanic island arc (Fig. 3.5b). The data of southern core fall distinctly away with more affinity to continental margin signatures (Fig.

3.5b). The downcore profiles clearly reflect increasing Th/Yb ratios from north to south core (Fig 3.6d), suggesting that the northern basin received more basic composition than other locations of the Andaman basin.

Fractionation indices such as total REE( $\Sigma$ REE), PAAS (Post-Archaean Australian Shale)[Taylor and McLennan, 1985] normalized La/Yb were calculated to decipher the changes in source material which could be influenced by change in river course, onset/offset of a particular source with past climatic changes. The close resemblance in total REE of three cores represents that the source area for entire record remained same individually for all the cores. Down core  $\Sigma$ REE varied between 78-144ppm in core SK168 (Fig. 3.6a) and displayed a cyclic pattern whereas the  $\Sigma$ REE in central core (AAS11) showed a narrow range of 70 to 90ppm except some samples at 28ka and the southern core (RVS02) showing a range of 80 to 140 ppm by displaying similar to SK168 (Fig. 3.6a). The southern core (RVS02) show higher(La/Yb)<sub>n</sub> ratios throughout the record indicates the supply from felsic sources. These results are consistent with the downcore major element data (high silica and low alumina content) and other plots discussed above, and suggests that the southern basin receives more material of felsic nature. The ratios Th/Yb and Ni/Co (Fig. 3.6c and 3.6d) in lithogenic fraction have been calculated to understand the source variations of different geologic reservoirs that help to check any oceanic crust/mantle material input to the study area. Th, Yb both enriched in continental rocks than mantle and oceanic crust and Ni, Co are enriched in ultrabasic and basic composition rocks [Turekian and Wedepohl, 1961]. The down core variation of Ni/Co in three cores (Fig. 3.6c) show similar pattern but southern core (RVS02) show low values during 20–8ka. The Th/Yb ratio can indicate the juvenile input to the marine sediments. A recent study on a sediment core (SK234-60) recovered near the Barren volcano of western AS [Awasthi et al., 2014]shows repeated episodes of juvenile input to core, but the present study of northern

and central cores of central basin (Fig. 3.6d) shows no remarkable input of juvenile material throughout the 54ka period. The absence of such kinks Th/Yb in southern core which is retrieved from Nicobar swarm region suggests neither Myanmar river watersheds nor Andaman-Nicobar archipelago are responsible for the kinks in SK234 core but most likely Barren volcanism, thus suggests the limitation of volcanic material of Barren island. The absence of such episodes of Th/Yb either in northern core SK168 or central core AAS11 further suggests the influence of barren volcanism is very less on sediments of the basin.

The  $^{87}\text{Sr}/^{86}\text{Sr}$ ,  $\epsilon_{\text{Nd}}$  and  $\epsilon_{\text{Hf}}$  values (Table 3.4) of surface sediments ranges from 0.714435 to 0.724732, -7.6 to -11.9 (Fig. 3.7b) and 0.25 to -9.96 (Fig. 3.8) respectively except one sample (SSK33/Gr02) that showed lowest radiogenic Sr isotopic value 0.705472 and highest radiogenic Nd and Hf isotopic values ( $\epsilon_{\text{Nd}} +3.94$  and  $\epsilon_{\text{Hf}}+13.51$  respectively) among samples of this study. Sr-Nd-Hf isotopes were analyzed in northern (SK168) and Sr-Nd isotopes on southern (RVS02) cores of the transect (Table 3.11 and 3.12). This isotopic work has substantiated the observations made from major, trace and rare earth elemental studies in order to understand chemical weathering and provenance changes which recorded in the study area. Marine sediments particularly in areas with complex tectonic domains such as in the Andaman Sea, isotopic data will help in deciphering multiple sources and to quantify the relative contribution from each of these sources. The  $^{87}\text{Sr}/^{86}\text{Sr}$ ,  $\epsilon_{\text{Nd}}$  and  $\epsilon_{\text{Hf}}$  values of SK168 range from 0.71414 to 0.72438, -9.24 to -11.24 (Fig. 3.7b) and -3.98 to +0.2 respectively (Fig. 3.8). The  $^{87}\text{Sr}/^{86}\text{Sr}$  and  $\epsilon_{\text{Nd}}$  of RVS02 core ranges from 0.721987 to 0.729454 and -12.7 to -10.9 respectively (Fig. 3.7b). All Andaman sediments (both surface and gravity core values) fall in Higher Himalayan sedimentary series in northern Indian Ocean Sr-Nd space (Fig. 3.7a), except one surface

sediment SSK33/Gr02. The sample SSK33/Gr02 falls in field defining ninetyeast ridge, Indonesian arc together with rocks-ash of Barren island [Awasthi *et al.*, 2010] as well andesite-diorite of Indo-Burman ranges [Mitchell *et al.*, 2012]. The close association of

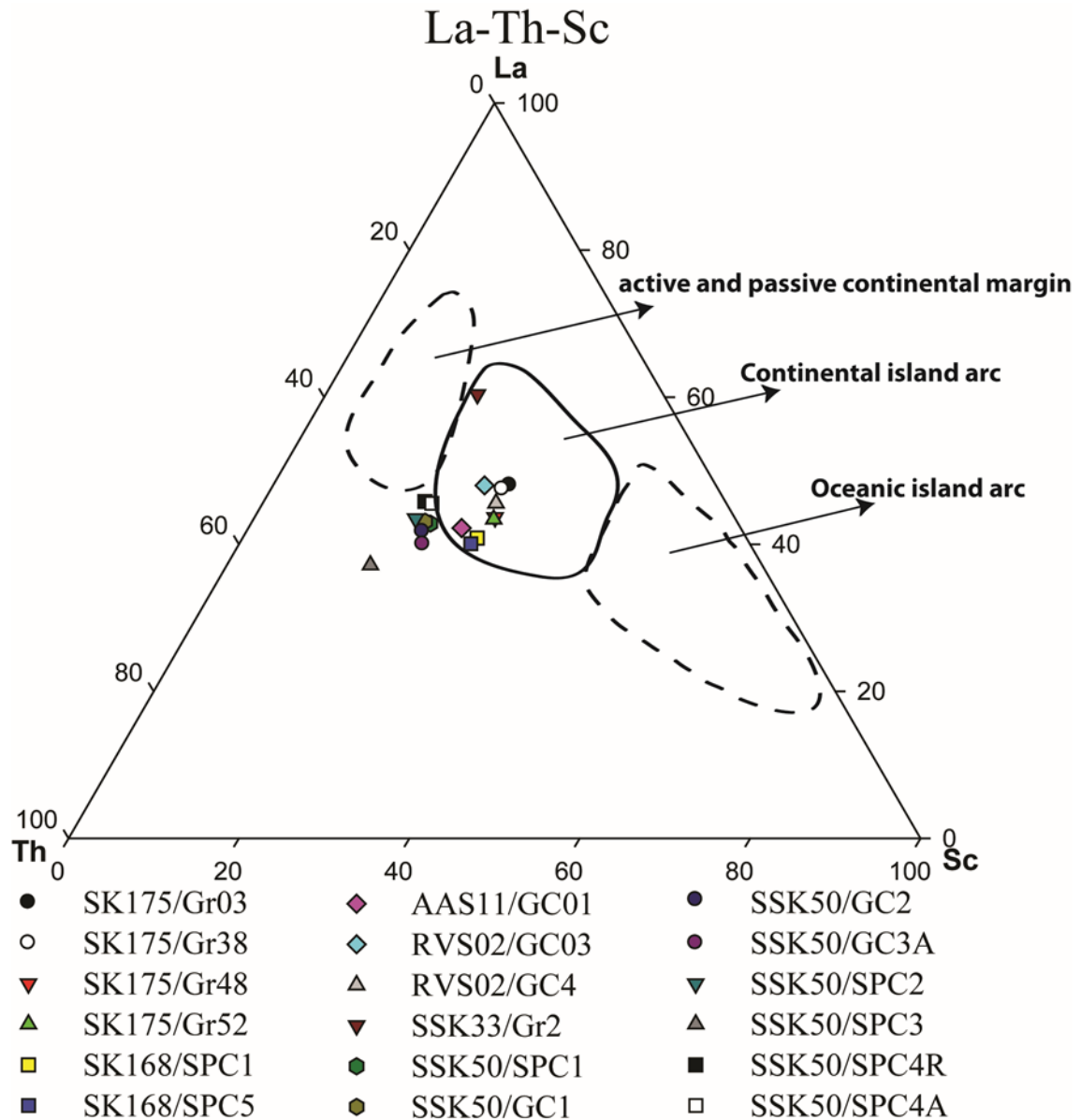


**Figure 3.5a:** *La-Th-Sc ternary diagram of all surface sediments studied here. Discriminatory spaces of continental margins and island arcs are shown.*

SSK33/Gr02 to Barren island material in Sr-Nd plot (Fig. 3.7b) supports the previous understanding that the Barren and Narcondam islands are northward extension of western Andaman fault [Halder *et al.*, 1992]. A little deviation of these (Barren island material and SSK33/Gr02) values from Indonesian arc and close to ninetyeast ridge (NER) material suggests the role of subducted NER material in addition to western Andaman fault/ arc

derived material. Although all the sediments fall in higher Himalaya sedimentary series (Fig. 3.7a), they are well differentiated among them. Comparatively eastern, southeastern basins are less radiogenic (Nd) than central Andaman basin sediments and much lesser radiogenic (Nd) than western basin (Fig. 3.7a). The western basin shows high radiogenic

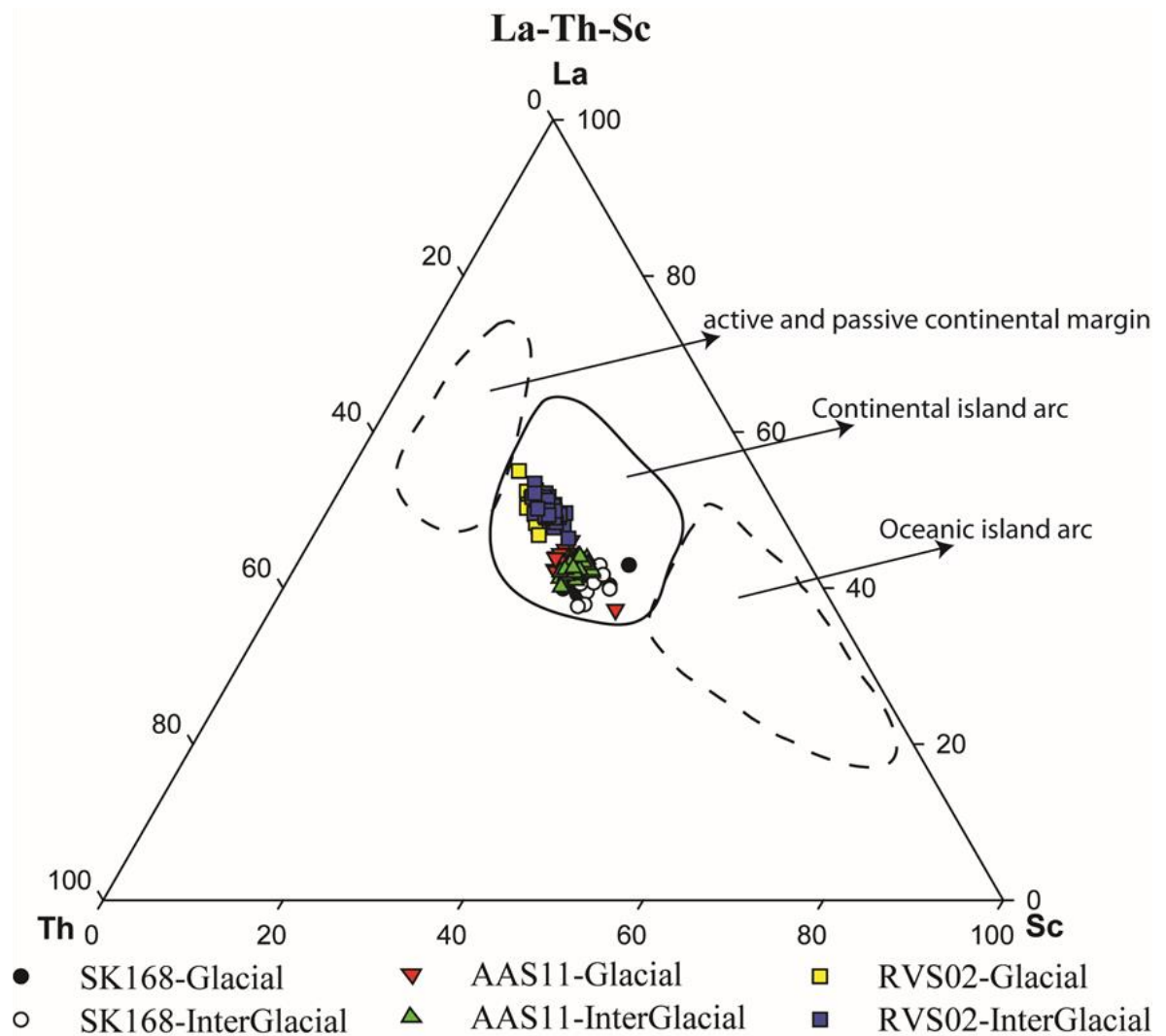


**Figure 3.5b:** *La-Th-Sc diagram of all subsurface sediments from three sediment cores. Glacial and interglacial sediments are plotted with a different symbol.*

(Nd) material probably derived from Andaman Islands and Indo-Burman ranges. Hafnium isotopes were used to understand the chemical weathering intensity at source areas and provenance of sediments, the hafnium isotopes were measured for the first time in Indian Ocean sediments. The Nd-Hf isotope values of all sediments (Table 3.10) are falling in and around zircon free array [Vervoort *et al.*, 1999] in Nd-Hf isotopic space (Fig. 3.8) except

SSK33/Gr02 that fall in between mid-Oceanic ridge basalt (MORB) and Oceanic island basaltic (OIB) isotopic composition.

### 3.3. Discussion:

The major, trace, rare earth elemental data along with Sr-Nd-Hf radiogenic isotope data, that plotted in various geochemical discriminative plots suggest four major lithogenic sedimentary zones the Andaman Sea. Primarily, Indo-Burman ranges are playing major role by contributing its signatures through rivers of Irrawaddy off western Marthaban shelf and other rivers off Arakan coast. Secondly, Sino-Burman ranges derived material is transported through rivers of Salween, Sittang, Tavoy and Tanintaryi. The Andaman-Nicobar Islands may also seem to having its control over sediments of the basin but to a limited geographic area. Finally, but importantly 'western Andaman fault' through its arc derived material also seem to influence the lithology of the basin. Strontium and neodymium isotope data of 15 sediments were plotted in Sr-Nd plot of northeastern Indian Ocean and its land mass values (Fig. 3.7a). All Andaman basin sediments were falling in Higher Himalaya sedimentary series except seamount sediment (SSK33/Gr02) that falls in ninet east ridge rocks space (Fig. 3.7a). The entire range of  $^{87}\text{Sr}/^{86}\text{Sr}$  and  $\epsilon_{\text{Nd}}$  values of this study varies from 0.705472 to 0.724732 and 3.9 to -11.9 respectively and along with other published values of Andaman basin broadly suggests the entire spread in this plot varies in between composition of Indonesian arc and High Himalaya crystalline material. However, the elemental and isotopic composition of the Andaman lithogenic material suggests four major geographical zones in the basin where the imprints of specific geological reservoirs are noticed, which are described below.

### 3.3.1. Indo-Burman Ranges:

The geochemical analyses on shelf samples collected off the Myanmar rivers like Irrawaddy, Salween, Sittang, Tanintaryi implies the signatures of their particular river material. The low alumina and titanium content (Table 3.2) in shelves of Arakan – Irrawaddy than Sittang – Salween – Tanintaryi located on east probably reflects the

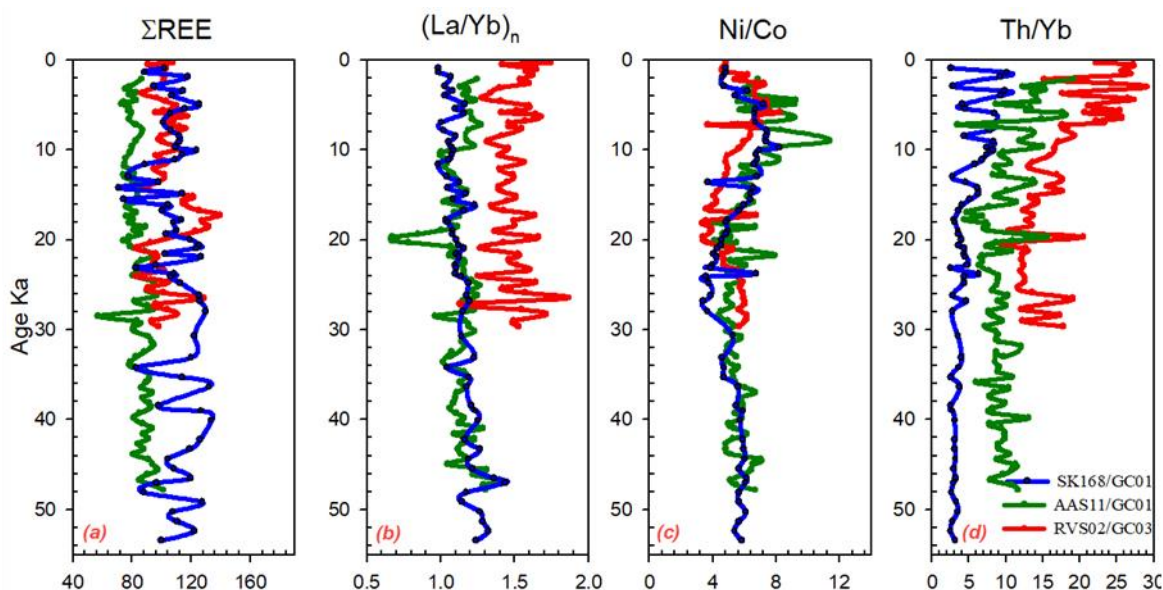


**Figure 3.6:** Downcore variation of  $\Sigma\text{REE}$ ,  $(\text{La}/\text{Yb})_n$ ,  $\text{Ni}/\text{Co}$  and  $\text{Th}/\text{Yb}$  ratios of SK168, AAS11 and RVS02 cores. The southern core shows different  $\text{La}/\text{Yb}$  and  $\text{Th}/\text{Yb}$  ratios, similar to major elemental variation.

lithological differences in their watersheds. The provenance indicator  $\epsilon_{\text{Nd}}$  also shows  $\sim 2\epsilon_{\text{Nd}}$  and  $\sim 9\epsilon_{\text{Nd}}$  units variation within these two regimes and tracks the present day pathways of terrigenous sediment transport to the deep Andaman Sea. The more radiogenic  $\epsilon_{\text{Nd}}$  and less radiogenic Sr in Irrawaddy mouth shelf sample SK175/Gr38 ( $\epsilon_{\text{Nd}}$  -8.72 and 0.713429) is very similar to the Arakan shelf sample SK175/Gr03 ( $\epsilon_{\text{Nd}}$  -8.88 and 0.714849) (Table 3.4) and agrees well with reported Irrawaddy sediment values of  $\epsilon_{\text{Nd}}$  -8.3 and -8.6 [Colin *et al.*, 1999; Allen *et al.*, 2008] and implies that the eastern and western part of Indo-Burman ranges (IBR) are contributing near similar Nd signal to the open ocean, either through Arakan, Rakhine rivers in western IBR or through Irrawaddy river on eastern IBR. The signatures of the Irrawaddy control the major parts of the basin and even reported that

reached up to 5°N on ninetyeast ridge also [Ahmad et al., 2005]. Though, the Nd-isotopic values of middle part of Irrawaddy river, where river Chindwin merges to the Irrawaddy are

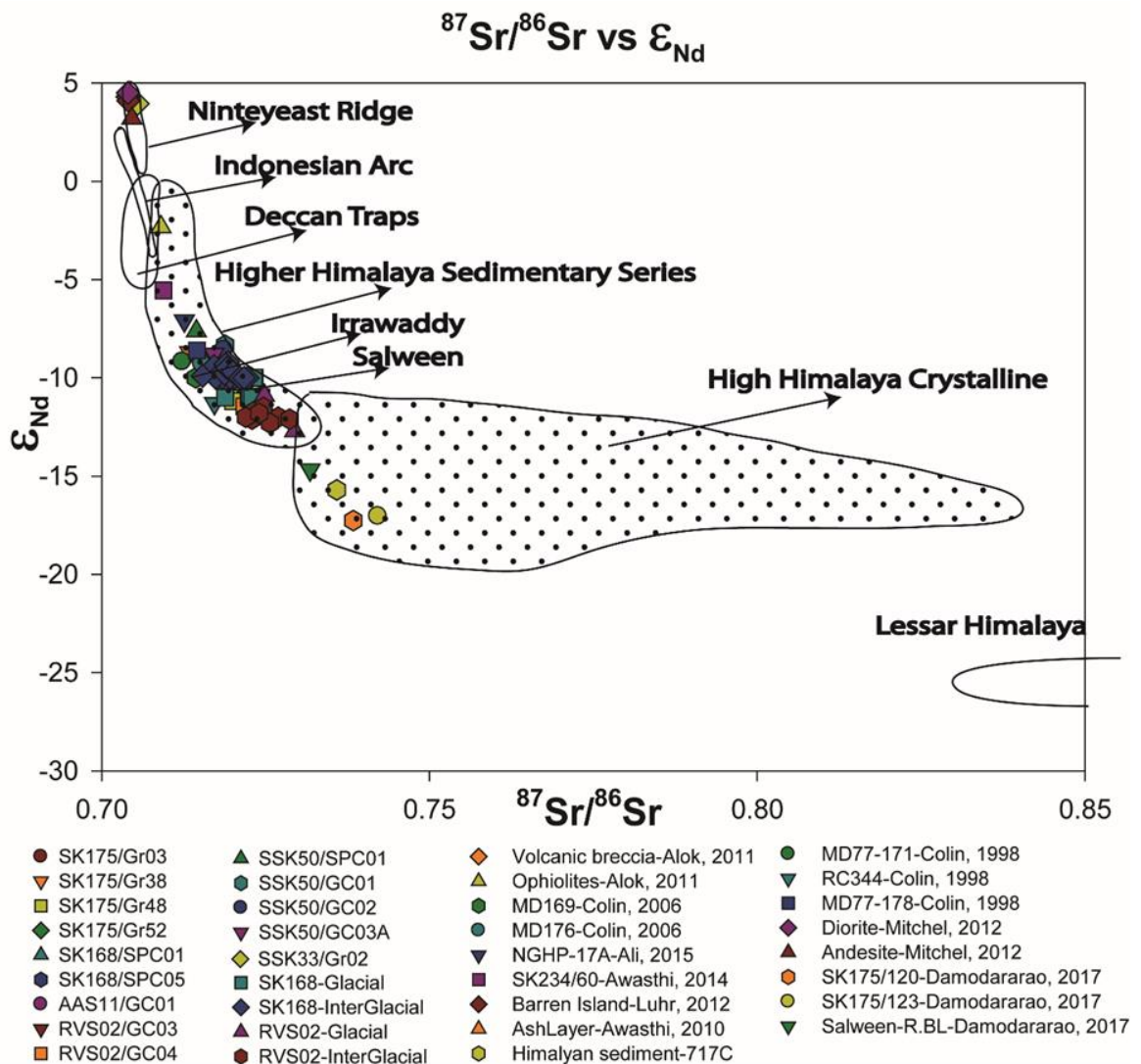


**Figure 3.7a:** A plot of  $^{87}\text{Sr}/^{86}\text{Sr}$  vs  $\epsilon_{\text{Nd}}$  of all sediments used for this study and other available sediments from the northeastern Indian Ocean. The discriminative spaces are re-drawn from Colin et al, [1999]. Most of the samples fall in a broad field defining Higher Himalayan crystalline series where the 3 Myanmar river end-members also fall.

less radiogenic ( $\epsilon_{\text{Nd}}$  -13.75 to 0.25) [Licht et al., 2016], the presence of recent volcanic dykes, flysch, mud volcanoes and ophiolites [Mitchell et al., 2007; Allen et al., 2008; Licht et al., 2013, 2016; Awasthi et al., 2014] probably makes Irrawaddy material to be more radiogenic (Nd-isotopic values).

The isotopic data of the northern core SK168 (this work –Alcock ridge complex/plateau) exhibits a narrow range of Nd isotopes ( $\epsilon_{Nd}$  -11.24 to -9.24; average  $-10.15 \pm 0.46$ ) (Fig. 3.7d) which fall very close to other published central Andaman basin (CAB) values (MD77-169 [Colin *et al.*, 2006] of Sewell seamount (here after MD169) and RC12-344 [Colin *et al.*, 2006] (hereafter RC344)), ( $\epsilon_{Nd}$  -11.5 to -9.5; average  $-10.56 \pm 0.3$ ) implies the CAB region of Andaman Sea had received material from a same source during the last two glacial cycles. Another record MD77-176 (hereafter MD176) located close to Irrawaddy mouth shows high radiogenic Nd [Colin *et al.*, 2006] of -9.2 to -7.7 with average value of  $-8.67 \pm 0.43$  (Fig. 3.7e). High radiogenic  $\epsilon_{Nd}$  in MD176 is similar to Arakan shelf (SK175/3 - this study) and Irrawaddy mouth (SK175/38 - this study) sediments. All these 3 areas seem to reflect the dominant supply from Irrawaddy; whereas the CAB cores has contribution of low radiogenic Nd material from Salween and Sittang rivers. The slight enrichment of unradiogenic material in glacial sediments of CAB cores may be due to climatic change (intensified NE monsoon and weakened SW monsoon in the Myanmar plains). The possibility of addition of material from Andaman islands to the CAB is ruled out due to absence of major rivers on islands and the presence of coral reefs which grew since LGM [Ray *et al.*, 2013].

### **3.3.2. Sino-Burman Ranges:**

Shelf sediments off rivers Salween (SK175/52;  $\epsilon_{Nd}$  -10.37 and 0.721543) and Sittang (SK175/48;  $\epsilon_{Nd}$  -11.19 and 0.720063) have distinctly low radiogenic values reflecting a dominance of old crustal material in the flood plains of Salween and Sittang. The river Salween originates in eastern syntaxes of Himalaya and flows through south-eastern Tethyan tectonic belt [Roger *et al.*, 2003; Chen *et al.*, 2007], while river Sittang

originates and flows entirely from Shan Plateau of Sino-Burman ranges (SBR). The clockwise movement of stronger monsoon currents probably mix the Irrawaddy, Salween and Sittang sediments well during the transport [Ramaswamy *et al.*, 2004; Rao *et al.*, 2005] and deposition in the Central Andaman basin. Two recent studies [Cao *et al.*, 2015; Damodararao *et al.*, 2016] on eastern shelf off Mergui islands at varied depth indicates

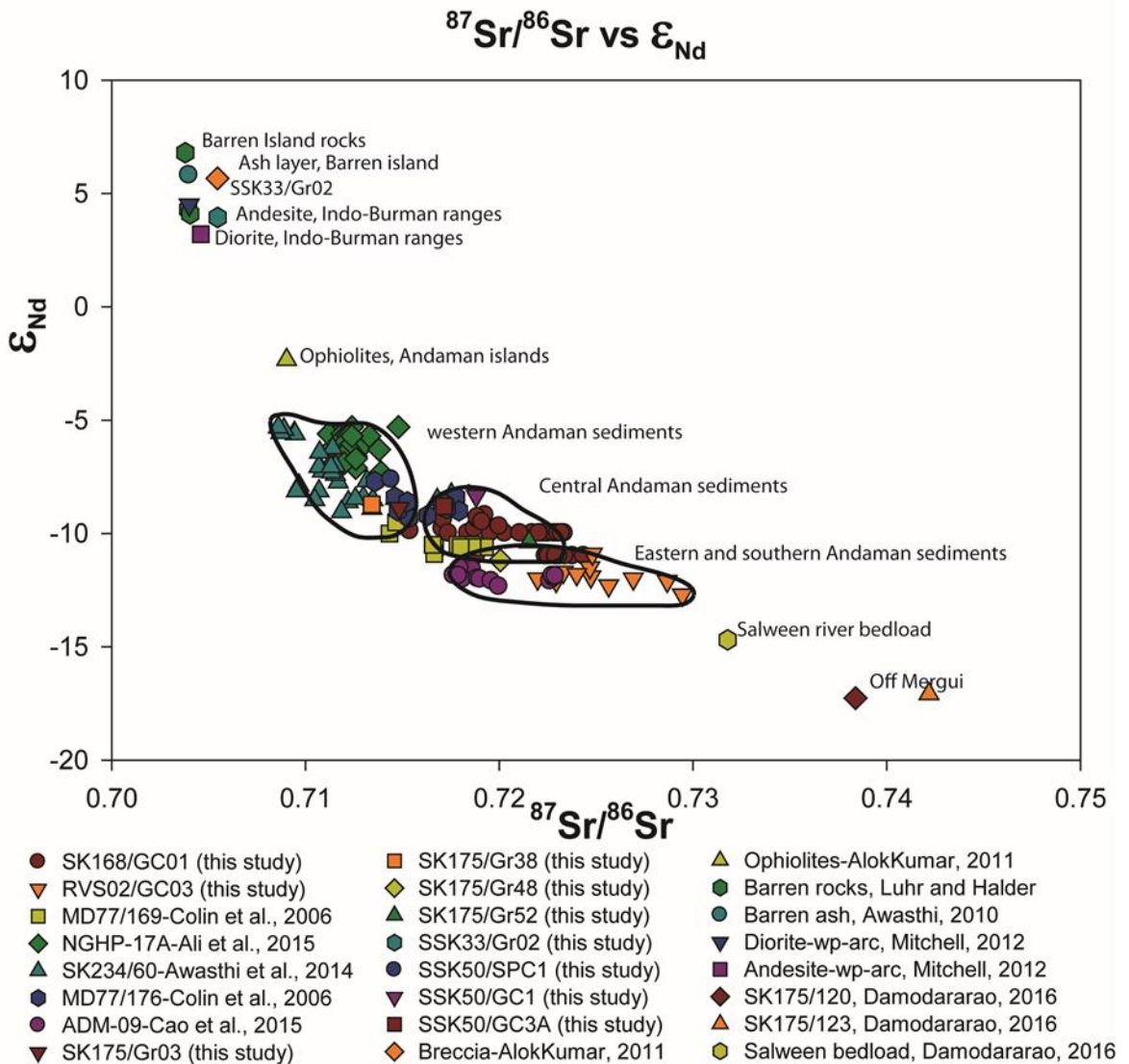


**Figure 3.7b:** A plot of  $^{87}\text{Sr}/^{86}\text{Sr}$  vs  $\epsilon_{\text{Nd}}$  of all available downcore data of Andaman Sea. Distinct geographic zonation is seen in the elemental data too.

eastern Andaman basin is isolated from more radiogenic Irrawaddy river material to this area. Although a clear domination of interglacial characterized SW monsoon intensification made Irrawaddy to dominate other rivers, it seems to have less influence in the eastern region of Andaman Sea. The lowest radiogenic Nd and highest radiogenic Sr

values reported ( $\epsilon_{Nd} \sim -17$  and 0.740292; Table 3.4) from off Mergui shelf [Damodararao *et al.*, 2016], suggests the considerable contribution of Tanintaryi river to the basin (Table 3.4). A 26ka Sr-Nd isotopic study on a core [Cao *et al.*, 2015] retrieved in southeastern slope of the basin clearly shows single source in both glacial-interglacial climatic conditions (Fig. 3.7d). The river Tanintaryi being a major drainage watershed of this old granites of southern Myanmar/western Thailand, the high radiogenic Sr and low radiogenic Nd isotopic numbers ( $\epsilon_{Nd} -25.4$  and 0.7685) [Nakapadungrat *et al.*, 1984] of this region implies the major source to the eastern shelf, but having minimal impact on central Andaman basin sediments. Sr-Nd isotopic study on the southern core of the transect of present study (RVS02/GC03) seems to have received very similar lithogenic source as ADM-09 core location [Cao *et al.*, 2015] and suggests the southeastern side and southwestern side of the Andaman basin received similar type of sediment sources at least since last 30ka (Table 3.7). The low radiogenic  $^{87}Sr/^{86}Sr$  observed (Fig. 3.7d) in ADM-09 core than RVS02/GC03 core might be due to differences in leaching protocols. Samples of ADM-09 core was treated with only 0.25M acetic acid before complete digestion [Cao *et al.*, 2015], whereas RVS02/GC03 samples were subjected to 1M Hydroxylamine Hydrochloride (HH) in 25% acetic acid in addition to buffered acetic acid to make sure to remove all other components in order to get pure lithogenic fraction (see Rutberg *et al* 2000 and Bayon *et al* 2002). Although, the core RVS02 is located on the western side of the basin, the local volcanic and islandic influence is not seen and suggests the southwestern basin is different from northwestern basin. As the clock-wise movement of monsoonal currents brings Irrawaddy-Salween-Sittang material effectively but may push this Mergui material to southern basin further more. The absence of considerable changes in southern basin core RVS02 implies a minimal exchange (at least inflow) of lithogenic material through 'Great Channel' during both glacial-interglacial periods.

### 3.3.3. Andaman-Nicobar Islands:

The sediments collected east side of the Andaman archipelago (includes northern-middle-southern Andaman) in varying depths (n=8; sample number 11 to 18) does not show any

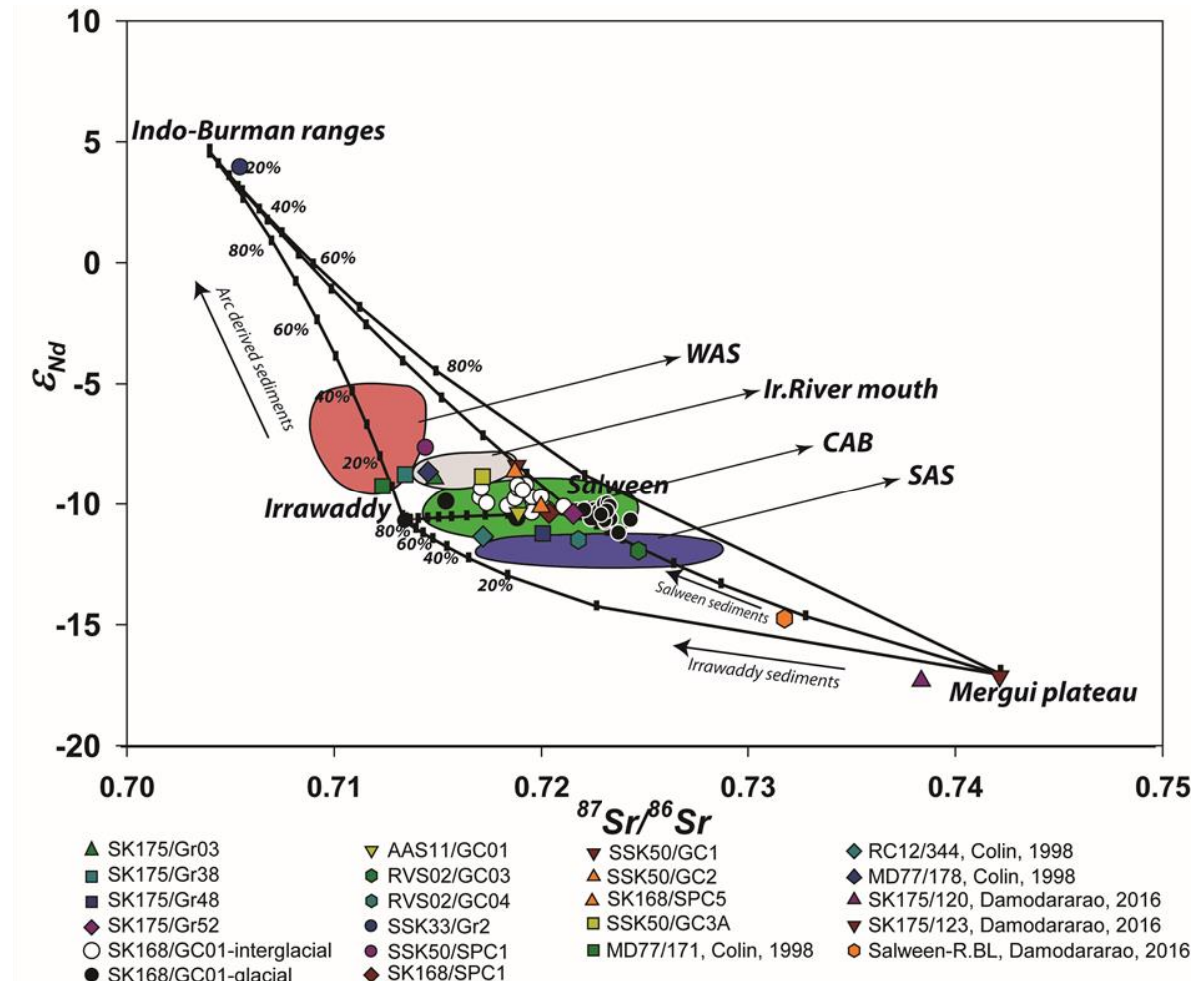


**Figure 3.7c:** A mixing diagram of  $^{87}Sr/^{86}Sr$  vs  $\epsilon_{Nd}$  showing all available surface sediment and downcore data plotted along with data generated for this present study. Four possible end-members viz., the IBR, Irrawaddy, Salween-Sittang and Mergui Plateau are plotted. While the CAB and SAB sediments fall within the end-members, WAS sediments seems to have additional source

differences in TAS diagram among other samples of the basin. They are falling in mixed composition “andesite”, probably resulted by mixing of basic islandic signatures with felsic terrigenous sources in the north. While, samples collected west side of the south Andaman and one beach sample in Corbyn’s cove beach shows high silica concentration (~82 % of  $SiO_2$ ) and plots beyond the TAS diagram. The island sourced sediments fall in

gabbro weathering trend of A-CN-K diagram (Fig. 3.3a) and fall as a separate group in A-

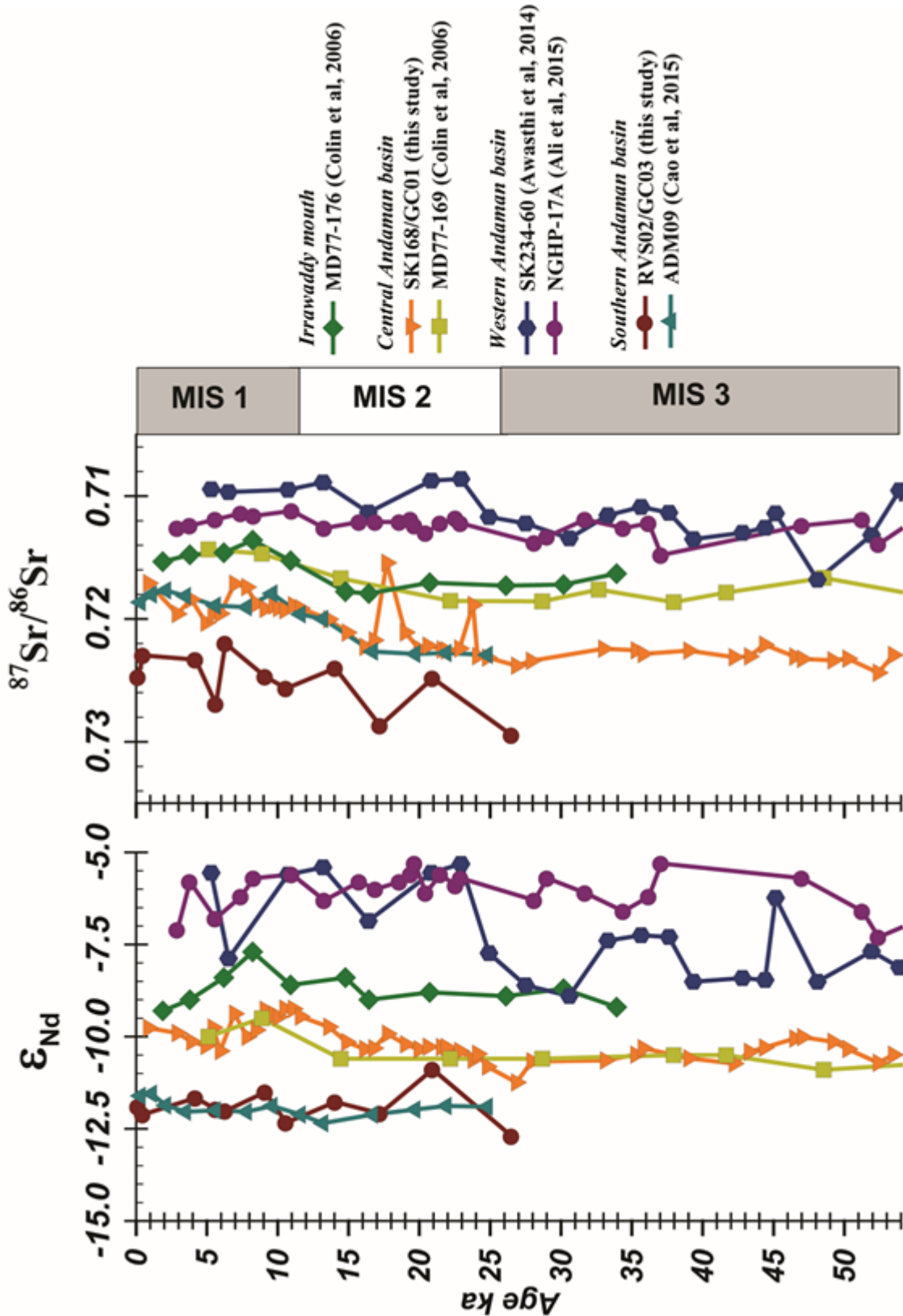


Figure 3.7d: Sr-Nd isotopic data of all available sediment cores of the Andaman Sea along with northern and southern cores (SK168 and RVS02) of this study. WAS sediments plot away from CAB cores.

CNK-FM diagram (Fig. 3.4a) with more affinity towards FM apex. In trace elemental ternary plot La-Th-Sc, all these samples fall in none of the discriminative arc-plots (Fig.

3.5a) possibly because of high thorium concentration. This abnormal behavior of these samples in the above major-trace discriminative plots suggest the presence of plume derived material in Andaman island rocks [Jafri *et al.*, 1990].

Two records from the western part of Andaman Sea [Awasthi *et al.*, 2014; Ali *et al.*, 2015] (Fig. 2.1) have reported high radiogenic Nd. The range of  $\epsilon_{Nd}$  (-7.3 to -5.3) and the average value of  $-6.04 \pm 0.53$  (Fig. 3.7c) of core NGHP-17A [Ali *et al.*, 2015] lies between beach sediment values of middle Andaman, Neil islands ( $\epsilon_{Nd}$  -5.1 and -7.6) [Ali *et al.*, 2015] and SSK50/SPC01, SSK50/GC01, SSK50/GC02 and SSK50/GC3A ( $\epsilon_{Nd}$ -7.6 to -8.8 - this study) suggests a major contribution from the local sources to the western AS. In another core SK234 [Awasthi *et al.*, 2014] collected near Barren volcano,  $\epsilon_{Nd}$  vary between -9.0 and -5.3 (average  $-7.4 \pm 1.1$ ) and  $^{87}Sr/^{86}Sr$  0.70861 to 0.71680 (Fig. 3.7c). The major portion of SK234 record has high radiogenic  $\epsilon_{Nd} > -8.0$  and less radiogenic Sr  $< 0.712$ . This core was found to have multiple ash layers [Awasthi *et al.*, 2010] ( $\epsilon_{Nd}$   $5.75 \pm 0.54$ ) derived from Barren volcanism and less likely to receive terrigenous sediments from the Myanmar rivers [Rodolfo, 1969]. As shown above, when the average values of  $\epsilon_{Nd}$  in the Andaman sediment are compared, a regional variation in the source provenance of the detrital sediments of the Andaman Sea can be constructed. The CAB region is depleted by  $\sim 2$   $\epsilon_{Nd}$  units relative to Irrawaddy mouth region, and  $\sim 4$   $\epsilon_{Nd}$  units relative to the western region (NGHP-17A and SK234). The observed high radiogenic Nd of NGHP-17A core and the large excursions in isotopic ratios of SK234 (Barren) are not seen in the CAB cores and suggest that the central Andaman Sea has little supply from island and the volcanic sources in the western AS (Fig. 3.7d). The ophiolite data [Kumar, 2011] of Andaman Islands fall in between western basin sediment zone and arc material zone and further suggests these ophiolites were derived from mixing composition of Myanmar derived sediments and arc derived material.

#### **3.3.4. Western Andaman fault:**

Subduction of Indian plate under Sumatra-Indonesia resulted in the formation of numerous volcanoes and rate of subduction controls the intensity of Indonesian volcanic eruptions [Chesner and Rose, 1991; Chesner et al., 1991; Turner et al., 2003]. The geochemistry also varies distinctly from east to west, with low crustal contamination in east and more in the west near the Sunda region. The western Andaman Fault (WAF) lies above the forearc, and consists of numerous volcanoes areal and sub-areal. Among them, two prominent volcanoes Barren (active) and Narcondam (dormant) in the north and a seamount chain in the south (Kamesh Raju et al., 2012) are connected. While the rocks of Barren and Narcondam volcanoes were studied thoroughly [Luhr and Haldar, 2006; Chandrasekharam et al., 2009; Sheth et al., 2009, 2011; Ray et al., 2013], nearly none is available on entire WAF. An attempt is made in the present study to assess the elemental geochemistry of sediments those collected in and around seamounts in the south as well surface sediment around Narcondam and Barren islands. Distinctly high calcium in these sediment samples (Table 3.2) collected around either Barren island or seamounts on the WAF denotes the influence of forearc material in sediments of the basin. High radiogenic neodymium and low strontium values are characteristic of andesite-diorite type of rocks in Indo-Burman ranges [Mitchell et al., 2012], volcanic sediment of inner wedge of IBR (Wuntho-Popa arc) [Licht et al., 2016], north Andaman basin located Barren-Narcondam island rocks [Luhr and Haldar, 2006; Streck et al., 2011], ash layers found in sediment core off Barren island [Awasthi et al., 2014], volcanic breccia derived from mud-volcanoes of Andaman islands [Kumar, 2011] and in the sediments from a seamount in the southern Andaman basin (SSK33/Gr02; this study). The geochemical similarities in between rocks, ashes of Barren island and rocks from seamount tops in southern basin as well surface sediments of the present study suggest WAF may be another lithogenic material supplier to

the basin. But a thorough sampling and a detailed survey is required to quantify the WAF input to the basin. The detailed survey on arc systematics may further help in deciphering the role of NER in spreading center and plume derived material in Andaman archipelago.

### 3.3.5. Nd-Hf based provenance inferences:

Hafnium isotopes were measured on surface sediments (n=14; Table 3.4) and subsections of northern core SK168 (n=44; Table 3.11), representing the first data from the Indian Ocean, to understand past provenance changes in source areas of sediments. Further, the combined use of Hf and Nd isotope systematic offers a unique perspective of silicate weathering (e.g., Bayon *et al.*, 2009). Due to fractionation of  $^{176}\text{Lu}$  into  $^{176}\text{Hf}$ , different arrays develop in  $\epsilon_{\text{Nd}}$  vs  $\epsilon_{\text{Hf}}$  plot (Fig. 3.8) which can be used to understand the source of the material from which it is derived primarily. Older rocks on terrestrial array are less radiogenic with younger rocks being more radiogenic and plot in another end. The zircon-rich and zircon-free arrays also suggested [Bayon *et al.*, 2009], due to high affinity of hafnium to zircons. The Sea water array is represented by ferromanganese nodules and other seawater authigenic precipitates which is defined by high  $\epsilon_{\text{Hf}}$  and low to intermediate values of  $\epsilon_{\text{Nd}}$  (Fig. 3.8). The geographic configuration of Indo-Burman ranges (IBR), Central Myanmar basin (CMB) and Sino-Burman ranges (SBR) consists of complex tectonic arrangements, like accreted continental crust, volcanic arcs, and suture zones that constitute the remnants of closed oceanic basins [Metcalf, 1996, 2006, Ridd, 2009a, 2009b; Dopieralska *et al.*, 2012]. The IBR has formed from the thick column of sediment (~10km) being scrapped off the subducting Indian plate under Burma /Sibumasu terrane [Bender, 1983; Curray, 2005; Allen *et al.*, 2008; Gireesh, 2010]. The  $\epsilon_{\text{Hf}}$  values in

lithogenic fraction vary between  $-0.4$  to  $+13.5\epsilon_{\text{Hf}}$  in surface sediments and  $-4$  to  $+0.25$  in SK168 (Table 3.4). Although a minor variation is seen between glacial ( $-2\epsilon_{\text{Hf}}$ ) mean and interglacial ( $-1.6\epsilon_{\text{Hf}}$ ) mean values of the core SK168, a clear demarcation in  $\epsilon_{\text{Hf}}$  vs  $\epsilon_{\text{Nd}}$  plot

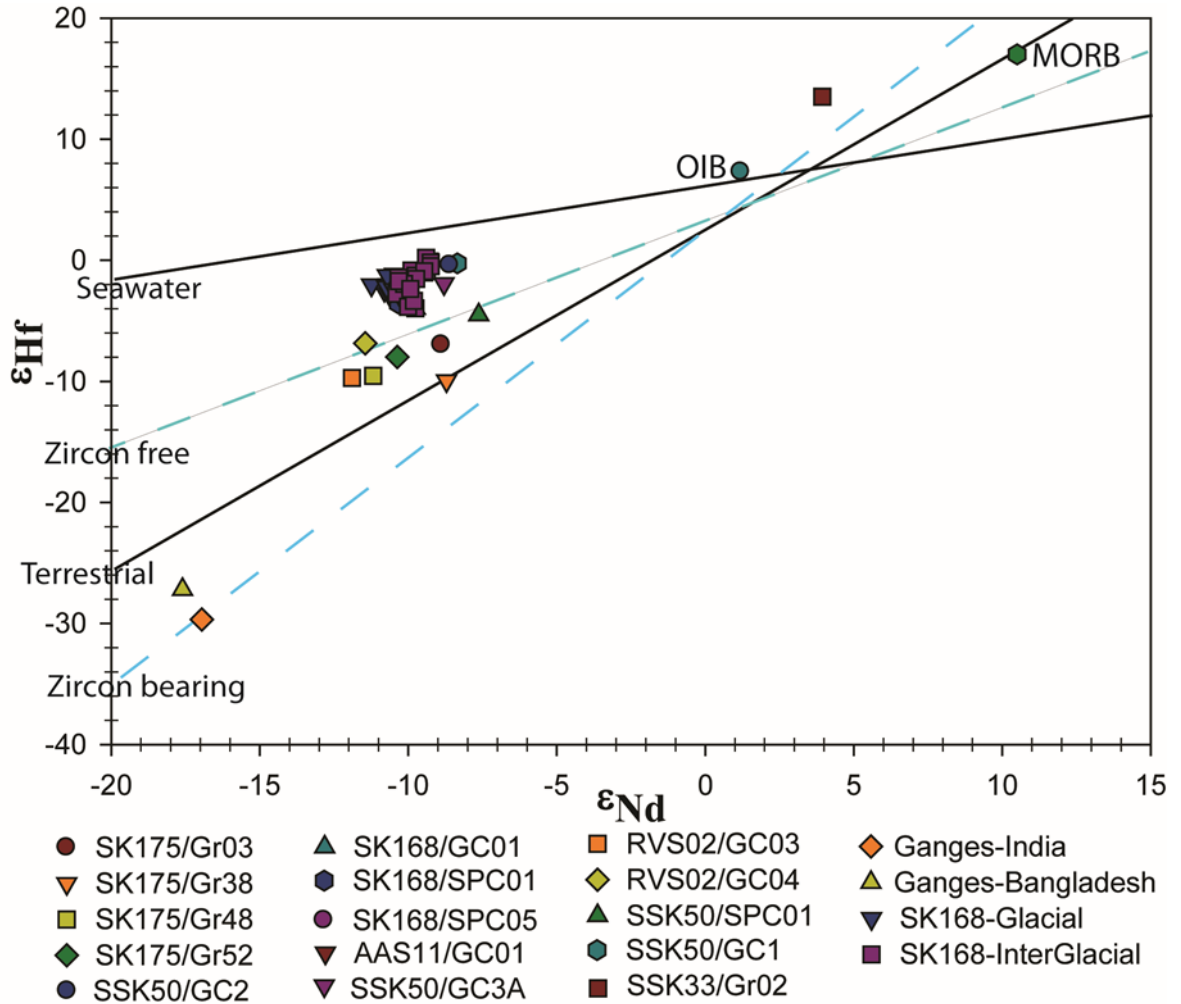


**Figure 3.8:**  $\epsilon_{\text{Nd}}$  vs.  $\epsilon_{\text{Hf}}$  of all available surface sediments and 44 subsections of core SK168 of Andaman Sea along with Ganges sediment in India and Bangladesh as well MORB-Mid-Oceanic Ridge Basalt and OIB-Oceanic Island Basalt composition. The seawater array is re-drawn from Vervoort et al, [2007] and zircon-free and zircon-bearing arrays are re-drawn from Bayon et al, [2009].

(Fig. 3.8) was noticed during these climatic regimes (which is similar to  $\epsilon_{\text{Nd}}$  of same core).

The interglacial sediments gained more radiogenic nature in both Hf and Nd resulting in a shift towards MORB end (Fig. 3.8). The Hf isotopic measurement was carried out on pure lithogenic fraction (non-carbonate and non-oxide/hydroxide fractions) after 7 days of

complete digestion to ensure all the zircons were digested. The  $\epsilon_{\text{Hf}}$  values of SK168 ( $1.8\epsilon_{\text{Hf}}; n=44$ ) are neither close to -26 (Ganges) nor +18 (MORB), but seem to represent the mixing of extreme end members]. The  $\epsilon_{\text{Hf}}$  values in shelf sediments off Salween and Sittang are -8 and -9.5, off Irrawaddy are -10 and off Arakan coast are -7. The Andaman sediments ( $-1.8\epsilon_{\text{Hf}}$ ) and the Myanmar shelf sediments ( $-7$  to  $-10\epsilon_{\text{Hf}}$ ) are more radiogenic than neighboring Ganges sediments ( $-30\epsilon_{\text{Hf}}$  India;  $-27\epsilon_{\text{Hf}}$  Bangladesh; [Garcon *et al.*, 2013] reflecting the variation in source rock lithology. This high radiogenic hafnium in lithogenic sediments is possible if DM/old continental crust ( $-20 \epsilon_{\text{Hf}}$ ) mixes with recent volcanic material like MORB ( $+15 \epsilon_{\text{Hf}}$ ). The microplate Sibumasu may have a large influence on tectonic arrangements of present day Myanmar. The Sibumasu was sandwiched between India and IndoChina plates and resulted in repeated collisions. These series of collisions resulted in forming Sino Burman ranges and Indo Burman ranges and these tectonic movements could have influenced the geochemical properties.

During weathering process, more radiogenic Hf is released to aqueous system along with mobile elements by retaining unradiogenic Hf in source terranes, mainly due to retention of chemically resistant zircons which have unradiogenic Hf [Patchett *et al.*, 1984; White *et al.*, 1986]. This is called as zircon effect and causes the incongruent weathering. The zircons are most stable minerals and have the lowest Lu/Hf ratio and this ratio decreases with time due to  $^{176}\text{Lu}$  decay to  $^{176}\text{Hf}$ . This is the reason for spacing of old continental crust and recent mid oceanic ridge basalt (MORB) in either end of Nd-Hf terrestrial array. But similar increases in radiogenic Nd and Hf in SK168 may rule out the possibility of the zircon effect in the study area. The similar increase in radiogenic nature

in hafnium isotopes along with neodymium isotopes during interglacial period probably indicates slight enrichment of juvenile material in the source area

**3.3.6. Sr-Nd mixing diagram:** A simple Sr-Nd mixing diagram is presented with four possible dominant sources (interpreted above) to the study area as the end-members (Fig. 3.7c). The 4-end members considered here are: i) the end-member with extreme unradiogenic (Nd) and high  $^{87}\text{Sr}/^{86}\text{Sr}$  value of Mergui Plateau ( $-17.1\epsilon_{\text{Nd}}$  and  $0.742183$  respectively) [Damodararao *et al.*, 2016], (ii) extreme radiogenic (Nd) and low  $^{87}\text{Sr}/^{86}\text{Sr}$  value of Indo-Burman ranges ( $4.5\epsilon_{\text{Nd}}$  and  $0.704$ ) [Mitchell *et al.*, 2007], (iii) the Irrawaddy river sediment values ( $-10.7\epsilon_{\text{Nd}}$  and  $0.7133$ ) [Colin *et al.*, 1999], representing IBR influenced western Myanmar region and (iv) off Salween river sediment value ( $-10.4\epsilon_{\text{Nd}}$  and  $0.721543$  this study), representing SBR influenced eastern Myanmar region. All available and newly generated Sr-Nd isotopic data (for this study) of sediments are plotted in this mixing plot (Fig. 3.7c). A clear zonation is seen in this plot (Figures 3.7b and 3.7c) displaying maximum radiogenic signatures observed in western Andaman Sea (WAS) sediments and sediments around Irrawaddy mouth as well Arakan shelf. The two long records SK234 and NGHP-17A [Awasthi *et al.*, 2014; Ali *et al.*, 2015], Neil and middle Andaman beach sediments [Ali *et al.*, 2015], surface sediment of MD77-171 [Colin *et al.*, 1999] and four surface sediments (SSK50/SPC01, SSK50/GC01, SSK50/GC02 and SSK50/GC3A-this study) of western Andaman Sea fall closer to this discriminative space suggests that the WAS is dominated by high radiogenic material probably from local volcanic, islandic sources or from IBR. The data of Irrawaddy river mouth core (MD77-176) [Colin *et al.*, 2006], surface sediment MD77-186 [Colin *et al.*, 2006] off Arakan coast and two shelf sediments of present study (SK175/03 and SK175/38) suggests that river Irrawaddy carrying radiogenic (Nd) material to open Sea is either through western Marthaban shelf or through Arakan shelf. The location of discriminative spaces of WAS

and Irrawaddy river mouth sediments (Fig. 3.7c) falling in between IBR and Irrawaddy sediment end-members clearly shows the domination of IBR material in these two areas, but the overflowing of WAS space beyond the IBR-Irrawaddy mixing line clearly supports the interpretation of additional contribution from volcanic and island material to WAS sediments. The central Andaman basin (CAB) sediments occupy a major portion of the plot and form a broad discriminative space in this Sr-Nd mixed plot (Fig. 3.7c). CAB cores like MD77/169 [Colin *et al.*, 2006] and SK168 (this study) fall in this space along with other CAB surface sediments (SK168/SPC01, SK168/SPC05, RVS02/GC04 and AAS11/GC01) as well Sittang river mouth sediment (SK175/48). The present day-CAB sediments fall in between Irrawaddy and Salween river mouth sediment end-members, suggests that the present day sedimentation in the CAB region is mainly controlled by supplies from these two rivers. The glacial CAB sediments however plot outside the Salween end member, away from the Irrawaddy but fall on the line connecting IBR and Mergui Plateau end-members supporting the interpretation of Salween as the major glacial source with additions from low radiogenic Nd sources of MP. The SAS space, that includes southeastern core ADM-09 [Cao *et al.*, 2015], southwestern core RVS02/GC03 (this study) and surface sediment SS172-4038 [Bhushan, 2008] distinctly fall below CAB sediments, away from IBR sources but with a spread between Irrawaddy and MP type of sources supporting the earlier interpretation of clock-wise sediment movement from east to west.

**3.3.7. Sm-Nd based  $T_{DM}$  calculations:** The Sm-Nd depleted model age [DePaolo, 1980]  $T_{DM}$  is calculated for both the cores SK168 and RVS02 (Tables 3.11 and 3.12). The  $T_{DM}$  values of SK168 varies from 1.14 to 1.46Ga and the average remained close to 1.33Ga for both glacial and interglacial sediments, which suggests that the provenance to northern core location remained same through the climatic change. The  $T_{DM}$  of shelf sediments off

Arakan and Irrawaddy (1.26 and 1.28Ga respectively) fall very close to SK168 downcore values, while the ages for southern core RVS02 vary from 1.45 to 1.53Ga with an average of 1.5Ga are slightly older than the Salween and Sittang shelf sediments(1.44 and 1.36Ga respectively) which may suggest an additional contribution of older material (possibly Tanintaryi). The  $T_{DM}$  ages of cores SK168, RVS02 and shelf sediments correspond to the interpretation of sources from Sr-Nd plot (Fig. 3.7d).

### 3.4. Conclusions:

- A large database of elemental and isotope geochemistry of sediments, generated in this work covering the entire Andaman Sea in space and time gave clues about possible sources and sedimentary pathways to the basin. The north-south increase in silica with a reduction in alumina content over silica suggests a reduced basic composition towards southern parts of the basin.
- Elemental and isotopic analysis of shelf sediments that are retrieved off Myanmar rivers helped in defining the end-member composition of each of these rivers to the deep sea. The gradual decrease in lighter REE (Nd as a component) during 54 to 23ka (in SK168) with constant  $\epsilon_{Nd}$  strongly suggests Nd isotopes as a promising provenance indicator. The  $\epsilon_{Nd}$  of river mouths bracketing all central Andaman sediments, suggests the Myanmar river systems Irrawaddy, Salween and Sittang (ISS) are the major terrigenous material suppliers to the central Andaman Sea in both glacial-interglacial periods.
- The more radiogenic  $\epsilon_{Nd}$  in Irrawaddy mouth is very similar to the Arakan shelf, and agrees well with reported Irrawaddy sediment value and implies that the eastern and

western part of Indo-Burman ranges (IBR) are contributing near similar Nd signal to the open ocean, either through Arakan, Rakhine rivers in western IBR or through Irrawaddy river on eastern IBR.

- The shelf sediments off rivers Salween and Sittang have distinctly low radiogenic values reflecting a dominance of old crustal material in the flood plains of Salween and Sittang. The low radiogenic (Nd) material in downcore Sr-Nd data of ADM-09 (southeastern basin) and RVS02/GC03 (southwestern basin) implies less control of Irrawaddy derived high radiogenic material in southern basin throughout its record spanning both glacial-interglacial climatic periods.
- The occurrence of  $\sim 17\epsilon_{Nd}$  near Mergui plateau shows the Mergui Plateau as the lowest radiogenic (Nd) end member to the Andaman Sea.
- The high resolution Sr-Nd isotopic study on SK168 along with other CAB core MD169 show a small shift in sources towards more radiogenic (Nd) since  $\sim 15ka$  to 5ka suggests the domination of Irrawaddy material over Salween and Sittang sources.
- Western Andaman Basin (WAB) represents the more radiogenic endmember than other regions of the Andaman Sea. Four new isotopic data on surface sediments along with published long records suggests the importance of local islandic sources and Barren volcanism. But, the absence of such more radiogenic values in CAB sediments shows the limited geographic influence of WAB sources. The absence of observed excursions in WAB core (SK234) in CAB cores (SK168 and MD169) further suggests the limited contribution of WAB sources to the deep sea.
- The geochemical and isotopic studies on deep sea cores collected in north-south transect in addition to several surface sediments covering the major physiographic domains of the Andaman Sea suggests four major lithogenic zones of the basin viz., a) a zone that has Indo-Burman range (IBR) derived sediment, with Irrawaddy river

being the major supplier, b) a zone that has supplies from the watersheds of eastern Myanmar rivers like Salween-Sittang-Tanintaryi, c) the western part of the basin which receives sediments mainly from the Andaman archipelago and local volcanism, and, d) the seamounts and volcanics associated with Western Andaman fault (WAF).

- Presence of Mergui Plateau derived material in southern core RVS02 implies the role of SW monsoonal currents in carrying sediments in clock wise direction on the broad eastern shelf and their deposition in southern Andaman region.
- Calculated  $T_{DM}$  (Nd-model) ages of northern and the southern core also supports the interpretations drawn from Sr-Nd plot viz., the dominant supply of Irrawaddy derived IBR material in the northern and central Andaman basin region while the southern Andaman Sea receiving sediments from Salween, Sittang regions and the Mergui Plateau with high  $T_{DM}$  model ages. Sr-Nd mixing diagram with four end-members has shown the relative affinity and possible mixing patterns of different end-members in CAB, SAS and WAS sediments.
- New Hf-isotope data along with Nd-isotopes on the lithogenic fraction of SK168 shows how/why the eastern Himalayas (and/or Myanmar terranes) are different from central Himalayas. They fall in high radiogenic space, belongs to sea water array implies the hydrothermal influence. This might be due to tectonic evolution of Myanmar terranes.

**Table 3.1.** Location and water depths of all sediment samples studied here. Also shown are details of published literature on sediment samples in and around Andaman Sea used in the interpretations. Serial Numbers are same as those shown in Fig. 2.1

Sr.No	Sample Name	Lat °N	Long °E	Water Depth (m)	Reference
1	SK175/Gr03	17.49	94.46	49	This study
2	SK175/Gr38	15.4	95.23	18	This study
3	SK175/Gr48	15.26	96.5	22	This study
4	SK175/Gr52	15.01	97.25	28	This study
5	SK168/GC01	11.7	94.48	2064	This study
6	SK168/SPC01	11.17	94.73	3047	This study
7	SK168/SPC05	10.31	94.49	3132	This study
8	AAS11/GC01	9.1	94.28	2909	This study
9	RVS02/GC03	7.7	93.97	2301	This study
10	RVS02/GC04	10.92	94.75	3618	This study
11	SSK50/GC01	12.11	92.89	44	This study
12	SSK50/GC02	11.52	92.82	608	This study
13	SSK50/GC03A	10.76	93.11	1347	This study
14	SSK50/SPC01	11.46	92.99	868	This study
15	SSK50/SPC02	11.52	92.82	623	This study
16	SSK50/SPC03	11.53	92.77	253	This study
17	SSK50/SPC04R	12.05	92.87	54.2	This study
18	SSK50/SPC04A	12.1	92.88	43.3	This study
19	SSK33/Grab02	7.37	94.39	2557	This study
20	SSD18/GC01	13.4	94.34	2137	This study
21	SSD18/GC03	11.78	93.85	2181	This study
22	SSD18/SPC02	12.4	94.27	1335	This study
23	SSD18/SPC03	10.63	94.3	2880	This study
24	SSD18/DR03	13.13	94.1	1664	This study
25	SSD18/DR08	10.67	94.05	2618	This study
26	SSD18/DR09	9.03	94.63	2000	This study
27	SSD18/DR10	10	94.1	1321	This study
28	SSK98/1/Gr-01	6.755	93.87	35.2	This study
29	SSK98/1/GC-01	6.588	94.49	32	This study
30	SSK98/1/Dr-06	6.911	94.59	1824	This study
31	SSK98/1/Gr-07	12.78	94.19	63	This study
32	Corbyn's cove beach	11.64	94.75	0.2	This study
33	SSK98/2/SPC-01	12.29	93.84	724	This study
34	SSK98/2/SPC-02	13.76	94.9	1122	This study
35	SSK98/2/SPC-03	13.71	93.99	1397	This study
36	SSK98/2/SPC-04	13.49	93.19	96	This study
37	SSK98/2/SPC-06	12.49	93.08	85	This study

Table 3.1. Continued...

38	<b>SSK98/2/SPC-07</b>	12.51	93.03	48	This study
39	<b>SSK98/2/SPC-08</b>	12.45	92.97	30	This study
40	<b>SSK98/2/SPC-12</b>	12.11	92.47	101	This study
41	<b>SSK98/2/SPC-13</b>	12.1	92.36	158	This study
42	<b>SSK98/2/Gr-01</b>	12.12	92.26	515	This study
43	<b>SSK98/2/Gr-04</b>	12.1	91.98	1604	This study
44	<b>SSK98/2/Gr-05</b>	12.09	91.92	2030	This study
45	<b>Seamount rocks- Andesitic Dacite</b>	7.93	94.05	517	Kamesh Raju et al., 2012
46	<b>Seamount rocks- Rhyolite</b>	7.94	94.04	373	Kamesh Raju et al., 2012
47	<b>MD77-169</b>	10.2	95.05	2360	Colin et al., 2006
48	<b>RC12-344</b>	12.77	96.07	2140	Colin et al., 2006
49	<b>MD77-171</b>	11.75	94.15	1760	Colin et al., 2006
50	<b>MD77-176</b>	14.5	93.12	1375	Colin et al., 2006
51	<b>MD77-178</b>	17.18	93.08	2459	Colin et al., 2006
52	<b>SK234-60</b>	12.1	94.08	2000	Awasthi et al., 2014
53	<b>NGHP-17A</b>	10.75	93.1	1356	Ali et al., 2015
54	<b>ADM-09</b>	9.56	96.07	1242	Cao et al., 2016
55	<b>SK-175/120</b>	12.51	97.5	80	Damodara Rao et al., 2016
56	<b>SK-175/123</b>	12.25	97	175	Damodara Rao et al., 2016
57	<b>Salween R. BL</b>	16.53	97.62	NA	Damodara Rao et al., 2016
58	<b>SS172-4035</b>	13.01	94.12	2337	Bhushan, 2008
59	<b>SS172-4037</b>	10.82	94.65	3250	Bhushan, 2008
60	<b>SS172-4038</b>	6.55	94.24	1314	Bhushan, 2008

**Table 3.2.** Major element content and calculated weathering indices Al/K, CIA\*, CIW and PIA of surface sediments of Andaman Sea

Sr.No	Sample Name	SiO <sub>2</sub> (%)	Al <sub>2</sub> O <sub>3</sub> (%)	TiO <sub>2</sub> (%)	K <sub>2</sub> O (%)	Na <sub>2</sub> O (%)	CaO (%)	Al/K	CIA*	CIW	PIA
1	SK175/Gr03	73.4	15.3	0.8	1.9	0.9	0.3	4.2	81.3	89.2	87.6
2	SK175/Gr38	74.9	16.3	0.8	2.1	1.9	0.7	4.1	75.3	79.2	76.5
3	SK175/Gr48	65.1	20.8	1.0	2.7	1.1	0.3	4.1	81.5	90.3	88.8
4	SK175/Gr52	65.6	20.5	1.0	2.7	1.1	0.3	4.1	81.3	90.1	88.6
5	SK168/GC01	54.3	17.1	0.7	2.3	0.9	1.5	4.1	81.6	80.6	78.1
6	SK168/SPC01	55.1	17.8	0.7	2.4	0.5	0.5	4.0	83.9	91.4	90.1
7	SK168/SPC05	64.0	18.3	0.8	2.4	0.6	0.4	4.1	83.7	91.8	90.6
8	AAS11/GC01	61.3	15.9	0.7	2.4	1.0	1.1	3.6	79.2	81.5	78.7
9	RVS02/GC03	68.1	12.8	0.7	2.2	1.0	0.9	3.1	75.8	79.1	75.5
10	RVS02/GC04	66.2	18.0	0.8	2.7	0.9	0.5	3.7	80.4	87.8	85.9
11	SSK50/GC01	61.9	18.3	0.9	2.2	0.7	0.5	4.4	83.5	89.6	88.2
12	SSK50/GC02	65.3	15.7	0.8	1.8	1.0	0.8	4.7	81.8	84.1	82.3
13	SSK50/GC03A	64.5	15.3	0.9	2.1	1.0	0.6	4.0	80.0	85.1	83.0
14	SSK50/SPC01	60.3	16.8	0.9	2.1	0.7	0.4	4.4	83.4	89.9	88.6
15	SSK50/SPC02	57.7	16.5	0.9	2.0	1.0	0.5	4.4	81.3	86.3	84.6
16	SSK50/SPC03	70.4	10.5	0.8	1.2	1.5	1.3	4.6	73.4	68.9	65.9
17	SSK50/SPC04R	60.9	17.1	1.0	2.1	1.1	0.5	4.3	80.9	86.6	84.8
18	SSK50/SPC04A	62.6	15.9	0.9	2.0	1.0	0.5	4.3	80.6	85.9	84.0
19	SSK33/Grab02	70.4	12.9	0.0	1.2	3.0	1.8	5.9	67.5	61.1	58.6
20	SSD18/GC01	58.0	16.8	0.8	2.3	0.7	0.9	3.9	82.0	86.0	84.0
21	SSD18/GC03	53.5	16.0	0.8	1.8	0.8	2.0	4.8	83.0	76.3	73.9
22	SSD18/SPC02	55.3	17.1	1.1	0.8	1.7	6.8	11.3	82.3	53.0	51.7
23	SSD18/SPC03	55.2	16.8	0.8	2.4	0.6	0.4	3.7	82.4	90.5	88.9
24	SSD18/DR03	57.1	17.0	0.8	2.3	0.7	0.8	3.9	82.1	86.4	84.4
25	SSD18/DR08	54.8	18.3	0.8	2.9	0.6	0.5	3.4	81.4	90.4	88.7
26	SSD18/DR09	58.7	15.7	0.7	2.3	0.7	0.6	3.7	81.5	87.4	85.4
27	SSD18/DR10	57.7	16.0	0.7	2.2	0.6	0.7	3.8	82.1	87.6	85.7
28	SSK98/1/Gr-01	39.8	12.2	0.6	1.4	0.7	1.4	4.7	82.4	76.9	74.5
29	SSK98/1/GC-01	65.8	13.4	0.7	2.0	0.9	1.1	3.6	78.7	79.9	76.9
30	SSK98/1/Dr-06	50.6	19.7	0.8	0.3	1.4	10.0	30.5	87.8	48.9	48.4
31	SSK98/1/Gr-07	49.9	19.0	0.8	0.7	1.3	8.8	15.6	87.1	51.2	50.2
32	Corbyn's cove	91.5	3.6	0.4	0.4	0.6	0.8	5.5	72.0	58.5	55.8
33	SSK98/2/SPC-01	49.7	20.9	0.8	0.4	1.6	10.4	27.0	87.2	49.2	48.6
34	SSK98/2/SPC-02	59.8	16.7	0.8	2.4	0.7	0.6	3.7	81.5	88.4	86.5
35	SSK98/2/SPC-03	57.7	16.9	0.8	2.3	0.7	0.5	3.9	82.5	89.0	87.3
36	SSK98/2/SPC-04	79.2	6.9	0.3	0.8	0.8	0.9	4.9	76.6	70.4	67.7
37	SSK98/2/SPC-06	86.1	5.1	0.3	0.5	0.8	0.7	5.8	73.4	66.3	64.0
38	SSK98/2/SPC-07	76.9	9.7	0.6	1.1	1.1	0.5	4.7	76.3	77.9	75.6
39	SSK98/2/SPC-08	66.6	13.4	0.8	1.5	1.2	0.3	4.7	78.9	84.3	82.4
40	SSK98/2/SPC-12	92.2	3.9	0.5	1.0	0.6	0.5	2.2	66.6	68.0	61.0

Table 3.2. Continued...

41	SSK98/2/SPC-13	87.7	4.8	1.0	1.1	0.6	0.5	2.3	69.2	72.6	66.5
42	SSK98/2/Gr-01	85.7	7.1	0.5	1.7	0.9	1.0	2.2	68.1	69.0	62.0
43	SSK98/2/Gr-04	62.4	14.4	0.5	2.8	1.1	1.1	2.8	75.1	79.2	75.1
44	SSK98/2/Gr-05	58.4	15.2	0.8	2.2	0.8	1.4	3.7	80.4	79.8	76.9
45	Seamount rocks- Andesitic Dacite	64.4	15.5	0.8	0.8	4.2	5.0	10.1			
46	Seamount rocks- Rhyolite	71.1	15.0	0.5	0.6	4.6	3.6	18.6			
47	Barren lava-1832	51.1	21.3	0.8	0.4	3.0	11.3	29.3			
48	Barren lava-scoria-1991	54.9	17.7	1.2	0.6	4.0	8.4	15.1			
49	Barren lava-1995	51.5	21.6	0.8	0.4	3.0	11.3	27.5			
50	Barren Ash-1995	50.9	21.9	0.8	0.4	2.8	11.5	30.2			
51	Barren lava-2000	50.8	21.2	2.0	0.4	2.9	11.2	29.4			
52	SK234-60	NA	17.7	NA	1.4	5.2	3.0	6.93	73.4	55.1	53
53	ADM-09	33.7	11.3	0.4	1.7	17.0	NA	3.49	NA	NA	NA
54	SK-175/120	NA	0.9	0.1	0.5	0.1	0.1	1.04	51.1	71.6	52.6
55	SK-175/123	NA	2.6	0.4	0.8	0.1	0.2	1.84	65.9	83.3	77.3
56	Salween R. BL	NA	11.5	0.8	1.9	0.5	0.9	3.21	71.8	82.6	79.5

**Table 3.3.** Trace elemental content (in ppm), ratios of Rb/Sr,  $La_n/Yb_n$  and Total REE concentrations of surface sediments of Andaman Sea

Sr.No	Sample Name	Rb	Sr	La	Nd	Yb	Hf	Pb	Rb/Sr	$\Sigma$ REE	$La_n/Yb_n$
1	SK175/Gr03	90.2	61.6	23.2	19.8	1.3	0.5	6.1	1.5	108	1.4
2	SK175/Gr38	79.9	85.3	16.6	13.3	0.9	-0.7	6.3	0.9	75	1.4
3	SK175/Gr48	179.0	82.0	29.3	23.1	1.6	1.1	12.8	2.2	130	1.4
4	SK175/Gr52	153.1	75.3	27.9	21.8	1.4	-0.7	10.9	2.0	123	1.5
5	SK168/GC1	124.2	101.7	21.2	17.7	1.6	3.1	70.2	1.2	102	1.0
6	SK168/SPC1	134.5	77.2	23.6	20.0	1.4	2.2	128.0	1.7	108	1.2
7	SK168/SPC5	137.2	68.2	24.0	19.1	1.4	2.6	8.3	2.0	105	1.2
8	AAS11/GC1	107.4	121.4	18.6	14.9	1.1	-	9.7	0.9	86	1.3
9	RVS02/GC3	118.0	101.3	22.8	18.2	1.0	1.4	54.0	1.2	107	1.8
10	RVS02/GC4	152.6	84.6	27.3	23.0	1.4	1.8	18.0	1.8	123	1.5
11	SSK50/GC1	112.8	77.5	23.9	20.1	1.9	3.2	19.8	1.5	110	0.9
12	SSK50/GC2	108.5	66.3	23.8	19.7	1.7	2.9	16.2	1.6	107	1.0
13	SSK50/GC3A	110.9	109.5	23.1	18.6	1.8	3.6	49.0	1.0	104	1.0
14	SSK50/SPC1	79.1	77.1	16.3	14.2	1.4	2.8	4.7	1.0	77	0.8
15	SSK50/SPC02	110.7	100.5	23.3	22.0	1.6	-	10.4	1.1	107	1.0
16	SSK50/SPC03	56.4	104.1	15.3	17.3	1.5	-	6.4	0.5	80	0.8
17	SSK50/SPC04R	119.4	101.1	23.6	22.6	1.6	-	9.1	1.2	107	1.1
18	SSK50/SPC04A	110.4	100.6	23.8	23.0	1.5	-	9.1	1.1	111	1.2
19	SSK33/Gr2	21.4	643.3	12.4	11.5	2.8	3.2	76.0	0.0	74	0.3
20	MD77-169	117.3	129.7	NA	24.0	NA	NA	NA	0.9	NA	NA
21	RC12-344	NA	106.3	NA	29.1	NA	NA	NA	NA	NA	NA
22	MD77-171	NA	162.8	NA	21.5	NA	NA	NA	NA	NA	NA
23	MD77-176	124.7	113.0	NA	24.2	NA	NA	NA	1.1	NA	NA
24	MD77-178	NA	98.9	NA	16.8	NA	NA	NA	NA	NA	NA
25	SK234-60	108.4	64.0	14.0	12.0	1.7	1.9	7.2	1.7	67	0.6
26	SK-175/120	NA	10.0	NA	4.3	NA	NA	NA	NA	NA	NA
27	SK-175/123	NA	16.0	NA	16.5	NA	NA	NA	NA	NA	NA
28	Salween R. BL	NA	70.0	NA	21.3	NA	NA	NA	NA	NA	NA

**Table 3.4.** Nd, Sr and Hf isotopic composition of surface sediments of Andaman Sea

Sr.No	Sample Name	$^{87}\text{Sr}/^{86}\text{Sr}$	$^{143}\text{Nd}/^{144}\text{Nd}$	$\epsilon_{\text{Nd}}$	$^{176}\text{Hf}/^{177}\text{Hf}$	$\epsilon_{\text{Hf}}$
1	SK175/Gr03	0.714849	0.512183	-8.9	0.282571	-7
2	SK175/Gr38	0.713429	0.512191	-8.7	0.282487	-10
3	SK175/Gr48	0.720063	0.512065	-11.2	0.282499	-9.5
4	SK175/Gr52	0.721543	0.512106	-10.4	0.282543	-8
5	SK168/GC01	0.717078	0.512137	-9.8	0.282657	-4
6	SK168/SPC01	0.720374	0.512108	-10.3	0.282668	-3.6
7	SK168/SPC05	0.719989	0.512121	-10.1	0.28271	-2.1
8	AAS11/GC01	0.718884	0.512108	-10.3	0.282696	-2.6
9	RVS02/GC03	0.724732	0.512028	-11.9	0.282494	-9.7
10	RVS02/GC04	0.721787	0.512051	-11.5	0.282575	-6.9
11	SSK50/SPC01	0.714435	0.512247	-7.6	0.282642	-4.5
12	SSK50/GC01	0.718818	0.51221	-8.3	0.282762	-0.3
13	SSK50/GC02	0.718713	0.512197	-8.6	0.282757	-0.4
14	SSK50/GC03A	0.717153	0.512187	-8.8	0.282715	-1.9
15	SSK33/Grab02	0.705472	0.51284	3.9	0.283151	13.5
16	MD77-169	0.71434	0.512125	-10	NA	NA
17	RC12-344	0.71665	0.512059	-11.3	NA	NA
18	MD77-171	0.71233	0.512164	-9.2	NA	NA
19	MD77-176	0.71534	0.512162	-9.3	NA	NA
20	MD77-178	0.71453	0.512199	-8.6	NA	NA
21	SK234-60	0.70944	0.512354	-5.5	NA	NA
23	NGHP-17A	0.7126	0.512274	-7.1	NA	NA
22	ADM-09	0.718636	0.512043	-11.6	NA	NA
23	SK-175/120	0.7384	0.511753	-17.3	NA	NA
24	SK-175/123	0.742183	0.511763	-17.1	NA	NA
25	Salween R. BL	0.731794	0.511885	-14.7	NA	NA
26	SS172-4035	0.7125	NA	-8.95	NA	NA
27	SS172-4037	0.7164	NA	-10.21	NA	NA
28	SS172-4038	0.7138	NA	-11.55	NA	NA
29	Barren Is rocks	0.70395	0.512857	4.3	NA	NA
30	Barren Is rocks	0.703804	0.512985	6.8	NA	NA
31	Barren Scoria	0.704053	0.512846	4.1	NA	NA

**Table. 3.5.** Major element content and calculated Al/K, CIA\*, CIW and PIA in sediments from the core SK168/GC01 shown against subsurface depth and age.

Mean depth (cm)	Age (ka)	SiO <sub>2</sub> (%)	Al <sub>2</sub> O <sub>3</sub> (%)	TiO <sub>2</sub> (%)	K <sub>2</sub> O (%)	CaO (%)	Na <sub>2</sub> O (%)	Al/K	CIA*	CIW	PIA
1	0.88	54.3	17.1	0.7	2.3	1.5	0.9	4.8	82	81	78
5	1.39	55.5	17.3	0.7	2.3	1.3	0.9	4.7	81	81	79
9	1.89	55.3	17.3	0.7	2.4	1.2	0.9	4.7	81	83	81
17	2.9	56	17.4	0.7	2.3	1.1	0.8	4.8	82	84	82
21	3.41	56.4	17.2	0.7	2.3	1.3	0.9	4.8	81	82	79
25	3.92	56.1	17.1	0.7	2.4	1.2	0.9	4.6	81	83	80
33	4.93	56.3	17.6	0.7	2.4	0.8	0.6	4.7	83	88	86
37	5.43	56.3	17.5	0.7	2.4	1.1	0.7	4.7	82	85	82
41	5.94	56.5	17.6	0.7	2.4	1.1	0.8	4.6	82	84	82
49	6.95	56.9	17.9	0.8	2.3	1.2	0.8	4.9	82	83	81
56	7.83	55.5	17.3	0.8	2.3	1.3	0.9	4.8	81	82	79
61	8.47	56.9	18	0.8	2.4	0.7	0.7	4.9	83	88	87
66	9.1	56.3	17.7	0.8	2.4	0.9	0.8	4.7	82	86	84
71	9.73	55.6	17.6	0.8	2.4	1.1	0.8	4.7	82	84	82
73.5	10.05	55.7	17.5	0.7	2.3	0.9	0.7	4.8	82	86	84
77.5	10.5	55.5	17.7	0.8	2.4	1.3	0.8	4.7	82	83	81
83.5	11.1	55.5	17.8	0.8	2.4	1.2	0.8	4.8	82	84	81
88.5	11.59	56.1	18.8	0.8	2.5	1	0.8	4.8	83	86	84
101	12.96	55.1	18	0.8	2.4	1.3	0.7	4.7	83	83	81
106	13.6	54.8	18.2	0.8	2.8	1	0.9	4.1	80	85	82
111	14.23	54.7	18.1	0.8	2.5	1.1	0.7	4.6	82	85	83
116	14.87	54.6	18.4	0.7	2.6	0.8	0.7	4.6	83	87	86
121	15.51	54.4	18.7	0.7	2.6	0.8	0.7	4.5	82	87	86
126	16.14	53.8	18.7	0.7	2.7	1.1	0.8	4.4	82	85	83
131	16.78	53.9	18.6	0.8	2.7	1.2	0.8	4.4	82	84	82
138.5	17.74	54.2	18.6	0.8	2.6	1.9	0.9	4.6	81	79	76
141	18.06	54.4	18.4	0.8	2.6	1.8	0.9	4.6	81	79	77
148.5	19.01	55	18.5	0.8	2.8	1	0.8	4.3	81	85	83
151	19.33	54.4	18.3	0.8	2.7	1.2	0.9	4.3	81	83	81
156	19.97	54	18.3	0.8	2.7	1	0.8	4.2	81	85	83
161	20.61	54.5	18.5	0.8	2.8	1	0.8	4.2	81	85	83
163.5	20.92	54.3	18.3	0.8	2.8	0.9	0.8	4.2	81	86	84
168.5	21.56	54.5	18.3	0.8	2.8	1.1	0.9	4.2	80	84	82
171	21.88	54.8	18	0.8	2.8	0.8	0.8	4.2	81	86	84
178.5	22.84	54.6	18.2	0.8	2.8	0.8	0.8	4.1	81	86	84
181	23.15	54.2	18.1	0.8	2.7	1.1	0.7	4.2	81	85	82
186	23.79	54.6	18	0.7	2.5	1.1	0.8	4.6	82	85	83
188.5	24.11	54.4	18	0.8	2.8	1.1	0.8	4.1	80	85	82
191	24.79	55.1	18.4	0.8	2.9	0.7	0.8	4.1	81	88	86

Table. 3.5. *Continued...*

196	26.16	54.3	18.3	0.8	2.9	1.2	0.7	4.1	81	84	82
198.5	26.85	55.5	18.4	0.8	3	0.8	0.9	4	80	87	84
202.5	27.95	55.1	18.4	0.7	2.8	1	0.8	4.1	81	85	83
212.5	30.69	54.4	18.3	0.8	2.8	0.8	0.8	4.1	81	87	85
227.5	33.13	54.9	18.5	0.8	2.8	0.8	0.8	4.2	81	87	84
237.5	34.2	55.2	18.5	0.8	2.8	1.2	1	4.3	80	83	80
247.5	35.27	52.7	17.7	0.7	2.7	1.3	0.7	4.2	81	84	81
257.5	36.34	55.2	18.8	0.8	2.8	0.8	0.8	4.3	81	87	85
277.5	38.48	54.6	18.5	0.7	2.8	0.8	0.7	4.3	82	88	86
282.5	39.01	55.1	18.8	0.8	2.8	0.7	0.7	4.2	82	89	87
292.5	40.08	55	18.5	0.7	2.9	0.7	0.7	4.1	81	89	87
312.5	42.22	55.4	18.5	0.7	2.9	0.6	0.7	4.1	81	89	87
322.5	43.29	54.9	18.4	0.7	2.9	0.7	0.7	4.1	81	88	86
332.5	44.36	55.3	18.6	0.7	2.9	0.6	0.7	4.1	81	90	88
342.5	45.43	55.5	18.7	0.7	2.9	0.5	0.7	4.1	81	90	88
352.5	46.5	55.7	18.7	0.7	2.9	0.8	0.7	4.1	81	88	86
357.5	47.04	55.6	18.6	0.7	2.9	0.7	0.7	4.1	81	88	86
367.5	48.11	55.8	18.4	0.7	2.9	0.7	0.8	4	81	88	85
377.5	49.18	54.6	18.1	0.8	2.9	0.9	0.7	4	81	87	84
387.5	50.25	55.2	18.5	0.7	2.8	0.6	0.7	4.2	82	89	87
397.5	51.32	55.2	18.4	0.8	2.9	0.8	0.7	4.1	81	88	86
407.5	52.39	55.5	18.3	0.7	3	0.8	0.7	3.9	80	88	85
417.5	53.46	55.1	18.5	0.7	2.9	0.6	0.7	4	81	89	87

*\*excluded CaO (%) in CIA formula as it is showing no variation.*

**Table. 3.6.** Major element content and calculated Al/K, CIA\*, CIW and PIA in sediments from the core AAS11/GC01 shown against subsurface depth and age.

Mean depth (cm)	Age ka	SiO <sub>2</sub> (%)	Al <sub>2</sub> O <sub>3</sub> (%)	TiO <sub>2</sub> (%)	K <sub>2</sub> O (%)	CaO (%)	Na <sub>2</sub> O (%)	Al/K	CIA*	CIW	PIA
8.5	2.1	61.3	15.87	0.74	2.39	1.12	0.95	4.2	79	81	79
13.5	3	55.8	15.1	0.66	2.26	2.8	0.92	4.3	79	70	66
16.5	3.2	58.3	15.46	0.68	2.3	2.36	1	4.3	79	72	69
22	3.7	58.3	15.41	0.69	2.3	1.83	0.84	4.3	80	77	73
24	3.9	58	15.16	0.68	2.28	2.14	0.86	4.2	80	74	71
32	4.5	62.4	15.81	0.75	2.33	0.93	0.78	4.3	81	84	82
34	4.6	58.1	15.08	0.65	2.21	2.5	0.83	4.4	80	72	68
37	4.9	54.9	14.54	0.64	2.12	3.08	0.86	4.4	80	67	64
40.5	5.3	56	14.96	0.67	2.21	2.72	0.86	4.3	80	70	66
44	5.7	56.3	15.13	0.68	2.18	2.8	0.84	4.4	80	70	66
45.5	5.9	63.5	16.48	0.78	2.37	0.94	0.79	4.4	81	85	82
52	6.6	62.8	16.28	0.76	2.38	1.17	0.85	4.4	80	82	80
57	7.2	51.3	16.85	0.7	2.43	3.41	0.73	4.4	82	69	66
62	7.8	61.4	16.66	0.79	2.3	1.01	0.84	4.6	81	84	82
72	9	62.2	16.44	0.8	2.27	1.06	0.8	4.6	81	84	81
77	9.6	60.3	16.15	0.78	2.26	1.26	0.95	4.6	80	81	78
82	10.3	54.7	15.47	0.72	2.22	2.31	1.07	4.4	79	72	69
87	10.9	56.1	15.5	0.72	2.19	2.02	1.13	4.5	79	74	70
92	11.5	57.6	15.68	0.75	2.24	1.81	0.89	4.5	80	77	74
94	11.8	50.3	14.55	0.65	2.09	4.08	1.21	4.4	77	61	57
100.5	12.6	57.6	16.03	0.75	2.27	2.02	0.79	4.5	81	76	73
102	12.8	53	15.39	0.69	2.22	3.46	0.8	4.4	81	67	63
107	13.4	59.4	16.9	0.79	2.39	1.09	0.69	4.5	82	84	82
112	14	58.8	16.79	0.78	2.36	1.36	0.71	4.5	82	82	80
117	14.6	55.6	16.12	0.74	2.32	2.4	0.79	4.4	81	74	71
122	15.2	57.4	16.75	0.76	2.42	1.76	0.74	4.4	81	79	76
127	15.8	55.2	15.27	0.71	2.16	2.38	0.94	4.5	80	72	69
132	16.4	51.5	16.07	0.71	2.42	3.25	0.94	4.2	79	68	64
137	17	55	16.71	0.78	2.56	1.99	0.71	4.2	81	78	74
142	17.4	58.4	17.1	0.82	2.61	0.97	0.66	4.2	81	86	83
147	17.8	52.7	16.48	0.72	2.46	3.95	0.85	4.3	80	66	62
152	18.1	55	16.44	0.74	2.52	2.98	0.95	4.2	79	70	66
157	18.5	59.7	17.4	0.82	2.59	1.17	0.76	4.3	81	84	81
162	18.9	56.7	16.45	0.73	2.46	2.51	0.94	4.3	80	73	69
167	19.3	62.2	16.33	0.7	2.47	1.48	1.36	4.2	77	77	73
172	19.7	65.8	15.62	0.62	2.4	1.15	1.83	4.1	74	75	72
177	20.1	58.3	14.29	0.53	2.23	2.89	1.78	4.1	73	64	59
182	20.3	58.4	15.59	0.64	2.41	2.75	1.55	4.1	75	67	63
187	20.8	54.5	15.94	0.7	2.47	3.06	0.98	4.1	79	69	65

Table 3.6. Continued...

192	21.3	61.2	16.66	0.78	2.53	1.04	0.77	4.2	81	84	82
197	21.7	61.1	16.41	0.75	2.55	1.06	0.88	4.1	80	83	80
202	22.3	55.3	16.27	0.72	2.51	2.68	0.77	4.1	80	73	69
207	22.8	55.5	16.32	0.72	2.53	2.67	0.8	4.1	80	73	69
212	23.4	54.5	15.98	0.71	2.49	2.63	0.78	4.1	80	73	69
217	24	57.6	16.52	0.75	2.6	1.83	0.78	4.1	80	78	75
222	24.5	58.3	16.82	0.78	2.65	1.64	0.74	4	81	80	77
227	25.1	59.7	16.96	0.81	2.74	0.95	0.79	3.9	80	85	82
232	25.7	58.4	16.33	0.77	2.6	1.73	0.81	4	80	78	75
237	26.2	59.9	17.06	0.81	2.68	0.94	0.76	4.1	81	85	83
242	26.8	60.2	16.89	0.79	2.67	0.9	0.81	4	80	85	83
247	27.3	60.6	16.59	0.78	2.57	1.07	0.79	4.1	80	84	81
252	27.9	59.1	16.81	0.76	2.62	0.93	0.83	4.1	80	85	82
257	28.5	59	16.82	0.76	2.62	0.9	0.83	4.1	80	85	82
262	29	57.1	16.31	0.75	2.54	1.56	0.84	4.1	80	79	76
267	29.6	59.3	17.03	0.79	2.81	1.3	0.95	3.9	79	81	78
272	30.2	56.3	16.41	0.72	2.52	1.62	0.88	4.1	80	79	76
277	30.7	59.2	17.16	0.77	2.63	1.02	0.72	4.2	81	85	83
282	31.3	59.1	17.03	0.76	2.67	0.98	0.68	4.1	81	85	83
287	31.9	58.4	16.28	0.76	2.56	1.17	0.68	4.1	81	83	81
292	32.4	58.6	16.46	0.75	2.53	1.19	0.7	4.2	81	83	81
287	33	59.4	17.25	0.75	2.58	1.07	0.7	4.3	81	85	82
302	33.6	56.5	16.74	0.7	2.52	1.9	0.75	4.2	81	78	75
307	34.1	58.8	16.97	0.74	2.59	1.78	0.75	4.2	81	79	76
312	34.7	56.6	16.95	0.71	2.54	1.48	0.71	4.3	81	81	79
317	35.3	60.5	17.33	0.75	2.57	1.25	0.71	4.3	82	83	81
322	35.8	54.8	17.04	0.69	2.57	2.34	0.82	4.2	81	75	72
327	36.4	61.7	17.49	0.77	2.65	1.06	0.79	4.2	81	84	82
332	37	60.4	17.3	0.75	2.6	1.3	0.76	4.2	81	83	80
337	37.6	55.7	16.64	0.69	2.5	1.98	0.82	4.2	80	77	74
342	38.1	60.1	17.54	0.76	2.61	0.74	0.69	4.3	82	88	86
347	38.7	55.6	16.7	0.69	2.48	2.22	0.84	4.3	80	75	72
352	39.3	55.2	16.44	0.68	2.52	2.49	0.74	4.2	81	74	71
357	39.8	60.9	17.24	0.76	2.6	0.86	0.67	4.2	82	87	84
362	40.4	55.6	16.51	0.71	2.56	2.31	0.79	4.1	80	75	71
367	41	59.7	17.25	0.77	2.68	0.81	0.65	4.1	81	87	85
372	41.6	60.3	17.43	0.77	2.63	0.89	0.66	4.2	82	87	84
377	42.1	58.5	17.6	0.74	2.67	0.95	0.67	4.2	82	86	84
382	42.7	56	17.12	0.71	2.63	1.92	0.74	4.1	81	78	75
387	43.3	56.5	16.68	0.72	2.6	1.74	0.79	4.1	80	79	76
392	43.8	59.2	16.97	0.75	2.58	1.39	0.77	4.2	81	82	79

397	44.4	60	16.71	0.76	2.64	0.97	0.86	4	80	84	81
402	45	59.9	16.56	0.73	2.59	1.3	0.74	4.1	81	82	79

**Table 3.6.** *Continued...*

407	45.6	59.5	17.44	0.75	2.67	1.06	0.68	4.2	81	85	83
412	46.1	57.9	16.47	0.73	2.6	1.92	0.78	4	80	78	74
417	46.7	58.2	16.78	0.75	2.74	1.45	0.75	3.9	80	81	78
422	47.3	60.5	16.48	0.77	2.69	1.15	0.75	3.9	80	83	80
427	47.8	61.4	16.67	0.75	2.66	1	0.76	4	80	84	82

\*excluded CaO (%) in CIA formula as it showing no variation.

**Table 3.7.** *Major element content and calculated Al/K, CIA\*, CIW and PIA in sediments from the core RVS02/GC03 shown against subsurface depth and age.*

Mean depth (cm)	Age ka	SiO <sub>2</sub> (%)	Al <sub>2</sub> O <sub>3</sub> (%)	TiO <sub>2</sub> (%)	K <sub>2</sub> O (%)	CaO (%)	Na <sub>2</sub> O (%)	Al/K	CIA*	CIW	PIA
7.5	0.3	68.1	12.8	0.7	2.2	0.9	1	3.7	76	79	75
11.5	0.5	69.3	12.1	0.7	2.2	1.3	1.1	3.5	74	74	70
22.5	1	69.8	12.2	0.7	2.1	1.4	1.2	3.6	74	73	69
30.5	1.3	72.3	11.8	0.7	2.2	1.1	1.1	3.4	74	76	71
40.5	1.7	68.6	12.3	0.7	2.2	1.6	1.2	3.6	74	72	67
52.5	2.2	71.8	11.9	0.7	2.2	1.2	1.2	3.4	73	74	69
60.5	2.6	70.3	12.2	0.7	2.3	1.3	1.2	3.5	73	74	69
70.5	3.1	66.3	12.2	0.7	2.1	1.5	1.1	3.6	74	72	68
82.5	3.7	58.2	11.3	0.6	2	3.5	1.3	3.7	72	57	52
92.5	4.2	67.6	12.2	0.6	2.1	1.4	1.3	3.7	73	72	68
101	4.6	69.6	12.1	0.7	2.2	1.8	1.4	3.5	72	68	64
111	5.1	68.1	12.9	0.7	2.2	1.5	1.2	3.7	75	73	69
121	5.6	70.2	12.7	0.7	2.3	1.3	1.2	3.6	74	74	70
131	5.9	64.5	12	0.6	2.1	2	1.2	3.6	74	68	63
141	6.1	69.2	12.1	0.7	2.3	1.1	1.1	3.4	74	76	71
151	6.3	70.7	12	0.7	2.3	1	1.2	3.3	73	76	72
161	6.5	69.9	12.5	0.7	2.3	0.9	1.1	3.5	74	78	74
171	6.8	69	12.8	0.7	2.4	0.8	1.1	3.4	74	80	76
181	7	68	12.9	0.7	2.2	0.8	1	3.7	76	81	77
191	7.2	65.2	13	0.7	2.2	1.1	1	3.8	77	78	74
201	7.4	63.4	13.5	0.7	2.3	1.5	1.2	3.8	75	74	70
211	7.7	65.3	13.9	0.7	2.4	1.3	1.2	3.8	76	77	73
221	8.4	62.7	13.3	0.7	2.2	1.6	1.1	3.8	76	73	69
231	9.1	62.7	13.4	0.7	2.2	1.6	1.1	3.9	76	74	70
241	9.9	60	12.4	0.7	2.1	1.4	1	3.7	76	75	71
251	10.6	63.3	13	0.7	2.2	1.8	1.1	3.7	76	72	67
261	11.3	62.8	12.8	0.7	2.3	2.1	1.1	3.6	75	69	65

271	12.1	62.1	13.7	0.7	2.2	1.8	1	4	77	74	70
-----	------	------	------	-----	-----	-----	---	---	----	----	----

**Table 3.7.** *Continued...*

281	12.8	62.7	13.2	0.7	2.2	1.8	1.1	3.8	76	72	68
291	13.5	62.4	13	0.7	2.2	1.9	1.1	3.9	76	72	68
301	14.1	63.5	15.1	0.7	2.2	1.9	1.1	4.4	79	74	71
311	14.6	62.8	13.3	0.7	2.1	1.8	1.1	4	77	73	69
321	15.1	65.1	13.7	0.8	2.4	1	1	3.6	76	80	76
331	15.6	59.7	13.4	0.7	2.2	2.5	1.1	3.8	76	68	64
341	16.2	61.5	14.1	0.7	2.3	2	1	3.8	77	73	69
351	16.7	61.1	14.3	0.7	2.4	1.6	1	3.8	77	76	72
361	17.2	63.3	14.1	0.7	2.5	1.6	1.1	3.7	76	75	71
371	17.9	62.2	14.4	0.8	2.5	1.5	1	3.7	77	77	73
381	18.5	60.9	14.3	0.7	2.4	1.7	1.1	3.7	76	75	71
391	19.1	61.5	14.1	0.7	2.4	1.6	1	3.8	77	76	72
401	19.7	70.1	13.6	0.8	2.5	0.6	1.1	3.4	75	82	79
411	20.3	61.4	14.3	0.7	2.4	1.4	1	3.8	77	77	74
421	20.9	55.6	13.1	0.6	2.2	3.4	1.4	3.8	74	61	56
431	21.6	63.1	14.2	0.7	2.5	1.1	1	3.7	77	79	76
441	22.2	60.4	14.3	0.7	2.4	1.4	1	3.8	77	77	73
451	22.8	61.6	14.5	0.7	2.4	1	0.9	3.8	78	81	78
461	23.4	63	14.5	0.7	2.5	1	1	3.7	77	80	77
471	24	54.5	13.1	0.6	2.2	3.6	1.4	3.8	74	60	55
481	24.7	65.2	12.9	0.7	2.3	1.1	1.1	3.5	75	78	74
491	25.3	55.6	13.1	0.7	2.3	3.6	1.3	3.7	74	60	55
501	25.9	60.8	12.7	0.7	2.3	2.5	1.2	3.6	74	66	61
511	26.5	68.8	12.6	0.7	2.4	0.9	1.1	3.3	74	78	74
521	27.1	64	13.9	0.7	2.2	1.4	1.6	4.1	74	73	69
531	27.8	64.2	14.6	0.8	2.4	0.6	1	3.8	78	84	81
541	28.4	67.4	13.3	0.7	2.4	0.9	1	3.5	76	80	77
551	29	62.1	14	0.7	2.3	1.3	1	3.8	77	78	74
561	29.6	64.3	14	0.8	2.4	0.8	0.9	3.7	77	82	79

*\*excluded CaO (%) in CIA formula as it showing no variation*

**Table 3.8.** Trace elemental content (ppm), ratios of Ni/Co, Rb/Sr, Th/Yb, La<sub>n</sub>/Yb<sub>n</sub> and Total REE concentrations of the core SK168/GC01 shown against sediment depth and age

Mean Depth (cm)	Age ka	Co	Ni	Rb	Sr	La	Yb	Th	Ni/Co	Rb/Sr	Th/Yb	TREE	La <sub>n</sub> /Yb <sub>n</sub>
1	0.88	26	126	124	102	21	2	13	4.8	1.2	8.2	102	1
5	1.39	21	100	130	120	18	1	12	4.8	1.1	8.7	88.3	1
9	1.89	24	112	134	128	26	2	16	4.6	1	9	117	1.1
17	2.9	23	108	137	87	18	1	12	4.7	1.6	9.2	94.5	1
21	3.41	16	99	134	129	26	2	16	6.2	1	9.1	114	1.1
25	3.92	19	100	127	118	23	2	15	5.4	1.1	8.9	107	1
33	4.93	17	125	149	95	29	2	18	7.2	1.6	9.9	125	1.2
37	5.43	16	107	140	103	25	2	16	6.7	1.4	9.6	115	1.1
41	5.94	16	106	135	124	24	2	13	6.6	1.1	8.6	106	1.2
49	6.95	15	97	124	111	22	2	14	6.7	1.1	8.5	101	1
56	7.83	15	114	131	125	23	2	14	7.4	1	8.5	106	1
61	8.47	16	115	140	89	25	2	15	7.4	1.6	9.1	112	1.1
66	9.1	17	124	144	129	25	2	15	7.4	1.1	9	112	1.1
71	9.73	16	132	136	128	24	2	15	8.2	1.1	8.9	109	1.1
73.5	10.05	18	121	141	129	28	2	17	6.9	1.1	8.8	124	1.1
77.5	10.5	18	120	144	132	25	2	16	6.7	1.1	9	114	1.1
83.5	11.1	18	122	147	128	23	2	15	6.8	1.1	9.1	109	1.1
88.5	11.59	18	122	138	111	18	1	12	6.6	1.2	9	88.5	1
101	12.96	19	129	134	91	16	1	9.6	6.8	1.5	8.8	77.4	1
106	13.6	31	114	156	96	20	1	13	3.7	1.6	10.5	97.6	1.1
111	14.23	20	132	141	109	13	1	9.6	6.6	1.3	10.4	70.6	1.1
116	14.87	19	120	140	111	26	2	16	6.4	1.3	10	114	1.2
121	15.51	19	124	142	95	14	1	11	6.4	1.5	11.2	74.2	1.1
126	16.14	20	119	137	105	23	1	13	6	1.3	9.5	104	1.2
131	16.78	21	118	142	108	21	1	14	5.6	1.3	10.4	100	1.2
138.5	17.74	23	111	139	114	25	2	15	4.9	1.2	8.4	113	1
141	18.06	22	104	135	111	24	2	14	4.8	1.2	8.3	108	1.1
148.5	19.01	23	114	150	95	24	2	15	4.9	1.6	9.4	110	1.1
151	19.33	25	121	147	101	22	2	14	4.8	1.4	9.5	103	1.1
156	19.97	27	124	160	106	25	2	17	4.6	1.5	9.9	119	1.1
161	20.61	29	131	159	106	27	2	17	4.5	1.5	9.6	125	1.1
163.5	20.92	26	112	160	100	27	2	17	4.3	1.6	9.7	123	1.2
168.5	21.56	28	113	154	104	21	1	14	4.1	1.5	10.2	102	1.1
171	21.88	28	120	166	107	28	2	17	4.2	1.5	9.5	126	1.1
178.5	22.84	28	112	164	100	19	1	13	4	1.7	10.3	95.8	1.1
181	23.15	29	112	147	85	16	1	11	3.9	1.7	10.3	82.7	1.1
186	23.79	18	123	138	122	24	2	15	6.7	1.1	9.3	108	1.1
188.5	24.11	31	110	165	105	22	1	15	3.6	1.6	10.5	106	1.1
191	24.79	28	105	160	92	25	2	16	3.8	1.7	10.6	112	1.2

**Table 3.8.** *Continued...*

196	26.16	31	119	168	110	28	2	17	3.9	1.5	10.1	125	1.2
202.5	27.95	33	121	170	105	28	2	18	3.7	1.6	9.9	130	1.2
212.5	30.69	27	141	173	103	26	2	17	5.3	1.7	10	122	1.1
227.5	33.13	26	120	165	100	26	2	16	4.6	1.7	10.6	120	1.2
237.5	34.2	24	112	154	88	16	1	10	4.7	1.7	9.5	82.3	1
247.5	35.27	26	121	165	106	24	2	16	4.7	1.6	10.7	114	1.2
257.5	36.34	24	132	175	106	29	2	18	5.6	1.7	9.9	132	1.2
277.5	38.48	23	123	167	89	20	1	14	5.5	1.9	12	97.7	1.2
282.5	39.01	21	122	177	96	28	2	18	5.9	1.8	10.7	126	1.2
292.5	40.08	21	119	181	98	30	2	19	5.7	1.8	10.6	134	1.3
312.5	42.22	21	121	181	97	27	2	18	5.9	1.9	10.2	126	1.2
322.5	43.29	19	115	178	98	26	2	17	6	1.8	11.1	119	1.3
332.5	44.36	20	120	178	89	23	1	14	6	2	10	104	1.2
342.5	45.43	21	120	184	92	23	1	16	5.7	2	11.7	108	1.2
352.5	46.5	20	121	178	97	27	1	17	6.1	1.8	11.6	120	1.4
357.5	47.04	20	119	157	85	21	1	10	6.1	1.9	9.2	96.6	1.4
367.5	48.11	21	119	173	87	18	1	12	5.7	2	10	87.9	1.2
377.5	49.18	19	108	170	104	28	2	17	5.6	1.6	9.3	127	1.2
387.5	50.25	20	124	172	91	23	1	16	6.1	1.9	12.1	107	1.3
397.5	51.32	21	121	172	93	24	1	16	5.7	1.8	11.4	111	1.3
407.5	52.39	25	136	179	97	27	2	17	5.4	1.8	11.1	122	1.3
417.5	53.46	19	109	182	89	22	1	13	5.8	2.1	10.1	99.8	1.2

$La_n/Yb_n$  are normalized ratios to Post Archean Australian Shale-PAAS (Taylor and McLennan, 1985)

**Table. 3.9.** Trace elemental content (ppm), ratios of Ni/Co, Rb/Sr, Th/Yb, La<sub>n</sub>/Yb<sub>n</sub> and Total REE concentrations of the core AAS11/GC01 shown against sediment depth and age

Mean depth (cm)	Age ka	Co	Ni	Rb	Sr	La	Yb	Th	Ni/Co	Rb/Sr	Th/Yb	TREE	La <sub>n</sub> /Yb <sub>n</sub>
8.5	2.1	6.1	42	107	121	19	1.1	11	6.9	0.9	10.1	86	1.2
13.5	3	8.6	54	88	150	17	1.1	9.3	6.2	0.6	8.6	78	1.1
16.5	3.2	7.2	43	89	135	16	1	9.6	6	0.7	9.5	75	1.2
22	3.7	7.7	49	97	124	18	1.1	10.4	6.4	0.8	9.4	82	1.2
24	3.9	7.2	46	93	129	17	1.1	10	6.4	0.7	9.2	78	1.2
32	4.5	5.5	51	107	101	18	1.1	11.5	9.2	1.1	10.8	83	1.2
34	4.6	8.5	47	88	137	16	1	9.6	5.6	0.6	9.5	74	1.2
37	4.9	8	74	82	150	15	1	9.1	9.1	0.5	9.1	73	1.1
40.5	5.3	8.1	49	90	144	16	1.1	9.7	6.1	0.6	9	78	1.1
44	5.7	7.9	49	87	144	17	1.1	9.6	6.2	0.6	9.1	77	1.1
45.5	5.9	5.2	43	104	101	17	1	11.2	8.3	1	10.8	79	1.2
52	6.6	5.9	52	101	106	17	1	10.6	8.8	1	10.5	78	1.2
57	7.2	16.5	92	103	145	18	1	10.4	5.6	0.7	10.1	83	1.3
62	7.8	6.7	56	112	107	19	1.2	11	8.3	1	9.5	87	1.2
72	9	5.6	64	99	106	18	1.1	10.5	11.4	0.9	9.5	82	1.2
77	9.6	6.5	51	96	115	18	1.1	10.2	7.9	0.8	9.6	80	1.2
82	10.3	9.7	70	92	126	17	1.2	9.5	7.2	0.7	7.9	78	1
87	10.9	8.3	67	90	116	16	1.1	9.2	8.2	0.8	8	76	1
92	11.5	8.5	63	95	109	16	1.1	9.7	7.4	0.9	8.7	75	1
94	11.8	11.2	65	81	167	16	1.2	9.2	5.8	0.5	8	75	1
100.5	12.6	8	55	99	115	18	1.2	11.2	6.9	0.9	9.3	82	1.1
102	12.8	9.4	55	83	138	16	1.1	9.8	5.9	0.6	9.2	74	1.1
107	13.4	7.9	46	101	93	17	1.1	11.6	5.8	1.1	10.6	80	1.1
112	14	8.2	53	94	107	19	1.3	12.7	6.4	0.9	10.2	90	1.1
117	14.6	9.1	58	101	126	18	1.1	11.8	6.4	0.8	10.5	83	1.2
122	15.2	8.5	52	93	100	18	1.2	12	6.2	0.9	10.2	84	1.1
127	15.8	8.5	56	88	129	18	1.3	10	6.5	0.7	7.9	82	1
132	16.4	9.4	53	104	125	16	1	10.4	5.7	0.8	10.1	76	1.2
137	17	10.6	55	96	97	17	1.2	11.3	5.2	1	9.7	83	1.1
142	17.4	8.6	44	99	75	15	1	10.9	5.2	1.3	11.1	76	1.1
147	17.8	13	64	95	155	17	1.2	10.6	4.9	0.6	8.8	81	1
152	18.1	11.7	49	95	117	16	1.1	10	4.2	0.8	8.8	78	1.1
157	18.5	8.2	55	101	87	19	1.2	12.4	6.7	1.2	10.1	89	1.1
162	18.9	11.1	57	98	113	17	1.3	10.9	5.1	0.9	8.7	81	1
167	19.3	8	37	98	95	18	1.5	11	4.7	1	7.1	86	0.8
172	19.7	5.2	26	84	80	16	1.7	9.2	5.1	1.1	5.4	78	0.7

Table 3.9. Continued...

177	20.1	8.5	35	73	123	15	1.6	8.1	4.1	0.6	5	74	0.7
182	20.3	9	50	86	119	16	1.5	9.3	5.5	0.7	6.2	78	0.8
187	20.8	11.9	56	94	128	17	1.2	10.4	4.7	0.7	9	79	1.1
192	21.3	7.4	48	96	90	19	1.3	12.3	6.4	1.1	9.6	89	1.1
197	21.7	8.7	69	103	96	20	1.4	12.8	7.9	1.1	9.4	95	1.1
202	22.3	12	61	110	127	18	1.1	10.7	5.1	0.9	9.3	86	1.2
207	22.8	11.1	67	111	139	17	1.1	10.4	6.1	0.8	9.4	83	1.1
212	23.4	11.5	57	118	124	18	1.1	10.3	4.9	0.9	9.2	84	1.2
217	24	9.1	49	108	100	17	1.1	10.1	5.4	1.1	9.5	80	1.2
222	24.5	8.6	49	120	104	20	1.2	11.7	5.7	1.2	9.7	93	1.2
227	25.1	9.5	47	122	88	20	1.2	12.1	4.9	1.4	10.4	95	1.3
232	25.7	9.3	48	111	104	19	1.2	11.7	5.2	1.1	9.8	90	1.2
237	26.2	8.9	43	119	89	20	1.2	12.3	4.9	1.3	10.2	96	1.2
242	26.8	8.9	44	115	78	17	1.1	10.4	4.9	1.5	9.5	82	1.1
247	27.3	8.1	42	116	88	19	1.2	11.7	5.2	1.3	9.9	90	1.2
252	27.9	12.2	55	117	89	19	1.1	11.7	4.5	1.3	10.2	90	1.2
257	28.5	11.4	50	97	73	12	0.9	7.6	4.4	1.3	8.6	57	1
262	29	9.3	46	118	103	18	1.1	11.1	4.9	1.1	9.9	83	1.2
267	29.6	10.2	55	118	87	17	1.1	10.3	5.4	1.4	9.6	81	1.2
272	30.2	10.3	50	113	102	17	1	11.3	4.8	1.1	10.9	81	1.2
277	30.7	7.1	41	115	81	20	1.3	11.6	5.8	1.4	9.3	91	1.1
282	31.3	7.5	40	118	82	20	1.3	12.2	5.3	1.4	9.5	93	1.1
287	31.9	7.5	37	113	89	20	1.3	12.3	4.9	1.3	9.7	94	1.2
292	32.4	7.3	40	120	79	18	1.3	11.1	5.5	1.5	8.7	82	1.1
287	33	9.5	46	125	81	19	1.3	11.5	4.9	1.5	8.9	88	1.1
302	33.6	10.4	52	102	96	16	1.2	10.3	5	1.1	8.7	78	1
307	34.1	8.3	46	117	92	17	1.1	10.6	5.6	1.3	9.4	80	1.1
312	34.7	9.8	51	119	95	19	1.2	11.7	5.2	1.3	9.8	89	1.2
317	35.3	7.7	41	118	93	19	1.2	12.3	5.3	1.3	10.2	92	1.2
322	35.8	11.4	62	108	115	19	1.2	11.2	5.4	0.9	9.1	90	1.1
327	36.4	6.8	41	117	82	18	1.1	11.1	6	1.4	9.9	86	1.2
332	37	7.4	50	115	90	20	1.3	11.9	6.7	1.3	9.1	93	1.1
337	37.6	8.9	51	115	102	19	1.2	11.2	5.7	1.1	9	87	1.1
342	38.1	7.5	44	115	76	19	1.3	12	5.9	1.5	9.1	91	1.1
347	38.7	9.7	57	118	121	19	1.3	11.8	5.9	1	9.1	92	1.1
352	39.3	10.1	55	109	124	18	1.2	11.1	5.4	0.9	9.3	85	1.1
357	39.8	5.7	33	120	76	17	1.1	11.4	5.9	1.6	10.7	81	1.2
362	40.4	7.8	39	123	113	18	1.2	11.2	5	1.1	9.2	87	1.1
367	41	7.2	39	127	80	20	1.1	13	5.4	1.6	11.3	93	1.3

**Table. 3.9.** *Continued...*

372	41.6	6.2	38	117	75	19	1.3	11.8	6.2	1.6	9.3	87	1.1
377	42.1	8.8	46	125	84	19	1.1	13.1	5.3	1.5	11.4	91	1.2
382	42.7	10.4	50	114	102	18	1.1	11.3	4.8	1.1	10.1	84	1.1
387	43.3	10.1	49	125	104	19	1.2	11.3	4.8	1.2	9.2	88	1.1
392	43.8	7.7	40	111	87	17	1.1	10.7	5.1	1.3	9.7	81	1.1
397	44.4	7.3	52	123	89	19	1.2	11.7	7	1.4	9.7	91	1.2
402	45	6.4	42	126	101	20	1.4	12	6.6	1.2	8.7	94	1
407	45.6	8.6	55	137	107	21	1.2	13.8	6.4	1.3	11.8	97	1.3
412	46.1	8.8	52	124	123	19	1.1	12.3	5.9	1	10.8	90	1.2
417	46.7	9.3	48	128	100	18	1	11.9	5.1	1.3	12.3	85	1.4
422	47.3	7.9	43	132	100	20	1.2	12.7	5.5	1.3	11	94	1.3
427	47.8	6.3	42	145	103	22	1.2	13.8	6.7	1.4	11.3	101	1.3

$L a_n / Y b_n$  are normalized ratios to Post Archean Australian Shale-PAAS (Taylor and McLennan, 1985)

**Table. 3.10.** Trace elemental content (ppm), ratios of Ni/Co, Rb/Sr, Th/Yb, La<sub>n</sub>/Yb<sub>n</sub> and Total REE concentrations of the core RVS02/GC03 shown against sediment depth and age

Mean depth (cm)	Age ka	Co	Ni	Rb	Sr	La	Yb	Th	Ni/Co	Rb/Sr	Th/Yb	TREE	La <sub>n</sub> /Yb <sub>n</sub>
7.5	0.33	5.1	29	118	101	23	1	12	5.7	1.2	12.3	108	1.7
11.5	0.5	3.9	22	110	105	19	1	10	5.7	1	10.5	90.9	1.4
22.5	0.95	4.2	23	112	110	22	1	11	5.4	1	10.8	103	1.6
30.5	1.28	3.8	20	108	96	20	0.9	10	5.3	1.1	10.9	94	1.6
40.5	1.67	4.9	25	110	116	22	1	11	5.1	0.9	11	101	1.6
52.5	2.17	4.1	20	116	110	21	1	11	4.8	1	10.8	102	1.5
60.5	2.58	4.7	26	114	111	21	1	11	5.5	1	11.3	101	1.6
70.5	3.09	4.9	26	113	118	20	1.1	11	5.3	1	10.4	94.7	1.4
82.5	3.7	7.1	33	94	176	18	1	9	4.7	0.5	9.6	86.3	1.3
92.5	4.21	4.4	23	108	112	20	1.2	10	5.3	1	9	96.9	1.3
101	4.62	5	25	107	124	21	1.1	11	5	0.9	9.5	103	1.4
111	5.13	6.1	31	112	115	23	1.1	11	5.2	1	10.4	110	1.6
121	5.64	4.7	25	113	107	21	1	11	5.2	1.1	11	101	1.5
131	5.86	5.8	29	106	134	20	1	10	4.9	0.8	9.7	95.8	1.4
141	6.09	4.5	23	114	107	24	1.1	12	5	1.1	11	114	1.6
151	6.31	4.1	21	117	102	24	1.1	11	5.2	1.2	10.9	116	1.7
161	6.54	4.2	22	114	93	22	1	11	5.3	1.2	11.5	106	1.7
171	6.76	4.2	22	116	84	23	1.1	11	5.3	1.4	10.5	108	1.6
181	6.99	4.4	25	114	87	22	1.1	11	5.6	1.3	10.4	104	1.5
191	7.21	5.3	32	118	98	21	1	12	6.1	1.2	11	102	1.5
201	7.43	6.6	36	120	118	23	1.2	11	5.5	1	9.7	112	1.5
211	7.66	6.3	35	123	109	24	1.2	12	5.5	1.1	10	115	1.5
221	8.39	6.2	33	110	111	21	1.1	10	5.3	1	9.4	99.6	1.4
231	9.13	6.5	36	109	112	21	1.2	11	5.5	1	8.9	101	1.3
241	9.86	6.3	33	111	106	23	1.2	11	5.2	1.1	9.7	111	1.5
251	10.6	6.2	34	106	117	20	1.1	10	5.5	0.9	9.7	95.9	1.4
261	11.34	6.4	36	108	132	22	1	11	5.5	0.8	11	104	1.6
271	12.07	6.5	37	103	107	20	1	10	5.6	1	9.8	94.6	1.4
281	12.81	6.5	35	104	118	22	1.1	11	5.4	0.9	10.2	102	1.5
291	13.54	5.9	32	102	117	20	1	10	5.5	0.9	9.6	97.1	1.4
301	14.07	6.6	38	98	110	19	1	10	5.7	0.9	9.9	89.3	1.4
311	14.6	5.6	33	101	110	19	1	10	5.9	0.9	10	92.5	1.4
321	15.12	8.4	45	147	98	25	1.2	14	5.3	1.5	11.3	121	1.5
331	15.65	8.9	46	129	169	24	1.2	12	5.2	0.8	10.2	114	1.5
341	16.18	9.3	44	142	141	25	1.3	13	4.8	1	9.8	117	1.3
351	16.7	8.7	42	150	138	26	1.4	14	4.8	1.1	10.2	125	1.4

Table. 3.10. Continued...

361	17.23	8.8	41	148	136	29	1.3	14	4.7	1.1	11.1	139	1.6
371	17.85	9.9	44	151	122	27	1.3	14	4.4	1.2	10.8	127	1.5
381	18.47	12.6	51	149	125	27	1.3	14	4	1.2	10.6	132	1.5
391	19.09	11.1	53	145	117	26	1.4	14	4.8	1.2	10.1	123	1.4
401	19.71	3.9	22	117	74	22	1	11	5.8	1.6	11.6	107	1.7
411	20.33	8.8	39	116	90	19	1	10	4.4	1.3	10.5	92.4	1.4
421	20.95	10.2	39	91	133	17	1	9	3.8	0.7	9.1	82.4	1.3
431	21.56	7.1	34	109	87	20	1	11	4.8	1.3	11.5	95.8	1.5
441	22.18	9.7	41	119	92	20	1	11	4.3	1.3	10.9	95.5	1.5
451	22.8	8.7	40	117	78	20	0.9	11	4.6	1.5	11.7	94.3	1.5
461	23.42	8.7	36	118	81	21	1	12	4.2	1.5	11.9	101	1.6
471	24.04	9.9	41	92	136	17	1	9	4.2	0.7	8.9	82.2	1.2
481	24.66	8.2	37	123	94	22	1	12	4.6	1.3	12.1	105	1.6
491	25.28	9.3	38	104	166	19	1	10	4.1	0.6	10.1	90.7	1.4
501	25.9	9.3	38	108	131	21	1	11	4.1	0.8	11.1	101	1.6
511	26.52	6.8	29	128	94	27	1.1	13	4.3	1.4	12	128	1.8
521	27.14	7.9	35	106	98	19	1.2	10	4.5	1.1	7.8	95.9	1.1
531	27.75	9.6	42	107	79	21	1	12	4.4	1.4	12.2	104	1.5
541	28.37	6.8	28	129	88	23	1	13	4.2	1.5	12.8	110	1.7
551	28.99	9.2	42	124	96	19	0.9	11	4.6	1.3	11.7	93.3	1.5
561	29.61	7.5	34	129	85	21	1	12	4.5	1.5	12.6	97.9	1.5

$L a_n / Y b_n$  are normalized ratios to Post Archean Australian Shale-PAAS (Taylor and McLennan, 1985)

**Table 3.11.** Nd, Sr and Hf isotopic composition of core SK168/GC01.

Age ka	$^{87}\text{Sr}/^{86}\text{Sr}$	$\pm 2\text{SE}$	$^{176}\text{Hf}/^{177}\text{Hf}$	$\pm 2\text{SE}$	$\epsilon_{\text{Hf}}$	$^{143}\text{Nd}/^{144}\text{Nd}$	$\pm 2\text{SE}$	$\epsilon_{\text{Nd}}$	$T_{\text{DMGa}}$
0.88	0.71708	16	0.282657	4	-3.98	0.512137	6	-9.8	1.2
2.9	0.71959	16	0.282745	6	-0.84	0.512131	6	-9.9	1.14
3.92	0.7184	14	0.282718	4	-1.81	0.512119	5	-10	1.41
4.93	0.7203	11	0.282711	4	-2.07	0.512112	6	-10	1.34
5.43	0.71958	18	0.282733	6	-1.26	0.512138	6	-9.8	1.29
5.94	0.71956	11	0.282691	4	-2.77	0.512105	6	-10	1.46
6.95	0.71714	17	0.282744	6	-0.89	0.512157	6	-9.4	1.39
7.83	0.7174	15	0.28266	3	-3.84	0.512125	4	-10	1.46
8.47	0.71876	11	0.282674	3	-3.36	0.512135	13	-9.8	1.33
9.1	0.71918	20	0.282766	5	-0.12	0.512163	5	-9.3	1.38
9.73	0.71891	20	0.282775	5	0.2	0.512156	6	-9.4	1.34
10.05	0.71912	11	0.282741	5	-1.01	0.512153	6	-9.5	1.37
10.5	0.71928	15	0.282764	3	-0.18	0.512164	7	-9.2	1.37
11.1	0.71889	18	0.282755	5	-0.49	0.512164	7	-9.3	1.33
11.59	0.71913	16	0.282743	3	-0.91	0.512153	5	-9.5	1.29
13.6	0.72002	10	0.282725	4	-1.54	0.512139	5	-9.7	1.19
14.87	0.7211	14	0.282714	4	-1.96	0.512118	7	-10	1.39
16.14	0.72226	21	0.282729	4	-1.43	0.512108	4	-10	1.35
16.78	0.72173	10	0.28272	3	-1.73	0.512109	7	-10	1.3
17.74	0.71542	11	0.282702	7	-2.36	0.512129	4	-9.9	1.32
19.01	0.7211	11	0.282723	3	-1.64	0.512115	6	-10	1.3
19.97	0.7224	30	0.282735	5	-1.2	0.512108	6	-10	1.33
20.61	0.72218	17	0.282721	5	-1.7	0.512111	6	-10	1.33
21.56	0.72248	11	0.282716	4	-1.89	0.512111	8	-10	1.32
21.88	0.72256	13	0.282718	5	-1.8	0.512111	8	-10	1.34
22.84	0.72241	18	0.282732	5	-1.31	0.512105	6	-10	1.35
23.79	0.71885	23	0.282693	4	-2.69	0.512093	4	-11	1.26
24.11	0.72302	29	0.282736	10	-1.17	0.512101	5	-11	1.45
24.79	0.72313	10	0.282699	4	-2.48	0.512084	5	-11	1.39
26.85	0.7238	25	0.282711	8	-2.04	0.512062	6	-11	1.43
27.95	0.72341	11	0.282712	5	-2.01	0.512091	6	-11	1.34
33.13	0.72242	11	0.282691	4	-2.75	0.512092	4	-11	1.35
35.27	0.72254	9	0.282706	4	-2.24	0.5121	4	-11	1.31
35.8	0.72285	10	0.282729	3	-1.43	0.512109	6	-10	1.3
39.01	0.72257	17	0.28271	4	-2.1	0.512095	3	-11	1.33
42.22	0.7231	25	0.282706	4	-2.21	0.512088	3	-11	1.37
43.29	0.72304	12	0.282707	3	-2.19	0.512104	7	-10	1.37
44.36	0.72208	20	0.282687	4	-2.9	0.51211	5	-10	1.26
46.5	0.72306	15	0.282702	5	-2.36	0.512123	5	-10	1.34
47.04	0.72324	16	0.282707	9	-2.19	0.512125	5	-10	1.3
49.18	0.72336	15	0.282682	6	-3.08	0.512118	5	-10	1.3

**Table 3.11.** *Continued...*

50.25	0.72323	30	0.282735	6	-1.21	0.512108	5	-10	1.36
52.39	0.72438	13	0.282733	6	-1.26	0.512089	4	-11	1.37
53.46	0.72294	18	0.282701	5	-2.41	0.5121	6	-11	1.28

**Table 3.12.** *Nd and Sr isotopic compositions of core RVS02/GC03.*

Age (ka)	$^{87}\text{Sr}/^{86}\text{Sr}$	$\pm 2\text{SE}$	$^{143}\text{Nd}/^{144}\text{Nd}$	$\pm 2\text{SE}$	$\epsilon_{\text{Nd}}$	$T_{\text{DM}}$ (Ga)
0.14	0.724732	13	0.512028	4	-11.9	
0.5	0.722949	14	0.512017	6	-12.1	1.49
4.21	0.723313	11	0.51204	7	-11.7	1.5
5.64	0.726927	15	0.512024	9	-12	1.49
6.31	0.721987	10	0.512022	9	-12	1.48
9.13	0.724687	15	0.512048	9	-11.5	1.53
10.6	0.725652	10	0.512006	6	-12.3	1.51
14.07	0.724002	11	0.512035	5	-11.8	1.53
17.23	0.728675	12	0.512018	8	-12.1	1.45
20.95	0.724815	17	0.51208	8	-10.9	1.46
26.52	0.729454	20	0.511987	7	-12.7	1.51

*Note: 2SE (twice the standard errors) are on the final quoted significant figures. Calculated with  $(^{143}\text{Nd}/^{144}\text{Nd})_{\text{CHUR}} = 0.512638$  [Jacobsen and Wasserberg, 1980]. Errors for  $\epsilon_{\text{Nd}}$  are given as 2SD, the external reproducibility of JNdi  $^{143}\text{Nd}/^{144}\text{Nd} = 0.512105 \pm 17$  which translates to  $\pm 0.33$   $\epsilon_{\text{Nd}}$  units. (TDM) Depleted mantle model ages estimate using measured  $^{143}\text{Nd}/^{144}\text{Nd}$  and  $^{147}\text{Sm}/^{144}\text{Nd}$  ratios following DePaolo (1980).*

## CHAPTER 4

Climatic control on lithogenic  
sedimentation in the Andaman Sea  
during late Quaternary period

## 4.1. Introduction

Past climatic conditions are interpreted from several proxies such as aeolian dust deposited in marine sedimentary column, speleothem records from limestone caves, thickness and color of the tree rings, moisture content variation, abundances of pollen in sedimentary column, abundances of microfossils and their isotopic variation. The interpretations based on lithogenic sedimentation are usually about the changes in run-off or erosion in the source areas. Very few studies carried out are based on chemical weathering fluctuations. The chemical weathering plays a crucial role in the cycle of ice-green houses by regulating the atmosphere carbon dioxide content through negative feedback [Walker *et al.*, 1981; Berner *et al.*, 1983; Lasaga *et al.*, 1994]. The key driver of chemical weathering intensification is humidity and the humidity in the Northern Indian Ocean is related to the key regional climatic phenomenon monsoon. Indian Ocean Monsoon (IOM) is a major result of pressure gradient variation in between Indian Ocean and continental part of south Asia, can be a major driver of sediment transport from erosion and weathering through Himalayan river systems Ganges-Brahmaputra-Indus-Irrawaddy (GBII) which combinedly carry about 20% of global sediment discharge to the world Oceans. The major depocenters for sediments transported from these rivers are the submarine fan systems viz., the Bengal, Indus and the Nicobar in the Northern Indian Ocean. History of orogeny and erosion of Himalayas is recorded by these fan systems [Curry and Moore, 1971; France-Lanord *et al.*, 1993; Einsele *et al.*, 2017]. Recent Bengal Fan seismic stratigraphy built by Krishna *et.al.* (2016) has shown a distinct increase in sediment discharge (~140 m/m.y.) by Ganges-Brahmaputra during the Oligocene–Miocene (~23 Ma) marking the start of turbidity system corresponding to rapid exhumation of the Himalaya, which intensified the erosional process and commencement of Bengal Fan sedimentation possibly related to Indian monsoon. In fact, the tectonic

activity of Tibetan Plateau uplift has been believed to have driven the increased chemical weathering rates which may have led to decrease in atmospheric CO<sub>2</sub> over the past 40 million years [Raymo and Ruddiman, 1992]. Clift *et al.*, (2008) have presented weathering records from the South China Sea, Bay of Bengal and Arabian Sea, reconstructed the Neogene Asian monsoon climate from these records and have shown a correlation between the rate of Himalayan exhumation and monsoon intensity over the past 23 Myr and have attributed this link to a dynamic coupling between Neogene climate and both erosion and deformation in the Himalaya. While a number of Himalayan erosional records are published, only one weathering record is known from the Andaman Sea [Colin *et al.*, 1999] which has reflected the climate regime in Indo-Burman ranges. Andaman Sea has well constrained sources [Rodolfo, 1968; Colin *et al.*, 1998, 1999, 2006; Kurian *et al.*, 2008; Awasthi *et al.*, 2014; Damodararao *et al.*, 2016; Miriyala *et al.*, 2017], the rivers flowing through geological terranes of Indo-Burman ranges, Sino-Burman ranges, Mergui Plateau, Arakan mountains, Rakhine coast being the major sediment suppliers. The climate regime of these source terranes are not entirely similar to that prevailing in the Himalaya and thus the Andaman sediments may record the climatic signatures prevailing in these regions which are not well constrained. Unlike in the Bengal Fan, the sedimentation rates published so far are near linear in regions like northern AS [Colin *et al.*, 2006; Rashid *et al.*, 2007], north central AS [Alagarsamy *et al.*, 2010a; Sijinkumar *et al.*, 2010], western AS [Awasthi *et al.*, 2014; Ali *et al.*, 2015], south Central AS [Colin *et al.*, 1999], southeastern AS [Cao *et al.*, 2015] and southwestern AS [Sijinkumar *et al.*, 2015] for the late Quaternary period providing good archives of tectonic-climatic linkage.

The Late Quaternary (LQ) period is a suitable test case as various climatic instabilities like transition of last glacial–interglacial period (termination of Weichselian glacial cycle), Last Glacial Maximum (LGM), Boling Alleroid (BA), Younger Dryas (YD)

and ice rafting events at poles were witnessed. The high resolution sedimentary records can explain the instabilities in IOM in relation with other global climatic events.

As discussed the sedimentary pathways to the Andaman Sea in sources chapter, the central Andaman region is the best place to study the climatic changes that took place in the Myanmar watersheds. The study on sediment cores collected in N-S transect of the basin further explains the geographical variation in sediment deposition in addition to climatic influence. Elemental and isotopic geochemistry of well dated sediment cores has been used to reconstruct the linkage of lithogenic sedimentation to climatic changes that took place in the Myanmar watersheds. Most of the studies undertaken so far have emphasized on the paleoceanography and monsoonal changes in the Andaman Sea (see for e.g., *Naqvi et.al.*, 1994; *Rashid et.al.*, 2007, 2011; *Sijinkumar et.al.*, 2010, 2011, 2015, 2016a, 2016b; *Gebregiorgis et.al.*, 2016) showing a need to improve our understanding of source terrains.

The role of chemical weathering has been considered only in studies dealing with geological time-scales, because it was thought to react slowly to climatic changes. Some of the recent reports have shown that the effect on chemical weathering can be felt on shorter time-scales. For example, a rapid increase in the chemical weathering flux in Iceland (up to 30% increase over four decades) in response to high-latitude climate change [*Gislason et al.*, 2009] was reported. Further, a recent modeling study of MacKenzie River basin, an Arctic watershed has estimated that the CO<sub>2</sub> consumption flux related to weathering processes would increase by more than 50% for an atmospheric CO<sub>2</sub> doubling by the end of this century [*Beaulieu et al.*, 2012]. In this context, paleoweathering records of climate change regime would be useful to assess their linkage. Major climatic changes occurred during the glacial-interglacial cycles during the Quaternary. The current interglacial has

also witnessed short term but profound climatic changes such as Bolling-Allerod (B-A), Younger Dryas (YD) and Little Ice Age. The records chosen for this study cover these time periods and give an opportunity to decipher the weathering changes that took place. Within Myanmar watersheds, river Irrawaddy is considered as the major contributor for sediment and fresh water to the Andaman Sea and the pulses of Irrawaddy are reported to have reached the equatorial Indian Ocean [Ahmad *et al.*, 2005]. The present day rainfall on Irrawaddy watersheds, IBR (including Rakhine Mountains, Chin and Arakan hills) is high and about 5050mm per annum [Stamp, 1940; Furuichi *et al.*, 2009] and probably brings in a large sediment supply to the oceans. However, about 90% of the present-day rainfall accounts for SW monsoonal precipitation. In other areas of the northern Indian Ocean, paleoclimatic reconstructions suggest that NE monsoon has played a dominant role during glacial conditions (e.g., Sarkar *et.al.*, 1990). The rainfall scenario during glacials is unknown and the NE-monsoonal control on sediment supply to the Andaman Sea is unknown. Thus, this study of lithogenic sedimentation with time covering the last 3 isotopic stages may provide some clues to improve our understanding of climatic changes in Myanmar watersheds.

## 4.2. Results & Preliminary observations

**4.2.1. Chemical weathering proxies:** Total 206 subsections of three well dated sediment cores SK168/GC01 (11°42N, 94°29E), AAS11/GC01 (9°06N, 94°17E) and RVS02/GC03 (7°42N, 93°58E) as well 44 surface sediments (Fig. 2.1) were analyzed for major, trace, rare earth elements to delineate the chemical weathering imprints in the Andaman Sea (AS). The selection of sediment core sites was to achieve a reasonably representative geographical variation in climatic changes in neighboring land masses. All three cores

reached up to marine isotopic stages III covering the last glacial maximum-deglacial period-interglacial climatic periods which would help to check climatic influence on lithogenic sediment removal from source rocks. As discussed in the earlier chapter the

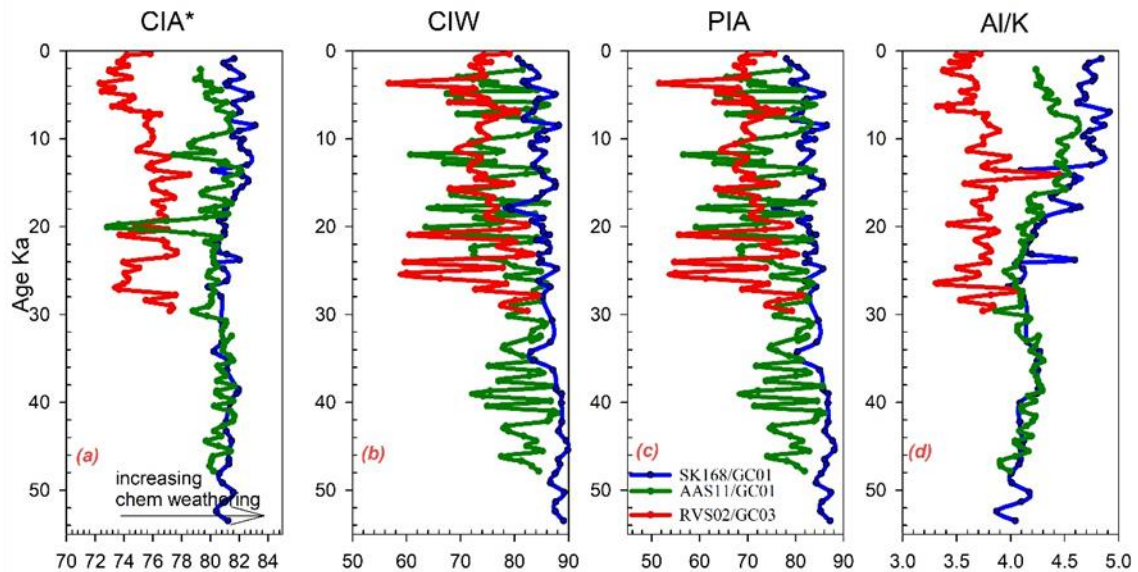


**Figure 4.1:** Different indices of alteration of all three gravity cores obtained from major element analysis plotted against age. CIA=Chemical index of alteration [Nesbitt and Young, 1982]; CIW=Chemical index of weathering [Harnois, 1988]; PIA= Plagioclase index of alteration [Fedo et al., 1995] and elemental ratio of alumina and potassium.

so

source discriminative plots such as TAS, A-CN-K, A-CNK-FM, La-Th-Sc, Sr-Nd, Nd-Hf and Pb-Pb have suggested that the northern (SK168) and central cores (AAS11) recorded climatic response in Myanmar watersheds while the southern core (RVS02) recorded more information about the climatic changes in southern Myanmar/western Thailand region.

In order to decipher the chemical weathering intensity in the source area, well established weathering proxies like CIA-Chemical Index of Alteration [Nesbitt and Young, 1982], CIW-Chemical Index of Weathering [Harnois, 1988], PIA-Plagioclase Index of Alteration [Fedo et al., 1995] and elemental ratios like Al/K [Taylor and McLennan, 1985; Yarincik et al., 2000], Rb/Sr were calculated. The intensity of chemical weathering tells about prevailed climatic conditions. Chemical index of alteration (CIA) [Nesbitt and

Young, 1982] is indicative of leaching of labile elements during chemical weathering with respect to resistive elements. The average values of CIA (SK168 81.3, AAS11 80.16 and RVS02 75.3) indicate source area has experienced moderate chemical weathering (Fig. 4.1a) except an offset of low CIA values in sediments representing LGM (last glacial maximum during 21 to 18ka) possibly indicating the domination of physical weathering

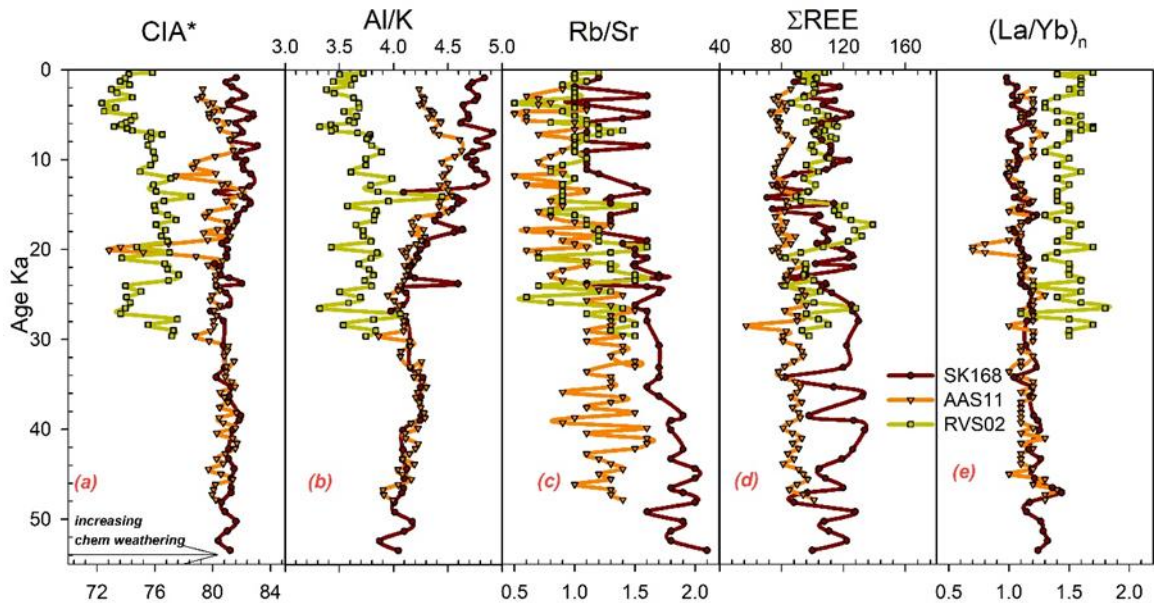


**Figure 4.2:** Downcore variation of  $\Sigma\text{REE}$ ,  $(\text{La}/\text{Yb})_n$ ,  $\text{Ni}/\text{Co}$  and  $\text{Th}/\text{Yb}$  ratios of all three cores plotted against age.  $n$ =normalized to Post Australian Archean Shale [Taylor and McLennan, 1985].

r

responding to arid climate prevailed then. The intensity of chemical weathering of sediments can be inferred from aluminum to potassium ratio (Al/K). Aluminum is one of the resistant elements and potassium is highly mobile during weathering of lithogenic material. The trace elemental ratio Rb/Sr also can be used as an indicator of arid environment. Rubidium being typical of arid and dry environment, while strontium is a mobile element in weathering profile. A distinct change in weathering proxies Al/K and Rb/Sr is noticed during last glacial-interglacial transition (deglacial) reflecting a climatic change (Fig. 4.1d). Near similar variations in CIA and PIA records implies that there was no additional K supply to the study area by K-metamorphism or through turbidites to any of the area studied here. Changes in CIA and Al/K variation (Fig. 4.1) in the northern core

(SK168) and central core (AAS11) of the transect are similar during three climatic phases (glacial-deglacial-interglacial). Lack of such changes in these proxies in southern core (RVS02) implies that the climatic variation in source terranes of southern core either are not strong or not significant enough to be imprinted. Intensified chemical weathering is observed in the northern and central cores during interglacial period than glacial period,

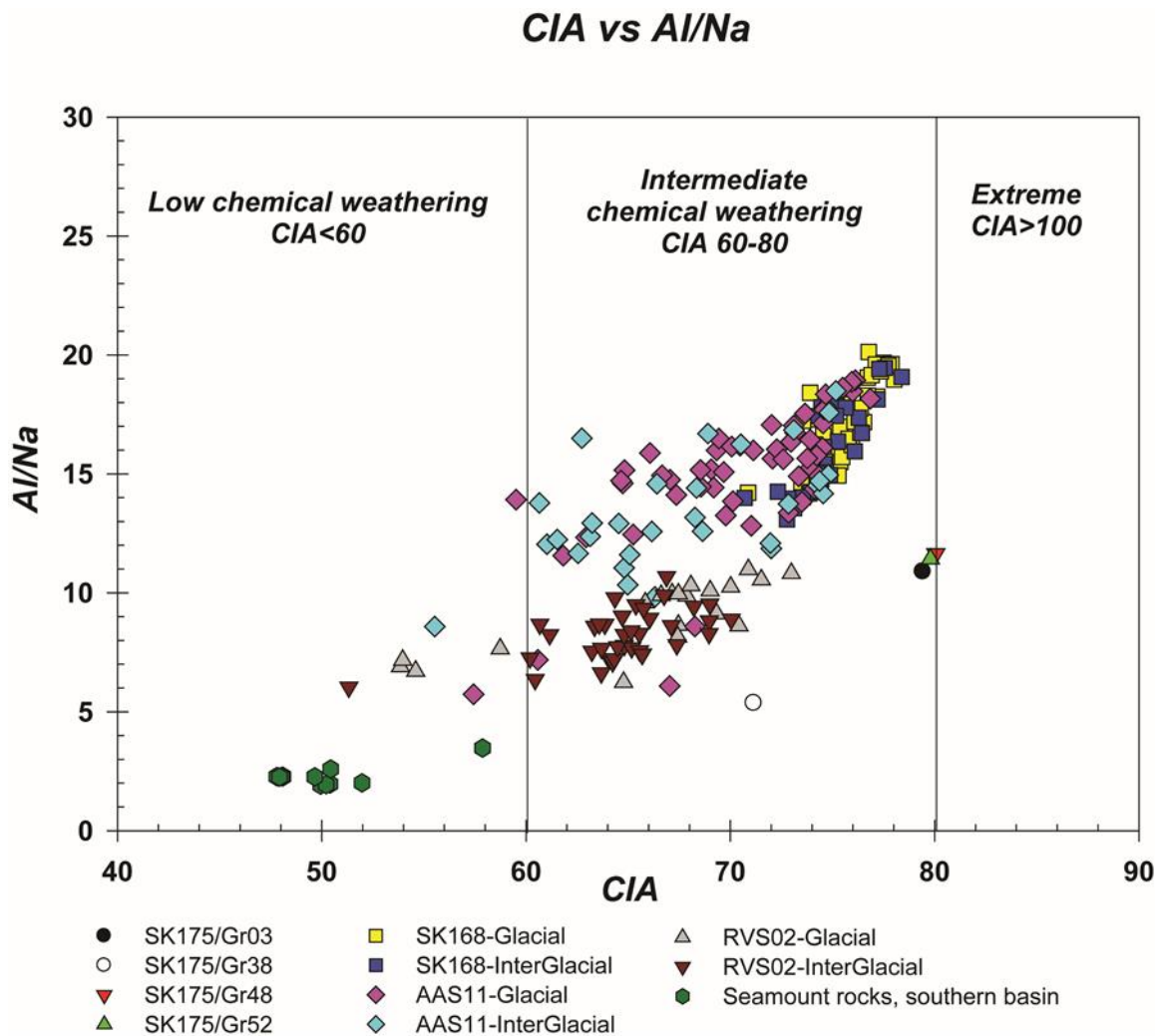


**Figure 4.3:** *CIA vs Al/Na binary plot of glacial and interglacial sediments of all three cores along with shelf sediments off Myanmar river mouths and seamount rocks [Kamesh Raju et al, 2012]. Majority of the samples fall in the intermediate/moderate weathering domain*

w

hile the transition period (deglacial) showing a well defined intermediate pattern. The distinct variation observed in CIA\*, Al/K and Rb/Sr (Fig. 4.2), but a small change in source indicators (La/Yb)<sub>n</sub>, ΣREE implies that the chemical weathering proxies established

from lithogenic fraction were not biased by changes in the sources. The triangular plots A-CN-K and A-CNK-FM were employed to see how weathering trends varied in these geochemical discriminative plots. The chemical weathering indices ranges also postulated next to A-CN-K plot (Fig. 3.3b), the ranges can be compared as both triangular plot and CIA formulae uses molecular proportions of major oxides [Nesbitt and Young, 1982; Nath et al., 2000; Selvaraj and Chen, 2006]. The northern core (SK168) shows maximum CIA values than central core (AAS11), while southern core displays lowest ranges of CIA

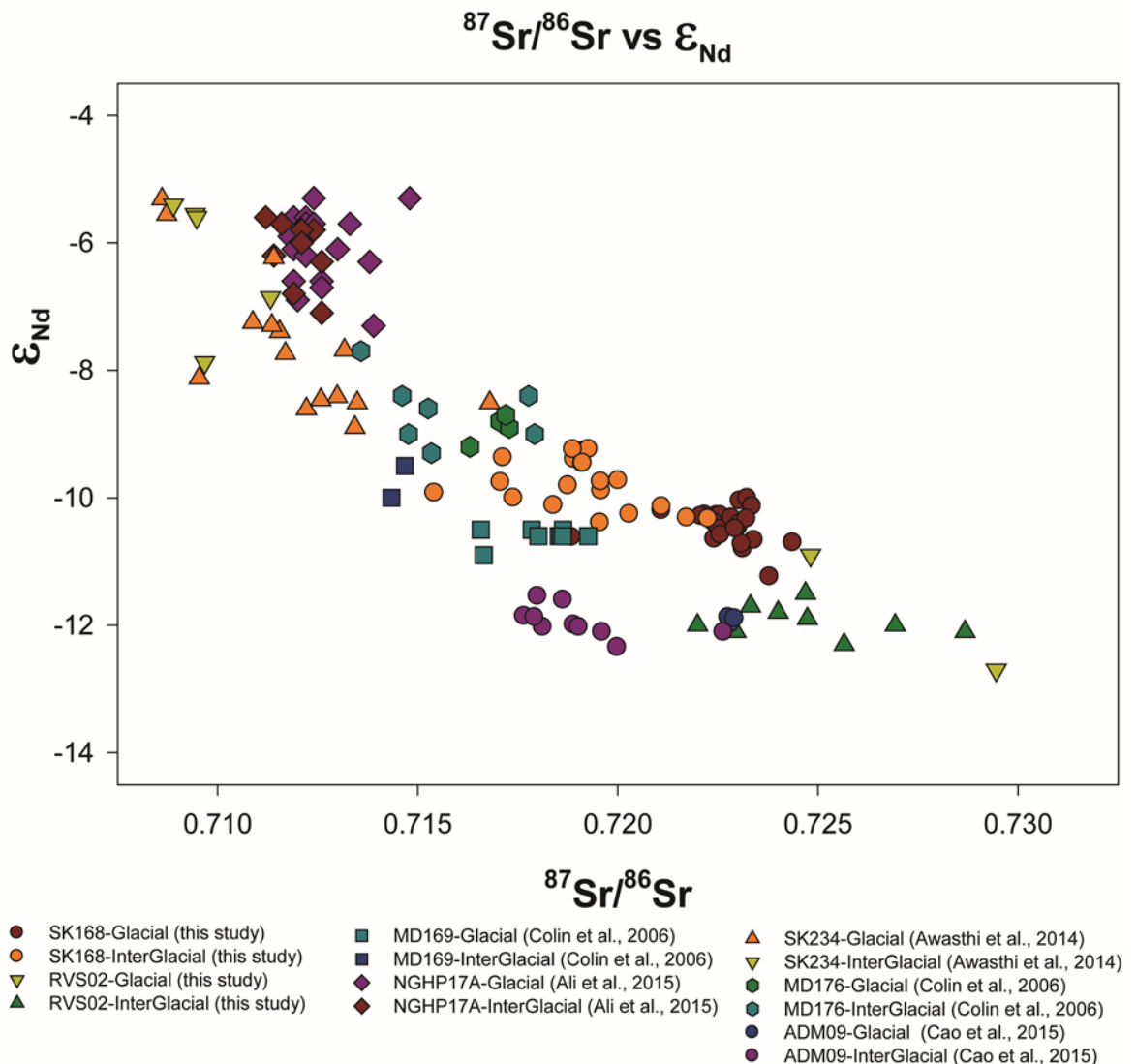


**Figure 4.4:**  $\epsilon_{\text{Nd}}$  versus  $^{87}\text{Sr}/^{86}\text{Sr}$  of glacial and interglacial sediments of published data [Colin et al, 2006; Awasthi et al, 2014; Ali et al, 2015; Cao et al, 2015] and two cores of the present study [SK168 and RVS02].

among three cores of this study. The interglacial sediments of northern two cores display

more alteration as they fall close to  $\text{Al}_2\text{O}_3$  apex. CIA values of all 3 sediments cores are plotted against Al/Na, along with shelf sediments (off Myanmar) and the seamount rocks of southern Andaman basin (Fig. 4.3) to decipher the weathering trends. The northern core (SK168) displayed high CIA\* values and Al/Na ratios, while central core (AAS11) shows relatively lower CIA and Al/Na values than the northern core. The southern core in contrast has displayed lowest values among all the three cores. The seamount rock values show very low CIA values (~50) implies fresh rock material [Nesbitt and Young, 1982; Nath et al., 2000; Selvaraj and Chen, 2006] and the shelf sediments displayed highest CIA values with the basinal sediments falling in between. The low Al/Na values in the shelf sediments than deep sea cores may reflect the size sorting due to the influence of hydrodynamic conditions at river mouths.

**4.2.2. Radiogenic Isotopes in lithogenic fraction:** Strontium and neodymium isotopic analyses were performed on total of 44 subsections of northern core SK168 and 11 subsections of southern core RVS02 (Fig. 2.1 and Tables 3.11, 3.12). This isotopic work has substantiated the observations made from major, trace and rare earth elemental studies in order to understand chemical weathering and provenance changes which recorded in the study area. The  $^{87}\text{Sr}/^{86}\text{Sr}$  and  $\epsilon_{\text{Nd}}$  values range from 0.71414 to 0.72438, -9.24 to -11.24 and 0.721987 to 0.729454, -12.7 to -10.9 for SK168 and RVS02 respectively (Fig. 4.4). The high radiogenic Sr ( $^{87}\text{Sr}/^{86}\text{Sr}$ ) isotopic values were observed in SK168 during glacial than interglacials while this difference is not seen in RVS02 core. The downcore  $\epsilon_{\text{Nd}}$  values of both the cores display a small variation ( $\sim\Delta 1.6\epsilon_{\text{Nd}}$  and  $\sim\Delta 1.8\epsilon_{\text{Nd}}$  respectively). The values of the provenance indicator  $\epsilon_{\text{Nd}}$  in SK168 are very close to another central

Andaman core MD77-169 [Colin *et al.*, 2006], while the  $\epsilon_{Nd}$  of RVS02 ranges very close to southeastern shelf slope core ADM-09 [Cao *et al.*, 2015] implying that the sediment sources are different for these two core sites (Fig. 3.9d). The  $\epsilon_{Nd}$  study of surface sediments of this study (n=14) and other published values also suggests that the sources of central basin (SK168) are different to the southern basin (RVS02 location).

### 4.3. Discussion

**4.3.1. Past climatic reconstructions using chemical weathering proxies:** Distinct changes in isotopic and geochemical data indicative of chemical weathering in source areas during

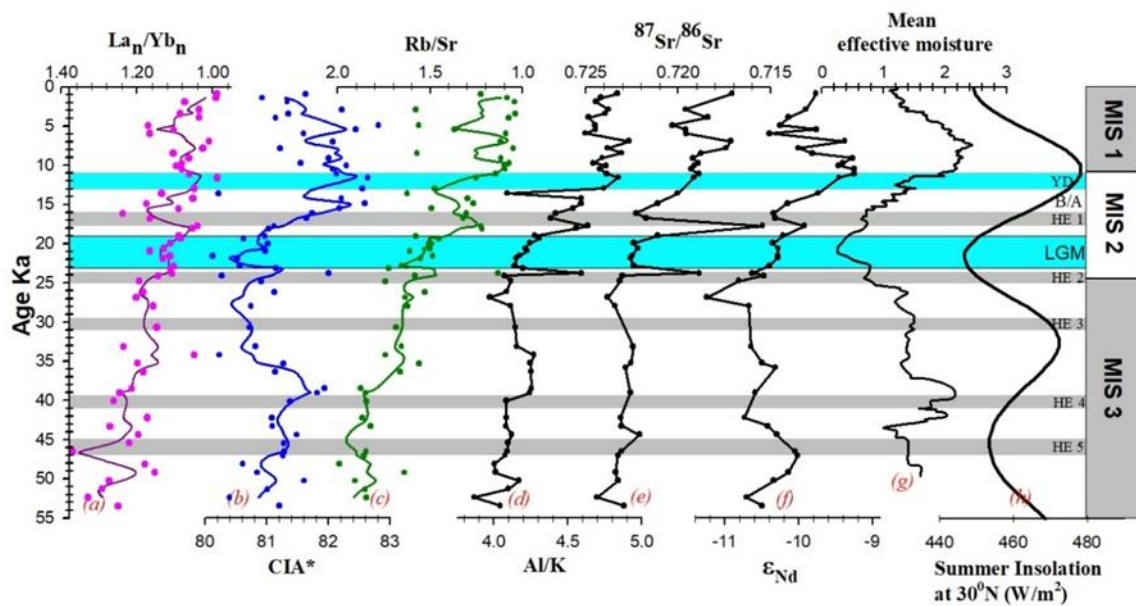


**Figure 4.5:** Downcore plots of SK168 (northern core); (a)  $La_n/Yb_n$  ratio and 3-point moving average; (b) Chemical Index of Alteration\* and 3-point moving average (CIA\*-excluding CaO [Colin *et al.*, 2006]) calculated from molar proportions of major elements; (c) elemental ratio of rubidium to strontium and its 3-point moving average; (d) elemental ratio of aluminium to potassium; (e)  $^{87}Sr/^{86}Sr$ ; (f)  $\epsilon_{Nd}$ ; (g) mean effective moisture of Asia [Herzschuh, 2006]; (h) summer insolation at  $30^\circ N$  [Berger, 1978].  $La_n/Yb_n$ ,  $Rb/Sr$  and  $Sr/Sr$  are in reverse order to get best fit with other plots.

d

eglacials implies the northern core (SK168) is a well preserved archive of the climatic

changes. Thus, a high resolution study was conducted, with 44 analyses of Sr-Nd-Hf radiogenic isotopes and geochemistry of major-trace-rare earth elements in 62 subsections to reconstruct paleo-climatic conditions in Myanmar watersheds. Comparatively, the low sedimentation rates (8cm/ka) in this record (than other two records) has allowed the reconstruction of 54 kyr record of lithogenic sedimentation, silicate weathering and the climate change at source area

The Al/K and Rb/Sr ratios were recognized as good indicators of chemical weathering at source areas. The sensitivity of these proxies to track and quantify the chemical weathering intensity is well established [Nesbitt and Young, 1982; Nath et al., 2000; Colin et al., 2006; Selvaraj and Chen, 2006; Wei et al., 2006; Wan et al., 2009]. Al is relatively conservative during weathering process, while K tends to be enriched in weathering products during moderate weathering, but depleted during extreme weathering. Therefore, high Al/K ratio in sediments can be regarded as indicator of extreme chemical weathering (e.g., [Nesbitt et al., 1980]). Variation in Rb/Sr ratio primarily reflects the geochemistry of fluid-rock interaction, where more mobile Sr will be leached out partly into solution during weathering, while the immobile Rb stays with the residue. The elemental ratios Al/K and Rb/Sr (Fig. 4.2 and Tables 3.5, 3.6, 3.7) of all three cores shows variation in between their glacial and interglacial time slices. A first peak in CIA\*, Al/K and Rb/Sr is observed during the boundary of marine isotopic stages II and III, while the second peak at 17.7ka implies a first kick of chemical weathering intensification at source areas after the LGM. Early Holocene is marked by signatures of intensified chemical weathering, probably influenced by Holocene optimum climatic conditions (HCO) at source areas. The saw tooth pattern in all proxies however suggests that the Holocene period experienced more climatic excursions than glacials.

### 4.3.2. Climatic forcing on lithogenic sedimentation:

Temporal changes in chemical weathering intensity interpreted from proxies Al/K, Rb/Sr, CIA and  $^{87}\text{Sr}/^{86}\text{Sr}$  (Fig. 4.5) mark three broad time periods in this 54ka record, the glacial (54 to 17.7ka), the deglacial (17.7 to 11.6ka) and interglacial periods (11.6ka to present day). The overall CIA\* (defined in caption of Fig. 4.3) ranges from 80 to 83,

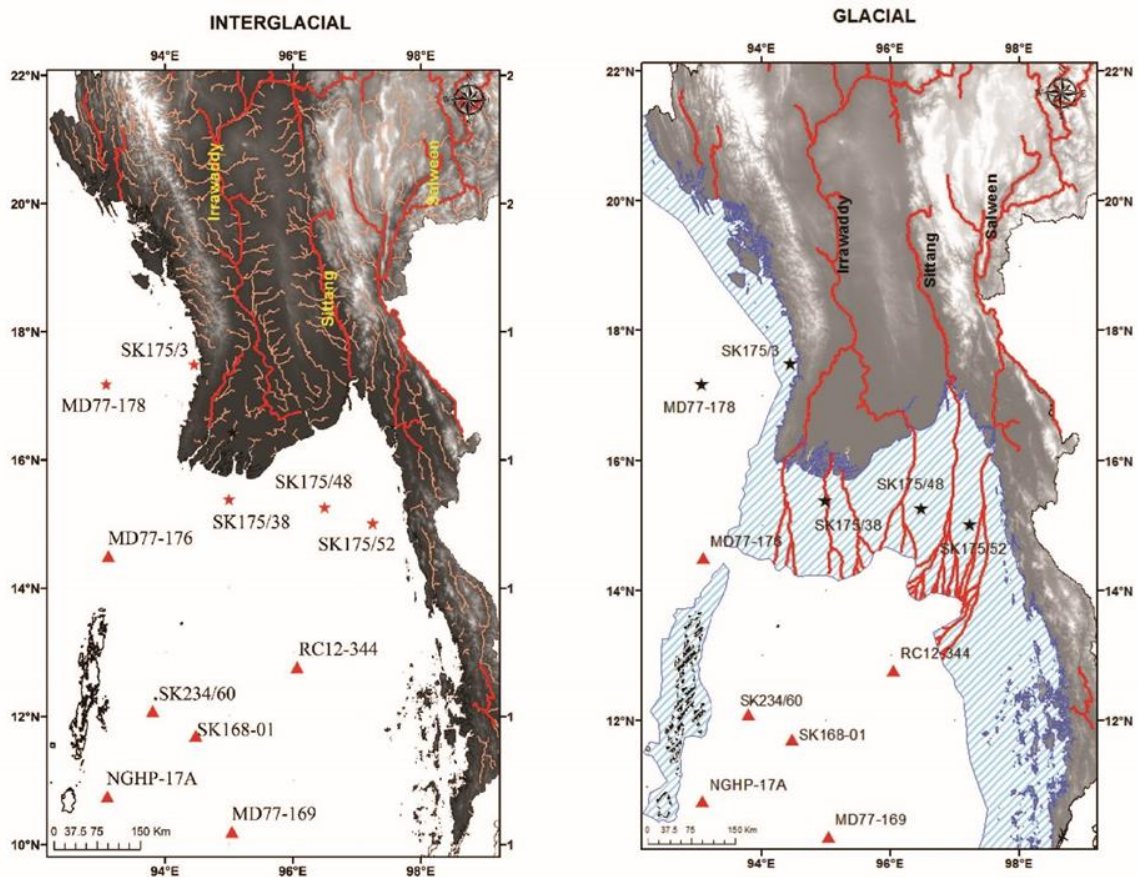


**Figure 4.6:** Present day and reconstructed river catchments during interglacial and glacial periods respectively. Increased catchments during interglacials due to increased vegetated and soil zone areas. Additional catchments (orange) during interglacials would facilitate produce more weathered material. During glacials, due to less catchment area, low infiltration and high runoff are expected. Exposed shelf during glacials (reconstructed-shaded area, below 120MSL of present day).

implies moderate to high chemical weathering in the source regions. The average Al/K ratios are low (4.2) in glacial, high (4.8) in interglacial with intermediate values (4.6) during deglacial since LGM reflecting the highest degree of chemical weathering during interglacial period. Rb/Sr ratios on an average are low during interglacials (1.2) and the deglacial period (1.4) than glacials (1.7), the reduction of Rb with an increase in Sr as an

effect of enhanced chemical weathering. The same is reflected with low  $^{87}\text{Sr}/^{86}\text{Sr}$  ratios during interglacial ( $0.71882 \pm 0.007$  n=15) and deglacial ( $0.71994 \pm 0.007$  n=6) and higher ratios ( $0.72238 \pm 0.007$  n=25) in glacial sediments (Fig. 4.5e). Higher  $^{87}\text{Sr}/^{86}\text{Sr}$  ratios during glacials show the dominance of physical weathering. Least radiogenic value (0.71542) is noticed at 17.7ka, probably reflecting the transition to warmer climate and increased chemical weathering. Chemical weathering changes were not evident during YD probably responding more to local summer insolation and/or due to insufficient sediment residence time for the chemical weathering to take place. Low radiogenic Sr during 9-7ka of Holocene implies increased chemical weathering, consistent with the timings of increased monsoon induced erosion in the western Himalayas [Clift *et al.*, 2008]. Interestingly the highest effective moisture is recorded at same time (9-7ka) in Asian moisture (Fig. 4.5g), and strongly suggest that 9-7ka is an intensified monsoonal event in south Asian climate.

The reduced salinity from 36 to 31psu between 16 and 4ka in a record from Ganges river mouth (126KL) of Bay of Bengal [Kudrass *et al.*, 2001], shows that intensification of summer monsoon with initiation of interglacial climate (Fig. 4.7). This increased fresh water input is reflected in  $\delta^{18}\text{O}_{\text{sw}}$  records of western BoB (SK218) [Govil and Naidu, 2011] and the Andaman Sea (RC344) [Rashid *et al.*, 2007], and shows that the entire Northeastern Indian Ocean received fresh water during this intensified SW monsoon [Sijinkumar *et al.*, 2016a]. These monsoonal records are synchronous to summer insolation at 30°N [Berger, 1978] implying the role of solar insolation in enhancing SW monsoon.

The SW monsoon has weakened and NE monsoon has strengthened during glacials [Fontugne and Duplessy, 1986; Duplessy *et al.*, 1992]. The impact of southward shifting of the locus of Intertropical Convergent Zone (ITCZ) and increased rainfall in rivers of

southern Arakan coast were found to have contributed LGM sediments with high radiogenic Nd to Bay of Bengal [Burton and Vance, 2000; Stoll et al., 2007]. The lack of such radiogenic Nd in the glacial central Andaman basin-CAB (both in Alcock (this study) and the Sewell plateau record [Colin et al., 2006]) suggests that the rivers flowing through

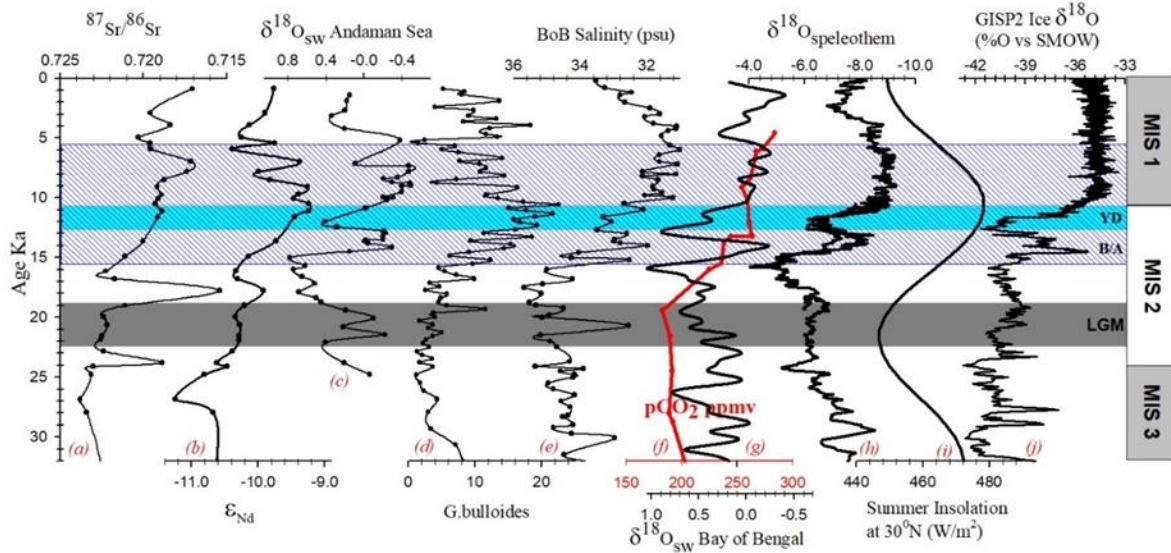


**Figure 4.7:** Downcore plots of (a)  $^{87}\text{Sr}/^{86}\text{Sr}$  of SK168; (b)  $\epsilon\text{Nd}$  of SK168; (c)  $\delta^{18}\text{O}_{\text{sw}}$  of Andaman Sea of RC12-344 [Rashid et al., 2007]; (d) Planktonic foraminifer (*Globigerina Bulloides*) % in SK168 [Sijinkumar et al., 2010]; (e) Salinity record in 126KL core of Bay of Bengal [Kudrass et al., 2001]; (f)  $p\text{CO}_2$  [Petit et al., 1999]; (g)  $\delta^{18}\text{O}_{\text{sw}}$  of middle-west Bay of Bengal from SK218 [Govil and Naidu, 2011]; (h)  $\delta^{18}\text{O}$  of stalagmites of Chinese caves [Wang, 2001; Yuan et al., 2004]; (i) summer insolation at  $30^\circ\text{N}$  [Berger, 1978]; (j)  $\delta^{18}\text{O}$  of ice core from Greenland ice-sheet program GISP2 [Blunier and Brook, 2001]. For clarity we have restricted the time series records to 32ka. The blue color shaded region represents the period with coeval increase in chemical weathering and the deglacial monsoon.

SBR (Salween and Sittang) may be the major contributors to the CAB. Absence of such radiogenic Nd shifts in these CAB cores suggests the dominance of NE monsoon during glacial times, which ultimately brought unradiogenic Nd from river basins of Salween and Sittang of SBR. During glacials, due to the sea level fall and exposure of shelf, eastward flowing currents would have weakened and isolated Irrawaddy from Salween and Sittang sources (Fig. 4.6). The time series plot of  $\epsilon\text{Nd}$  displays two humps of radiogenic nature during 53 to 42ka and 15.5 to 5.5ka periods (Fig. 4.5). The first radiogenic event at 53 to 42ka occurred during low summer insolation, coincident with Heinrich event 5 recognized in North Atlantic Ocean. There was no change in  $\epsilon\text{Nd}$  during LGM at 23 to 19ka

[Sijinkumar *et al.*, 2010] as the source remained constant in this peak of arid climate. High radiogenic  $\epsilon_{Nd}$  (-9.92) and a peak in all chemical weathering proxies (Fig. 4.5) with the occurrence of first warm event in effective moisture content of Asian atmosphere [Herzschuh, 2006] at 17.7ka marks this period as the first trigger of warm climate since the LGM. But it took more than 2 thousand years to show a clear impact of warm climate possibly due to coverage of ice sheets formed during glacials. The significant shift in radiogenic nature of Nd at 15.5ka may mark the beginning of effect of warm period and increased monsoon which continued upto 5.5ka. This increased radiogenic Nd input is also observed in other two Myanmar river fed low resolution records of Sewell seamount (MD169) and Irrawaddy river mouth (MD176) [Colin *et al.*, 2006] during this period of SW monsoonal intensification [Rashid *et al.*, 2007]. Interestingly, changes in all chemical weathering proxies Al/K, Rb/Sr,  $^{87}Sr/^{86}Sr$  co-vary with this high radiogenic Nd event and establishes a link between enhanced chemical weathering and supply of radiogenic Nd to deep central Andaman Sea.

The present day rainfall data during 1988-1997 (Department of Meteorology and Hydrology of Myanmar) shows the dominance of SW monsoon (~92%) over NE monsoon on the plains of Myanmar Rivers. As major part of Central Myanmar Basin has a dry zone (CDZ) formed due to rain shadow of Rakhine mountains, the sediment loads of Irrawaddy will have much influence of IBR flux [Stamp, 1940; Furuichi *et al.*, 2009]. CDZ receives very low rainfall ~600mm, while the northern and southern part of CDZ receives around 2300 and 1200mm of rainfall respectively. But, these are much lower than IBR located on western side of Irrawaddy basin (Rakhine, Chin and Arakan hills) which receives about 5050mm. Thus IBR may have a larger control on sediment of Irrawaddy that is carried to the deep sea.

The Mg/Ca values of RC344 core shows the Sea Surface Temperature (SST) during early Holocene (27.9°C) is closer to modern August SST (28.6°C) [Rashid *et al.*, 2007]. Thus if one considers the present day rainfall (5050mm) is similar to that during the deglacial to mid Holocene, it is possible that IBR catchment could be the potential source for the weathered materials to Irrawaddy river.

The interglacial climate is known for high humidity, large day-night temperature variations, high monsoonal precipitation, together leading to increase in vegetation cover, soil zone and rain water residence time which is more acidic due to increased atmospheric CO<sub>2</sub> [Petit *et al.*, 1999] content (Fig. 4.7). All these would favor an increased chemical weathering conditions at the source region.

Atmospheric CO<sub>2</sub> concentrations in the Northern Hemisphere is said to lead the global temperature making it an important driver of deglacial warming [Shakun *et al.*, 2012]. With the rise in atmospheric pCO<sub>2</sub> concentrations, the deglacial warming initiated at 17ka is coeval with the intensification of chemical weathering in Myanmar watersheds (Fig. 4.7). This implies that the atmospheric CO<sub>2</sub> rise was a trigger for monsoon, which in turn had intensified the silicate weathering in the source regions. A part of risen deglacial CO<sub>2</sub> would have been consumed during the deglacial to mid-Holocene weathering.

Given that the basic and ultrabasic materials tend to weather more quickly than the high crystalline rocks because of textural differences [Meybeck, 1989], the IBR region which is characteristic of recent volcanic dykes, ophiolites, mud volcanoes, flysch [Mitchell *et al.*, 2007; Allen *et al.*, 2008; Licht *et al.*, 2013, 2016; Awasthi *et al.*, 2014] could have weathered preferentially. It is probable that the increased catchments due to intensified monsoon might have energized the supply of radiogenic Nd to the total sediment discharge of Irrawaddy River.

A 54ka lithogenic sediment depositional record from the Andaman Sea tracked monsoon variations, weathering patterns, and provenance changes with time. Climate-

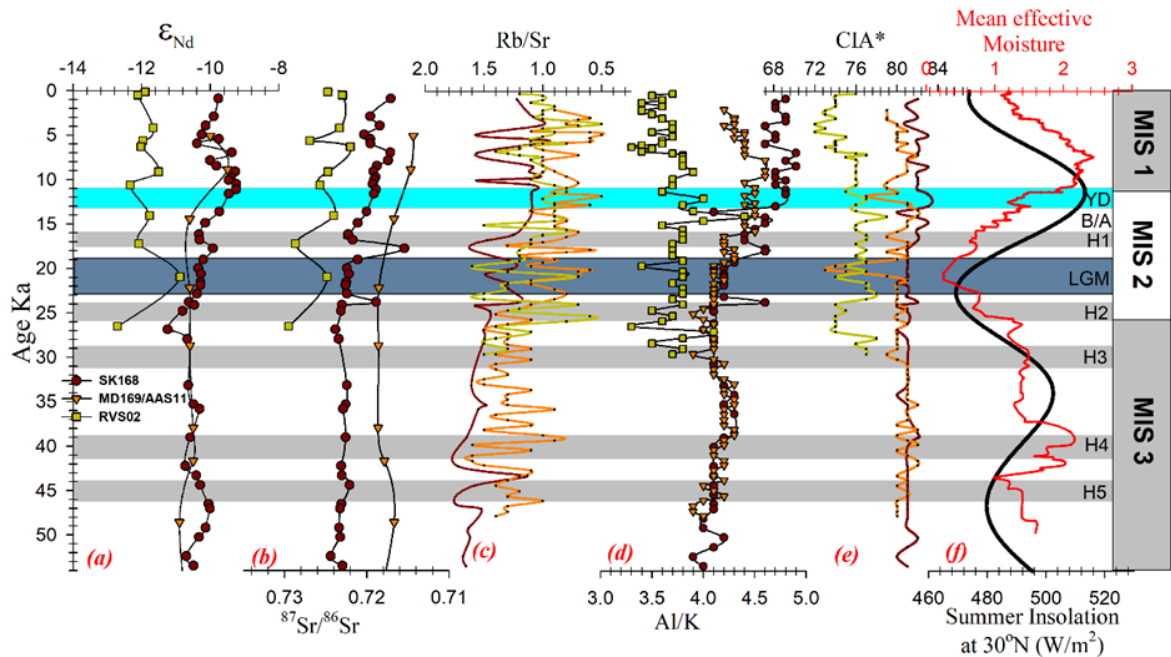


**Figure 4.8:** a) downcore plots of  $\epsilon_{Nd}$  of SK168 (north central basin), MD169 (south central basin), RVS02 (southern basin); b) downcore plots of  $^{87}Sr/^{86}Sr$  of SK168 (north central basin), MD169 (south central basin), RVS02 (southern basin); c) Rb/Sr of SK168 (north central basin), AAS11 (south central basin), RVS02 (southern basin); d) Al/K of SK168 (north central basin), AAS11 (south central basin), RVS02 (southern basin); e) CIA\* of SK168 (north central basin), AAS11 (south central basin), RVS02 (southern basin); f) Mean effective Moisture of [Herzschuh, 2006] and Summer Insolation at 30°N [Berger, 1978].

driven changes in chemical weathering and erosion in the Myanmar river catchments on these time scales is evident. More importantly, the inferred silicate weathering intensity is synchronous with the strengthening of summer monsoon during the deglaciation to mid-Holocene and these changes closely follow changes in regional and global climate. Nd isotope records suggest that over the last 54ka, detrital sediments are primarily sourced from the Myanmar rivers Salween, Sittang along with Irrawaddy. The glacial contrasts between Nd isotopic composition in the Bay of Bengal and the Andaman Sea suggest that the Andaman Sea was isolated from Bay of Bengal during low sea-levels.

In contrast to the northern and central cores of central Andaman basin, the elemental and isotopic results of southern core RVS02 have not displayed any climatic influence like glacial-interglacial climatic changes (Fig. 4.8). No remarkable changes in CIA, Al/K, Rb/Sr and  $^{87}\text{Sr}/^{86}\text{Sr}$  suggests that the southern Andaman basin received lithogenic sources from a region where the glacial-interglacial impacts were not significant. The Sr-Nd concentrations and variations of this southern core are very similar to the other south eastern core ADM-09, studied by Cao et al (2016). The absence of radiogenic Nd peak during 15.5 to 5.5ka in these cores suggests, these locations were not influenced by Irrawaddy material during SW-monsoonal intensification. A high resolution study on this core may help understand the reasons for not recording the glacial-interglacial changes. Absence of pronounced deglacial response (that is observed in CAB cores) in two published records from WAS [Awasthi et al., 2014; Ali et al., 2015] suggests the western Andaman Sea received more material from Andaman islandic or local volcanic sources than Myanmar watersheds.

### **4.3.3. Global linkage of Indian Ocean dynamics:**

As discussed above, the chemical weathering records of Andaman Sea shows Holocene experienced more climatic oscillations than glacials in the Myanmar watersheds (Fig. 4.8). In this section, the geochemical and chemical weathering records of Holocene period of northern core SK168 are compared with other monsoonal records of northern Indian Ocean (Fig. 4.9) for understanding the regional climatic phenomena.

As an effect of deglacial intensification of SW monsoon over IBR that lithologically consisting juvenile material and Irrawaddy supplied this juvenile material

(radiogenic Nd) to the Andaman Sea. The highest radiogenic Nd event during ~11.5 to 8.5ka (Fig. 4.7) suggests the peak of SW monsoon during early Holocene [Rashid *et al.*, 2011]. The increased radiogenic Nd along with increased mass accumulation rates (Ti based) and drastic fall in Al/K, K/Rb and CIA (Fig. 4.10) altogether suggests the enhanced monsoonal erosion suppressed the weathering during 11.5 to 8.5ka in Indo-Burman ranges. Following this, increased chemical weathering in source areas is evident from the proxies,

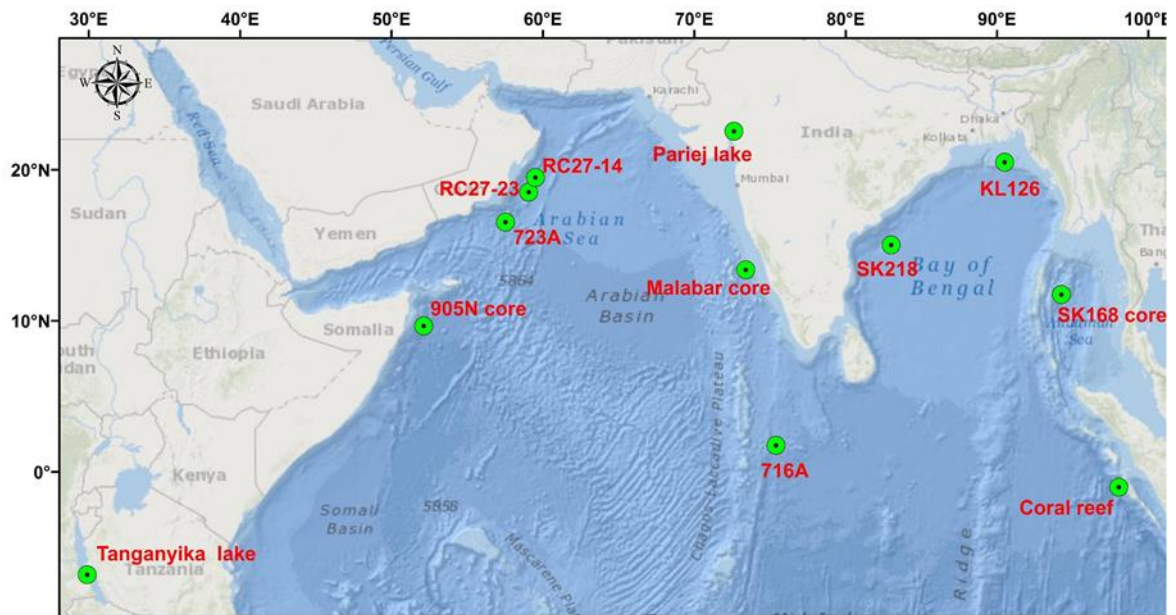


**Figure 4.9:** Holocene monsoonal precipitation changes in the Andaman Sea compared with those from the western and eastern Arabian Sea and from the Bay of Bengal and Africa which are inferred from proxy data: a)  $\delta^{13}C_{wax}$  of Tanganyika lake [Tierney and DeMenocal, 2013]; b)  $^{87}Sr/^{86}Sr$  data of dust fraction of 905 core off Somalia [Jung *et al.*, 2014]; c) *G.Bullodites* (%) of ODP723A core [Naidu and Melmgren, 1995]; d)  $\delta^{15}N$  of RC27-23 and RC27-14 cores off Oman [Altabet *et al.*, 2002]; e) Perij lake level fluctuations [Raj *et al.*, 2015]; f) *G.bullodites* (%) of Malabar core [Saraswat *et al.*, 2016]; h) *G.Bullodites* (%) of ODP716A core [Gupta *et al.*, 2010]; i)  $\delta^{18}O_{sw}$  record of SK218 core of western BoB [Govil and Naidu, 2011]; j) Salinity record of Ganges mouth core [Kudrass *et al.*, 2001]; k) *G.bullodites* (%) of SK168 core [Sijinkumar *et al.*, 2010] and l) Coral reef record of Mentawai island [Abram *et al.*, 2003].

Al/K, K/Rb and  $^{87}Sr/^{86}Sr$  from ~8.5 to 6.5ka soon after erosional event (~11.5 to 8.5ka) (Fig. 4.10) manifesting a response to the Holocene Climatic Optimum period (HCO) for this area. The monsoon induced erosion (11.5 to 8.5ka) in Myanmar and the deglacial ice sheet retreat might have exposed fresh rock material to facilitate an increase in the

chemical weathering (during 8.5 to 6.5ka) with the warm and moist conditions prevailed then. The intensified monsoon interpreted from erosion and weathering proxies here are reflected in  $\delta^{18}\text{O}$  of Mawmluh cave in Meghalaya, Northeast India [Dutt *et al.*, 2015] during ~11ka to ~6.5ka (Fig. 4.11) and a drastic rise in Asian moisture [Herzschuh, 2006] during the same period (but with a peak at 7.5ka). At the same period, low  $\delta^{18}\text{O}_{\text{sw}}$  values in Andaman Sea [Rashid *et al.*, 2007] and western Bay of Bengal [Govil and Naidu, 2011] implies salinity changes induced by increased monsoonal precipitation, implying the climate over the Northeast Indian Ocean also responding to HCO. A detailed study [Goodbred S. and Kuehl, 2000] on 50 boreholes covering the Ganges-Brahmaputra delta shows huge sediment deposition in between 11 to 7ka and the peak in low salinity at ~8ka recorded at Ganges river mouth [Kudrass *et al.*, 2001] suggests the role of intensified SW monsoon over Himalayan terrains during the early Holocene period. Interestingly, total fertile species (Fig. 4.11–unpublished data combined abundance of *G. bulloides*, *G. falconensis* and *G. glutinata* – indicator of monsoon-driven productivity- of the SK168 shows a drastic increase in its population during intensified chemical weathering period (8.5 to 6.5ka) suggested both the Andaman Sea and the Myanmar terrains experienced monsoon intensification. The high erosional event (11.5 to 8.5ka) along with intensified chemical weathering period (~8.5 to 6.5ka) in SK168 makes the time period 11.5 to 6.5ka as a monsoonal event over Irrawaddy and river flood plains of Myanmar. The decreased salinity and increased G-B river sedimentation rates of Ganges-Brahmaputra rivers, low speleothem  $\delta^{18}\text{O}$  values as well reduced  $\delta^{18}\text{O}_{\text{sw}}$  of Bay of Bengal and Andaman Sea during the monsoonal event recognized in lithogenic sedimentation of Andaman Sea (SK168) further suggests the entire northeastern Indian Ocean and its rim countries experienced intensified monsoon during (11.5 to 6.5ka) early Holocene.

The intensified monsoon period (11.5 to 6.5ka) was followed by a period of distinct low chemical weathering during 6.5 and 5ka indicated by increased radiogenic Sr reflected in  $^{87}\text{Sr}/^{86}\text{Sr}$  ratio, decreased Al/K, K/Rb and CIA (Fig. 4.10) possibly in response to reduced moisture and precipitation. This again is synchronous with a drastic rise of  $\delta^{18}\text{O}$  of Mawmluh cave [Dutt *et al.*, 2015] in the Meghalaya region of India and decreased productivity in the Andaman Sea (fall in total fertile species in SK168- Fig. 4.11), the low stands of Perij lake at 6.6ka [Raj *et al.*, 2015], death of Indonesian coral reefs at ~6.6ka [Abram *et al.*, 2003], reduced influx to Tibetan lakes [Hong *et al.*, 2003; Bird *et al.*, 2014] and other studies suggested that the eastern part of Northern Indian Ocean and many parts of south Asia experienced low monsoon during 6.5 to 5ka. Further,  $^{10}\text{Be}$  derived precipitation record [Zhou *et al.*, 2015] shows monsoonal reduction during 6.5 to 5ka recorded in Chinese loess, hence this 6.5 to 5ka dry period is apparently not only limited to eastern Indian Ocean but the entire Asian region.

A peak in chemical weathering intensity at ~3.8ka coincide with the occurrence of overflow of Perij lake at ~3.6ka and a rise in fertile species in the Andaman Sea during ~5 to 3.2ka period suggests another period of increased monsoonal precipitation soon after dry middle Holocene period over Indian and Myanmar landmasses and northeastern Indian Ocean. In summary, the early to late Holocene in the Northeastern Indian Ocean has witnessed two major episodes of enhanced monsoonal precipitation sandwiching one episode of reduced monsoonal precipitation.

These Holocene monsoonal records of northeastern and eastern Indian Ocean are compared to the monsoonal records of western Indian Ocean and eastern Africa to assess if these changes are regional in nature. In contrast to the high precipitation noticed at 8.5 to 6.5 ka and 5 to 3.4 ka in the northeastern Indian Ocean region, a study on African lakes

[Gasse, 2000] shows low stands of lakes at ~8ka and 4ka and overflow at 6.6ka when a dry mid-Holocene phase was seen in the northeastern region (Fig. 4.12). Further, two aridification steps (8.5 to 6.2ka and till 3.8ka) were observed in dust ( $^{87}\text{Sr}/^{86}\text{Sr}$ ) record of western Indian Ocean core [Jung *et al.*, 2004] (Fig. 4.12). The east-west contrast is further

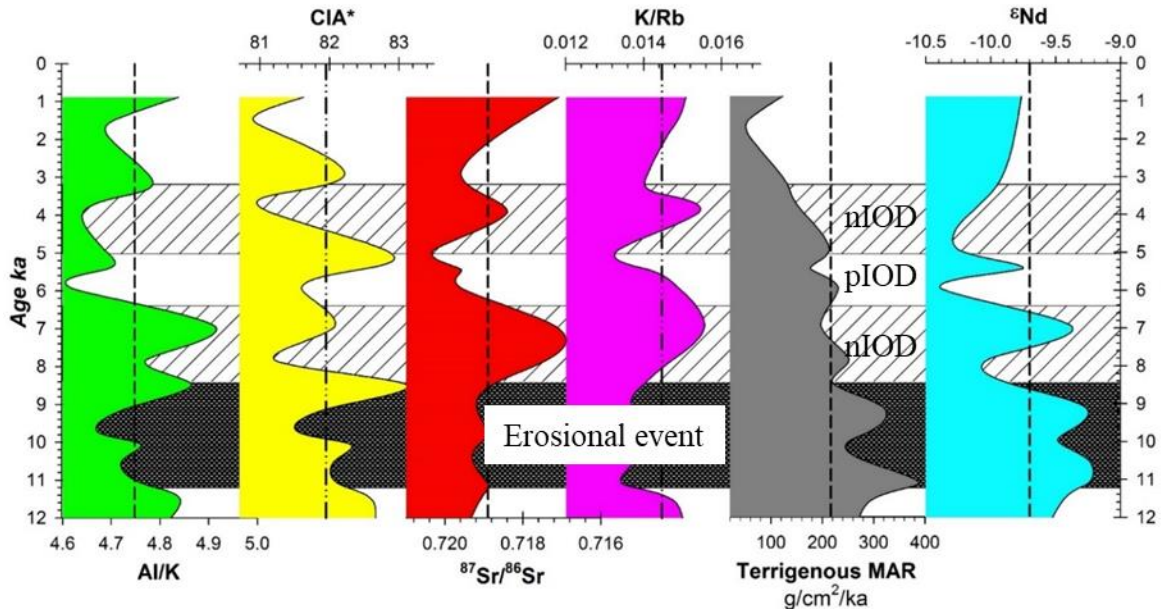


**Figure 4.10:** Erosional and weathering proxy data of SK168 core during Holocene period. a) Aluminium to potassium ratio; b) Chemical Index of Alteration\* (CIA-Nesbitt and Young, 1982) calculated from molar proportions of major elements and CIA\*-excluding CaO [Colin *et al.*, 2006]; c)  $^{87}\text{Sr}/^{86}\text{Sr}$  isotopic ratio variation; d) Potassium to rubidium ratio; e) Mass accumulation ratio of terrigenous matter, based on titanium concentration [Yarincik *et al.*, 2000] and f)  $\epsilon_{\text{Nd}}$  used as a provenance indicator.

supported by an increased grass type of vegetation than a forest type vegetation during 8.8 to 6.2ka and at ~5 to 3.2ka are recorded in Tanganyika lake [Tierney and DeMenocal, 2013] implying a weak monsoonal period. This dry period during 5 to 3.2ka is well recognized by several records which centers at 4.2ka; the 4.2 ka event reflected in high salinity in Red Sea [Arz *et al.*, 2006], a major drought condition recognized in dust and dolomite content in the Gulf of Oman [Thompson *et al.*, 2002] and demise of Akkadian empire due to reduced monsoonal precipitation [Cullen *et al.*, 2000], increased windiness in the Arabian peninsula [Overpeck *et al.*, 1996], arid period in Higher Garhwal Himalayas and northwestern India [Phadtare, 2000] and reduction in Indus river outflow

[Staubwasser *et al.*, 2003] altogether suggests reduced monsoon over WIO and eastern Africa. On the other hand, a high monsoonal period is sandwiched in between above two dry periods, when a drastic increase in forest type of vegetation observed during 6.5 to 5ka in  $\delta^{13}\text{C}_{\text{wax}}$  record [Tierney and DeMenocal, 2013] (Fig. 4.11) and increased terrestrial organic matter flux recorded in (BIT index) of Challa lake [Wolff *et al.*, 2011] of western equatorial Indian Ocean implies the presence of monsoonal extremities on either sides of northern Indian Ocean when the Northeastern Indian Ocean has witnessed a dry climate. The precipitation proxies discussed here have displayed a distinct east-west contrast in monsoon and questions the validity of considering whole of Northern Indian Ocean as a single climatic unit.

**4.3.3.1. Wind proxies during Holocene:** For assessing the wind strength variation of past, several proxies such as the presence of aeolian sediments are used. For inferring the monsoonal wind-driven upwelling, the surface dwelling planktic foraminifer *G.bulloides* has been extensively used [Anderson and Carrington, 1993; Naidu and Malmgren, 1995; Gupta *et al.*, 2003, 2010; Sijinkumar *et al.*, 2010]. We compiled all available *G.bulloides* records of northern Indian Ocean like SK168 (Eastern Indian Ocean-EIO) [Sijinkumar *et al.*, 2010], ODP716A (central Indian Ocean-CIO) [Gupta *et al.*, 2010], off Malabar core (Arabian Sea) [Saraswat *et al.*, 2016] and ODP723A (western Indian Ocean-WIO) [Naidu and Malmgren, 1995] (Fig. 4.14) to assess the regional variation in wind driven upwelling during the Holocene period. Gupta *et al.* (2010) has attributed the drastic decrease in the *G.bulloides* population in ODP716A to strengthening pIOD (positive-Indian Ocean Dipole) as an effect of major decrease of IEW (Indian Ocean Equatorial Westerlies) which resulted in heavier floods in eastern Africa (western Indian Ocean) and drought conditions and wildfires in Australia (southeastern Indian Ocean).

Low abundance in *G.bulloides* in western Indian Ocean core (723A) representing reduced upwelling in western Indian Ocean during 8.5 to 6.5ka [Naidu and Malmgren, 1995], is synchronous with arid period identified in dust  $^{87}\text{Sr}/^{86}\text{Sr}$  record off Somalia [Jung et al., 2004] and  $\delta^{13}\text{C}_{\text{wax}}$  record in Lake Tanganyika [Tierney and DeMenocal, 2013] suggests

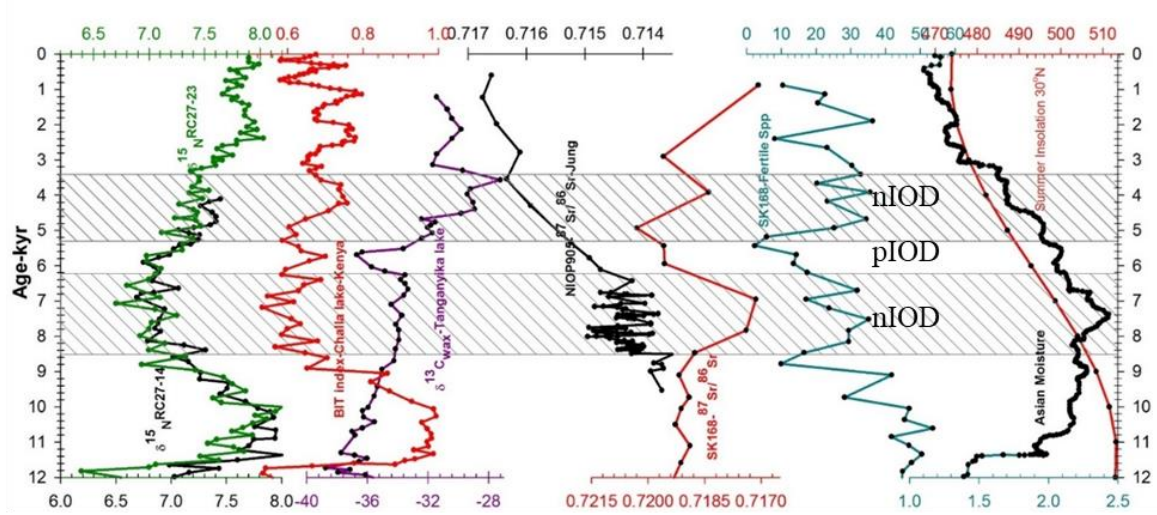


**Figure 4.11:** Climatic and precipitation proxy data of northern Indian Ocean. References can be found in figure 4.9 except BIT index of Challa lake of Kenya [Wolff et al, 2011], total fertile species of SK168 core [Sijinkumar et al, unpublished data], Asian mean moisture content [Herzschuh, 2006] and summer insolation curve [Berger, 1979].

that the period 8.5 to 6.5ka in the western Indian Ocean is a reduced monsoon period. While central Indian Ocean record (716A) shows low *G.bulloides* population in the first half of first period (8.5 to 7.2 ka) was less, with a gradual increase in population from ~7.2ka. The low *G.bulloides* abundance in another record (Malabar core) in same longitude as of CIO core close to western coast of India also shows this gradual increase of *G.bulloides* population initiated at ~ 6.5ka (Fig. 4.14). But, this increased productivity has continued till 3.8ka suggests a minimum control of eastern African climate over eastern Arabian Sea. In contrast, the northeastern core SK168 has shown enhanced productivity (fertile species) as well as increased *G.bulloides* during these two WIO dry periods. In the central part of the northern Indian Ocean, the proliferation of upwelling productivity indicator *G.bulloides* in the Central Indian Ocean core ODP716A has commenced at ~7ka, which is ~2ka later than that seen in the Eastern Indian Ocean core SK168 This east-west

contrast in early Holocene is not seen in Malabar core too Interestingly, the Holocene productivity patterns interpreted from the  $\delta^{15}\text{N}$  isotopic study [Altabet *et al.*, 2002] of Western Indian Ocean coincides with terrestrial organic matter flux recorded in (BIT index) of Challa lake [Wolff *et al.*, 2011]. In summary, a clear east-west contrast of

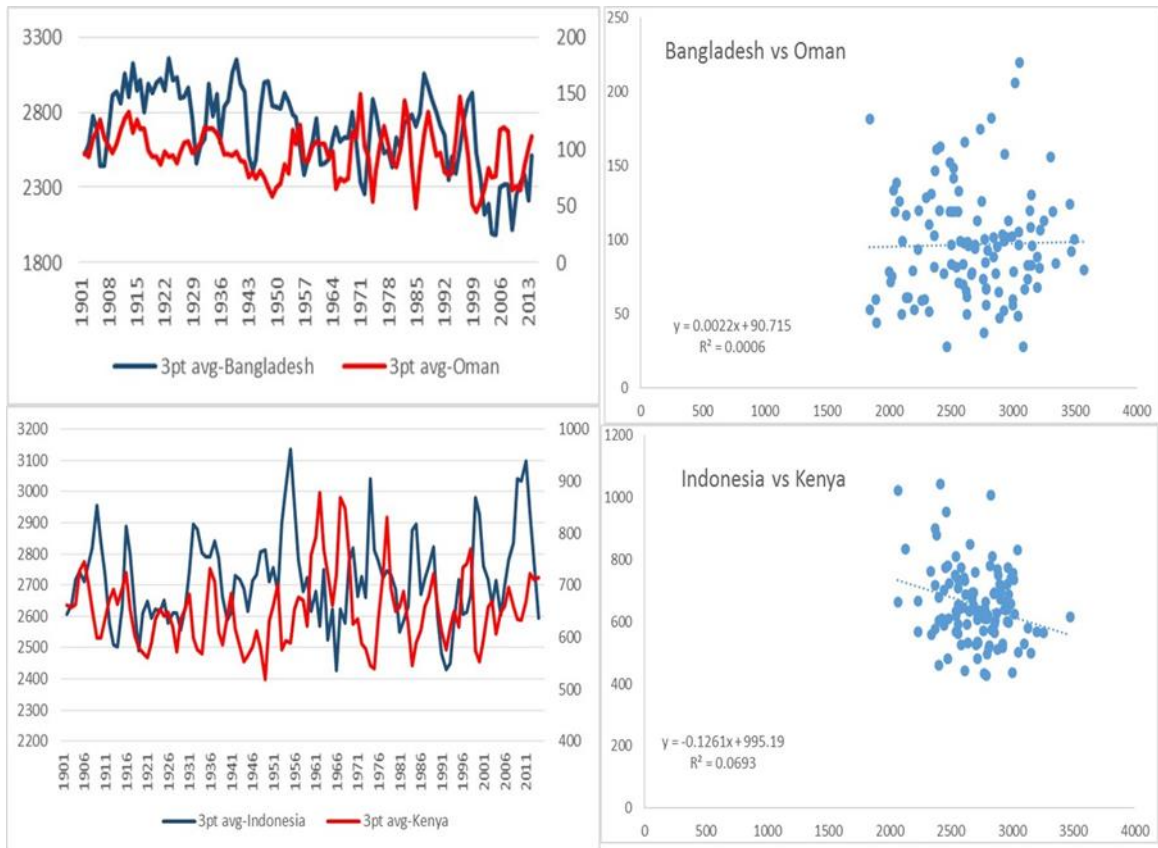


**Figure 4.12:** Historical rainfall c(for the last112 years) contrast between east Indian and west Indian Ocean land masses. In the top panel, Bangladesh and Oman data have been used and in the bottom panel, Indonesia data is compared with Kenya. The data is taken from CRU [Haris *et al.*, 2014].

p

recipitation and the wind-intensity is evident for the Northern Indian Ocean from the data presented above. The east-west contrast is similar to Indian Ocean Dipole phenomenon, when an alternating heat gradient between the eastern and western equatorial Indian Ocean persists representing positive and negative Dipole (e.g., Saji *et.al.*, 1999) which is an internal dynamics mechanism in the Indian Ocean but can impact the global climate as well [Saji and Yamagata, 2003]. Alternatively, this is a reflection of present day Bay of

Bengal-Arabian Sea contrast in heat budget, wind patterns, precipitation etc [Shenoi *et al.*, 2002].

To check if the above shown east-west contrast in Holocene precipitation is reflected in the modern time, the annual precipitation data of 90 years from 1905 to 2015 for Indonesia and Kenya to represent eastern and the western regions of the equatorial Indian Ocean were extracted (Fig. 4.12) from CRU [Harris *et al.*, 2014]. The extracted data is plotted in Fig. 4.12 which shows a near inverse relation with low correlation but suggests the existence of extremities of equatorial Indian Ocean. A comparison is also made for Bangladesh and Oman to represent the stations in the northern Indian Ocean region (Fig. 4.12) where a similar contrast is seen in our record. If the contrast is IOD-driven, this suggests that the IOD impact is not limited to equatorial region alone but may extend its influence to higher latitudes.

"The IOD involves an aperiodic oscillation of sea-surface temperatures, between "positive", "neutral" and "negative" phases. A positive phase sees greater-than-average sea-surface temperatures and greater precipitation in the western Indian Ocean region, with a corresponding cooling of waters in the eastern Indian Ocean—which tends to cause droughts in adjacent land areas of [Indonesia](#) and [Australia](#). The negative phase of the IOD brings about the opposite conditions, with warmer water and greater precipitation in the eastern Indian Ocean, and cooler and drier conditions in the west. The IOD also affects the strength of monsoons over the Indian subcontinent."  
([https://en.wikipedia.org/wiki/Indian\\_Ocean\\_Dipole](https://en.wikipedia.org/wiki/Indian_Ocean_Dipole))

The number of IOD events vary with time. In a 42 year record from January 1958 to December 1999, Saji and Yamagata (2003) have identified 9 positive (pIOD) and 10 negative IOD events from land rain and temperature data. Over the geological time-scales,

there are few interpretations of prevalence of IOD influencing the regional climate and monsoon. From a record from the central equatorial Indian Ocean (ODP716A), Gupta et al., (2010) have attributed the drastic decrease of *G.bulloides* population during mid-Bruhnes period (300-250ka) to strengthening IOD (positive-Indian Ocean Dipole) as an effect of major decrease of IEW (Indian Ocean Equatorial Westerlies), which is also

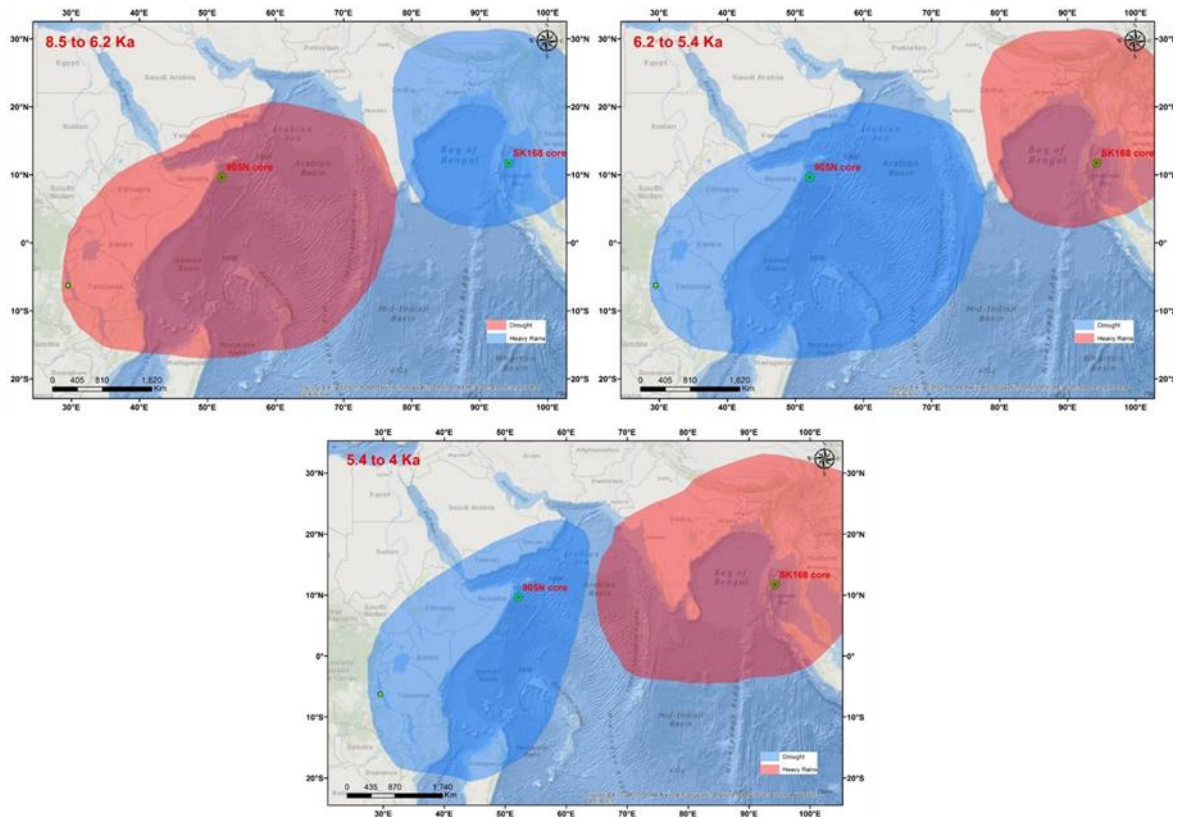


**Figure 4.13:** Regional variability of precipitation and East-West monsoonal contrast during three periods of Holocene epoch in the Northern Indian Ocean reconstructed from paleo-data.

supported with the occurrence of heavier floods in eastern Africa and drought conditions in Australia. A couple of records to my knowledge were found to have IOD influence. From a 8ka record from Mauritian lowland, *de Boer et.al.*, (2013) have found an anti-phased relationship of climate dynamics with the western tropical Australia during the middle Holocene and have interpreted this as a prolonged configuration of a negative mode of the Indian Ocean Dipole (IOD) and also considered the repeated decadal-scale wet events in the Mauritian lowlands occurring every  $\sim 350$  years to reflect short positive IOD-like

events [Boer *et al.*, 2013]. From the coral geochemical records from the equatorial eastern Indian Ocean, Abram *et al.* (2007) have identified 4 IOD events of longer duration of strong surface Ocean cooling during the last 6500 years associated with droughts that peaked later than those expected by El Niño forcing alone. Here, we propose the Holocene

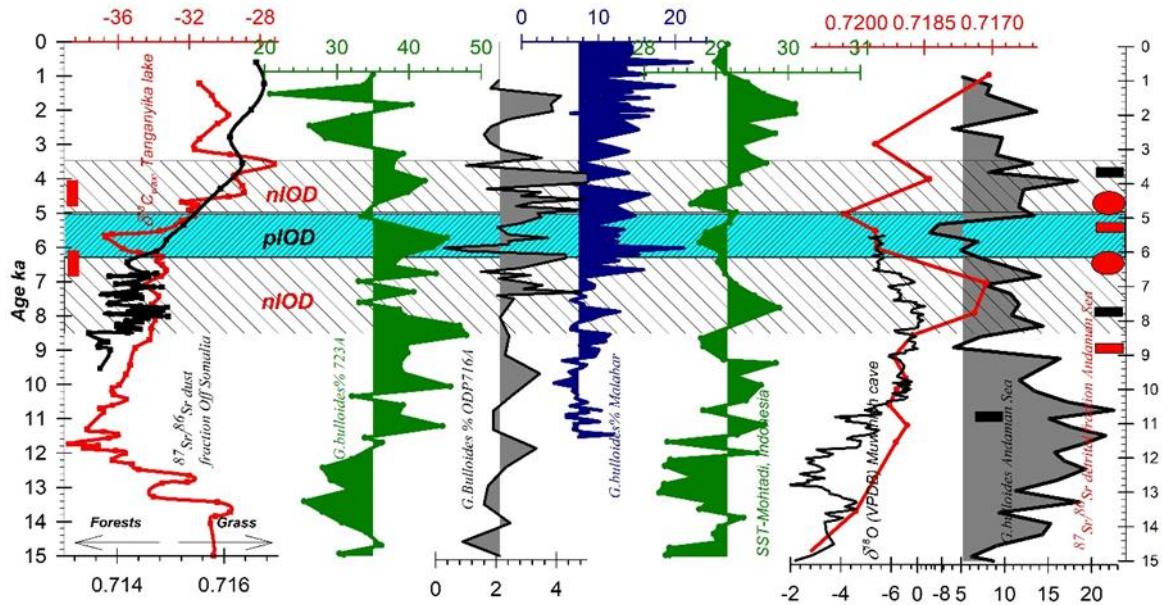


**Figure 4.14:** Sr isotope records of western (published) and eastern Indian Ocean (this study) are compared with wind proxies (upwelling indicators in oceans), monsoonal records from land in Africa, NE India.  $^{87}\text{Sr}/^{86}\text{Sr}$  isotope record off Somalia [Jung *et al.*, 2004];  $\delta^{13}\text{C}$  record from lake Tanganyika [Tierney and DeMenocal, 2013]; Variation of *G. bulloides* population from west to east Indian Ocean records [Naidu and Melmgren, 1995, Gupta *et al.*, 2010, Sijinkumar *et al.*, 2010]; SST record off Indonesia [Mohtadi *et al.*, 2014];  $^{87}\text{Sr}/^{86}\text{Sr}$  isotope record of Andaman Sea core (this study);  $\delta^{18}\text{O}$  record of Mawmulah cave [Dutt *et al.*, 2015]; the boxes and ellipsoids on the right end indicate lake level fluctuations (red – low level; black – increased lake levels) in India. Boxes on the extreme left indicate Holocene IOD events reported in an Indonesian island [Abram *et al.*, 2003].

c

changes in east-west contrast to prevalence of change in IOD modes, a negative Indian Ocean dipole mode during 8.5 to 6.5ka, 5 to 3.4ka with a positive mode sandwiched in between them (Fig. 4.13). The two negative phases identified here are similar to that found during Mid-Brunhes (300-250ka) but shorter in duration. The pIOD between ~6.5 to 5ka is when the African monsoon would have triggered, which was also identified as mid-Holocene climate transition in a core of eastern Arabian Sea [Saraswat *et al.*, 2016] but

with a reduced precipitation in Myanmar terrains ( $^{87}\text{Sr}/^{86}\text{Sr}$  of SK168) and the Andaman Sea [Sijinkumar *et al.*, 2010]. The drastic increase in forest type vegetation from grass type in African climate, shrinkage of western Indian lakes, reduction in Indonesian coral growth [Abram *et al.*, 2003], reduced chemical weathering in Myanmar terrains, fresh water input to Bay of Bengal, reduced productivity in fertile species of Andaman Sea altogether suggests the 6.5 to 5ka event as a strong pIOD in Indian Ocean. At 5ka, the effect of pIOD is reduced in both sides of Indian Ocean with the establishment of nIOD with warmed climate in east and cold climate in western Indian Ocean. This coupled exchange of phases in IOD is also supported by the  $\delta^{13}\text{C}_{\text{wax}}$  record (Fig. 4.14) of Tanganyika lake of Western Africa [Tierney and DeMenocal, 2013]. The less *G.bulloides* population in both central and western Indian Ocean records (Fig. 4.14) during first nIOD (8.5 to 6.5ka) suggests the prevailed arid climate over the entire Arabian Sea and African land masses. While during second nIOD (5 to 3.4ka), only the western Arabian Sea faced arid climate and eastern Arabian Sea and central Indian Ocean were same as that prevailed in the eastern Indian Ocean. The east-west contrast is stronger in the first nIOD (8.5 to 6.5ka) event compared to that of later nIOD event (5 to 3.4ka) possibly because of strengthened ENSO [Abram *et al.*, 2007]. Each of these 3 events are nearly 1500 yrs in duration and may represent the periods of increased influence of these modes. However, there may be smaller events within these mega events which are not deciphered because of time resolution the core covers.

#### 4.4. Conclusions

- The high resolution elemental and isotopic geochemistry studies carried out on deep-sea cores in a N-S transect from the Andaman Sea have helped to reconstruct

the geochemical history of lithogenic sedimentation since the last 54ka of the late Quaternary period. The northern and central cores of CAB with principle contribution from Irrawaddy, Salween and Sittang river systems responded more to the climatic changes in Myanmar watersheds. The chemical weathering proxies Al/K, Rb/Sr, CIA and  $^{87}\text{Sr}/^{86}\text{Sr}$  were able to capture the major changes prevailed during the deglacial climate. A rise in chemical weathering intensity at 17.7ka marks the recurrence of humid climate increase in Asian moisture content and may represent the first trigger of deglacial warming after the LGM. Increased summer insolation, atmospheric  $\text{CO}_2$ , moisture content, removal of vegetation cover and exposure of soil zone combinedly promoted the chemical weathering at 15.5 which continued until ~5.5ka in response to deglacial to mid-Holocene summer monsoonal intensification. A clear deglacial response suggests that the chemical weathering is not a later amplifier of climate change but operates in tandem. This study highlights the importance of contribution of Salween and Sittang river systems to the Andaman Sea in addition to Irrawaddy, which is considered as the dominant river system in the Northeastern Indian Ocean. Especially during glacial climates, the domination of Salween and Sittang derived SBR material is evident. The absence of more radiogenic Nd during glacials than late Holocene in the Andaman Sea (as observed in BoB) clearly suggests AS was isolated from the Bay of Bengal especially in sediment supply during low stands of sea-level during glacials.

- Radiogenic (Nd) hump during 15.5 to 5.5ka in both CAB cores as well in Irrawaddy river mouth core suggests, chemical weathering intensification on IBR terrains as a result of deglacial SW-monsoonal intensification made a significant impact on sediment supply to the Andaman Sea.

- Deglacial climatic impact signals were weak in southern core and the other published southeastern Andaman core which suggests that the monsoon and the weathering in south Myanmar and Thailand land masses, the source areas for these sediments, were not as significant as they are in northern Myanmar terrains.
- An east-west contrast, similar to Indian Ocean Dipole (IOD) phenomena, in precipitation and monsoon in the northern Indian Ocean was observed when the Holocene chemical weathering record of this study was compared with other precipitation records of the northern Indian Ocean. Distinct dissimilarities especially between the humidity and dust records in the western Indian Ocean and the African land mass with the monsoonal precipitation signatures in the eastern Indian Ocean. In all, two negative IOD-like events (8.5 to 6.5ka and 5 to 3.4ka) sandwiching one positive IOD like event (6.5 to 5ka) was noticed. This study suggests the prevalence of strong and mega-IOD like events within the early to mid-Holocene with reduced influence since the strengthening of ENSO phenomenon during the late Holocene. The east-west contrast as well as the temporal changes in alignment of Indian monsoon with the eastern and western regions of the northern Indian Ocean shows a regional variability of Indian monsoon in time and space and cautions the consideration of monsoon changes at one location at a given time to represent the South Asian Monsoon in general for the entire area.

## CHAPTER 5

# Summary and Conclusions

This study presents the results obtained and interpretations drawn from a comprehensive elemental and isotope geochemical data generated on the lithogenic fraction of 44 surface sediments and 3 well-dated sediment cores from a north-south transect from the Andaman Sea to delineate the sources, to decipher the temporal changes of late Quaternary lithogenic sedimentation, to interpret the erosion and weathering patterns in the Myanmar watersheds and in the other neighboring geological terrains and to study the climate-weathering-climate linkage during the LGM, deglaciation and the Holocene. The study is based on major, trace, rare-earth elements and the radiogenic isotopes like strontium, neodymium and hafnium in the lithogenic fraction. Elemental concentrations, their ratios, geochemical discrimination tracers (such as CIA, PIA etc.), isotope-isotope relations, ternary and mixing diagrams were used for the interpretations.

Before summarizing and concluding the present study, it is felt pertinent to highlight a similar study carried out elsewhere in the world. An excellent work using Al/K, CaO%,  $\epsilon_{Nd}$  and  $\epsilon_{Hf}$  in a sediment core recovered off Congo river mouth of equatorial Africa by Bayon *et.al.* [2012] has shown that the migration of human settlement has intensified the chemical weathering changes, greater than that induced by climate in the Congo river watersheds. The work of Bayon *et.al.*, and that presented here thus suggests that a knowledge of natural and man-made changes in the adjacent terrestrial watersheds are required before gleaning the paleoclimatic information from lacustrine and marine sedimentary records.

Important findings, interpretations and key conclusions drawn from this study are listed below.

- A large database of elemental and isotope geochemistry of sediments, generated in this work covering the entire Andaman Sea in space and time gave clues about possible sources and sedimentary pathways to the basin. The north-south increase in silica with

a reduction in alumina content over silica suggests a reduced basic composition towards southern parts of the basin.

- Elemental and isotopic analysis of shelf sediments that are retrieved off Myanmar rivers helped in defining the end-member composition of each of these rivers to the deep sea. The gradual decrease in lighter REE (Nd as a component) during 54 to 23ka (in SK168) with constant  $\epsilon_{Nd}$  strongly suggests Nd isotopes as a promising provenance indicator for this area. The  $\epsilon_{Nd}$  of river mouths bracketing all central Andaman sediments, suggests that all major Myanmar river systems Irrawaddy, Salween and Sittang (ISS) are principal carriers of terrigenous material to the central Andaman Sea in both glacial-interglacial periods.
- The more radiogenic  $\epsilon_{Nd}$  in sediments from Irrawaddy mouth is very similar to those in Arakan shelf, and agrees well with reported Irrawaddy sediment value and implies that the eastern and western part of Indo-Burman ranges (IBR) are contributing near similar Nd signal to the open ocean, either through Arakan, Rakhine rivers in western IBR or through Irrawaddy river on eastern IBR.
- The shelf sediments off rivers Salween and Sittang have distinctly low radiogenic values reflecting a dominance of old crustal material in the flood plains of Salween and Sittang. The low radiogenic (Nd) material in downcore Sr-Nd data of ADM-09 (southeastern basin) and RVS02/GC03 (southwestern basin) implies less control of Irrawaddy derived high radiogenic material in southern basin throughout its record spanning both glacial-interglacial climatic periods.
- The occurrence of  $\sim -17$   $\epsilon_{Nd}$  near Mergui Plateau shows the Mergui Plateau as the lowest radiogenic (Nd) end member to the Andaman Sea.

- The high resolution Sr-Nd isotopic study on SK168 along with other CAB core MD169 show a small shift in sources towards more radiogenic (Nd) from ~15ka to 5ka suggests the domination of Irrawaddy material over Salween and Sittang sources.
- Western Andaman Basin (WAB) represents the more radiogenic end member than other regions of the Andaman Sea. Four new isotopic data on surface sediments along with published long records suggests the importance of local islandic sources and Barren volcanism. But, the absence of such more radiogenic values in CAB sediments shows the limited geographic influence of WAB sources. The absence of observed excursions in WAB core (SK234) in CAB cores (SK168 and MD169) further suggests the limited contribution of WAB sources to the deep sea.
- The geochemical and isotopic studies on deep sea cores collected in north-south transect in addition to several surface sediments covering the major physiographic domains of the Andaman Sea suggests four major lithogenic zones of the basin viz., a) a zone that has Indo-Burman range (IBR) derived sediment, with Irrawaddy river being the major supplier; b) a zone that has supplies from the watersheds of eastern Myanmar rivers like Salween-Sittang-Tanintaryi; c) the western part of the basin which receives sediments mainly from the Andaman archipelago and local volcanism, and; d) the seamounts and volcanics associated with Western Andaman fault (WAF).
- Presence of Mergui Plateau derived material in southern core RVS02 implies the role of SW monsoonal currents in carrying sediments in clock wise direction on the broad eastern shelf and their deposition in southern Andaman region.
- Calculated  $T_{DM}$  (Nd-model) ages of northern and the southern core also supports the interpretations drawn from Sr-Nd plot viz., the dominant supply of Irrawaddy derived IBR material in the northern and central Andaman basin region while the southern Andaman Sea receiving sediments from Salween, Sittang regions and the Mergui

Plateau with high  $T_{DM}$  model ages. Sr-Nd mixing diagram with four end-members has shown the relative affinity and possible mixing patterns of different end-members in CAB, SAS and WAS sediments.

- New Hf-isotope data along with Nd-isotopes on the lithogenic fraction of SK168 shows how/why the eastern Himalayas (and/or Myanmar terrains) are different from central Himalayas. They fall in high radiogenic space, belongs to sea water array implies the hydrothermal influence. This might be due to tectonic evolution of Myanmar terranes.
- The high resolution elemental and isotopic geochemistry studies carried out on deep-sea cores in a N-S transect from the Andaman Sea have helped to reconstruct the geochemical history of lithogenic sedimentation since the last 54ka of the late Quaternary period. The northern and central cores of CAB with principle contribution from Irrawaddy, Salween and Sittang river systems responded more to the climatic changes in Myanmar watersheds. The chemical weathering proxies Al/K, Rb/Sr, CIA and  $^{87}\text{Sr}/^{86}\text{Sr}$  were able to capture the major changes prevailed during the deglacial climate. A rise in chemical weathering intensity at 17.7ka marks the recurrence of humid climate, increase in Asian moisture content and may represent the first trigger of deglacial warming after the LGM. Increased summer insolation, atmospheric  $\text{CO}_2$ , moisture content, removal of vegetation cover and exposure of soil zone combinedly promoted the chemical weathering at 15.5 which continued until ~5.5ka in response to deglacial to mid-Holocene summer monsoonal intensification. A clear deglacial response suggests that the chemical weathering is not a later amplifier of climate change but operated in tandem. This study highlights the importance of contribution of Salween and Sittang river systems to the Andaman Sea in addition to Irrawaddy, which is considered as the dominant river system in the Northeastern Indian Ocean.

Especially during glacial climates, the domination of Salween and Sittang derived SBR (Sino-Burman ranges) material is evident. The absence of more radiogenic Nd during glacials than late Holocene in the Andaman Sea (as observed in BoB) clearly suggests that the AS was isolated from the Bay of Bengal especially in sediment supply during low stands of sea-level during glacials.

- Radiogenic (Nd) hump during 15.5 to 5.5ka in both CAB cores as well in Irrawaddy river mouth core suggests, chemical weathering intensification on IBR terrains as a result of deglacial SW-monsoonal intensification made a significant impact on sediment supply to the Andaman Sea.
- Deglacial climatic impact signals were weak in southern core and the other published southeastern Andaman core which suggests that the weathering response to monsoon in south Myanmar and Thailand land masses (the source areas for these sediments) was poor compared to that in northern Myanmar terrains.
- An east-west contrast, similar to Indian Ocean Dipole (IOD) phenomena, in precipitation and monsoon in the northern Indian Ocean was observed when the Holocene chemical weathering record of this study was compared with other precipitation records of the northern Indian Ocean. Distinct dissimilarities especially between the humidity and dust records in the western Indian Ocean and the African land mass with the monsoonal precipitation signatures in the eastern Indian Ocean during the Holocene were noticed. In all, two negative IOD-like events (8.5 to 6.5ka and 5 to 3.4ka) sandwiching one positive IOD like event (6.5 to 5ka) was noticed. This study suggests the prevalence of strong and mega-IOD like events within the early to mid-Holocene. East-west contrast during the late Holocene was not so stark, possibly because of weakening of IOD like phenomenon with the strengthening of ENSO phenomenon. The east-west contrast as well as the temporal changes in alignment of

Indian monsoon with the eastern and western regions of the northern Indian Ocean shows a regional variability of Indian monsoon in time and space and cautions the consideration of monsoon changes at one location at a given time to represent the South Asian Monsoon in general for the entire area.

In summary, the work presented in this thesis has clearly demarcated the sediment pathways to the Andaman Sea in present day and during the last 54ka. In contrast to a general consideration of Irrawaddy being the predominant source, the isotopic data has shown that other two rivers Salween and Sittang flowing through Sino-Burman ranges also contribute sediments significantly to the Andaman Sea. The findings of role of SW monsoonal currents in carrying sediments in clock wise direction from east to south and the contribution from local volcanoes are new to this area. The relative contribution from different sources was found to vary between glacial and interglacial periods. Andaman Sea being a depocenter of sediments shed from Myanmar watersheds, the lithogenic sedimentation in well-characterized cores has allowed to visualize a clear climate-weathering/erosion linkage. Erosional and chemical weathering signals in the sediments were used as proxies for assessing the late Quaternary monsoonal changes in Myanmar watersheds for which a limited information is available. Chemical weathering was found to respond in tandem with climatic changes and was not a later amplifier. An east-west contrast in Holocene precipitation patterns, similar to Indian Ocean Dipole (IOD) phenomena, was found in the Northern Indian Ocean suggesting that a caution has to be exercised in considering a single monsoonal record to represent the regional monsoonal change for a given time period. The sediment record presented here has recorded three mega-IOD like events during the Holocene which are hitherto unknown for the Indian Ocean. But, do these extremities in internal dynamics of the Indian Ocean trigger any abrupt global climatic events is not known yet and has a potential for future studies.

# Bibliography

- Abram, N. J., M. K. Gagan, M. T. McCulloch, J. Chappell, and W. S. Hantoro (2003), Coral Reef Death During the 1997 Indian Ocean Dipole Linked to Indonesian Wildfires, *Science*, *301*(2003), 953–955, doi:10.1126/science.1083841.
- Abram, N. J., M. K. Gagan, Z. Liu, W. S. Hantoro, M. T. McCulloch, and B. W. Suwargadi (2007), Seasonal characteristics of the Indian Ocean Dipole during the Holocene epoch., *Nature*, *445*(7125), 299–302, doi:10.1038/nature05477.
- Achyuthan, H., M. Nagasundaram, A. T. Gourlan, C. Eastoe, S. M. Ahmad, and V. M. Padmakumari (2014), Mid-Holocene Indian Summer Monsoon variability off the Andaman Islands, Bay of Bengal, *Quat. Int.*, *349*, 232–244, doi:10.1016/j.quaint.2014.07.041.
- Ahmad, S. M., D. J. Patil, P. S. Rao, B. N. Nath, B. R. Rao, and G. Rajagopalan (2000), Glacial-interglacial changes in the surface water characteristics of the Andaman Sea: Evidence from stable isotopic ratios of planktonic foraminifera, *J. Earth Syst. Sci.*, *109*(1), 153–156, doi:10.1007/BF02719159.
- Ahmad, S. M., G. Anil Babu, V. M. Padmakumari, A. M. Dayal, B. S. Sukhija, and P. Nagabhushanam (2005), Sr, Nd isotopic evidence of terrigenous flux variations in the Bay of Bengal: Implications of monsoons during the last ~34,000 years, *Geophys. Res. Lett.*, *32*(22), 1–4, doi:10.1029/2005GL024519.
- Alagarsamy, R., C. F. You, B. N. Nath, and A. V. S. Kumar (2010), Determination of rare earth, major and trace elements in authigenic fraction of Andaman Sea (Northeastern Indian Ocean) sediments by Inductively Coupled Plasma-Mass Spectrometry, *Microchem. J.*, *94*(1), 90–97, doi:10.1016/j.microc.2009.09.007.
- Ali, S., E. C. Hathorne, M. Frank, D. Gebregiorgis, K. Stattegger, R. Stumpf, S. Kutterolf, J. E. Johnson, and L. Giosan (2015), South Asian monsoon history over the past 60 kyr recorded by radiogenic isotopes and clay mineral assemblages in the Andaman Sea, *Geochemistry, Geophys. Geosystems*, *16*(2), 505–521, doi:10.1002/2014GC005586.
- Allen, R., Y. Najman, A. Carter, D. Barfod, M. J. Bickle, H. J. Chapman, E. Garzanti, G. Vezzoli, S. Andò, and R. R. Parrish (2008), Provenance of the Tertiary sedimentary rocks of the Indo-Burman Ranges, Burma (Myanmar): Burman arc or Himalayan-derived?, *J. Geol. Soc. London.*, *165*(6), 1045–1057, doi:10.1144/0016-76492007-143.
- Altabet, M. A., M. J. Higginson, and D. W. Murray (2002), The effect of millennial-scale changes in Arabian Sea denitrification on atmospheric CO<sub>2</sub>, *Nature*, *415*(6868), 159–162, doi:10.1038/415159a.
- Anderson, D. L. T., and D. J. Carrington (1993), Modeling Interannual Variability in the Indian Ocean Using Momentum Fluxes From the Operational Weather Analyses of the United Kingdom Meteorological Office and European Centre for Medium Range Weather Forecasts, *J. Geophys. Res.*, *98*(7), 12,483–12,499.
- Arz, H. W., F. Lamy, and J. Pätzold (2006), A pronounced dry event recorded around 4.2 ka in brine sediments from the northern Red Sea, *Quat. Res.*, *66*(3), 432–441, doi:10.1016/j.yqres.2006.05.006.
- Awasthi, N., J. S. Ray, A. H. Laskar, A. Kumar, M. Sudhakar, R. Bhutani, H. C. Sheth, and M. G. Yadava (2010), Major ash eruptions of Barren Island volcano (Andaman Sea) during the past 72 kyr: Clues from a sediment core record, *Bull. Volcanol.*, *72*(9), 1131–1136, doi:10.1007/s00445-010-0408-1.

- Awasthi, N., J. S. Ray, A. K. Singh, S. T. Band, and V. K. Rai (2014), Provenance of the Late Quaternary sediments in the Andaman Sea: Implications for monsoon variability and ocean circulation, *Geochemistry Geophys. Geosystems*, *15*(2), 3890–3906, doi:10.1002/2014GC005462. Received.
- Le Bas, M. J., R. W. Le Maitre, A. Streckeisen, and B. Zanettin (1986), A chemical classification of volcanic rocks based on the total alkali silica diagram, *J. Petrol.*, *27*(3), 745–750, doi:10.1093/petrology/27.3.745.
- Baumeister, J. L. (2012), Chemical Weathering of the Mafic Minerals Serpentine and Olivine in Natural Environments, University of Nevada, Las Vegas.
- Bayon, G., C. R. German, R. M. Boella, J. a. Milton, R. N. Taylor, and R. W. Nesbitt (2002), An improved method for extracting marine sediment fractions and its application to Sr and Nd isotopic analysis, *Chem. Geol.*, *187*(3–4), 179–199, doi:10.1016/S0009-2541(01)00416-8.
- Bayon, G., K. W. Burton, G. Soulet, N. Vigier, B. Dennielou, J. Etoubleau, E. Ponzevera, C. R. German, and R. W. Nesbitt (2009), Hf and Nd isotopes in marine sediments: Constraints on global silicate weathering, *Earth Planet. Sci. Lett.*, *277*(3–4), 318–326, doi:10.1016/j.epsl.2008.10.028.
- Bayon, G., B. Dennielou, J. Etoubleau, E. Ponzevera, S. Toucanne, and S. Bermell (2012), Intensifying weathering and land use in Iron Age Central Africa., *Science*, *335*(6073), 1219–1222, doi:10.1126/science.1221820.
- Beaulieu, E., Y. Godd ris, Y. Donnadieu, D. Labat, and C. Roelandt (2012), High sensitivity of the continental-weathering carbon dioxide sink to future climate change, *Nat. Clim. Chang.*, *2*(5), 346–349, doi:10.1038/nclimate1419.
- Bender, F. (1983), *Geology of Burma*, Gebr. Borntraeger.
- Berger, A. (1978), Long-Term Variations of Daily Insolation and Quaternary Climatic Changes, *J. Atmos. Sci.*, *35*(12), 2362–2367, doi:10.1175/1520-0469(1978)035<2362:LTVODI>2.0.CO;2.
- Berner, R. A., A. C. Lasaga, and R. M. Garrels (1983), The carbonate-silicate geochemical cycle and its effect on atmospheric carbon dioxide over the past 100 million years., *Am. J. Sci.*, *283*(7), 641–683, doi:10.2475/ajs.283.7.641.
- Bhatia, M. R., and K. A. W. Crook (1986), Trace element characteristics of greywackes and tectonic setting discrimination of sedimentary basins, *Contrib. to Mineral. Petrol.*, *92*, 181–193, doi:10.1007/BF00375292.
- Bhushan, R. (2008), Geochemical and Isotopic studies in sediments and waters of the northern Indian Ocean, M.S. University of Baroda, Vadodara, India.
- Bird, B. W., P. J. Polisar, Y. Lei, L. G. Thompson, T. Yao, B. P. Finney, D. J. Bain, D. P. Pompeani, and B. A. Steinman (2014), A Tibetan lake sediment record of Holocene Indian summer monsoon variability, *Earth Planet. Sci. Lett.*, *399*, 92–102.
- Blunier, T., and E. J. Brook (2001), Timing of millennial-scale climate change in Antarctica and Greenland during the last glacial period., *Science*, *291*(5501), 109–12, doi:10.1126/science.291.5501.109.
- Boer, E. J. De, H. Hooghiemstra, F. B. V. Florens, C. Baider, S. Engels, V. Dakos, M. Blaauw, and K. D. Bennett (2013), Rapid succession of plant associations on the small ocean island of Mauritius at the onset of the Holocene, *Quat. Sci. Rev.*, *68*, 114–125, doi:10.1016/j.quascirev.2013.02.005.

- Broecker, W. S. (1994), Massive iceberg discharges as triggers for global climate change, *Nature*, 372(1 December), 421–424, doi:10.1038/372421a0.
- Burton, K. W., and D. Vance (2000), Glacial-interglacial variations in the neodymium isotope composition of seawater in the Bay of Bengal recorded by planktonic foraminifera, *Earth Planet. Sci. Lett.*, 176, 425–441.
- Cao, P., X. Shi, W. Li, S. Liu, Z. Yao, L. Hu, S. Khokiattiwong, and N. Kornkanitnan (2015), Sedimentary responses to the Indian Summer Monsoon variations recorded in the southeastern Andaman Sea slope since 26ka, *J. Asian Earth Sci.*, 114, 512–525, doi:10.1016/j.jseaes.2015.06.028.
- Chamley, H. (1989), Clay formation through weathering., in *Clay sedimentology.*, pp. 21–50, Springer-Verlag, Berlin.
- Chandrasekharam, D., A. P. Santo, B. Capaccioni, O. Vaselli, M. A. Alam, P. Manetti, and F. Tassi (2009), Volcanological and petrological evolution of Barren Island (Andaman Sea, Indian Ocean), *J. Asian Earth Sci.*, 35(5), 469–487, doi:10.1016/j.jseaes.2009.02.010.
- Chauhan, O. S., S. K. Patil, and J. Suneethi (2004), Fluvial influx and weathering history of the Himalayas since Last Glacial Maxima - Isotopic, sedimentological and magnetic records from the Bay of Bengal, *Curr. Sci.*, 87(4), 509–515.
- Chen, F., X.-H. Li, X.-L. Wang, Q.-L. Li, and W. Siebel (2007), Zircon age and Nd–Hf isotopic composition of the Yunnan Tethyan belt, southwestern China, *Int. J. Earth Sci.*, 96(6), 1179–1194, doi:10.1007/s00531-006-0146-y.
- Chesner, C. A., and W. I. Rose (1991), Stratigraphy of the Toba Tuffs and the evolution of the Toba Caldera Complex, Sumatra, Indonesia, *Bull. Volcanol.*, 53(5), 343–356, doi:10.1007/BF00280226.
- Chesner, C. A., W. I. Rose, A. Deino, R. Drake, and J. A. Westgate (1991), Eruptive history of Earth's largest Quaternary caldera (Toba, Indonesia) clarified, *Geology*, 19(3), 200–203, doi:10.1130/0091-7613(1991)019<0200:EHOESL>2.3.CO;2.
- Clift, P. D., K. V. Hodges, D. Heslop, R. Hannigan, H. Van Long, and G. Calves (2008a), Correlation of Himalayan exhumation rates and Asian monsoon intensity, *Nat. Geosci.*, 1(12), 875–880, doi:10.1038/ngeo351.
- Clift, P. D. et al. (2008b), Holocene erosion of the Lesser Himalaya triggered by intensified summer monsoon, *Geology*, 36(1), 79–82, doi:10.1130/G24315A.1.
- Colin, C., C. Kissel, D. Blamart, and L. Turpin (1998), Magnetic properties of sediments in the Bay of Bengal and the Andaman Sea: impact of rapid North Atlantic Ocean climatic events on the strength of the Indian monsoon, *Earth Planet. Sci. Lett.*, 160(3–4), 623–635, doi:10.1016/S0012-821X(98)00116-2.
- Colin, C., L. Turpin, J. Bertaux, A. Desprairies, and C. Kissel (1999), Erosional history of the Himalayan and Burman ranges during the last two glacial-interglacial cycles, *Earth Planet. Sci. Lett.*, 171(4), 647–660, doi:10.1016/S0012-821X(99)00184-3.
- Colin, C., L. Turpin, D. Blamart, N. Frank, C. Kissel, and S. Duchamp (2006), Evolution of weathering patterns in the Indo-Burman Ranges over the last 280 kyr: Effects of sediment provenance on  $^{87}\text{Sr}/^{86}\text{Sr}$  ratios tracer, *Geochemistry, Geophys. Geosystems*, 7(3), doi:10.1029/2005GC000962.
- Crowley, T. J., and G. R. North (1991), Paleoclimatology,

- Cullen, H. M., P. B. De Menocal, S. Hemming, F. H. Brown, T. Guilderson, and F. Sirocko (2000), Climate change and the collapse of the Akkadian empire: Evidence from the deep sea, *Geology*, 28(4), 379–382, doi:10.1130/0091-7613(2000)28<379:CCATCO>2.0.CO;2.
- Curry, J. R. (1994), Sediment volume and mass beneath the Bay of Bengal, *Earth Planet. Sci. Lett.*, 125(1–4), 371–383, doi:10.1016/0012-821X(94)90227-5.
- Curry, J. R. (2005), Tectonics and history of the Andaman Sea region, *J. Asian Earth Sci.*, 25(1), 187–232, doi:10.1016/j.jseaes.2004.09.001.
- Curry, J. R., and D. G. Moore (1971), Growth of the Bengal deep-sea fan and denudation in the Himalayas, *Bull. Geol. Soc. Am.*, 82(3), 563–572, doi:10.1130/0016-7606(1971)82[563:GOTBDF]2.0.CO;2.
- Curry, J. R., D. G. Moore, L. a Lawver, F. J. Emmel, R. W. Raitt, M. Henry, and R. M. Kieckhefer (1979), Tectonics of the Andaman Sea and Burma, *AAPG Mem.* 29, 29, 189–198.
- Damodararao, K., S. K. Singh, V. K. Rai, V. Ramaswamy, and P. S. Rao (2016), Lithology, Monsoon and Sea-Surface Current Control on Provenance, Dispersal and Deposition of Sediments over the Andaman Continental Shelf, *Front. Mar. Sci.*, 3(July), 1–15, doi:10.3389/fmars.2016.00118.
- Das, A., S. Krishnaswami, and A. Kumar (2006), Sr and 87Sr/86Sr in rivers draining the Deccan Traps (India): Implications to weathering, Sr fluxes, and the marine 87Sr/86Sr record around K/T, *Geochemistry, Geophys. Geosystems*, 7(6), 1–14, doi:10.1029/2005GC001081.
- DePaulo, D. J. (1980), Crustal growth and mantle evolution: inferences from models of element transport and Nd and Sr isotopes, *Geochim. Cosmochim. Acta*, 44(7), 1185–1196, doi:10.1016/0016-7037(81)90149-6.
- Derry, L. a., and C. France-Lanord (1996), Neogene Himalayan weathering history and river 87Sr/86Sr: impact on the marine Sr record, *Earth Planet. Sci. Lett.*, 142(1–2), 59–74, doi:10.1016/0012-821X(96)00091-X.
- Dopieralska, J., Z. Belka, P. Königshof, G. Racki, N. Savage, P. Lutat, and A. Sardud (2012), Nd isotopic composition of Late Devonian seawater in western Thailand: Geotectonic implications for the origin of the Sibumasu terrane, *Gondwana Res.*, 22(3–4), 1102–1109, doi:10.1016/j.gr.2012.01.009.
- Duplessy, J. C., L. Labeyrie, M. Arnold, M. Paterne, J. Duprat, and T. C. E. van Weering (1992), Changes in surface salinity of the North Atlantic Ocean during the last deglaciation, *Nature*, 358(6386), 485–488, doi:10.1038/358485a0.
- Dutt, S., A. K. Gupta, S. C. Clemens, H. Cheng, R. K. Singh, G. Kathayat, and R. Lawrence Edwards (2015), Abrupt changes in Indian summer monsoon strength during 33,800 to 5500 years B.P., *Geophys. Res. Lett.*, 42(13), 5526–5532, doi:10.1002/2015GL064015.
- Einsele, G., L. Ratschbacher, and A. Wetzel (1996), The Himalaya-Bengal Fan Denudation-Accumulation System during the past 20 Ma, *J. Geol.*, 104(2), 163–184.
- Fedo, C. M., H. W. Nesbitt, and G. M. Young (1995), Unravelling the effects of potassium metasomatism in sedimentary rocks and paleosols, with implications for paleoweathering conditions and provenance, *Geology*, 23(10), 921–924, doi:10.1130/0091-7613(1995)023<0921:UTEOPM>2.3.CO.
- Filippelli, G. M. (1997), Intensification of the Asian monsoon and a chemical weathering event in the late Miocene-early Pliocene: Implications for late Neogene climate change, *Geology*, 25(1), 27–

- 30, doi:10.1130/0091-7613(1997)025<0027:IOTAMA>2.3.CO.
- Fontugne, M. R., and J.-C. Duplessy (1986), Variations of the monsoon regime during the upper quaternary: Evidence from carbon isotopic record of organic matter in North Indian Ocean sediment cores, *Palaeogeogr. Palaeoclimatol. Palaeoecol.*, *56*(1–2), 69–88, doi:10.1016/0031-0182(86)90108-2.
- France-Lanord, C., L. Derry, and A. Michard (1993), *Evolution of the Himalaya since Miocene time: isotopic and sedimentological evidence from the Bengal Fan*, edited by P. J. Treloar and M. P. Searle.
- Frerichs, W. E. (1967), Distribution and ecology of foraminifera in the sediments of the Andaman Sea., University of southern California.
- Furuichi, T., Z. Win, and R. J. Wasson (2009), Discharge and suspended sediment transport in the Ayeyarwady River, Myanmar: Centennial and decadal changes, *Hydrol. Process.*, *23*(April), 1631–1641, doi:10.1002/hyp.
- Gaillardet, J., B. Dupré, P. Louvat, and C. J. Allègre (1999), Global silicate weathering and CO<sub>2</sub> consumption rates deduced from the chemistry of large rivers, *Chem. Geol.*, *159*(1–4), 3–30, doi:http://dx.doi.org/10.1016/S0009-2541(99)00031-5.
- Galy, A., and C. France-Lanord (1999), Weathering processes in the Ganges-Brahmaputra basin and the riverine alkalinity budget, *Chem. Geol.*, *159*(1–4), 31–60, doi:10.1016/S0009-2541(99)00033-9.
- Galy, A., and C. France-Lanord (2001), Higher erosion rates in the Himalay: Geochemical constraints on riverine fluxes, *Geology*, *29*(1), 23–26, doi:10.1130/0091-7613(2001)029<0023.
- Garçon, M., C. Chauvel, C. France-Lanord, P. Huyghe, and J. Lave (2013), ScienceDirect Continental sedimentary processes decouple Nd and Hf isotopes, *Geochim. Cosmochim. Acta*, *121*, 177–195.
- Gasse, F. (2000), Hydrological changes in the African tropics since the Last Glacial Maximum, *Quat. Sci. Rev.*, *19*, 189–211.
- Gebregiorgis, D., E. C. Hathorne, A. V. Sijinkumar, B. Nagender Nath, D. Nürnberg, and M. Frank (2016), South Asian summer monsoon variability during the last ~54 kysr inferred from surface water salinity and river run off proxies, *Quat. Sci. Rev.*, *138*, 6–15, doi:10.1016/j.quascirev.2016.02.012.
- Gireesh, R. (2010), Geophysical investigations of the andaman island arc- trench system and its collision with the ninety east ridge.
- Gislason, S. R. et al. (2009), Direct evidence of the feedback between climate and weathering, *Earth Planet. Sci. Lett.*, *277*(1–2), 213–222, doi:10.1016/j.epsl.2008.10.018.
- Goodbred S., J., and S. A. Kuehl (2000), Enormous Ganges-Brahmaputra sediment discharge during strengthened early Holocene monsoon, *Geology*, *28*(12), 1083–1086, doi:10.1130/0091-7613(2000)28<1083.
- Govil, P., and P. D. Naidu (2011), Variations of Indian monsoon precipitation during the last 32kyr reflected in the surface hydrography of the Western Bay of Bengal, *Quat. Sci. Rev.*, *30*(27–28), 3871–3879, doi:10.1016/j.quascirev.2011.10.004.
- Gupta, A. K., D. M. Anderson, and J. T. Overpeck (2003), Abrupt changes in the Asian southwest monsoon during the Holocene and their links to the North Atlantic Ocean., *Nature*, *421*(6921),

354–7, doi:10.1038/nature01340.

- Gupta, A. K., S. Sarkar, S. De, S. C. Clemens, and A. Velu (2010), Mid-Brunhes strengthening of the Indian Ocean Dipole caused increased equatorial East African and decreased Australasian rainfall, *Geophys. Res. Lett.*, *37*(6), 6–11, doi:10.1029/2009GL042225.
- Gupta, H., G. J. Chakrapani, K. Selvaraj, and S. J. Kao (2011), The fluvial geochemistry, contributions of silicate, carbonate and saline-alkaline components to chemical weathering flux and controlling parameters: Narmada River (Deccan Traps), India, *Geochim. Cosmochim. Acta*, *75*(3), 800–824, doi:10.1016/j.gca.2010.11.010.
- Halder, D., T. Laskar, P. C. Bandyopadhyay, N. K. Sarkar, and J. K. Bjswas (1992), Volcanic Eruption of the Barren Island Volcano, Andaman Sea, *J. Geol. Soc. India*, *39*(May), 411–419.
- Harnois, L. (1988), The CIW index: A new chemical index of weathering, *Sediment. Geol.*, *55*(3–4), 319–322, doi:10.1016/0037-0738(88)90137-6.
- Harris, I., P. D. Jones, T. J. Osborn, and D. H. Lister (2014), Updated high-resolution grids of monthly climatic observations - the CRU TS3.10 Dataset, *Int. J. Climatol.*, *34*(3), 623–642, doi:10.1002/joc.3711.
- Hein, C. J., V. Galy, A. Galy, C. France-Lanord, H. Kudrass, and T. Schwenk (2017), Post-glacial climate forcing of surface processes in the Ganges–Brahmaputra river basin and implications for carbon sequestration, *Earth Planet. Sci. Lett.*, *478*, 89–101, doi:10.1016/j.epsl.2017.08.013.
- Herzschuh, U. (2006), Palaeo-moisture evolution in monsoonal Central Asia during the last 50,000 years, *Quat. Sci. Rev.*, *25*(1–2), 163–178, doi:10.1016/j.quascirev.2005.02.006.
- Hong, Y. T. et al. (2003), Correlation between Indian Ocean summer monsoon and North Atlantic climate during the Holocene, *Earth Planet. Sci. Lett.*, *211*(3–4), 371–380, doi:10.1016/S0012-821X(03)00207-3.
- J. Streck, M., F. Ramos, A. Gillam, D. Halder, and R. A. Duncan (2011), The Intra-oceanic Barren Island and Narcondam Arc Volcanoes, Andaman Sea: Implications for Subduction Inputs and Crustal Overprint of a Depleted Mantle Source, in *Topics in Igneous Petrology*, pp. 241–273.
- Jacobson, A. D., J. D. Blum, C. P. Chamberlain, D. Craw, and P. O. Koons (2003), Climatic and tectonic controls on chemical weathering in the New Zealand Southern Alps, *Geochim. Cosmochim. Acta*, *67*(1), 29–46, doi:10.1016/S0016-7037(02)01053-0.
- Jafri, S. H., V. Balaram, and S. L. Ramesh (1990), Geochemistry of Andaman-Nicobar island basalts: A case for a possible plume origin, *J. Volcanol. Geotherm. Res.*, *44*(3–4), 339–347, doi:10.1016/0377-0273(90)90026-C.
- Janekarn, V., and J. Hylleberg (1989), Coastal and offshore primary production along the west coast of Thailand (Andaman Sea) with notes on physical-chemical variables., *Phuket Mar. Biol. Center. Res. Bull.*, *51*, 1–20.
- Jung, S. J. A., G. R. Davies, G. M. Ganssen, and D. Kroon (2004), Stepwise Holocene aridification in NE Africa deduced from dust-borne radiogenic isotope records, *Earth Planet. Sci. Lett.*, *221*(1–4), 27–37, doi:10.1016/S0012-821X(04)00095-0.
- Kamesh Raju, K. A., T. Ramprasad, P. S. Rao, B. Ramalingeswara Rao, and J. Varghese (2004), New insights into the tectonic evolution of the Andaman basin, northeast Indian Ocean, *Earth Planet. Sci. Lett.*, *221*(1–4), 145–162, doi:10.1016/S0012-821X(04)00075-5.

- Kamesh Raju, K. A., G. P. S. Murty, D. Amarnath, and M. L. M. Kumar (2007), The west Andaman fault and its influence on the aftershock pattern of the recent megathrust earthquakes in the Andaman-Sumatra region, *Geophys. Res. Lett.*, *34*(3), 1–5, doi:10.1029/2006GL028730.
- Kamesh Raju, K. A., D. Ray, A. Mudholkar, G. P. S. Murty, V. K. Gahalaut, K. Samudrala, A. L. Paropkari, R. Ramachandran, and L. Surya Prakash (2012), Tectonic and volcanic implications of a cratered seamount off Nicobar Island, Andaman Sea, *J. Asian Earth Sci.*, *56*(November 2007), 42–53, doi:10.1016/j.jseae.2012.04.018.
- Keller, G. H., and A. F. Richards (1967), Sediments of the Malacca strait, Southeast Asia, *J. Sediment. Petrol.*, *37*(1), 102–127.
- Konta, J. (1985), Mineralogy and chemical maturity of suspended matter, *Transp. carbon Miner. major world rivers, part III.*, 569–592.
- Krishna, K. S., M. Ismaiel, K. Srinivas, D. Gopala Rao, J. Mishra, and D. Saha (2016), Sediment pathways and emergence of Himalayan source material in the Bay of Bengal, *Curr. Sci.*, *110*(3), 363–372.
- Krishnaswami, S., J. R. Trivedi, M. M. Sarin, R. Ramesh, and K. K. Sharma (1992), Strontium isotopes and rubidium in the Ganga-Brahmaputra river system: Weathering in the Himalaya, fluxes to the Bay of Bengal and contributions to the evolution of oceanic  $^{87}\text{Sr}/^{86}\text{Sr}$ , *Earth Planet. Sci. Lett.*, *109*, 243–253.
- Kudrass, H. R., A. Hofmann, H. Dose, K. Emeis, and H. Erlenkeuser (2001), Modulation and amplification of climatic changes in the Northern Hemisphere by the Indian summer monsoon during the past 80 k.y., *Geology*, *29*(1), 63–66.
- Kumar, A. (2011), Geochemical and isotopic studies of rocks from the Barren Island Volcano and Andaman subduction zone, India, *PhD thesis*, 115–139.
- Kumar, S., A. Hazra, and B. N. Goswami (2014), Role of interaction between dynamics, thermodynamics and cloud microphysics on summer monsoon precipitating clouds over the Myanmar Coast and the Western Ghats, , 911–924, doi:10.1007/s00382-013-1909-3.
- Kurian, S., B. N. Nath, V. Ramaswamy, D. Naman, T. Gnaneshwar Rao, K. A. Kamesh Raju, K. Selvaraj, and C. T. A. Chen (2008), Possible detrital, diagenetic and hydrothermal sources for Holocene sediments of the Andaman backarc basin, *Mar. Geol.*, *247*(3–4), 178–193, doi:10.1016/j.margeo.2007.09.006.
- Lasaga, A. C., J. M. Soler, J. Ganor, T. E. Burch, and K. L. Nagy (1994), Chemical weathering rate laws and global geochemical cycles, *Geochim. Cosmochim. Acta*, *58*(10), 2361–2386, doi:10.1016/0016-7037(94)90016-7.
- Licht, A., C. France-Lanord, L. Reisberg, C. Fontaine, A. N. Soe, and J.-J. Jaeger (2013), A palaeo Tibet-Myanmar connection? Reconstructing the Late Eocene drainage system of central Myanmar using a multi-proxy approach, *J. Geol. Soc. London.*, *170*(6), 929–939, doi:10.1144/jgs2012-126.
- Licht, A., L. Reisberg, C. France-Lanord, A. Naing Soe, and J. J. Jaeger (2016), Cenozoic evolution of the central Myanmar drainage system: Insights from sediment provenance in the Minbu Sub-Basin, *Basin Res.*, *28*(2), 237–251, doi:10.1111/bre.12108.
- Limmer, D. R., C. M. Kohler, S. Hillier, S. G. Moreton, A. R. Tabrez, and P. D. Clift (2012a), Chemical weathering and provenance evolution of Holocene-Recent sediments from the Western Indus Shelf, Northern Arabian Sea inferred from physical and mineralogical properties, *Mar.*

- Geol.*, 326–328, 101–115, doi:10.1016/j.margeo.2012.07.009.
- Limmer, D. R., P. Bning, L. Giosan, C. Ponton, C. M. Köhler, M. J. Cooper, A. R. Tabrez, and P. D. Clift (2012b), Geochemical record of Holocene to Recent sedimentation on the Western Indus continental shelf, Arabian Sea, *Geochemistry, Geophys. Geosystems*, 13(1), 1–26, doi:10.1029/2011GC003845.
- Luhr, J. F., and D. Haldar (2006), Barren Island Volcano (NE Indian Ocean): Island-arc high-alumina basalts produced by troctolite contamination, *J. Volcanol. Geotherm. Res.*, 149, 177–212, doi:10.1016/j.jvolgeores.2005.06.003.
- MacFarlane, A. W., A. Danielson, H. D. Holland, and S. B. Jacobsen (1994), REE chemistry and Sm-Nd systematics of late Archean weathering profiles in the Fortescue Group, Western Australia, *Geochim. Cosmochim. Acta*, 58(7), 1777–1794.
- Metcalfe, I. (1996), Gondwanaland dispersion, Asian accretion and evolution of eastern Tethys\*, *Aust. J. Earth Sci.*, 43(6), 605–623, doi:10.1080/08120099608728281.
- Metcalfe, I. (2006), Palaeozoic and Mesozoic tectonic evolution and palaeogeography of East Asian crustal fragments: The Korean Peninsula in context, *Gondwana Res.*, 9(1–2), 24–46, doi:10.1016/j.gr.2005.04.002.
- Meybeck, M. (1989), *Pathways of major elements from land to ocean through rivers*.
- Milliman, J. D., and R. H. Meade (1983), World-wide delivery of river sediment to the Oceans, *J. Geol.*, 91(1), 1–21.
- Milliman, J. D., and J. P. M. Syvitski (1992), Geomorphic/Tectonic Control of Sediment Discharge to the Ocean: The Importance of Small Mountainous Rivers, *J. Geol.*, 100(5), 525–544, doi:10.1086/629606.
- Miriyala, P., N. P. Sukumaran, B. N. Nath, P. B. Ramamurthy, A. V Sijinkumar, B. Vijayagopal, V. Ramaswamy, and T. Sebastian (2017), Increased chemical weathering during the deglacial to mid-Holocene summer monsoon intensification, *Sci. Rep.*, 1–15, doi:10.1038/srep44310.
- Mitchell, A., S. L. Chung, T. Oo, T. H. Lin, and C. H. Hung (2012), Zircon U-Pb ages in Myanmar: Magmatic-metamorphic events and the closure of a neo-Tethys ocean?, *J. Asian Earth Sci.*, 56, 1–23, doi:10.1016/j.jseaes.2012.04.019.
- Mitchell, A. H. G., M. T. Htay, K. M. Htun, M. N. Win, T. Oo, and T. Hlaing (2007), Rock relationships in the Mogok metamorphic belt, Tatkon to Mandalay, central Myanmar, *J. Asian Earth Sci.*, 29(5–6), 891–910, doi:10.1016/j.jseaes.2006.05.009.
- Nagasundaram, M., H. Achyuthan, and S. M. Ahmad (2014), Monsoonal changes inferred from the Middle to Late Holocene sediments off Landfall Island, North Andaman, *Arab. J. Geosci.*, 7(9), 3513–3523, doi:10.1007/s12517-013-1010-6.
- Naidu, P. D., and B. A. Malmgren (1995), A 2,200 years periodicity in the Asian monsoon system, *Geophys. Res. Lett.*, 22(17), 2361–2364.
- Nakapadungrat, S., R. D. Beckinsale, and S. Suensilpong (1984), Geochronology and geology of Thai granites., in *Applications of Geology and the National Development*, pp. 75–93.
- Naqvi, W. A., C. D. Charles, and R. G. Fairbanks (1994), Carbon and oxygen isotopic records of benthic foraminifera from the Northeast Indian Ocean: implications on glacial-interglacial atmospheric CO<sub>2</sub> changes, *Earth Planet. Sci. Lett.*, 121, 99–110.

- Nath, B. N. (2001), Geochemistry of sediments, in *The Indian Ocean: A perspective, vol. 2, Oxford & IBH, New Delhi (India)*, pp. 645–689.
- Nath, B. N., and A. V. Mudholkar (1989), Early diagenetic processes affecting nutrients in the pore waters of Central Indian Ocean cores, *Mar. Geol.*, 86(1), 57–66, doi:10.1016/0025-3227(89)90018-2.
- Nath, B. N., K. Kunzendorf, and W. Plüger (2000), Influence of Provenance, Weathering and Sedimentary Processes on the Elemental Ratios Of the Fine Grained Fraction of the Bedload Sediments from the Vembanad Lake and the Adjoining Continental Shelf, South-West Coast of India, *J. Sediment. Res.*, 70(1), 1081–1094, doi:10.1306/100899701081.
- Nath, B. N., S. M. Gupta, P. G. Mislankar, B. R. Rao, G. Parthiban, I. Roelandts, and S. K. Patil (2005), Evidence of Himalayan erosional event at ~0.5Ma from a sediment core from the equatorial Indian Ocean in the vicinity of ODP Leg 116 sites, *Deep Sea Res. Part II Top. Stud. Oceanogr.*, 52(14–15), 2061–2077, doi:10.1016/j.dsr2.2005.05.011.
- Nesbitt, H. W., and G. M. Young (1982), Early Proterozoic climates and plate motions inferred from major element chemistry of lutites, *Nature*, 299(5885), 715–717, doi:10.1038/299715a0.
- Nesbitt, H. W., G. Markovics, and R. G. Price (1980), Chemical processes affecting alkalis and alkaline earths during continental weathering., *Geochim. Cosmochim. Acta*, 44(11), 1659–1666, doi:10.1016/0016-7037(80)90218-5.
- Nobi, E. P., E. Dilipan, T. Thangaradjou, K. Sivakumar, and L. Kannan (2010), Geochemical and geo-statistical assessment of heavy metal concentration in the sediments of different coastal ecosystems of Andaman Islands, India, *Estuar. Coast. Shelf Sci.*, 87(2), 253–264, doi:10.1016/j.ecss.2009.12.019.
- Ota, Y. et al. (2017), Effects of intensification of the Indian Summer Monsoon on northern Andaman Sea sediments during the past 700 years, *J. Quat. Sci.*, 32(4), 528–539, doi:10.1002/jqs.2947.
- Overpeck, J., D. Rind, a Lacis, and R. Healy (1996), Possible role of dust-induced regional warming in abrupt climate change during the last glacial period, *Nature*, 384(6608), 447–449, doi:10.1038/384447a0.
- Patchett, P. J., W. M. White, H. Feldmann, S. Kielinczuk, and A. W. Hofmann (1984), Hafnium/rare earth element fractionation in the sedimentary system and crustal recycling into the Earth's mantle, *Earth Planet. Sci. Lett.*, 69(2), 365–378, doi:10.1016/0012-821X(84)90195-X.
- Petit, R. J., D. Raynaud, I. Basile, J. Chappellaz, C. Ritz, M. Delmotte, M. Legrand, C. Lorius, and L. Pe (1999), Climate and atmospheric history of the past 420,000 years from the Vostok ice core, Antarctica, *Nature*, 399, 429–413, doi:10.1038/20859.
- Phadtare, N. R. (2000), Sharp Decrease in Summer Monsoon Strength 4000–3500 cal yr B.P. in the Central Higher Himalaya of India Based on Pollen Evidence from Alpine Peat, *Quat. Res.*, 53, 122–129, doi:10.1006/qres.1999.2108.
- Phillips, S. C., J. E. Johnson, M. B. Underwood, J. Guo, L. Giosan, and K. Rose (2014), Long-timescale variation in bulk and clay mineral composition of Indian continental margin sediments in the Bay of Bengal, Arabian Sea, and Andaman Sea, *Mar. Pet. Geol.*, 58(PA), 117–138, doi:10.1016/j.marpetgeo.2014.06.018.
- Prins, M. A., G. Postma, J. Cleveringa, A. Cramp, and N. H. Kenyon (2000), Controls on terrigenous sediment supply to the Arabian Sea during the late quaternary: The Indus fan, *Mar. Geol.*, 169(3–4), 327–349, doi:10.1016/S0025-3227(00)00086-4.

- Rahaman, W., S. K. Singh, R. Sinha, and S. K. Tandon (2009), Climate control on erosion distribution over the Himalaya during the past ~100 ka, *Geology*, *37*(6), 559–562, doi:10.1130/G25425A.1.
- Raj, R., L. S. Chamyal, V. Prasad, A. Sharma, J. K. Tripathi, and P. Verma (2015), Holocene climatic fluctuations in the Gujarat Alluvial Plains based on a multiproxy study of the Pariyaj Lake archive, western India, *Palaeogeogr. Palaeoclimatol. Palaeoecol.*, *421*, 60–74, doi:10.1016/j.palaeo.2015.01.004.
- Ramaswamy, V., P. . Rao, K. . Rao, S. Thwin, N. S. Rao, and V. Raiker (2004), Tidal influence on suspended sediment distribution and dispersal in the northern Andaman Sea and Gulf of Martaban, *Mar. Geol.*, *208*(1), 33–42, doi:10.1016/j.margeo.2004.04.019.
- Rao, P. S., K. A. Kamesh Raju, T. Ramprasad, B. Nagender Nath, B. Ramalingeswara Rao, C. M. Rao, and R. R. Nair (1996), Evidence for hydrothermal activity in the Andaman Backarc Basin, *Curr. Sci.*, *70*(5), 379–385.
- Rao, P. S., V. Ramaswamy, and S. Thwin (2005), Sediment texture, distribution and transport on the Ayeyarwady continental shelf, Andaman Sea, *Mar. Geol.*, *216*(4), 239–247, doi:10.1016/j.margeo.2005.02.016.
- Rashid, H., B. P. Flower, R. Z. Poore, and T. M. Quinn (2007), A ~25 ka Indian Ocean monsoon variability record from the Andaman Sea, *Quat. Sci. Rev.*, *26*(19–21), 2586–2597, doi:10.1016/j.quascirev.2007.07.002.
- Rashid, H., E. England, L. Thompson, and L. Polyak (2011), Late Glacial to Holocene Indian Summer Monsoon Variability Based upon Sediment Records Taken from the Bay of Bengal, *J. Geophys. Res.*, *116*(2), 215–228, doi:10.3319/TAO.2010.09.17.02(TibXS)1.
- Ray, J. S., K. Pande, and N. Awasthi (2013), A minimum age for the active Barren Island volcano, Andaman Sea, *Curr. Sci.*, *104*(7), 934–939.
- Raymo, M. E., and W. F. Ruddiman (1992), Tectonic forcing of late Cenozoic climate, *Nature*, *359*(10), 117–122.
- Ridd, M. F. (2009a), Geological history of the Sibumasu Block in Peninsular Thailand: report of a Geologists' Association Field Meeting in 2007, *Proc. Geol. Assoc.*, *120*(2–3), 163–174, doi:10.1016/j.pgeola.2009.09.002.
- Ridd, M. F. (2009b), The Phuket Terrane: A Late Palaeozoic rift at the margin of Sibumasu, *J. Asian Earth Sci.*, *36*(2–3), 238–251, doi:10.1016/j.jseaes.2009.06.006.
- Rodolfo, K. S. (1968), Sediment of the Andaman Basin, northeastern Indian ocean, *Mar. Geol.*, *7*(1969), 371–402, doi:10.1016/0025-3227(69)90014-0.
- Rodolfo, K. S. (1969), Bathymetry and Marine Geology of the Andaman Basin, and Tectonic Implications for Southeast Asia, *Geol. Soc. Am. Bull.*, *80*(7), 1203–1230, doi:10.1130/0016-7606(1969)80.
- Roger, F., N. Arnaud, S. Gilder, P. Tapponnier, M. Jolivet, M. Brunel, J. Malavieille, Z. Xu, and J. Yang (2003), Geochronological and geochemical constraints on Mesozoic suturing in east central Tibet, *Tectonics*, *22*(4), 1–20, doi:10.1029/2002TC001466.
- Roonwal, G. S., G. P. Glasby, and R. Chugh. (1997), Mineralogy and geochemistry of surface sediments from the Bengal Fan, Indian Ocean, *J. Asian Earth Sci.*, *15*(1), 33–41.
- Rutberg, R. L., S. L. Goldstein, S. R. Hemming, and R. F. Anderson (2005), Sr isotope evidence for

- sources of terrigenous sediment in the southeast Atlantic Ocean: Is there increased available Fe for enhanced glacial productivity?, *Paleoceanography*, 20(1), 1–10, doi:10.1029/2003PA000999.
- Saji, N. H., and T. Yamagata (2003), Possible impacts of Indian Ocean Dipole mode events on global climate, *Clim. Res.*, 25(2), 151–169, doi:10.3354/cr025151.
- Saji, N. H., B. N. Goswami, P. N. Vinayachandran, and T. Yamagata (1999), A dipole mode in the tropical Indian Ocean, *Nature*, 401(6751), 360–363, doi:10.1038/43854.
- Saraswat, R., D. K. Naik, R. Nigam, and A. S. Gaur (2016), Timing, cause and consequences of mid-Holocene climate transition in the Arabian Sea, *Quat. Res.*, 1–8, doi:10.1016/j.yqres.2016.06.001.
- Sarin, M. M., S. Krishnaswami, J. R. Trivedi, and K. K. Sharma (1992), Major ion chemistry of the Ganga source waters: Weathering in the high altitude Himalaya, *Proc. Indian Acad. Sci. - Earth Planet. Sci.*, 101(1), 89–98, doi:10.1007/BF02839175.
- Sarkar, a, R. Ramesh, S. K. Bhattacharya, and G. Rajagopalan (1990), Oxygen isotope evidence for a stronger winter monsoon during the last glaciation, *Nature*, 343, 549–551.
- Sarma, V. V. S. S., and P. V. Narvekar (2001), A study on inorganic carbon components in the Andaman Sea during the post monsoon season, *Oceanol. Acta*, 24(2), 125–134, doi:10.1016/S0399-1784(00)01133-6.
- Selvaraj, K., and C. A. Chen (2006), Moderate Chemical Weathering of Subtropical Taiwan: Constraints from Solid-Phase Geochemistry of Sediments and Sedimentary Rocks, *J. Geol.*, 114(1), 101–116, doi:10.1086/498102.
- Shakun, J. D., P. U. Clark, F. He, S. A. Marcott, A. C. Mix, Z. Liu, B. Otto-Bliesner, A. Schmittner, and E. Bard (2012), Global warming preceded by increasing carbon dioxide concentrations during the last deglaciation, *Nature*, 484(7392), 49–54, doi:10.1038/nature10915.
- Shenoi, S. S. C., D. Shankar, and S. R. Shetye (2002), Differences in heat budgets of the near-surface Arabian Sea and Bay of Bengal: Implications for the summer monsoon, *J. Geophys. Res.*, 107, 1–14.
- Sheth, H. C., J. S. Ray, R. Bhutani, A. Kumar, and R. S. Smitha (2009), Volcanology and eruptive styles of Barren Island: An active mafic stratovolcano in the andaman sea, NE Indian Ocean, *Bull. Volcanol.*, 71(9), 1021–1039, doi:10.1007/s00445-009-0280-z.
- Sheth, H. C., J. S. Ray, A. Kumar, R. Bhutani, and N. Awasthi (2011), Toothpaste lava from the Barren Island volcano (Andaman Sea), *J. Volcanol. Geotherm. Res.*, 202(1–2), 73–82, doi:10.1016/j.jvolgeores.2011.01.006.
- Sijinkumar, A. V., B. N. Nath, and M. V. S. Guptha (2010), Late Quaternary record of pteropod preservation from the Andaman Sea, *Mar. Geol.*, 275(1–4), 221–229, doi:10.1016/j.margeo.2010.06.003.
- Sijinkumar, A. V., S. Clemens, B. N. Nath, W. Prell, R. Benshila, and M. Lengaigne (2016a),  $\delta^{18}\text{O}$  and salinity variability from the Last Glacial Maximum to Recent in the Bay of Bengal and Andaman Sea, *Quat. Sci. Rev.*, 135, 79–91, doi:10.1016/j.quascirev.2016.01.022.
- Sijinkumar, A. V., B. N. Nath, G. Possnert, and A. Aldahan (2011), Pulleniatina Minimum Events in the Andaman Sea (NE Indian Ocean): Implications for winter monsoon and thermocline changes, *Mar. Micropaleontol.*, 81(3–4), 88–94, doi:10.1016/j.marmicro.2011.09.001.
- Sijinkumar, A. V., B. N. Nath, M. V. S. Guptha, S. M. Ahmad, and B. R. Rao (2015), Timing and

- preservation mechanism of deglacial pteropod spike from the Andaman Sea, northeastern Indian Ocean, *Boreas*, 44(2), 432–444, doi:10.1111/bor.12099.
- Sijinkumar, A. V., B. Nagender Nath, and S. Clemens (2016b), North Atlantic climatic changes reflected in the Late Quaternary foraminiferal abundance record of the Andaman Sea, northeastern Indian Ocean, *Palaeogeogr. Palaeoclimatol. Palaeoecol.*, 446, 11–18, doi:10.1016/j.palaeo.2016.01.009.
- Stamp, D. L. (1940), The Irrawaddy River, *Geogr. J.*, 5(1885), 329–352.
- Staubwasser, M., F. Sirocko, P. M. Grootes, and M. Segl (2003), Climate change at the 4.2 ka BP termination of the Indus valley civilization and Holocene south Asian monsoon variability, *Geophys. Res. Lett.*, 30(8), 3–6, doi:10.1029/2002GL016822.
- Stoll, H. M., D. Vance, and A. Arevalos (2007), Records of the Nd isotope composition of seawater from the Bay of Bengal: Implications for the impact of Northern Hemisphere cooling on ITCZ movement, *Earth Planet. Sci. Lett.*, 255, 213–228, doi:10.1016/j.epsl.2006.12.016.
- Stuiver, M., and P. J. Reimer (1993), Extended  $^{14}\text{C}$  data base and revised CALIB 3.0  $^{14}\text{C}$  age calibration program, *Radiocarbon*, 35(1), 215–230.
- Taylor, S. T., and S. M. McLennan (1985), The continental crust: its composition and evolution, *Blackwell Sci. Publ.*, 312.
- Thamban, M., V. Purnachandra Rao, and R. R. Schneider (2002), Reconstruction of late Quaternary monsoon oscillations based on clay mineral proxies using sediment cores from the western margin of India, *Mar. Geol.*, 186(3–4), 527–539, doi:10.1016/S0025-3227(02)00268-2.
- Thompson, L. L. G. et al. (2002), Kilimanjaro ice core records: Evidence of Holocene climate change in tropical Africa, *Science*, 298(OCTOBER), 589–593, doi:10.1126/science.1073198.
- Tierney, J. E., and P. B. DeMenocal (2013), Abrupt Shifts in Horn of Africa Since the Last Glacial Maximum, *Science*, 342, 843–846, doi:10.1126/science.1240411.
- Tripathy, G. R., S. K. Singh, R. Bhushan, and V. Ramaswamy (2011), Sr–Nd isotope composition of the Bay of Bengal sediments: Impact of climate on erosion in the Himalaya, *Geochem. J.*, 45, 175–186.
- Turekian, K. K., and K. H. Wedepohl (1961), Distribution of the Elements in Some Major Units of the Earth's Crust, *Geol. Soc. Am. Bull.*, 72(February), 175–192.
- Turner, S., J. Foden, R. George, P. Evans, R. Varne, M. Elburg, and G. Jenner (2003), Rates and Processes of Potassic Magma Evolution beneath Sangeang Api Volcano, East Sunda Arc, Indonesia, 44(3), 491–515.
- Varkey, M. J., V. S. N. Murty, and A. Suryanarayana (1996), Physical Oceanography of the Bay of Bengal and Andaman Sea, *Oceanogr. Mar. Biol. An Annu. Rev.*, 34, 1–70.
- Venkatesan, M., E. Ruth, P. S. Rao, B. N. Nath, and B. R. Rao (2003), Hydrothermal petroleum in the sediments of the Andaman Backarc Basin, Indian Ocean, *Appl. Geochemistry*, 18(6), 845–861, doi:10.1016/S0883-2927(02)00180-4.
- Vervoort, J. D., P. J. Patchett, J. Blichert-toft, and F. Albarede (1999), Relationships between Lu–Hf and Sm–Nd isotopic systems in the global sedimentary system, 168, 79–99.
- Volk, T. (1987), Feedbacks between weathering and atmospheric  $\text{CO}_2$  over the last 100 million yearsQ, *Am. J. Sci.*, 287(8), 763–779, doi:10.2475/ajs.287.8.763.

- Walker, J. C. G., P. B. Hays, and J. F. Kasting (1981), Weathering rates in 106 gm km<sup>-2</sup> yr<sup>-1</sup> of dissolved SiO<sub>2</sub>. Parentheses signify, 86(1), 9776–9782.
- Wan, S., W. M. Kürschner, P. D. Clift, A. Li, and T. Li (2009), Extreme weathering/erosion during the Miocene Climatic Optimum: Evidence from sediment record in the South China Sea, *Geophys. Res. Lett.*, 36(19), doi:10.1029/2009GL040279.
- Wang, Y. J. (2001), A High-Resolution Absolute-Dated Late Pleistocene Monsoon Record from Hulu Cave, China, *Science*, 294(5550), 2345–2348, doi:10.1126/science.1064618.
- Wei, G., X.-H. Li, Y. Liu, L. Shao, and X. Liang (2006), Geochemical record of chemical weathering and monsoon climate change since the early Miocene in the South China Sea, *Paleoceanography*, 21(December), 1–11, doi:10.1029/2006PA001300.
- Weninger, B., O. Jöris, and U. Danzeglocke (2007), “CalPal-2007. Cologne radiocarbon calibration & palaeoclimate research package.”
- White, W. M., J. Patchett, and D. BenOthman (1986), Hf isotope ratios of marine sediments and Mn nodules: evidence for a mantle source of Hf in seawater, *Earth Planet. Sci. Lett.*, 79(1–2), 46–54, doi:10.1016/0012-821X(86)90039-7.
- Wolff, C., G. H. Haug, A. Timmermann, J. S. Sinninghe Damsté, A. Brauer, D. M. Sigman, M. A. Cane, and D. Verschuren (2011), Reduced Interannual Rainfall variability in East Africa During the Last Ice Age, *Science*, 333(August), 743–747.
- Yarincik, K. M., R. W. Murray, and L. C. Peterson (2000), Climatically sensitive eolian and hemipelagic deposition in the Cariaco Basin, Venezuela, over the past 578,000 years: Results from Al/Ti and K/Al, *Paleoceanography*, 15(2), 210–228, doi:10.1029/1999PA900048.
- Yuan, D. et al. (2004), Timing, duration, and transitions of the last interglacial Asian monsoon., *Science*, 304(5670), 575–578, doi:10.1126/science.1091220.
- Zhou, W., X. Xie, W. Beck, X. Kong, F. Xian, Y. Du, and Z. Wu (2015), Recent progress of <sup>10</sup>Be tracer studies in Chinese loess, *Nucl. Instruments Methods Phys. Res. Sect. B Beam Interact. with Mater. Atoms*, 361(June), 548–553, doi:10.1016/j.nimb.2015.02.061.

### **Publications:**

Pavan Miriyala, N. P. Sukumaran, B. Nagender Nath, P. B. Ramamurty, A.V. Sijinkumar, B. Vijayagopal, V. Ramaswamy & Tyson Sebastian. Increased chemical weathering during the deglacial to mid-Holocene summer monsoon intensification. Sci. Rep. 7, 44310; doi: 10.1038/srep44310 (2017).

### **Under preparation:**

Pavan Miriyala and B. Nagender Nath. Global control of Indian Ocean dynamics. (manuscript under preparation to submit in journal of *Science*)

# SCIENTIFIC REPORTS



OPEN

## Increased chemical weathering during the deglacial to mid-Holocene summer monsoon intensification

Received: 10 October 2016

Accepted: 06 February 2017

Published: 17 March 2017

Pavan Miriyala<sup>1</sup>, N. P. Sukumaran<sup>1</sup>, B. Nagender Nath<sup>2</sup>, P. B. Ramamurthy<sup>1</sup>, A. V. Sijinkumar<sup>3</sup>, B. Vijayagopal<sup>1</sup>, V. Ramaswamy<sup>2</sup> & Tyson Sebastian<sup>2</sup>

Chemical weathering and the ensuing atmospheric carbon dioxide consumption has long been considered to work on geological time periods until recently when some modelling and natural records have shown that the weathering-related CO<sub>2</sub> consumption can change at century to glacial-interglacial time scale. Last glacial to interglacial transition period is a best test case to understand the interplay between Pco<sub>2</sub>-temperature-chemical weathering when a pulse of rapid chemical weathering was initiated. Here we show, from a high resolution 54 ka record from the Andaman Sea in the northern Indian Ocean, that the chemical weathering responds to deglacial to mid-Holocene summer monsoon intensification in the Myanmar watersheds. The multi-proxy data (Al/K, CIA, Rb/Sr, <sup>87</sup>Sr/<sup>86</sup>Sr for degree of weathering and <sup>143</sup>Nd/<sup>144</sup>Nd for provenance) reveal an increase in silicate weathering with initiation of interglacial warm climate at ~17.7 ka followed by a major change at 15.5 ka. Inferred changes in chemical weathering have varied in tandem with the regional monsoonal proxies ( $\delta^{18}\text{O}_{\text{sw}}$ -salinity changes of Northern Indian Ocean, effective Asian moisture content and  $\delta^{18}\text{O}$  records of Chinese caves) and are synchronous with changes in summer insolation at 30°N and  $\delta^{18}\text{O}$  of GISP2 implying that chemical weathering was not a later amplifier but worked in tandem with global climate change.

Silicate weathering is the major process which consumes Pco<sub>2</sub> and preserves its imprints in the weathered products. While the weathering controlled solute transport in the present day streams/water bodies fail to detect the climatic link<sup>1</sup>, weathering rates in soils and small catchments were found to be linked to significant climate effect<sup>2</sup>. Consequently, the role of chemical weathering has been considered only in studies dealing with geological climatic evolution, because it was thought to react slowly to climatic changes. A recent report, of a rapid increase in the chemical weathering flux in Iceland (up to 30% increase over four decades) in response to high-latitude climate change<sup>3</sup>, however has challenged this idea. More recent modeling study of MacKenzie River basin, an Arctic watershed has supported this. At the current rate of anthropogenic emissions and increased atmospheric CO<sub>2</sub> and temperature, it was estimated that the CO<sub>2</sub> consumption flux related to weathering processes increases by more than 50% for an atmospheric CO<sub>2</sub> doubling by the end of this century<sup>4</sup>. In this context, paleoweathering records of climate change regime would be useful to assess their linkage. Major climatic changes occurred during the glacial-interglacial cycles during the Quaternary. The current interglacial has also witnessed short term but profound climatic changes such as Bolling-Allerod (B-A), Younger Dryas (YD) and Little Ice Age. Lab experiments by Berner (BLAG)<sup>5</sup>, Walker (WAGH)<sup>6</sup> Volk<sup>7</sup> and others<sup>1</sup> concluded “temperature as the driving force” based on rates of mineral dissolution by changing temperature and pH of fluids. Whether the climatic changes involving atmospheric temperature have triggered the erosion and weathering in the tropical areas is crucial in our assessment of climate-CO<sub>2</sub>-weathering linkages. Monsoon is the important climatic phenomenon in Asia which involves temperature and humidity changes both critical for silicate weathering. Here, we present a multi-proxy-based ~54 ka weathering record from the Alcock seamount complex in central Andaman Sea (Fig. 1

<sup>1</sup>Geochronology & Isotope Studies, CSIR-National Geophysical Research Institute, Hyderabad, India. <sup>2</sup>Geological Oceanographic Division, CSIR-National Institute of Oceanography, Goa, India. <sup>3</sup>Department of Geology, Central University of Kerala, Kerala, India. Correspondence and requests for materials should be addressed to P.M. (email: pavanmiriyala@ngri.res.in)

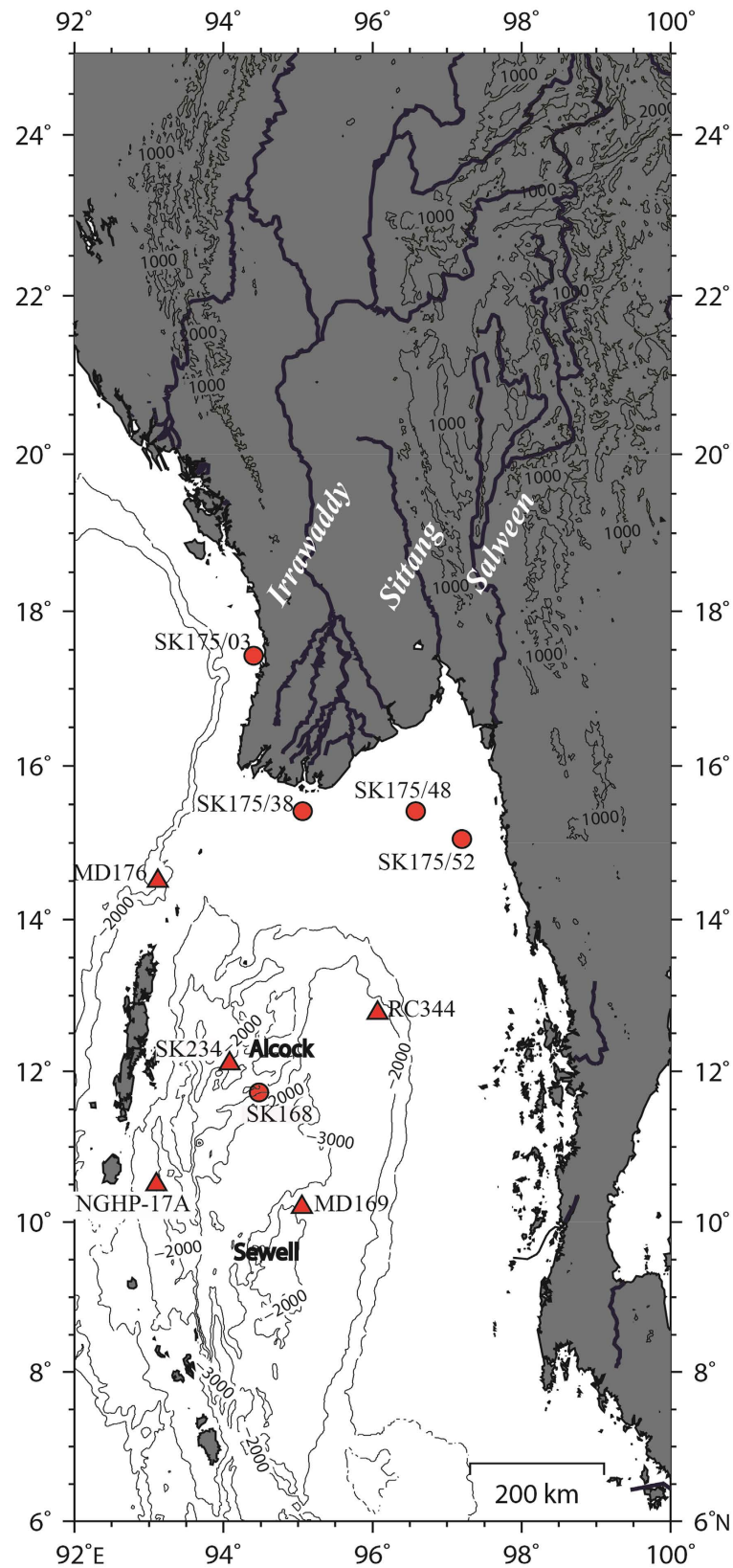


**Figure 1.** Location map (generated by using GMT<sup>68</sup> (v4.5)) of (a) elevation contours and river paths of Myanmar, bathymetry of the Andaman Sea along with; (b) Alcock and Sewell seamount complex; (c) shelf sediments of Arakan (SK175/3), river mouths off Irrawaddy (SK175/38), Sittang (SK175/48), Salween (SK175/52), gravity core SK168 (all from this study); (d) published records MD77-169, MD77-176, RC12-344<sup>12</sup>; SK234/60<sup>22</sup>; NGHP01-17A<sup>23</sup>.

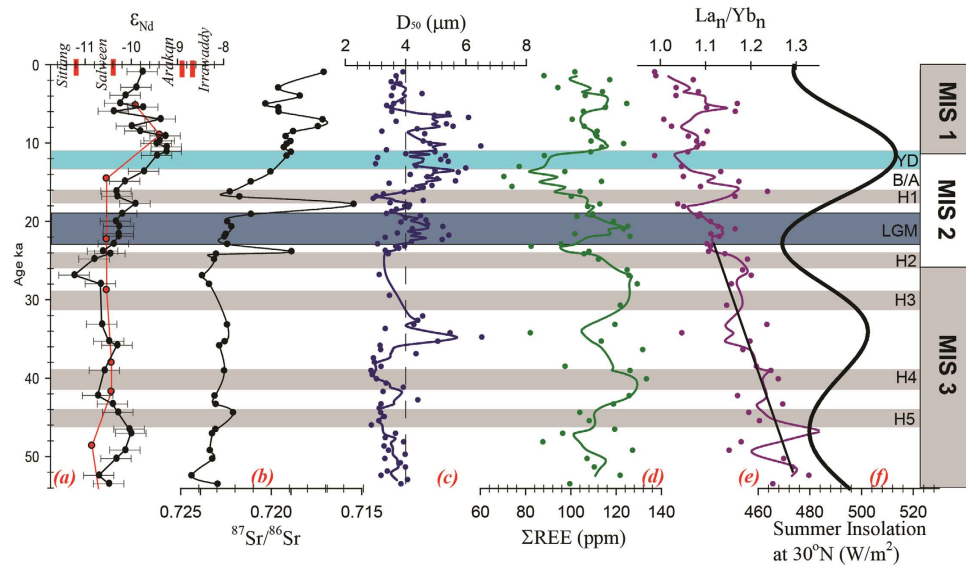


**Figure 2.** Downcore variations of (a)  $\epsilon_{Nd}$  of SK168 of Alcock seamount (this study - with 2sd error bars) and MD169 of Sewell seamount<sup>12</sup> in the Central Andaman Trough (CAT); (b)  $^{87}Sr/^{86}Sr$  of SK168 (this study); the 2sd errors of Sr isotopes are smaller than the symbol size; (c) 3-point moving average median grain size ( $D_{50}$ ), and dotted vertical line indicates average  $D_{50}$  for entire core; (d) 3-point moving average concentration of total rare earth elements; (e) 3-point moving average PAAS normalized ratios of light (La) to heavy (Yb) REE<sup>14</sup>; trend line for glacial period showing a reduction from  $\sim 1.3$  to 1.1; (f) summer insolation at  $30^{\circ}N$ <sup>30</sup>. Shaded regions denote the major climatic events (YD-Younger Dryas, B/A-Bolling/Allerod, H1-H5- Heinrich events and LGM-Last Glacial Maximum). MIS1-3 indicate marine isotope stages.

- SK168/GC1 hereafter referred as SK168), Northern Indian Ocean in the context of this debate (Supplementary, Materials and Methods).

Andaman basin is particularly suitable for such studies as it is a confined basin, separated from the Bay of Bengal by islands and sills, the contributing terrigenous sources<sup>8</sup> and the oceanography are well constrained<sup>9,10</sup>. The terrigenous sediments are principally derived from Myanmar rivers (Irrawaddy, Salween and Sittang) which combinedly supply more than 528 million tons of sediments annually, and are funneled through Gulf of Martaban to deep Andaman basin<sup>11</sup>. A single record of weathering is available for this area which covers a long period ( $\sim 280$  ka<sup>12</sup>) but with a low resolution ( $\sim 8$  data points covering the time period presented here) which precludes the study of weathering changes in response to multiple climatic events occurred since the Last Glacial Maximum (LGM). Past salinity and paleoceanographic variations were already elucidated<sup>13</sup> for the new weathering record presented here.

## Results and Interpretations

Grain size and geochemistry of lithogenic fraction of core SK 168 and Myanmar shelf sediments evaluates the changes in sediment provenance with varying time. The median grain size varied narrowly between 3 and  $7\mu m$  (Fig. 2) and hence the strontium isotope variation is not influenced by size fractionation. Median size displayed 3 periods (see Fig. 2 for 3-point moving average) of larger grain size at, 1) 36-33 ka, 2) 23-19 ka and 3) 15.5-7 ka. While the 36-33 ka and 15.5-7 ka peaks of coarsening coincide with 2 major peaks of solar insolation (Fig. 2), the 23-19 ka period marks the peak glacial time and probably reflects the intensification of physical weathering. As shown in later part of the paper, 15-7 ka is the period of increased monsoon (and runoff) and also associated with intensified chemical weathering. The shale normalized La to Yb ratio<sup>14</sup> (Fig. 2), has varied between 0.9 and 1.3 suggesting that the overall source has fluctuated between felsic to intermediate composition. The ratio shows a gradual decrease from the end of the record to LGM ( $La_n/Yb_n \sim 1.3$  to 1.1) and acquires a near-flat shale-normalized pattern and indicates that the sediment composition has either shifted from a dominantly felsic source to intermediate rock sources<sup>15</sup> or may suggest an efficient mixing in the drainage areas since the deglaciation. Between LGM to present day, the ratio fluctuates between 1 and 1.2 reflecting periods of minor changes in provenance or changing efficiency in sediment mixing. The major and trace element data of sediments from Myanmar continental shelf and SK168 are plotted in the geochemical discrimination plots (Fig. S3). All the samples from SK168 cluster closely, while the shelf samples fall at the edges of SK168 cluster (Fig. S3a), probably as a result of well mixing of Myanmar river materials. A slight shift in shelf values away from the SK168 in felsic-mafic ternary plot (Fig. S3b) might be due to higher Al content in shelf sediments due to its close proximity to the Myanmar river mouths.

The Sm-Nd depleted model age<sup>16</sup>  $T_{DM}$  calculated for SK168 core varies between 1.14 to 1.46 Ga and the average remained close to 1.33 Ga for both glacial and interglacial sediments, which suggests that the provenance remained same through the climatic change. The  $T_{DM}$  of shelf sediments (1.3 to 1.4 Ga) fall very close to SK168 values and thus the sediment deposited in Alcock area was mainly carried by Myanmar Rivers.

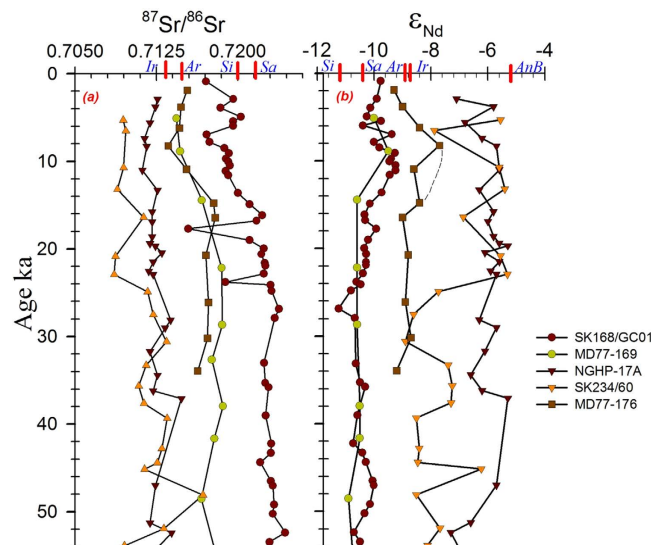


**Figure 3.** All available (a)  $^{87}\text{Sr}/^{86}\text{Sr}$  and (b)  $\epsilon_{\text{Nd}}$  records in and around Andaman Sea along with new Alcock seamount core data (SK 168 - this study). Dashed line in  $\epsilon_{\text{Nd}}$  of MD176 indicates proposed increase in radiogenic nature observed in central Andaman Sea cores. The red markings on x-axis indicate the isotopic values of sediments from continental shelf off river mouths and Middle Andaman island beach (names abbreviated). Ar-Arakan coast, Ir-off Irrawaddy, Sa-off Salween, Si-off Sittang and AnB-Andaman island beach sediment.

**Interpreting the provenance.** Nd isotopic compositions of the shelf sediments off river mouths Irrawaddy, Salween, Sittang and Arakan coast track the present day pathways of terrigenous sediment transport to the deep Andaman Sea. The more radiogenic  $\epsilon_{\text{Nd}}$  in Irrawaddy mouth shelf sample SK175/38 ( $\epsilon_{\text{Nd}} -8.72 \pm 0.33$ ) is very similar to the Arakan shelf sample SK175/3 ( $\epsilon_{\text{Nd}} -8.88 \pm 0.33$ ), and agrees well with reported Irrawaddy sediment value of  $\epsilon_{\text{Nd}} -8.3^{17}$  and implies that the eastern and western part of Indo-Burman ranges (IBR) are contributing near similar Nd signal to the open ocean, either through Arakan, Rakhine rivers in western IBR or through Irrawaddy river on eastern IBR. On the other hand, shelf sediments off rivers Salween (SK175/52;  $\epsilon_{\text{Nd}} -10.37 \pm 0.33$ ) and Sittang (SK175/48;  $\epsilon_{\text{Nd}} -11.19 \pm 0.33$ ) have distinctly low radiogenic values reflecting a dominance of old crustal material in the flood plains of Salween and Sittang. The river Salween originates in eastern syntaxes of Himalaya and flows through south-eastern Tethyan tectonic belt<sup>18,19</sup>, while river Sittang originates and flows entirely from Shan Plateau of Sino-Burman ranges (SBR). The clockwise movement of stronger monsoon currents probably mix the Irrawaddy, Salween and Sittang sediments well during the transport<sup>11,20</sup> and deposition in the Central Andaman basin.

The isotopic data of core SK168 (this work - northern half of the Central Andaman Trough - CAT) exhibits a narrow range of Nd isotopes ( $\epsilon_{\text{Nd}} -11.24$  to  $-9.24$ ; average  $-10.15 \pm 0.46$ ) (Fig. 3) which fall very close to other published CAT values (MD77-169<sup>12</sup> of Sewell seamount (here after MD169) and RC12-344<sup>12</sup> (hereafter RC344)), ( $\epsilon_{\text{Nd}} -11.5$  to  $-9.5$ ; average  $-10.56 \pm 0.3$ ) implies the CAT region of Andaman Sea had received material from a same source during the last two glacial cycles. Another record MD77-176 (hereafter MD176) located close to Irrawaddy mouth shows high radiogenic Nd<sup>12</sup> of  $-9.2$  to  $-7.7$  with average value of  $-8.67 \pm 0.43$  (Fig. 3b). High radiogenic  $\epsilon_{\text{Nd}}$  in MD176 is similar to Arakan shelf (SK175/3 - this study) and Irrawaddy mouth (SK175/38 - this study) sediments. All these 3 areas seem to reflect the dominant supply from Irrawaddy; whereas the CAT cores received low radiogenic Nd material from Salween and Sittang rivers. The slight enrichment of unradiogenic material in glacial sediments of CAT cores may be due to climatic change (intensified NE monsoon and weakened SW monsoon in the Myanmar plains). The possibility of addition of material from Andaman islands to the CAT is ruled out due to absence of major rivers on islands and the presence of coral reefs which grew since LGM<sup>21</sup>. Two other records from the western part of Andaman Sea<sup>22,23</sup> (Fig. 1) have reported high radiogenic Nd. The range of  $\epsilon_{\text{Nd}}$  ( $-7.3$  to  $-5.3$ ) and the average value of  $-6.04 \pm 0.53$  (Fig. 3b) of core NGHP-17A<sup>23</sup> lies between beach sediment values of middle Andaman ( $\epsilon_{\text{Nd}} -5.1 \pm 0.50$ )<sup>23</sup> and Neil islands ( $\epsilon_{\text{Nd}} -7.6 \pm 0.50$ )<sup>23</sup> suggesting a major contribution from the local sources to the western AS. In another core SK234<sup>22</sup> collected near Barren volcano,  $\epsilon_{\text{Nd}}$  vary between  $-9.0$  and  $-5.3$  (average  $-7.4 \pm 1.1$ ) (Fig. 3b) and  $^{87}\text{Sr}/^{86}\text{Sr}$  0.70861 to 0.71680 (Fig. 3a). The major portion of SK234 record has high radiogenic  $\epsilon_{\text{Nd}} > -8.0$  and less radiogenic Sr  $< 0.712$ . This core has multiple ash layers<sup>24</sup> ( $5.75 \pm 0.54$ ) derived from Barren volcanism and less likely to receive terrigenous sediments from the Myanmar rivers<sup>8</sup>. As shown above, when the average values of  $\epsilon_{\text{Nd}}$  in the Andaman sediment are compared, a regional variation in the source provenance of the detrital sediments of the Andaman Sea can be constructed. The CAT region is depleted by  $\sim 2 \epsilon_{\text{Nd}}$  units relative to Irrawaddy mouth region, and  $\sim 4 \epsilon_{\text{Nd}}$  units relative to the western region (NGHP-17A and SK234). The observed high radiogenic Nd of NGHP-17A core and the large excursions in isotopic ratios of SK234 (Barren) are not seen in the CAT cores and suggest that the central Andaman Sea has little supply from island and the volcanic sources in the western AS (Fig. S4). The close variation in glacial  $\epsilon_{\text{Nd}}$

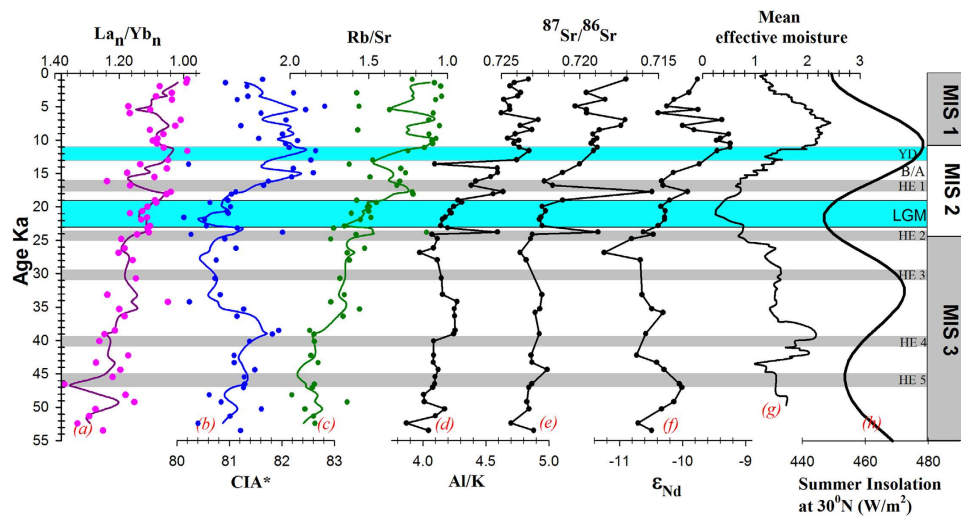


**Figure 4.** Downcore plots of SK168 (present study); (a)  $\text{La}_n/\text{Yb}_n$  ratio and 3 point moving average; (b) Chemical Index of Alteration\* and 3 point moving average ( $\text{CIA}^*$ -excluding  $\text{CaO}^{12}$ ) calculated from molar proportions of major elements; (c) elemental ratio of rubidium to strontium and its 3-point moving average; (d) elemental ratio of aluminium to potassium; (e)  $^{87}\text{Sr}/^{86}\text{Sr}$ ; (f)  $\epsilon_{\text{Nd}}$ ; (g) mean effective moisture of Asia<sup>36</sup>; (h) summer insolation at  $30^\circ\text{N}^{31}$ .  $\text{La}_n/\text{Yb}_n$ ,  $\text{Rb}/\text{Sr}$  and  $\text{Sr}/\text{Sr}$  are in reverse order to get best fit with other plots. Descriptions for shaded region can be found in Fig. 2 caption.

of SK168 with Salween and Sittang river mouth sediments and interglacial  $\epsilon_{\text{Nd}}$  with Irrawaddy river and Arakan coast suggest that the CAT region is mainly fed by the Irrawaddy-Salween-Sittang (ISS) river systems. Thus, the CAT is the most suitable location to explore the climatic impacts on Myanmar continental region.

The  $^{87}\text{Sr}/^{86}\text{Sr}$  ratio in core SK168 varies from 0.715421 to 0.724377 (Fig. 3a) which distinctly vary at different climatic regimes, with higher ratios in SK168 and other CAT cores during glacial and lower during humid interglacial periods implying reduced chemical weathering during glacial times and vice-versa during interglacials (Fig. 3a). The weighted average  $\epsilon_{\text{Nd}}$  values for the time slices representing glacial conditions (54–17.7 ka), the last glacial - interglacial transition (hereafter deglacial) (18–11.6 ka), and the interglacial starting at 11.6 ka are  $-10.43 \pm 0.20$  ( $n = 25$ ),  $-10 \pm 1.74$  ( $n = 6$ ) and  $-9.69 \pm 0.38$  ( $n = 15$ ) in SK 168 nearly brackets the range of values that we observe in the river mouth samples of Irrawaddy-Salween-Sittang (ISS) river systems.

A simple mixing calculation assuming two end members, of a less radiogenic end-member representing the Salween and Sittang rivers (weighted average  $\epsilon_{\text{Nd}} -10.79$ ) and a more radiogenic end member representing the river Irrawaddy and Arakan coast (weighted average  $\epsilon_{\text{Nd}} -8.82$ ), shows that during the glacial period, nearly 82% of the material came from the Salween and Sittang rivers and only 18% from the river Irrawaddy. For the deglacial, 60% of the detritus were sourced from Salween and Sittang rivers as against 40% from Irrawaddy. For the present interglacial, the Irrawaddy dominates the Salween and Sittang rivers by 56%. More importantly, the period between 15.5 and 5.5 ka, the main focus of this study, the Irrawaddy contributes more than 60% of the detritus material to our site. This calculation assumes that the river mouth samples represent the average composition of the catchment origin from which the rivers derive their loads. The new high resolution data of Nd isotopes of SK168 in combination with published CAT (MD169 and MD176)<sup>12</sup> records has helped in new interpretations. A shift towards high radiogenic Nd values is observed between 15.5 and 5.5 ka in SK168, which is not clearly visible in MD169 & MD176 due to low resolution but a kink of high radiogenic Nd at 9.8 ka<sup>12</sup> is synchronous in all records (Fig. 3b), implying a similar forcing mechanism that has taken place in the source area during the weathering. Although the CAT records show clear glacial-interglacial variability in  $\epsilon_{\text{Nd}}$  or  $^{87}\text{Sr}/^{86}\text{Sr}$ , no discernible changes are apparent during the North Atlantic climatic events of YD and B-A.

## Discussion

Temporal changes in chemical weathering intensity (interpreted from proxies  $\text{Al}/\text{K}$ ,  $\text{Rb}/\text{Sr}$ ,  $\text{CIA}^{25}$  and  $^{87}\text{Sr}/^{86}\text{Sr}$  – Fig. 4) mark three broad time periods in this 54 ka record, the glacial (54 to 17.7 ka), the deglacial (17.7 to 11.6 ka) and interglacial periods (11.6 ka to present day). The overall  $\text{CIA}^*$  (defined in Fig. 4) ranges from 80 to 83, implies moderate to high chemical weathering in the source regions. The average  $\text{Al}/\text{K}$  ratios are low (4.2) in glacial, high (4.8) in interglacial with intermediate values (4.6) during deglacial since LGM reflecting the highest degree of chemical weathering during interglacial period.  $\text{Rb}/\text{Sr}$  ratios on an average are low during interglacials (1.2) and during deglacial (1.4) than glacial (1.7), the reduction of Rb with an increase in Sr as an effect of enhanced chemical weathering. The same is reflected with low  $^{87}\text{Sr}/^{86}\text{Sr}$  ratios during interglacial ( $0.71882 \pm 0.007$   $n = 15$ ) and deglacial ( $0.71994 \pm 0.007$   $n = 6$ ) and higher ratios ( $0.72238 \pm 0.007$   $n = 25$ ) in glacial sediments (Fig. 3a). Higher  $^{87}\text{Sr}/^{86}\text{Sr}$  ratios during glacials shows the dominance of physical weathering. Least radiogenic value (0.71542) is noticed at 17.7 ka, the transition to warmer climate and increased chemical weathering. Chemical weathering changes were not evident during YD probably responding more to local summer insolation and/or due to insufficient sediment residence time for the chemical weathering to take place. Low radiogenic Sr during 9–7 ka of

Holocene implies increased chemical weathering, consistent with the timings of increased monsoon induced erosion in the western Himalayas<sup>26</sup>. Interestingly the highest effective moisture is recorded at same time (9–7 ka) in Asian moisture (Fig. 4), and strongly suggest that 9–7 ka is an intensified monsoonal event in south Asian climate.

The reduced salinity from 36 to 31psu between 16 and 4 ka in a record from Ganges river mouth (126KL) of Bay of Bengal<sup>27</sup>, shows that intensification of summer monsoon with initiation of interglacial climate. This increased fresh water input is reflected in  $\delta^{18}\text{O}_{\text{sw}}$  records of western BoB (SK218)<sup>28</sup> and the Andaman Sea (RC344)<sup>29</sup>, and shows that the entire Northeastern Indian Ocean received fresh water during this intensified SW monsoon<sup>13</sup>. These monsoonal records are synchronous to summer insolation at 30°N<sup>30</sup> implying the role of solar insolation in enhancing SW monsoon.

The SW monsoon has weakened and NE monsoon has strengthened during glacials<sup>31,32</sup>. The impact of southward shifting of the locus of Intertropical Convergence Zone (ITCZ) and increased rainfall in rivers of southern Arakan coast were found to have contributed LGM sediments with high radiogenic Nd to Bay of Bengal<sup>33,34</sup>. The lack of such radiogenic Nd in the glacial CAT (both in Alcock (this study) and the Sewell seamount record<sup>12</sup>) suggests that the rivers flowing through SBR (Salween and Sittang) may be the major contributors to the CAT. Absence of such radiogenic Nd shifts in these CAT cores suggests the dominance of NE monsoon during glacial times, which ultimately brought unradiogenic Nd from river basins of Salween and Sittang of SBR. During glacials, due to the sea level fall and exposure of shelf, eastward flowing currents would have weakened and isolated Irrawaddy from Salween and Sittang sources (Fig. S5). The time series plot of  $\epsilon_{\text{Nd}}$  displays two humps of radiogenic nature during 53 to 42 ka and 15.5 to 5.5 ka periods (Fig. 2). The first radiogenic event at 53 to 42 ka occurred during low summer insolation, coincident with Heinrich event 5 recognized in North Atlantic Ocean. There was no change in  $\epsilon_{\text{Nd}}$  during LGM at 23 to 19 ka<sup>35</sup> as the source remained constant in this peak of arid climate. High radiogenic  $\epsilon_{\text{Nd}}$  (−9.92) and a peak in all chemical weathering proxies (Fig. 4) with the occurrence of first warmth event in effective moisture content of Asian atmosphere<sup>36</sup> at 17.7 ka marks this period as the first trigger of warm climate. But it took more than 2 thousand years to show a clear impact of warm climate due to coverage of ice sheets formed during glacials. The significant shift in radiogenic nature of Nd at 15.5 ka may mark the beginning of warm period and increased monsoon which continued upto 5.5 ka. This increased radiogenic Nd input is also observed in other two Myanmar river fed low resolution records of Sewell seamount (MD169) and Irrawaddy river mouth (MD176)<sup>12</sup> during this period of SW monsoonal intensification<sup>29</sup>. Interestingly, changes in all chemical weathering proxies Al/K, Rb/Sr,  $^{87}\text{Sr}/^{86}\text{Sr}$  co-vary with this high radiogenic Nd event and establishes a link between enhanced chemical weathering and supply of radiogenic Nd to deep Andaman Sea.

The present day rainfall data during 1988–1997 (Department of Meteorology and Hydrology of Myanmar) shows the dominance of SW monsoon (~92%) over NE monsoon on the plains of Myanmar Rivers. As major part of Central Myanmar Basin has a dry zone (CDZ) formed due to rain shadow of Rakhine mountains, the sediment loads of Irrawaddy will have much influence of IBR flux<sup>37,38</sup>. CDZ receives very low rainfall ~600 mm, while the northern and southern part of CDZ receives around 2300 and 1200 mm of rainfall respectively. But, these are much lower than IBR located on western side of Irrawaddy basin (Rakhine, Chin and Arakan hills) which receives about 5050 mm. Thus IBR may have a larger control on sediment of Irrawaddy that is carried to the deep sea.

The Mg/Ca values of RC344 core shows the Sea Surface Temperature (SST) during early Holocene (27.9°C) is closer to modern August SST (28.6°C)<sup>29</sup>. Thus if one considers the present day rainfall (5050 mm) is similar to that during the deglacial to mid Holocene, it is possible that IBR catchment could be the potential source for the weathered materials to Irrawaddy river.

The interglacial climate is known for high humidity, large day-night temperature variations, high monsoonal precipitation, together leading to increase in vegetation cover, soil zone and rain water residence time which is more acidic due to increased atmospheric  $\text{CO}_2$ <sup>39</sup> content (Fig. 5). All these would favor an increased chemical weathering conditions at the source region.

Atmospheric  $\text{CO}_2$  concentrations in the Northern Hemisphere is said to lead the global temperature making it an important driver of deglacial warming<sup>40</sup>. With the rise in atmospheric  $\text{PCO}_2$  concentrations, the deglacial warming initiated at 17 ka is coeval with the intensification of chemical weathering in Myanmar watersheds (Fig. 5). This implies that the atmospheric  $\text{CO}_2$  rise was a trigger for monsoon, which in turn had intensified the silicate weathering in the source regions. A part of risen deglacial  $\text{CO}_2$  would have been consumed during the deglacial to mid-Holocene weathering.

Given that the basic and ultrabasic materials tend to weather more quickly than the high crystalline rocks because of textural differences<sup>41</sup>, the IBR region which is characteristic of recent volcanic dykes, ophiolites, mud volcanoes, flysch<sup>17,22,42–44</sup> could have weathered preferentially. It is probable that the increased catchments due to intensified monsoon might have energized the supply of radiogenic Nd to the total sediment discharge of Irrawaddy River.

A 54 ka lithogenic sediment depositional record from the Andaman Sea tracked monsoon variations, weathering patterns, and provenance changes with time. Climate-driven changes in chemical weathering and erosion in the Myanmar river catchments on these time scales is evident. More importantly, the inferred silicate weathering intensity is synchronous with the strengthening of summer monsoon during the deglaciation to mid-Holocene and these changes closely follow changes in regional and global climate. Nd isotope records suggest that over the last 54 ka, detrital sediments are primarily sourced from the Myanmar rivers Salween, Sittang along with Irrawaddy. The glacial contrasts between Nd isotopic composition in the Bay of Bengal and the Andaman Sea suggest that the Andaman Sea was isolated from Bay of Bengal during low sea-levels.

## Methods

For this study, sediment samples spanning the last 54 ka of a deep-sea core (SK-168/GC-01, 11°42'N, 94°29'E; 2064 m water depth) from the Andaman Sea and four Marthaban shelf sediments off Myanmar river mouths and Arakan coast were analyzed (Fig. 1). The core SK168/GC01 comprises of three distinct sediment layers,

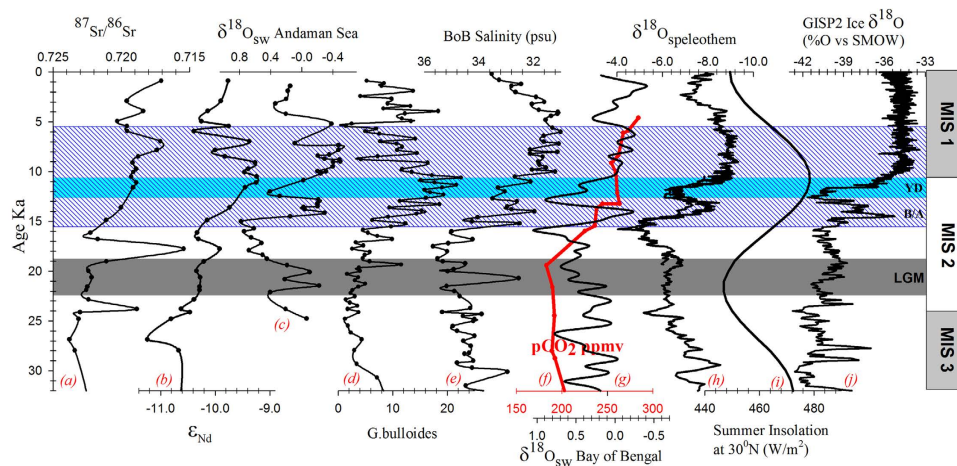


**Figure 5.** Downcore plots of (a)  $^{87}\text{Sr}/^{86}\text{Sr}$  of SK168 (present study); (b)  $\epsilon_{\text{Nd}}$  of SK168 (present study); (c)  $\delta^{18}\text{O}_{\text{sw}}$  of Andaman Sea of RC12-344<sup>29</sup>; (d) Planktonic foraminifer (*Globigerina Bulloides*) % in SK168<sup>35</sup>; (e) Salinity record in 126KL core of Bay of Bengal<sup>27</sup>; (f)  $\text{pCO}_2$ <sup>39</sup>; (g)  $\delta^{18}\text{O}_{\text{sw}}$  of middle-west Bay of Bengal from SK218<sup>28</sup>; (h)  $\delta^{18}\text{O}$  of stalagmites of Chinese caves<sup>69,70</sup>; (i) summer insolation at  $30^\circ\text{N}$ <sup>31</sup>; (j)  $\delta^{18}\text{O}$  of ice core from Greenland ice-sheet program GISP2<sup>71</sup>. For clarity we have restricted the time series records to 32 ka. Descriptions for shaded region except blue can be found in Fig. 2 caption. The blue color shaded region represents the period with coeval increase in chemical weathering and the deglacial monsoon.

dark yellowish brown colored clays in the top 10 cm and olive gray sediments between 30 cm to 420 cm (bottom of the core), while the 20 cm section of light olive gray sediments is sandwiched between these two layers. These sediments are extremely sticky and dominantly clayey in texture, containing tests of foraminifera. The downcore brown to grey color transition is typical of hemipelagic sediments with an oxidized top. Age model for core SK168 is well constrained<sup>45</sup> which is based on five AMS  $^{14}\text{C}$  dates performed on planktic foraminiferal tests and further refined by correlating  $\delta^{18}\text{O}$  *Globigerinoides* ruber record with the low-latitude isostack curve of Martinson *et al.*<sup>46</sup>. The sedimentation rate deduced from this age model averages about 7.8 cm/ka with a similar rate during Holocene and between 8 and 10 cm/ka during MIS 2 and 3. Of the four shelf surface sediments sampled close to the river mouth, three are from the river mouths of Irrawaddy (Sk175/38), Salween (175/48) and Sittang (SK175/52) rivers. One sample originates from a more remote location off the Arakan Coast (SK175/3). The Arakan and Irrawaddy shelf sediments are olive green and black clays while the Salween and Sittang shelf samples are brown colored terrigenous clays. The texture of sediments is silty clay except the Irrawaddy sediment which has a sandy clay texture. All the four sediments are poor in carbonate content<sup>47</sup>. The sediments studied here were collected during 168<sup>th</sup> and 175<sup>th</sup> expeditions of *O.R.V. Sagar Kanya*.

**Sr and Nd isotope analysis of lithogenic sediments.** Isotopic compositions of  $^{87}\text{Sr}/^{86}\text{Sr}$  and  $^{143}\text{Nd}/^{144}\text{Nd}$  were measured on the carbonate-free and Fe-Mn oxide free lithogenic fraction of the bulk sediments following a sequential leaching procedure<sup>48,49</sup>, in which carbonate was first removed using buffered acetic acid followed by Fe-Mn oxide coatings by strong reductive leaching with 1 M Hydroxylamine Hydrochloride (HH) in 25% acetic acid.

Briefly, an aliquot of ~300 mg of dry bulk sediment samples were leached in 20 ml 0.44 M acetic acid (buffered to pH5 by sodium acetate) in acid cleaned 50 ml centrifuge tubes on a shaker for 3 hrs at room temperature. The samples were then centrifuged and the acid containing dissolved carbonate was discarded. This step was repeated five times with fresh addition of buffered glacial acetic acid each time until no bubbles were discerned. The solid residue left over was washed incrementally three times with Milli-Q water, before the Fe-Mn oxides were removed by strong reductive leaching with 10 ml of 1 M HH in 25% acetic acid on a hotplate set at  $90^\circ\text{C}$  for three hours. Samples were centrifuged and the residue was then rinsed four times with Milli-Q water, dried in an oven at  $100^\circ\text{C}$  for a day and reweighed.

Sample dissolution and column chemistry for Sr and Nd generally follows the established procedure in our lab for the TIMS measurements<sup>50,51</sup>, but with some modifications such as dissolution in PARR Vessels and chemical separation using Savillex™ Teflon columns to accommodate Hf chemistry<sup>52</sup>. Approximately 100 mg of the detrital material was totally dissolved in a 3:1 ratio of double distilled concentrated HF:  $\text{HNO}_3$  in steel jacketed PARR vessels at  $180^\circ\text{C}$  for 4 days. Dissolved samples were nitrated twice to expel fluorides and re-dissolved in 6 M HCl. Following this conversion to chloride salts, and subsequent take up in 2.5N HCl, the sample solutions were virtually free of precipitates and an aliquot of 70% of the sample solution was preserved for the determination of Sr, and Nd isotope compositions.

Chemical separation of Sr and rare earth elements (for Nd) generally follows the conventional ion-exchange chromatography procedures<sup>52</sup> using Savillex™ Teflon columns ( $21\text{ cm} \times 0.64\text{ cm I.D.}$ ) charged with Bio-Rad® AG50W-X8 (200–400). Sr was eluted with 2.5M HCl and REEs with 6N HCl. Separation of Nd from other REEs was performed in quartz columns ( $10\text{ cm} \times 0.5\text{ cm I.D.}$ ) containing Teflon powder coated with HDEHP [di (2-ethylhexyl) ortho phosphoric acid] with 0.25N HCl.

Sr and Nd isotope ratios were measured using a Nu Plasma MC-ICPMS (Nu Instruments, UK) in static multi-collection mode at National Geophysical Research Institute (NGRI), Hyderabad. Analyses used 'On Peak Zeros' correction routine for the background blank and memory. Nd was measured in dry plasma mode using a Nu DSN 100 desolvating system and Sr analysis employed wet plasma mode. Sample solutions of Sr, and Nd were prepared in 2% (v/v) optima HNO<sub>3</sub>. Mass fractionation for Sr and Nd isotope ratios was corrected by normalization to <sup>86</sup>Sr/<sup>88</sup>Sr = 0.1194 and <sup>146</sup>Nd/<sup>144</sup>Nd = 0.7219. In the course of the five analytical sessions, standards measured every fourth sample gave the following mean values: <sup>87</sup>Sr/<sup>86</sup>Sr = 0.710254 ± 41 (58 ppm, 2σ, n = 18) for NIST SRM987 and <sup>143</sup>Nd/<sup>144</sup>Nd = 0.512105 ± 17 (33 ppm, 2σ, n = 18) for JNdi-1. The in-run precision quantified by twice the standard error (2SE) was on an average considerably smaller (21 ppm for Sr and 24 ppm for Nd) than the external reproducibility. Measured values were normalized to the accepted ratio of 0.710245 for NIST SRM987 <sup>87</sup>Sr/<sup>86</sup>Sr and 0.512115 for the JNdi-1 <sup>143</sup>Nd/<sup>144</sup>Nd<sup>53</sup>. Epsilon Nd values were calculated using chondritic value of <sup>143</sup>Nd/<sup>144</sup>Nd = 0.512638<sup>54</sup>.

Five analyses of USGS rock standard BCR-2 were used to assess the precision of the column chemistry and analytical procedure yielded <sup>87</sup>Sr/<sup>86</sup>Sr = 0.704985 ± 38 (54 ppm, 2σ, n = 5) and <sup>143</sup>Nd/<sup>144</sup>Nd = 0.512633 ± 7 (14 ppm, 2σ), similar to within errors of the published values of the standard<sup>55,56</sup>. All chemical procedures of leaching, digestions, chromatographic separations and purifications were performed in over pressurized HEPA filtered laminar flow hoods in the clean laboratory at NGRI, Hyderabad. The total procedural blanks were <100 pg for Sr, and ~25 pg for Nd (n = 5) insignificant compared to the size of the samples analyzed.

**Elemental Analysis.** Concentrations of major, trace and REE in the lithogenic fraction of the sediments were evaluated on 1N Hydrochloric (HCl) acid treated residue after removing the authigenic, biogenic and weakly bound exchangeable components. About 2 g salt free, oven dried powdered samples were treated initially with 20 ml 1N HCl for 4 hrs, then with additional 15 ml and agitated occasionally for every 30 minutes. Once the reactions ceased, the residues were washed thoroughly with MilliQ water four times, centrifuged and dried in an oven at 60 °C.

For the measurement of major elements, 0.55 gm of the sample powder was mixed with Spectromelt® A12 (Merck) flux and borate beads were prepared in a Minifuse2 induction furnace. Major elements were measured on Wavelength-Dispersive X-ray Fluorescence (XRF-WD; Axios, PANanalytical, The Netherlands) at the National Institute of Oceanography (NIO), Goa. Geological Survey of Japan reference material (JR-1) was analyzed simultaneously to monitor data quality. Accuracy and precision of the data are better than ± 4%. As the samples used were salt and carbonate-free, Na and Ca values presented here represent those present in lithogenic fraction only and thus suitable for calculating the weathering index CIA.

For trace and REE analyses, 50 mg of powdered samples were weighed into Teflon beakers and dissolved using a suprapure acid mixture of HF, HNO<sub>3</sub> and HClO<sub>4</sub> in a ratio of 7:3:1 on a hot plate. Following which, the digest was dissolved in 4 ml of 1:1 HNO<sub>3</sub> acid and made to 100 ml final volume with Milli-Q water. Elemental concentrations were analyzed by Inductively Coupled Plasma Mass Spectrometer (ICP-MS, X-series2 of Thermo Fisher) at NIO, Goa, with Rh as internal standard<sup>57</sup>. Along with the samples, geochemical reference standards of MAG-1, SCo-1, and AGV-1 were analyzed and the accuracy of trace and REE with reference to these standards was better than ± 3%.

**Size analysis.** Salt free sediments were wet sieved to collect the fraction less than 63 μm (silt and clay). Biogenic components (i.e. carbonate, organic matter and opal) in this fraction were removed sequentially by treatment with 1:4 acetic acid, 3% H<sub>2</sub>O<sub>2</sub> and hot Na<sub>2</sub>CO<sub>3</sub>. The grain size distribution of the treated sediments were measured using Malvern laser particle size analyzer (Mastersizer, 2000) with a Hydro 2000 MU wet sampling accessory using procedures<sup>58</sup> at NIO, Goa. Accuracy and analytical precision for D<sub>50</sub> (median grain size) was better than ± 1%.

**Geochemical and isotopic proxies of weathering.** Geochemical discrimination parameters and proxies of weathering such as the chemical index of alteration (CIA), elemental Al/K, Rb/Sr and <sup>87</sup>Sr/<sup>86</sup>Sr isotope ratios of the detrital sediments are used here to evaluate the intensity of chemical weathering the sediments have undergone in the source regions. The sensitivity of these proxies to track and quantify the chemical weathering intensity is well established<sup>59–64</sup>, but is only limited by grain size effect if any due to hydrodynamic sorting of sediments. CIA represents the molar proportions of more labile Na, K and Ca compared to immobile Al. A CIA value of 100 indicates intense chemical weathering, whereas values of 45–55 indicate virtually no weathering. Al is relatively conservative during weathering process, while K tends to be enriched in weathering products during moderate weathering, but depleted during extreme weathering. Therefore, high Al/K ratio in sediments can be regarded as to extreme chemical weathering (e.g., Nesbitt *et al.*<sup>65</sup>). Variation in Rb/Sr and <sup>87</sup>Sr/<sup>86</sup>Sr ratios primarily reflects the geochemistry of fluid-rock interaction, where more mobile Sr will be leached out partly into solution during weathering, while the immobile Rb stays with the residue. Thus during periods of intense chemical weathering, leaching of more Sr into solution could lower Rb/Sr and <sup>87</sup>Sr/<sup>86</sup>Sr ratios and vice versa if the physical weathering dominates.

**Oceanography of the Andaman Sea.** The present day oceanography of the Andaman Sea has been described by Sijinkumar *et al.*<sup>66</sup> (and references therein). Andaman Sea is a marginal sea located in the eastern part of the north-eastern Indian Ocean (Fig. 1). As in the case of the northern Bay of Bengal, the Andaman Sea receives annually large amount of fresh water from the Irrawaddy catchment with most of the outflow occurring during the summer to late fall<sup>29</sup>. As a result of a fresh water influx, salinity reduces to a minimum value during summer monsoon (July to August<sup>9</sup>). The annual average salinity at our core location (SK 168) is nearly 31.5‰<sup>66</sup>. As a result, a larger salinity gradient exists between the peak and inter monsoon periods. The annual surface

water temperature ranges from 28 to 30 °C and is well mixed to a depth of 50 m leading to stratification which hinders vertical mixing<sup>10</sup>. The Andaman Sea experiences, a seasonal reversal in surface circulation similar to that of the Arabian Sea. The maximum water depth in the Andaman Sea is 4400 m and it is inter-connected with the BoB via several openings viz., the Deep Prepares Channel, Ten Degree Channel, and the Great Channel. Similar to Arabian Sea, upwelling induced productivity changes is also reported from the Andaman Sea with a lower intensity mainly driven by cyclonic eddies. Biological productivity in the offshore Andaman region is ~0.8–1.0 mg C/m<sup>2</sup>/d compared to lesser values (<0.6 mg C/m<sup>2</sup>/d) observed in the coastal areas<sup>67</sup>.

**Data availability statement.** The entire geochemical and isotopic data related to the paper is made available in Tables S1 and S2 in the supplementary information.

## References

- White, A. F. & Brantley, S. L. The effect of time on the weathering of silicate minerals: why do weathering rates differ in the laboratory and field? *Chem. Geol.* **202**, 479–506 (2003).
- White, A. F. & Blum, A. E. Effects of climate on chemical weathering in watersheds. *Geochim. Cosmochim. Acta* **59**, 1729–1747 (1995).
- Gislason, S. R. *et al.* Direct evidence of the feedback between climate and weathering. *Earth Planet. Sci. Lett.* **277**, 213–222 (2009).
- Beaulieu, E., Godd eris, Y., Donnadi eu, Y., Labat, D. & Roelandt, C. High sensitivity of the continental-weathering carbon dioxide sink to future climate change. *Nat. Clim. Chang.* **2**, 346–349 (2012).
- Berner, R. A. Atmospheric carbon dioxide levels over Phanerozoic time. *Science* **249**, 1382–1386 (1990).
- Walker, J. C. G., Hays, P. B. & Kasting, J. F. A negative feedback mechanism for the long-term stabilization of Earth's surface temperature. *J. Geophys. Res.* **86**, 9776–9782 (1981).
- Volk, T. Feedbacks between weathering and atmospheric CO<sub>2</sub> over the last 100 million years. *American Journal of Science* **287**, 763–779 (1987).
- Rodolfo, K. S. Bathymetry and Marine Geology of the Andaman Basin, and tectonic implications for Southeast Asia. *Geol. Soc. Am. Bull.* **80**, 1203–1230 (1969).
- Varkey, M., Murty, V. S. & Suryanarayana, A. Physical Oceanography of the Bay of Bengal and Andaman Sea. *Oceanography and Marine Biology: An Annual Review* **34**, 1–70 (1996).
- Sarma, V. V. S. S. & Narvekar, P. V. A study on inorganic carbon components in the Andaman Sea during the post monsoon season. *Oceanol. Acta* **24**, 125–134 (2001).
- Ramaswamy, V. *et al.* Tidal influence on suspended sediment distribution and dispersal in the northern Andaman Sea and Gulf of Martaban. *Mar. Geol.* **208**, 33–42 (2004).
- Colin, C. *et al.* Evolution of weathering patterns in the Indo-Burman Ranges over the last 280 kyr: Effects of sediment provenance on <sup>87</sup>Sr/<sup>86</sup>Sr ratios tracer. *Geochemistry Geophys. Geosystems* **7**, Q03007 (2006).
- Sijinkumar, A. V. *et al.* δ<sup>18</sup>O and salinity variability from the Last Glacial Maximum to Recent in the Bay of Bengal and Andaman Sea. *Quat. Sci. Rev.* **135**, 79–91 (2016).
- Taylor, S. R. & McLennan, S. M. *The Continental Crust: Its composition and evolution* (1985).
- Piper, D. Z. Rare earth elements in the sedimentary cycle: A summary. *Chem. Geol.* **14**, 285–304 (1974).
- DePaolo, D. J. Crustal growth and mantle evolution: inferences from models of element transport and Nd and Sr isotopes. *Geochim. Cosmochim. Acta* **44**, 1185–1196 (1980).
- Allen, R. *et al.* Provenance of the Tertiary sedimentary rocks of the Indo-Burman Ranges, Burma (Myanmar): Burman arc or Himalayan-derived? *J. Geol. Soc. London.* **165**, 1045–1057 (2008).
- Roger, F. *et al.* Geochronological and geochemical constraints on Mesozoic suturing in east central Tibet. *Tectonics* **22**, 1–20 (2003).
- Chen, F., Li, X.-H., Wang, X.-L., Li, Q.-L. & Siebel, W. Zircon age and Nd–Hf isotopic composition of the Yunnan Tethyan belt, southwestern China. *Int. J. Earth Sci.* **96**, 1179–1194 (2007).
- Rao, P. S., Ramaswamy, V. & Thwin, S. Sediment texture, distribution and transport on the Ayeyarwady continental shelf, Andaman Sea. *Mar. Geol.* **216**, 239–247 (2005).
- Ray, J. S., Pande, K. & Awasthi, N. A minimum age for the active Barren Island volcano, Andaman Sea. *Curr. Sci.* **104**, 934–939 (2013).
- Awasthi, N., Ray, J. S., Singh, A. K., Band, S. T. & Rai, V. K. Provenance of the late Quaternary sediments in the Andaman Sea: Implications for monsoon variability and ocean circulation. *Geochemistry Geophys. Geosystems* **15**, 3890–3906 (2014).
- Sajid, A. *et al.* South Asian monsoon history over the past 60 kyr recorded by radiogenic isotopes and claymineral assemblages in the Andaman Sea. *Geochemistry, Geophys. Geosystems* **16**, 505–521 (2015).
- Awasthi, N. *et al.* Major ash eruptions of Barren Island volcano (Andaman Sea) during the past 72 kyr: Clues from a sediment core record. *Bull. Volcanol.* **72**, 1131–1136 (2010).
- Nesbitt, H. W. & Young, G. M. Early Proterozoic climates and plate motions inferred from major element chemistry of lutites. *Nature* **299**, 715–717 (1982).
- Clift, P. D. *et al.* Holocene erosion of the Lesser Himalaya triggered by intensified summer monsoon. *Geology* **36**, 79 (2008).
- Kudrass, H. R., Hofmann, A., Doose, H., Emeis, K. & Erlenkeuser, H. Modulation and amplification of climatic changes in the Northern Hemisphere by the Indian summer monsoon during the past 80 k.y. *Geology* **29**, 63–66 (2001).
- Govil, P. & Naidu, P. D. Variations of Indian monsoon precipitation during the last 32 kyr reflected in the surface hydrography of the Western Bay of Bengal. *Quat. Sci. Rev.* **30**, 3871–3879 (2011).
- Rashid, H., Flower, B. P., Poore, R. Z. & Quinn, T. M. A ~25 ka Indian Ocean monsoon variability record from the Andaman Sea. *Quat. Sci. Rev.* **26**, 2586–2597 (2007).
- Berger, A. Long-Term Variations of daily insolation and Quaternary Climatic Changes. *Journal of the Atmospheric Sciences* **35**, 2362–2367 (1978).
- Duplessy, J. C. *et al.* Changes in surface salinity of the North Atlantic Ocean during the last deglaciation. *Nature* **358**, 485–488 (1992).
- Fontugne, M. R. & Duplessy, J.-C. Variations of the monsoon regime during the upper Quaternary: Evidence from carbon isotopic record of organic matter in North Indian Ocean sediment cores. *Palaeogeogr. Palaeoclimatol. Palaeoecol.* **56**, 69–88 (1986).
- Burton, K. W. & Vance, D. Glacial-interglacial variations in the neodymium isotope composition of seawater in the Bay of Bengal recorded by planktonic foraminifera. *Earth Planet. Sci. Lett.* **176**, 425–441 (2000).
- Stoll, H. M., Vance, D. & Arealos, A. Records of the Nd isotope composition of seawater from the Bay of Bengal: Implications for the impact of Northern Hemisphere cooling on ITCZ movement. *Earth Planet. Sci. Lett.* **255**, 213–228 (2007).
- Sijinkumar, A. V., Nath, B. N. & Guptha, M. V. S. Late Quaternary record of pteropod preservation from the Andaman Sea. *Mar. Geol.* **275**, 221–229 (2010).
- Herzschuh, U. Palaeo-moisture evolution in monsoonal Central Asia during the last 50,000 years. *Quat. Sci. Rev.* **25**, 163–178 (2006).
- Stamp, D. L. The Irrawaddy River. *Geogr. J.* **5**, 329–352 (1940).

38. Furuichi, T., Win, Z. & Wasson, R. J. Discharge and suspended sediment transport in the Ayeyarwady River, Myanmar: Centennial and decadal changes. *Hydrol. Process.* **23**, 1631–1641 (2009).
39. Petit, R. J. *et al.* Climate and atmospheric history of the past 420,000 years from the Vostok ice core, Antarctica. *Nature* **399**, 429–413 (1999).
40. Shakun, J. D. *et al.* Global warming preceded by increasing carbon dioxide concentrations during the last deglaciation. *Nature* **484**, 49–54 (2012).
41. Meybeck, M. *Pathways of major elements from land to ocean through rivers. River Inputs to Ocean Systems* (1989).
42. Licht, A. *et al.* A palaeo Tibet-Myanmar connection? Reconstructing the Late Eocene drainage system of central Myanmar using a multi-proxy approach. *J. Geol. Soc. London.* **170**, 929–939 (2013).
43. Licht, A. *et al.* Cenozoic evolution of the central Myanmar drainage system: Insights from sediment provenance in the Minbu Sub-Basin. *Basin Res.* **28**, 237–251 (2016).
44. Mitchell, A. H. G. *et al.* Rock relationships in the Mogok metamorphic belt, Tatkon to Mandalay, central Myanmar. *J. Asian Earth Sci.* **29**, 891–910 (2007).
45. Sijinkumar, A. V., Nath, B. N. & Guptha, M. V. S. Late Quaternary record of pteropod preservation from the Andaman Sea. *Mar. Geol.* **275**, 221–229 (2010).
46. Martinson, D. G. *et al.* Age dating and the orbital theory of the ice-ages: development of a high-resolution 0 to 300,000 year chronostratigraphy. *Quat. Res.* **27**, 1–29 (1987).
47. Ramaswamy, V. & Rao, P. S. In *Geological Society, London, Memoirs* 231–240, doi: 10.1144/M41.17 (2014).
48. Rutberg, R., Hemming, S. & Goldstein, S. Reduced North Atlantic Deep Water flux to the glacial Southern Ocean inferred from neodymium isotope ratios. *Nature* **405**, 935–938 (2000).
49. Bayon, G. *et al.* An improved method for extracting marine sediment fractions and its application to Sr and Nd isotopic analysis. *Chem. Geol.* **187**, 179–199 (2002).
50. Banakar, V. K., Galy, A., Sukumaran, N. P., Parthiban, G. & Volvaiker, A. Y. Himalayan sedimentary pulses recorded by silicate detritus within a ferromanganese crust from the Central Indian Ocean. *Earth Planet. Sci. Lett.* **205**, 337–348 (2003).
51. Sukumaran, N. P., Pattan, J. N., Parthiban, G. & Bhaskar Rao, Y. J. Sr-Nd isotopic variations in the Central Indian Basin surface sediments. In *Goldschmidt 71743* (2010).
52. Sukumaran, N. P. *et al.* Sr, Nd, Hf and Pb isotopic characterization of the USGS BCR-2 standard: Results from the NGRI MC-ICPMS Facility. In *11th ismas-tricon* 518–521 (2009).
53. Tanaka, T. *et al.* JNdi-1: A neodymium isotopic reference in consistency with LaJolla neodymium. *Chem. Geol.* **168**, 279–281 (2000).
54. Jacobsen, S. B. & Wasserburg, G. J. Sm-Nd isotopic evolution of chondrites. *Earth Planet. Sci. Lett.* **50**, 139–155 (1980).
55. Weis, D. *et al.* High-precision isotopic characterization of USGS reference materials by TIMS and MC-ICP-MS. *Geochemistry, Geophys. Geosystems* **7** (2006).
56. Raczek, I., Jochum, K. P. & Hofmann, A. W. Neodymium and Strontium Isotope Data for USGS Reference GSP-1, GSP-2 and eight MPI-DING reference glasses. *Geostand. Newsl. J. Geostand. Geoanalysis* **27**, 173–179 (2001).
57. Pattan, J. N. & Parthiban, G. Do manganese nodules grow or dissolve after burial? Results from the Central Indian Ocean Basin. *J. Asian Earth Sci.* **30**, 696–705 (2007).
58. Ramaswamy, V. & Rao, P. S. Grain Size Analysis of Sediments from the Northern Andaman Sea: Comparison of Laser Diffraction and Sieve-Pipette Techniques. *J. Coast. Res.* **224**, 1000–1009 (2006).
59. Nesbitt, H. W. & Young, G. M. Early Proterozoic climates and plate motions inferred from major element chemistry of lutites. *Nature* **299**, 715–717 (1982).
60. Nath, B. N., Kunzendorf, K. & Plüger, W. Influence of provenance, weathering and sedimentary processes on the elemental ratios of the fine grained fraction of the bedload sediments from the Vembanad Lake and the adjoining continental shelf, South-West Coast of India. *J. Sediment. Res.* **70**, 1081–1094 (2000).
61. Colin, C. *et al.* Evolution of weathering patterns in the Indo-Burman Ranges over the last 280 kyr: Effects of sediment provenance on <sup>87</sup>Sr/<sup>86</sup>Sr ratios tracer. *Geochemistry, Geophys. Geosystems* **7** (2006).
62. Selvaraj, K. & Chen, C. A. Moderate chemical weathering of subtropical Taiwan: constraints from solid-phase geochemistry of sediments and sedimentary rocks. *J. Geol.* **114**, 101–116 (2006).
63. Wei, G., Li, X.-H., Liu, Y., Shao, L. & Liang, X. Geochemical record of chemical weathering and monsoon climate change since the early Miocene in the South China Sea. *Paleoceanography* **21**, 1–11 (2006).
64. Wan, S., Kürschner, W. M., Clift, P. D., Li, A. & Li, T. Extreme weathering/erosion during the Miocene Climatic Optimum: Evidence from sediment record in the South China Sea. *Geophys. Res. Lett.* **36**, 3–7 (2009).
65. Nesbitt, H. W., Markovics, G. & Price, R. G. Chemical processes affecting alkalis and alkaline earths during continental weathering. *Geochim. Cosmochim. Acta* **44**, 1659–1666 (1980).
66. Sijinkumar, A. V., Nath, B. N. & Clemens, S. North Atlantic climatic changes reflected in the Late Quaternary foraminiferal abundance record of the Andaman Sea, north-eastern Indian Ocean. *Palaeogeogr. Palaeoclimatol. Palaeoecol.* **446**, 11–18 (2016).
67. Janekarn, V. & Hylleberg, J. Coastal and offshore primary production along the west coast of Thailand (Andaman Sea) with notes on physical-chemical variables. *Phuket Mar. Biol. Center. Res. Bull.* (1989).
68. Wessel, P., Smith, W. H. F., Scharroo, R., Luis, J. & Wobbe, F. Generic Mapping Tools: Improved version released. *EOS Trans. AGU* **94**, 409–410 (2013).
69. Wang, Y. J. *et al.* A high-resolution absolute-dated late Pleistocene Monsoon record from Hulu Cave, China. *Science* **294**, 2345–2348 (2001).
70. Yuan, D. *et al.* Timing, duration, and transitions of the last interglacial Asian monsoon. *Science* **304**, 575–578 (2004).
71. Blunier, T. & Brook, E. J. Timing of millennial-scale climate change in Antarctica and Greenland during the last glacial period. *Science* **291**, 109–112 (2001).

## Acknowledgements

Directors of CSIR-NGRI and CSIR-NIO are acknowledged for permitting us to publish this work. Ship time was provided by MoES (Government of India). Isotope analyses at CSIR-NGRI, Hyderabad were supported by INDEX-LMP PSC0204. NPS acknowledges Y.J. Bhaskar Rao for support and encouragement. This is a contribution to CSIR networked projects GEOSINKS, GENIAS and INDEX. Mr. C. Moraes, Ms. Cliffla and Dr. Parthiban are thanked for their analytical support. We thank Mr. S. Dineshkumar for helping in figures generation. The Nu Plasma MC ICPMS at the NGRI, Hyderabad is a National Facility supported by DST-CSIR (NGRI & NIO). NIO Contribution No. 5992

## Author Contributions

B.N.N., N.P.S. and P.M. designed the study. P.M., B.N.N. and N.P.S. wrote the manuscript. S.A.V. has constructed the age model and identified the climatic events. N.P.S. generated the isotope data with the support from P.M., P.B.R. and B.V.G. P.M. and T.S. generated geochemical data. R.V. sampled the shelf and river mouth sediments

and provided inputs regarding the sediment pathways in the shelf. All authors were involved in the discussion and refinement of the final presentation.

### Additional Information

**Supplementary information** accompanies this paper at <http://www.nature.com/srep>

**Competing Interests:** The authors declare no competing financial interests.

**How to cite this article:** Miriyala, P. *et al.* Increased chemical weathering during the deglacial to mid-Holocene summer monsoon intensification. *Sci. Rep.* 7, 44310; doi: 10.1038/srep44310 (2017).

**Publisher's note:** Springer Nature remains neutral with regard to jurisdictional claims in published maps and institutional affiliations.



This work is licensed under a Creative Commons Attribution 4.0 International License. The images or other third party material in this article are included in the article's Creative Commons license, unless indicated otherwise in the credit line; if the material is not included under the Creative Commons license, users will need to obtain permission from the license holder to reproduce the material. To view a copy of this license, visit <http://creativecommons.org/licenses/by/4.0/>

© The Author(s) 2017